DIGITALCOMMONS
@WAYNESTATE

Wayne State University

Wayne State University Dissertations

1-1-2017

# An Investigation Of The Mechanism Of Traumatic Brain Injury Caused By Blast In The Open Field

Ke Feng
*Wayne State University,*

Follow this and additional works at: https://digitalcommons.wayne.edu/oa_dissertations

 Part of the Biomechanics Commons, and the Nanoscience and Nanotechnology Commons

Recommended Citation
Feng, Ke, "An Investigation Of The Mechanism Of Traumatic Brain Injury Caused By Blast In The Open Field" (2017). *Wayne State University Dissertations*. 1700.
https://digitalcommons.wayne.edu/oa_dissertations/1700

This Open Access Dissertation is brought to you for free and open access by DigitalCommons@WayneState. It has been accepted for inclusion in Wayne State University Dissertations by an authorized administrator of DigitalCommons@WayneState.

# AN INVESTIGATION OF THE MECHANISM OF TRAUMATIC BRAIN INJURY CAUSED BY BLAST IN THE OPEN FIELD

by

**KE FENG**

**DISSERTATION**

Submitted to the Graduate School

of Wayne State University,

Detroit, Michigan

in partial fulfillment of the requirements

for the degree of

**DOCTOR OF PHILOSOPHY**

2017

MAJOR: BIOMEDICAL ENGINEERING

Approved By:

| Advisor | Date |
|---|---|
| | |
| | |
| | |

**© COPYRIGHT BY**

**KE FENG**

**2017**

**All Rights Reserved**

## DEDICATION

*Dedicated to,*

*Xiuyu Guo and Zhijiang Feng, (my parents)*

**This work was not possible without your tremendous sacrifice for the family**

## ACKNOWLEDGEMENTS

This thesis would not have been possible without backing and assistance of numerous individuals.

I would like to express my genuine thanks to my advisor Dr. John Cavanaugh, for giving me the opportunity to join Spine lab and started this journey. His moral support, guidance, and supervision throughout the research work are highly acknowledged. I would also like to express my thanks to my thesis readers, Dr. Albert King, Dr. Liying Zhang, and Dr. Pamela VandeVord, for taking the time to serve on my thesis committee and providing feedback on my work. Special thanks to Dr. King Yang, Dr. Paul Begeman, Dr. Xin Jin, Dr. Srinivasu Kallakuri, Dr. Feng Zhu, Dr. Zhifeng Kou, whose doors are always open when I have questions. I am also grateful for Dr. Miriam Greenberg and Dr. Jingsheng Zhang for providing me with access with their lab equipment for much the work I completed.

To all my lab mates, both previous and present, Dr. Yan Li, Dr. Anil Kalra, Ms Liang Chen, Ms Deepti Guruprakash, Mr Tal Saif, Mr Runzhou Zhou, Mr Ming Shen, and Miss Natasha Gupta, you have made my time as a graduate student an amazing experience. Thank you for sharing your insights, knowledge, and time as we shared our successes and worked through our troubles over many late nights and weekends.

To my family and friends, I appreciate everyone's backing over my time at WSU. To my parents, Zhijiang Feng and Xiuyu Guo, thank you for your continued support and encouragement

to go further. To my husband, Wenxi Yu, and my daughter, Sheyung Yu, for their encouragement and patience during the final stages of this work.

I would also like to thank army research office for providing funding for this research. The research work was not possible without constant monetary support.

## TABLE OF CONTENTS

## LIST OF FIGURES

## LIST OF TABLES

# CHAPTER 1. INTRODUCTION

## 1.1 SIGNIFICANCE OF THE PROBLEM

In the last twenty years, blast-induced traumatic brain injury (bTBI) has gained increasing attention in the military for lack of effective treatment and prevention. From 2000-2014, over 310,000 US soldiers suffered from traumatic brain injury (TBI). Since 2007, the Department of Defense and the National Institutes of Health have spent more than $1 billion on TBI treatment, prevention, and research(Rosenfeld et al., 2013). Among which, bTBI caused by Improvised Explosive Devices (IED) is one of the leading reasons of TBI. Wojcik et al. compared data from several databases and found blasts accounted for 64% of all TBI in Iraq and 47% of those in Afghanistan.(Wojcik et al., 2010) In fact, bTBI has been called the "signature wound" of military service in numerous press reports.(Hoge et al., 2008) Not only in the war zone, but civilian neurosurgeons around the world also have encountered increasingly CNS blast injuries due to the terrorist bombing in urban environments (Rosenfeld et al., 2015; Rosenfeld et al., 2013). It is reported that between 2000 and 2003, more than 50% of terror-related injuries in Israel were the results of blast, mainly in the form of suicide bombers(Singer et al., 2005).

In the 1960's, investigations focused on injury from the blast were mainly on pulmonary, and gastrointestinal systems. The major reason was that blast fatality rate caused by hollow organs is higher than solid organs, like the brain (Clemedson, 1956). Much of the knowledge related to this area comes from extensive work of Richmond and Bowen (Bowen IG, 1968; Richmond et al., 1968; Richmond et al., 1962; White et al., 1965). They did a series of studies to predict the 50%

fatality rate of humans, and at the level of 70% pulmonary failure level the brain was not at risk of fatality or behavior changes(Bass et al., 2008). With the continuous improvement in personal protective equipment (PPE), the injury risk of pulmonary and gastrointestinal systems have been greatly decreased(Okie, 2005). However, with current equipment such as Kevlar helmets, the face and forehead are still not protected from penetrating wounds (Ling et al., 2009; Okie, 2005). Moreover, in the recent conflicts closed brain injuries from blast have outnumbered penetrating ones. (Wojcik et al., 2010) Among the 310,000 American soldiers, who were diagnosed with TBI between 2000 and 2016, more than 80% of them were classified as mild TBI (Figure 1-1).

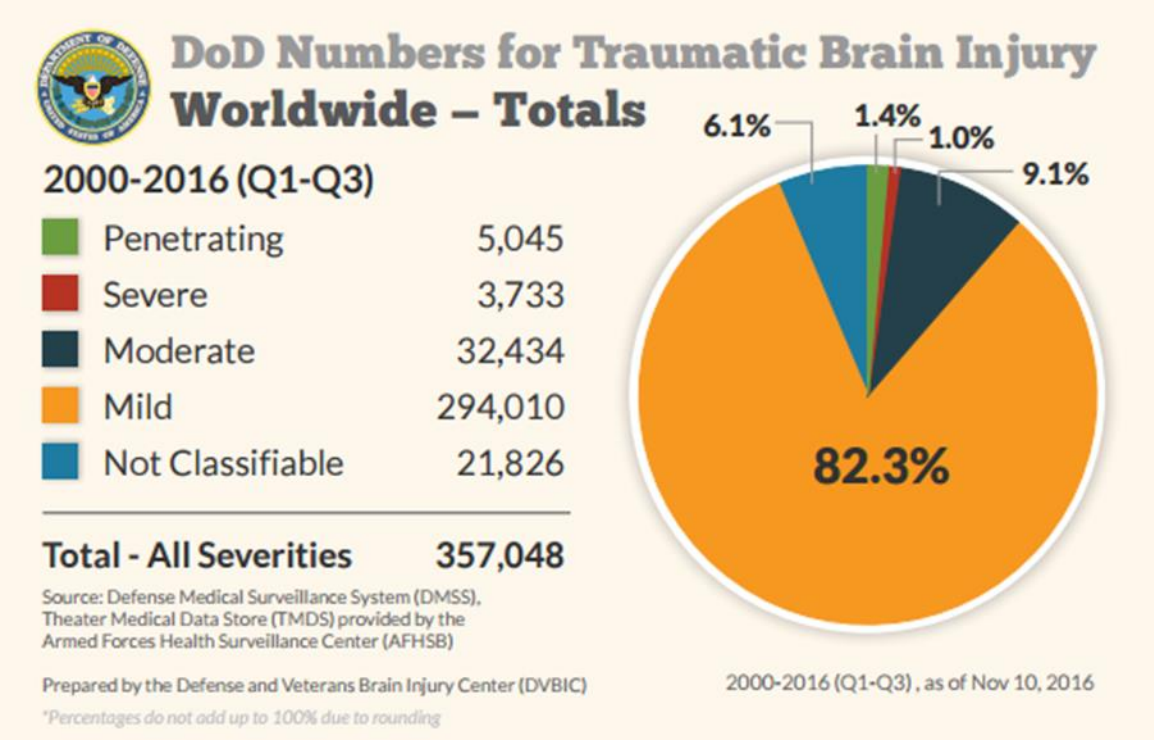


Figure 1-1: Total numbers of TBI diagnosed by Department of Defense (DoD)(2017; Ramasamy et al., 2014)

Research and statistics showed the sudden increased cases of mTBI began in 2006, which was consistent with the field data of an increased number of brain injuries due to blast exposures (Courtney and Courtney, 2015; Galarneau et al., 2008; Murray et al., 2005). Animal research has suggested that the blast level needed to cause fatality from an overpressure wave exposure to the head is greater than the peak overpressure needed to cause fatality from pulmonary injury. However, the blast level required to cause a mild/moderate brain injury may be similar to or less than that needed for pulmonary injury.(Rafaels et al., 2011; Rafaels et al., 2012) Therefore, there is a need to find out the mild/moderate injury tolerance curves in the human being.

Animal models are one of the crucial pathways to establish primary bTBI injury threshold. However, if traditional blast scaling is appropriate between species, many rodent models on blast TBI experiments using shock tubes provide blast overpressure conditions that are more similar to human long-duration nuclear blasts, not high explosive blasts. (Bass et al., 2012) Therefore, it is important to create clinical meaningful blasts that can represent in the real-world scenario. Computational modeling can help elucidate the comprehensive responses of the head and brain to blast.(Chafi et al., 2010; Lockhart et al., 2011; Moss et al., 2009; Nyein et al., 2010) One of the hypotheses is that the scalp may exacerbate the pressure effects in the brain.(Nyein et al., 2010) Others have shown that the skull flexure due to blast is a potential mechanism.(Moss et al., 2009) The distribution of ICP and the kinetics of the head have been simulated in several models.(Chafi et al., 2010; Lockhart et al., 2011; Wang et al., 2014)However, experimental data are still needed to validate these models.

Given the limitations in bTBI research, there is a need to develop reliable and more operationally relevant animal models. To characterize the effects of free-field blast on the head, this study exposed swine to free-field blasts generated by explosives at different incident overpressure (IOP) levels. Thus, the aim of this study was to provide data on the mechanical responses and injury outcomes of the swine in primary bTBI. To our knowledge, this would be the first set of published experimental biomechanical and pathology data from swine subjected to free-field blast overpressure.

## 1.2 OBJECTIVES AND STRUCTURE OF THESIS

This thesis focuses on understanding the mechanics of primary bTBI in a meaningful clinic scenario, and test if shock wave in this range can cause brain injury. The current blast research focuses either on the mechanics of brain responses to the shockwaves or the neurotrauma generated by the shockwaves. In terms of prevention, an improved understanding of the mechanics associated with pathological response of bTBI is needed. Figure 1-2 shows the framework of this study.

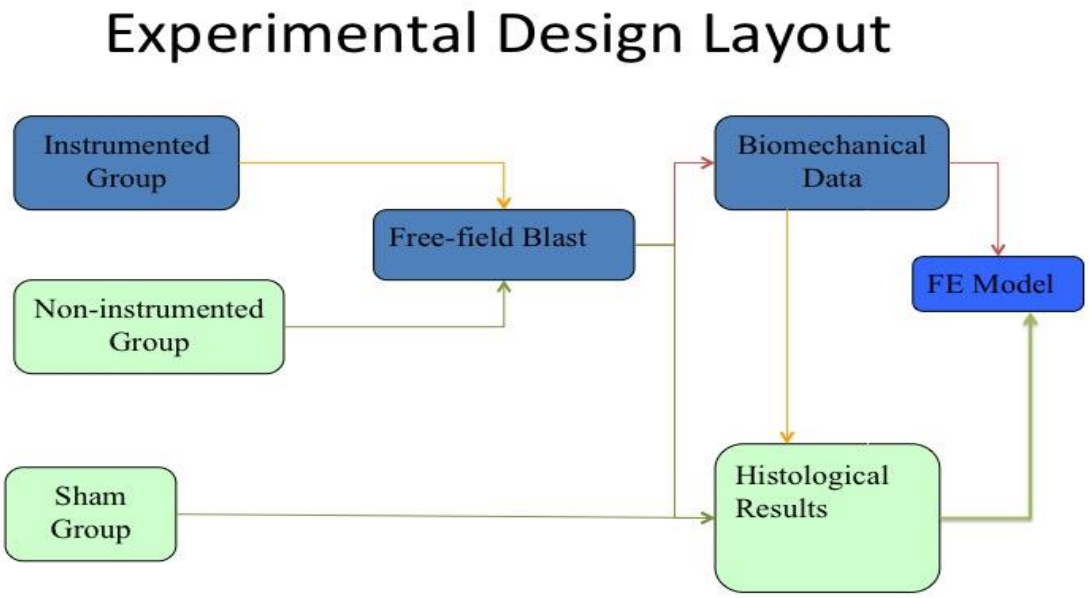


Figure 1-2: Flow chart of this study shows the layout of experiments.

The following chapter gives an overview of the current state of bTBI research. A general background of the current finding on primary bTBI is presented. This is followed by an overview of the central nervous system where details are presented from the system level down to the subcellular level. A definition for primary bTBI is presented, and a discussion is provided of the experimental models covering both the biomechanics and pathophysiology of primary bTBI. An experimental model for inducing primary bTBI is developed in Chapter 3. This model utilizes explosives-induced blasts in the open air to induce bTBI. The biomechanical responses of the brain and head are presented, including intracranial pressure (ICP) and kinematics of the head during blast. Chapter 4 presents changes in fluorescently labeled brain cells captured *in vivo* and under the same blast model. The acute changes of neural cells and apoptosis at different blast levels are discussed, qualitatively and quantitatively details the injury distributions for both those swine

undergoing bTBI and control group. Correlations between apoptotic cells and injured cells in the swine brain are presented. Finally, the implication and connection of this work to improving therapeutic interventions of bTBI are discussed (Chapter 5).

## 1.3 CONTRIBUTIONS TO RESEARCH FIELD

The research effort presented provides a basis for improving the fidelity of analytical approaches concerned with the evolution of bTBI. Insights into the blast induced traumatic brain injury require a firm comprehension of mechanics as well as an understanding of the process is required from clinical, pathological perspectives. Damage to brain propagates from a mechanical assault, but the injury development is influenced by structural changes that are observed at the cellular and subcellular level. It is understood that the loads applied at the macroscopic level of the individual are translated across length scales to the level of the cell in combinations of simple mechanical loads (tension, shear, and compression). It is important to understand how much of incident pressure can directly lead to degeneration of neuron cells and cell death in the CNS.

To approach this problem, an open field blast model is developed to replicate the real-world blasts. Two groups of swine were used to measure the mechanical responses and pathology, separately. We evaluated biomechanical responses of the brain in different regions and compared correlated it with IOP variable, including peak IOP, impulse, linear and angular head motions. We found the ICP had a good correlation with peak incident pressure (IOP). And there was little head motion induced by primary blast. In addition, we utilized Fluoro jade C (FJ-C) and Casepase-3 to evaluate the level of degenerating neurons and cellular death within the brain. It was confirmed

that at medium blast group (260 kPa) there was only increased amount of degenerating neurons but no sign of apoptosis compared with sham animals. At high blast level (370 kPa), we found both elevated FJ-C and Caspase-3 levels compared with sham group. These finding will help in developing the injury threshold of primary bTBI.

# CHAPTER 2. BACKGROUND

## 2.1 BLAST PHYSICS

A blast is characterized by a sharp, instantaneous, rise in ambient pressure and temperature that resulting from explosive detonation, then followed by exponential decay to a partial vacuum phase before gradually returning to the ambient pressure. Ideally, the open field blast wave, which is described as the Friedlander waveform, equation listed below, is composed of two phases: positive phase and negative phase. (Figure 1)

$$I_{max} = P_{so} t_s \left[\frac{1}{b} - \frac{1}{b^2}(1 - e^{-b})\right]$$

Where:

*P = Static pressure at any time t*

$P_{so}$ *= Maximum static overpressure*

*b = Experimentally determined waveform parameter*

$t_s$ *= Total time of the positive phase*

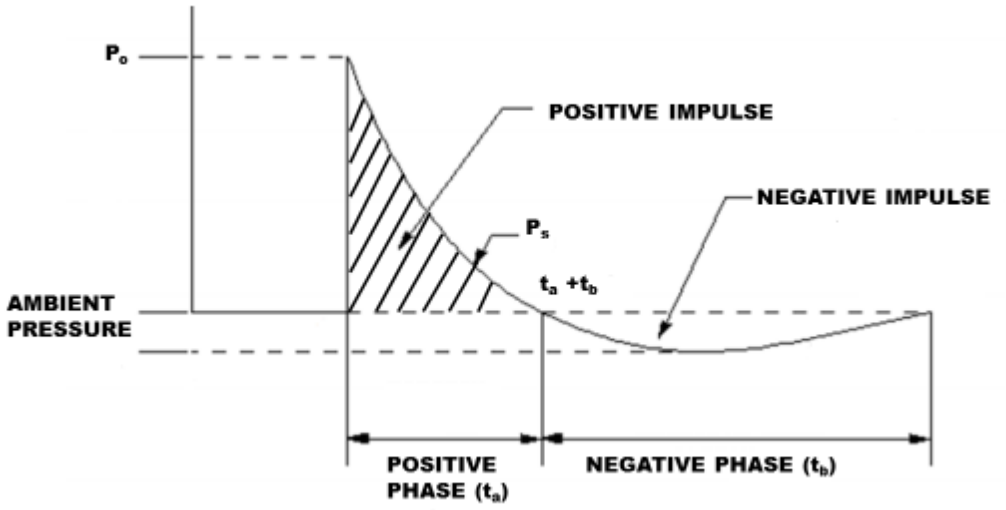


Figure 2-1: Ideal blast waveform (Friedlander Curve). It shows the steep pressure rise of the shock wave followed by a positive pressure phase and a negative pressure phase.

The time at which the pressure remains above normal ambient pressure is termed the duration of the blast wave. The blast impulse is the integral of the pressure in the positive phase and the duration of the blast wave. The peak pressure, the positive duration, and the impulse are believed to be the most important characteristics of the blast.

As the wave propagates away from the denotation, it decreases in magnitude and grows in duration (Figure 2-2).

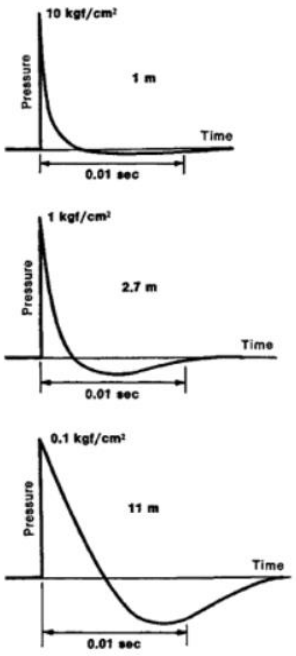


Figure 2-2: Blast wave attenuates with increasing distance (1 m, 2.7 m, 11 m) from the epicenter of an explosion. (Gubkin, K. E,1970).

Associated with the sudden rise in pressure there is also a blast wind due to the kinetic energy transmitted to the air particles(Wood, 1966). The blast wind is also called dynamic pressure. When the blast overpressure strikes the ground or other objects, it is reflected. The exact value of the reflected pressure depends on the incident wave and the angle at which it strikes the surface.

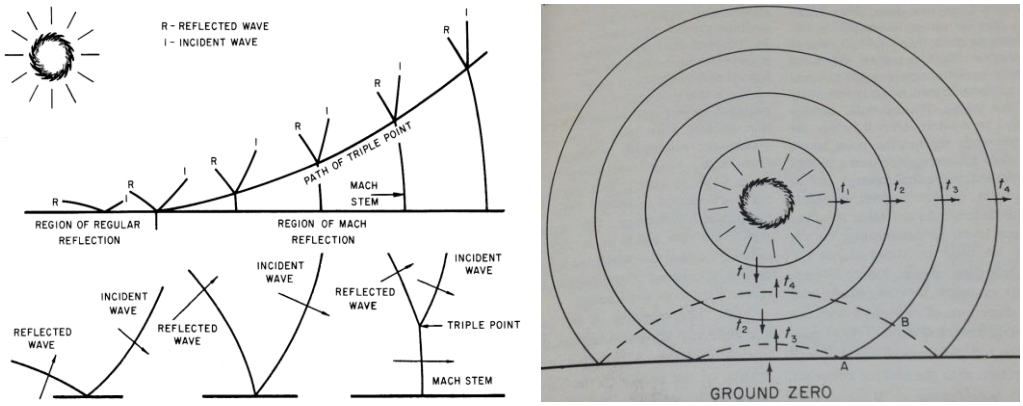


Figure 2-3: Left shows the timeline of reflected wave of a blast; right graph shows the formation of the “mach” stem.

At anywhere above the ground, there would be two separate waveforms. First, is the incident pressure, and then is the pressure from the reflected wave. Due to the compressed air and the heat, reflected wave travels faster than the incident wave, and eventually takes over the incident pressure and two front shocks merge into one. The merged overpressure called the “Mach stem” will have a horizontal angle. The point where the incident wave, reflected wave and the “Mach stem” meet is called the “triple points.” As the reflected wave continues to overtake the incident pressure, the range of the “Mach stem” also increases (Figure 2-3). Any object below the triple point would only have one peak overpressure the whole time. Moreover, this merged overpressure shares the same behavior as the typical blast shock wave, which has a sudden rise, then a positive phase following a negative phase.

The force the overpressure delivers upon a subject depends on the strength of the charge, distance from the blast, and the physical environment. In an enclosed space, the blast overpressure is complicated by multiple reflections of surface. The reflections are believed to complicate the deformation of the brain(Ling et al., 2009; Mayorga, 1997; Wang and Huang, 2013).

## 2.2 DEFINITION AND CLASSIFICATION OF TBI

The American Congress of Rehabilitation Medicine (ACRM) published the definition of TBI in 1993. For traditional close-head or penetrating type of brain injury (cTBI and pTBI), TBI was defined as an occurrence of head injury that is associated with any decreased level of conscience, amnesia, other neurological or neuropsychological abnormalities, skull fracture, diagnosed intracranial lesions, or death(1993). For mild TBI, the severity of the injury cannot

exceed in the following aspects: 1) loss of conscientiousness for approximately thirty minutes or less; 2) after 30 minutes an initial Glasgow Coma Scale (GCS) of 13-15; 3) post traumatic amnesia not greater than 24 hours. The 15-point GCS defines the severity of injury as mild (13-15), moderate (9-12), severe (3-8), and vegetative state (<3)(Teasdale and Jennett, 1974). Even though bTBI shares a lot of common symptoms with cTBI and pTBI, but the duration of the symptom varies a lot. Recognizing the specialty of bTBI, Okie et al. and Warden et al. proposed a new classification for bTBI: Mild bTBI is defined as loss of consciousness <1 h and post-traumatic amnesia <24 h after exposure to an explosive blast. Moderate bTBI is loss of consciousness for >1 but less than 24 h and amnesia lasting >1 but <7 days. Severe bTBI is loss of consciousness >24 h and amnesia >7 days(Okie, 2005; Warden and French, 2005). Typical mild bTBI does not involve skull fracture or other neurophysiological abnormalities that can be detected with current imaging technique.

Blunt TBI typically result in either diffuse or focal injuries or a combination of both. Focal injuries, readily observed using standard imaging techniques, include cortical contusions and subdural, epidural and intracerebral hematomas. The causes of blast-induced injury are usually complicated and can be due to one or more of the following mechanisms: 1) primary injury that directly results from the transmission of shock waves to the body, 2) secondary injury from fragments (shrapnel) that can cause penetrating wounds, 3) tertiary injury from blunt trauma caused by the blast wind which can throw the body against the ground or other obstructions, and 4) quaternary injury related to heat, smoke, chemicals and emission of electromagnetic pulses

(EMP)(Risling and Davidsson, 2012). This study focuses on the mild to moderate level of primary injury caused by pure shockwave loading.

The causes of blast-induced injury are usually complicated and composed of one or more of the following mechanisms: 1) primary injury that directly results from the transmission of shock waves to the body, 2) secondary injury from penetrating wounds related shrapnel fragments, 3) tertiary injury from blunt trauma resulting from blast wind caused by impact of the body against obstructions, and 4) quaternary injury related to heat, smoke, poisoned chemical and emission of electromagnetic pulses (EMP)(Risling and Davidsson, 2012).

**2.3 EXPERIMENTAL MODELS OF PRIMARY BTBI**

The mechanism of primary bTBI is still unclear. Researchers have noted the differences of primary bTBI compared with other blunt induced TBI. No visible bleeding, no effective histological staining, nevertheless it can result in the way of chronic behavior changes, etc. In mild bTBI, standard anatomical imaging techniques (MRI and computed tomography) generally fail to show focal lesions and most of the symptoms present as subjective clinical functional deficits.(Graner et al., 2013) Furthermore, clinical findings of long-term effects of mild, repeated bTBI varies widely. The effects include progressive affective liability, distractibility, executive dysfunction, memory disturbance, suicidal ideation, cognitive deficits and dementia (Goldstein et al., 2012; Rosenfeld et al., 2013). The neuropathology includes large-scale cortical perivascular tau pathology, disseminated microgliosis, astrocytosis, myelinated axonopathy, and progressive neurodegeneration (McKee et al., 2013). A similar description was first discovered in athletes with

repeated concussions (Omalu et al., 2005). bTBI is also often associated with the post-traumatic stress disorder (PTSD). The risk of PTSD might be increased by cognitive dysfunction (Stein and McAllister, 2009). However, the chronology of PTSD development remains uncertain.

All these findings indicate that the mechanism of primary bTBI could be different with other forms of TBI. Many experimental models and computer models have been developed since then (Table1-1). The proposed mechanisms need not to be mutually exclusive; however, the mechanical response of the brain under blast is crucial to understand the underlying injury mechanism. Considering the complex nature of this type of injury, computer modeling provides helpful insights on the mechanical responses following a primary blast injury.(Panzer et al., 2012; Zhang et al., 2013; Zhu et al., 2010; Zhu et al., 2012) However, with limited experimental data in this area, it is difficult to draw conclusions on injury mechanisms and threshold, and validate the computer models. Therefore, in this study, we developed an animal model under open-field blast conditions to evaluate the mechanical responses and its acute neuropathology consequences from primary bTBI.

Table 2-1: Primary bTBI mechanism studies.

| bTBI mechanisms study | | |
|---|---|---|
| *Mechanisms* | *Group* | *Type* |
| pressure interact with the brain | Chavko M, etc. (Chavko et al., 2007) | experimental |
| | Chavko M, etc. (Chavko et al., 2011) | experimental |
| | Bir C, etc.(C., 2011) | experimental |
| | Leonardi AD(Leonardi et al., 2011) | experimental |
| | Zhang L, etc. (Zhang et al., 2013) | computer models |
| | Shridharani JK (Shridharani et al., 2012) | experimental |
| | Ganpule SG, etc. (Ganpule et al., 2013) | experimental/computer model |
| | Kucherov KH. Etc. (Yan Kucherov, 2012) | computer models |
| | Taylor PA,etc.(Taylor and Ford, 2009) | Computer model |
| | Goeller J etc. (Goeller et al., 2012) | Computer models/surrogate |
| skull flexure | Bolander R, etc. (Bolander et al., 2011) | experimental |
| | Moss WC, etc(Moss et al., 2009) | Computer model |
| thoracic | Suneson A (Suneson et al., 1987, 1990) | experimental |
| | Cernak I, etc. (Cernak et al., 2011) | experimental |
| acceleration and deacceleration | Goldstein LE, etc. (Goldstein et al., 2012) | experimental |
| | Zhang L, etc. (Zhang et al., 2004) | computer models |
| | Courtney MW, etc. (Courtney and Courtney, 2011) | experimental |
| Generation of Piezoelectric properties of bones | Lee KY,etc. (Lee et al., 2011) | computer models |

## 2.4 GENERATION OF BLAST IN EXPERIMENTAL MODELS

Most studies have utilized shock tubes to produce overpressure.(Rafaels et al., 2012) The distinct advantages of shock tube are its economical function for tests in laboratories and high reproducability of the desired overpressure by applying membranes of the same thickness. Its ease of scheduling compared with field tests including severe restrictions of weather, explosives handling, and availability of personnel make the shock tube tests a prevalent choice. However, one should note that the parameters of the overpressure generated in conventional shock tubes can be different from a free-field blast wave. Some shock tubes generate shockwaves with prolonged positive duration outside the realm of real world situations.(Reneer et al., 2011; Sundaramurthy and Chandra, 2014) The test animal size is limited by the shock tube test section and there could be non-negligible complex reflections within the shock tube. These characteristics would make the corresponding mechanical responses different from those bTBI injuries in free-field blasts, in which test subjects can be exposed to a simple Friedlander wave without interference from reflections. Additionally, blast testing in the open field with proper settings can provide relevant physical parameters of blast conditions similar to those in the battlefield. In the real world, reflections of the shock wave from the ground are inevitable. Due to the complexities of gas-dynamic shock reflection phenomena, the reflected and incident waves merge into a new wave front called the "Mach stem". (Ben-Dor, 2007) To minimize the effect of reflected waves, it is necessary to locate the “triple point” within the “Mach stem” region utilizing appropriate standoff distances and the heights of burst.

The measurement of shock wave propagation patterns in an *in vivo* brain remains a significant challenge. Much research has been conducted with rats and swine to measure the ICP responses in the brain using shock tubes.(Bauman et al., 2009; Chavko et al., 2007; Leonardi et al., 2011; Long et al., 2009; Shridharani et al., 2012) However, in most of the studies only a few sensors were installed and, in some cases, there was no detailed description of sensor locations.(Bauman et al., 2009; Chavko et al., 2007; Leonardi et al., 2011) This lack of accurate information constitutes an impediment to a full understanding of how a pressure wave interacts with various parts of the brain. In addition, the brain structures and skull thickness vary widely between different animals. Yucatan swine, six to eight months in age, have a similar body mass (50-60) and skull thickness (6-17 mm) as human. Biomechanical responses of swine to blast overpressure are expected to be closer to those of the human and thus it would be more appropriate to study them instead of the small animals like rodents.

There are several ways to produce blast overpressure in blast researches. Open-field blasts, shock tube, and blast tube blasts are the three common types of sources used to produce shock waves A shock tube consists of two separate chambers: the driver section, where compressing the gas; and the driven section, where the shock wave propagates, creates the pressure. The two sections are separated by a frangible membrane, which ruptures at a pressure that is directly proportional to its thickness. Many blast studies have been conducted on shock tubes(Rafaels et al., 2012) (Table 2-1).

Table 2-2: Animal models on the investigation of mechanical responses of bTBI.

| Research group | Animal model | Blast type | Findings |
|---|---|---|---|
| Shridharani et al. | Rat | Shock Tube | First report on ICP |
| | | | The positive duration was longer than in air |
| Leonardi et al. | Rat | Shock Tube | Increased ICP compared with IOP |
| Saljo et al. | Swine | Shock Tube | Blast overpressure only on thorax introduced little ICP |
| Shridharani et al. | Swine | Shock Tube | Information of IOP including peak pressure and durations |
| | | | ICP readings were significantly lower compared with Surface Sensor reading. |
| | | | Linear acceleration results correlated well with ICP data |
| Bauman et al. | Swine | Shock Tube | ICP readings were lower compared with Surface Sensor reading. |
| Chen et al. | Goat | Open air | ICP reading was significantly lower compared with IOP |

The principles behind blast tubes are the same as with shock tube, where the former uses a small explosive charge to generate high pressures to mimic high-pressure level blasts. The major advantages of shock tube compared to the open-field blast are: 1. the desired pressure level is highly repeatable since the pressure purely depends on the thickness of the membrane and the length of the driven chamber. 2. It is easier to get a long blast impulse in the shock tube by modifying the configuration of the shock tube. However, open-field blasts are still very crucial and irreplaceable to study the biological effect when studying bTBI. Firstly, unlike in the real blast event, where the waveform goes to all the directions and with a single peak pressure, shock tube can only produce waveforms in one direction and the peak pressure is more prolonged over particular time. Secondly, any zone within the shock tube will be affected by the arrival of disturbances and gas dynamic features. Therefore, to understand the biomechanical responses to the blast wave, this study was carried out in the free field, and the blast was produced by explosives. The disadvantages of free-field blasts also need to be considered. Firstly, the explosives can create considerable variance in IOP under similar experimental conditions. Secondly, reflections from the ground and other obstacles can complicate the blast overpressure. Lastly, this type of experiment requires specific open field space and all the equipment needs proper placement and protection from the blast.

## 2.5 INJURY TOLERANCE STUDIES ON OTHER SOFT ORGANS

Pulmonary and the gastrointestinal system were found to be the most fragile parts under blast. In the past 70 years, much effort was made to find the relationship between blasts and thoracic injury.

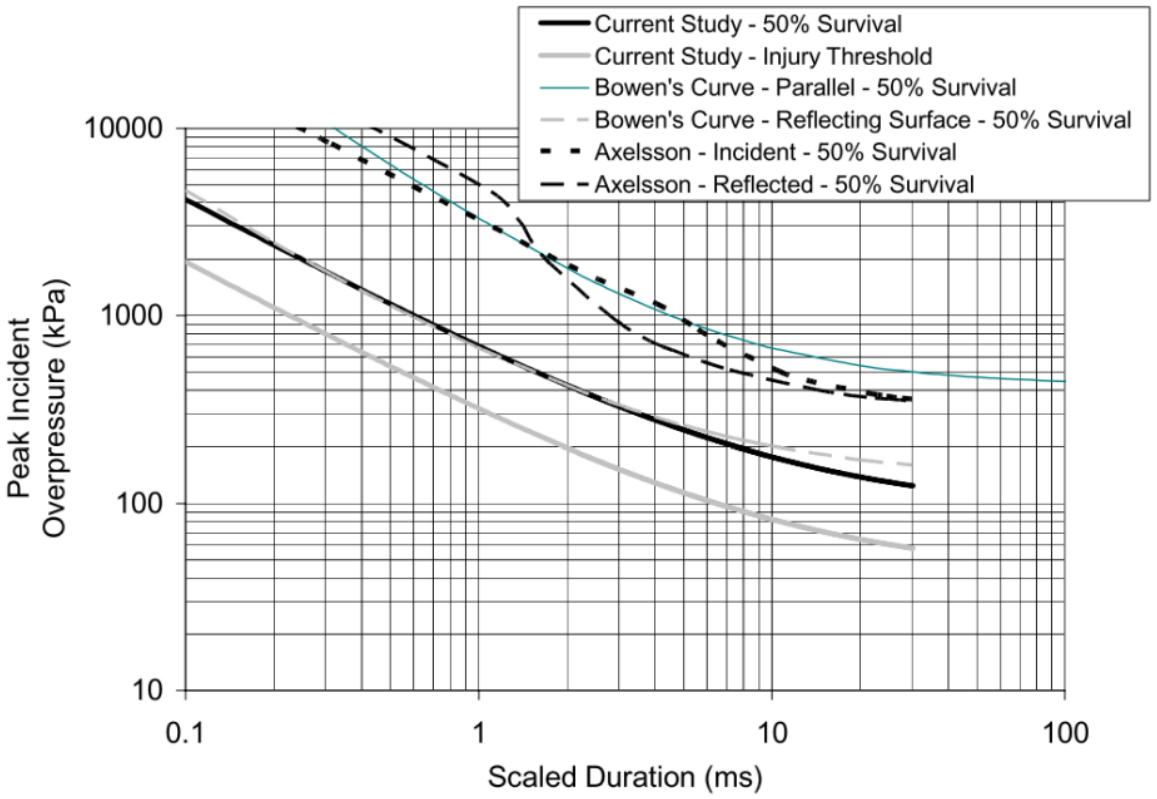


Figure 2-4: Incident overpressure/ duration of blast developed by Bowen, Bass, etc.

The biological tolerance level was defined and using the improved personal protective equipment (PPE), the mortality rate and injuries on the body has significantly dropped. However, there still is no effective ways to protect the brain from bTBI due to lack of knowledge on the mechanism of bTBI. Such lack of understanding has recently been highlighted as a problem by Bass as well as by Elder (Bass et al., 2012; Elder et al., 2014). Each of these groups underscored that progress in the field is highly unlikely until the mechanisms become known. To resolve this widely recognized problem, we presented here to identify the relevant interactions between blast pressure and injury level of the brain.

## 2.6 ANATOMICAL AND STRUCTURAL SIMILARITIES OF BRAIN BETWEEN HUMAN AND SWINE

Yucatan minipigs, which have an adult body weight of 70-90 kg, 6-month weight of 46 kg, are one of the commonly used purpose-bred laboratory minipigs. The pig brain weighs in the range of 80-180 g, depending on its body size and breed. Its brain volume is about 160 $mm^3$ ， the thickness of the cerebral cortex is around 0.22 cm(Hofman, 1985). This number is higher than human skull with average of 7 mm. Its cortical gyrification is more comparable to primates than that of rat using the dimensionless isomorphy factor. The pig brain has a value of 50, the human brain is around 65, whereas the lissencephalic rat brain has less than 10 (Mayhew, 1992; Mayhew et al., 1996). Anatomy studies of the porcine brain showed pigs share a lot of same structures with that of human. The basic structure of the porcine brain includes, telencephalon (Cerebral cortex), diencephalon, mesencephalon, brain stem, and cerebellum. A semi-diagrammatic representation of a sagittal section through the head is given in figure2-5. In addition, the total number of neocortical neurons in pig brain is around 400 million. In comparison, rat brain has a total number of 21 million. In the human cerebral cortex, there is around 20 billion neurons. Currently, major brain structures are identified and labelled in pig atlas (Roura et al., 2016).

There are also differences in the pig brain compared with that of human. The brain occupies a small region of the skull, especially in the adult swine. The organization of the main cortical lobes in the pig is different from that of primate, lacking the pronounced caudal expansion and curvature of the progressive telencephalon. There is a large, pneumatized frontal sinus in the pig

brain. In the 3-month old pig, the sinuses are confined to the anterior region. However, in older animals the frontal bone is traversed by the sinus virtually in two layers.

The gyrencephalic pig brain resembles the human brain more in anatomy and physiology than do the brains of commonly used small laboratory animals. The size of the pig brain permits the identification of cortical and subcortical structures by imaging techniques. Additionally, pigs have advantages over primates for economic and ethical reasons. In spite of its large body size, pigs have substantial advantages of being an experimental animal for modeling human brains.

In this study, Yucatan was chosen as the test animal mainly because of its similar body weight to humans and its inbred nature, which diminishes variability in the experimental data.

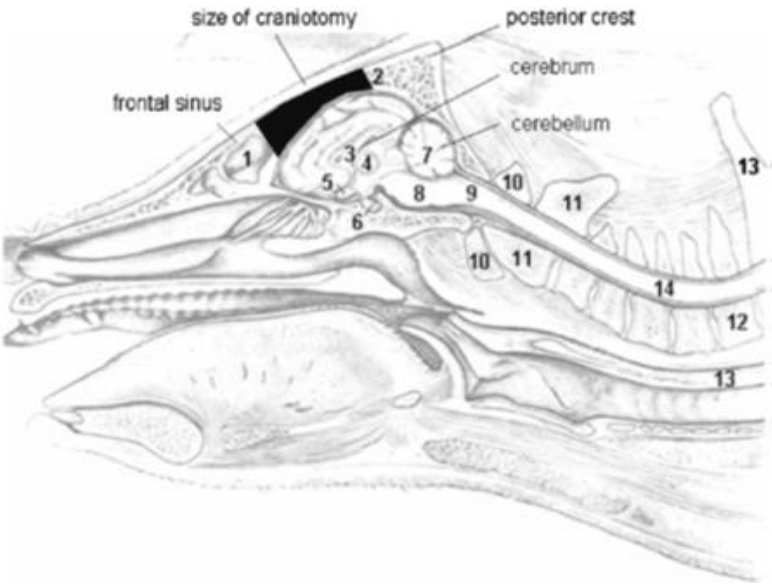


Figure 2-5: A semi-diagrammatic representation of a sagittal section through the head. 1 frontal sinuses, 2 skull, 3 hemisphere, 4 interhemispheric commissura, 5 chiasm, 6 pituitary, 7 cerebellum, 8 brainstem, 9 medulla, 10 atlas, 11 axis, 12 vertebral column, 13 anterior spinal processes, 14 spinal cord(Swindle, 1984)

## 2.7 QUANTIFICATION OF CELLULAR INJURY AND APOPTOSIS

TBI has been categorized as primary injury and secondary injury(Li et al., 2015). The primary injury results from damage from an external force or decrease in cerebral blood flow during ischemia. The second injury, characterized by neuronal loss, happens within minutes or from hours to days after the injury. Several pathological process, including disruption of the blood-brain barrier, necrosis, apoptosis, inflammation and oxidative stress, have been reported to contribute to the neuronal loss in the second injury phase(Cornelius et al., 2013; Hu et al., 2009; Shetty et al., 2014; Xu et al., 2013; Yatsiv et al., 2005). Among these process, apoptosis is a major cause of post-traumatic neuronal loss (Springer, 2002). About two third of TBI-induced cell death was caused by apoptosis (Zhang et al., 2005). Apoptosis can be initiated through intrinsic or extrinsic cell-signaling pathways (Ghavami et al., 2009; Salvesen, 2002). Both pathways converge on caspase-3, a protein that acts as the cell's executioner. Upon activation of apoptosis signaling, procaspase-3 is cleaved to yield active caspase-3, which in turn initiates organized degradation of cellular organelles (Walters et al., 2009). Therefore, the active form of caspase-3 is a widely used marker of apoptosis(Bardet et al., 2008; Bressenot et al., 2009).

TBI leads to a series of cellular events that contribute to the initiation of apoptosis in neuronal cells. TBI caused tissue damage and subsequent inflammation leads to excessive release of excitatory neurotransmitters, and thereby results in increase of intracellular and mitochondrial $Ca^{2+}$ levels (Cheng et al., 2012), which triggers apoptosis (Mattson and Chan, 2003; Uguz et al., 2009). The $Ca^{2+}$ overload also contributes to ROS production (Cheng et al., 2012), which promote

apoptosis (Abdul-Muneer et al., 2015). Furthermore, TBI damages blood-brain barrier, whose disruption is closely associated with neuronal apoptosis (Shetty et al., 2014). Taken together, neuron apoptosis in second injury is induced by a variety of cellular events and stimuli. The exact post-TBI signal that triggers neuronal apoptosis is not clear.

FJ-C staining is a technique widely used for the labeling of degenerating neurons. Compared with traditional methods such as hematoxylin and eosin (H & E) and Nissl stains, FJ-C staining exhibited better specificity and simplicity (Bian et al., 2007; Schmued et al., 1997; Schmued et al., 2005). Numerous TBI studies have applied FJ-C staining in the detection of neuron desecration (Hua et al., 2012; Kuehn et al., 2011; Li et al., 2016; Shellington et al., 2011; Wang et al., 2012). However, it is worth noting that the mechanism whereby FJ-C specifically labels degenerating neurons is not clear. Neither the molecules that bind to FJ-C in degenerating neurons have been well characterized.

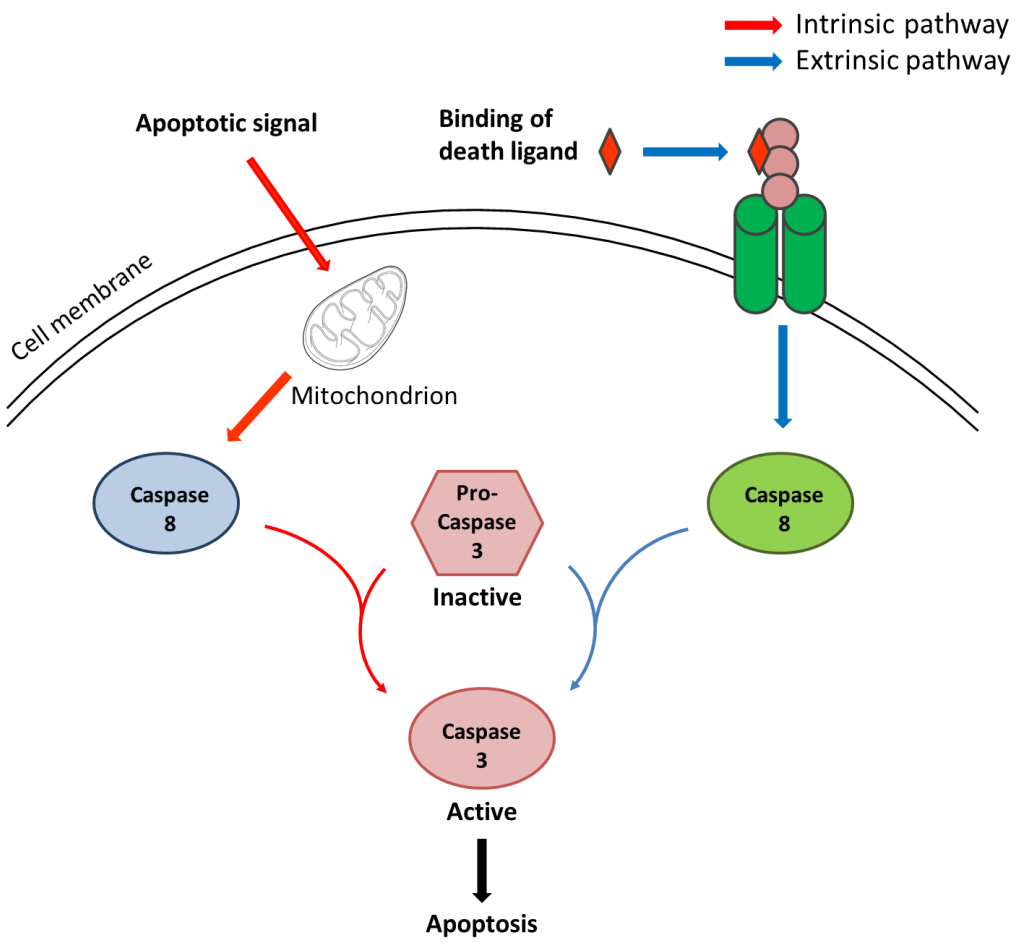


Figure 2-5: Caspase-3 activation. Apoptosis begins with the activation of the intrinsic pathway or the extrinsic pathway, which in turn activate downstream enzyme caspase-9 and caspase-8 respectively. Active caspase-9 and caspase-8 facilitate the cleavage of pro-capsase-3 to generate active caspase-3, which results in the irreversible apoptosis.

# CHAPTER 3. BIOMECHANICAL RESPONSES OF SWINE SUBJECT TO FREE-FIELD BLASTSANATOMICAL DIFFERENCES

## 3.1 MATERIALS AND METHODS

### 3.1.1 Animal preparation

This research protocol was reviewed and approved by the Institutional Animal Care and Use Committee and the USAMRMC ACURO. Five instrumented Yucatan swine (age 6-8 months, weight 50-60 kg) were exposed to repeated frontal free-field blasts to collect biomechanical data. Before instrumentation, all swine were acclimated for 6-8 days before tests to their new housing conditions. On the test date, the animal was transported in an ambulance to the blast site (ARES, Port Clinton, Ohio) under anesthesia (ketamine 20mg/kg intra muscular and xylazine 2mg/kg intra muscular). The ambulance was equipped with an examination table and equipment for physiological monitoring to ensure maintenance of the proper anesthetic level. Once at the test site, a surgical procedure to install ICP sensors was performed. Blood pressure, oxygen saturation, heart rate and respiratory rate were monitored before and in between blast exposures. During the tests the animal was maintained under anesthesia (propofol 12-20 mg/kg/hr Constant-Rate Infusion). To expose the swine to open field blast, the animal was placed prone in a specially designed canvas sling with holes for the extremities. The sling was supported by a steel body frame which was suspended from a metal I-beam that was 3.7 m off the ground. The I-beam was supported by two, steel A-frames, as shown in Figure 1. The body frame was tied down to the A-frames with straps to prevent excessive motion due to the blast wind. To prevent thoracic injuries from primary blast,

the torso was wrapped in a lead sheet that had a density of 39 kg/m$^2$. A piece of 1.6 cm thick foam padding was placed between of the lead sheet and the animal. The snout of the animals was secured by webbing material to support the head during blast tests.

3.1.2 Free-field blast procedure

3.6 kg of C-4 was packed into a spherical shape to generate blast waves. The height of burst (HOB) was controlled by suspending the C4 from a metal chain and a 2-inch thick metal plate placed under the charge to eliminate debris and assure consistence of the reflected wave. To generate different levels of IOP, the explosive was placed at varying distances from the pig's head. Three levels of IOP were used in this study. Since the goal was to evaluate mechanical responses in non-fatal primary bTBI, the pressure levels were selected based on previous swine studies that were tested using shock tubes.(Bauman et al., 2009; Shridharani et al., 2012) These three pre-determined peak IOP levels were nominally designated as low (150 kPa), medium (300 kPa), and high (400 kPa). To attain a pure Friedlander waveform, the height of the triple point as a function of the horizontal distance from a given charge weight was calculated for a range of HOB.(De Rosa et al., 1992; Ivanov et al., 2001) The HOB of the charge was computed to be 0.8 - 0.91 m with the height of the head of the test subject at or less than 0.91 m. The estimated horizontal distances from the charge and the HOB to produce the three different blast pressure levels were further verified by a finite element simulation (ConWep card in LS-Dyna, LSTC, Livermore, CA).

To record the IOP profile during each test, a pencil pressure sensor (137B24B, PCB Piezotronics, Depew, NY,) was placed near the animal at the level of its eyes while two backup

pencil sensors were placed at the same height along a circular arc with a radius equal to the desired standoff distance. The sensors were mounted on a metal frame that was bolted to the concrete ground. A total of nine blast tests run at three standoff distances were conducted first to validate and finalize the calculated standoff distances based on the IOP measured from pencil probes. The current communication reports the results from frontal blast tests. Side and rear blasts were also performed but the results were not discussed due to inconsistent ICP sensor locations, scatter plots can be reviewed in appendix B.

### 3.1.3 Directional sensitivity test on ICP sensors

In this study, Kullite sensors (Kulite Semiconductor Products, Inc., XCL-072-100A) were used for capturing ICP. All the Kullite sensors were calibrated with PCB in the shock tube before field tests. (Figure 7) Peak values of each sensor were used to determine if it is functional. All the sensors which percentage error is bigger than 10% were excluded.

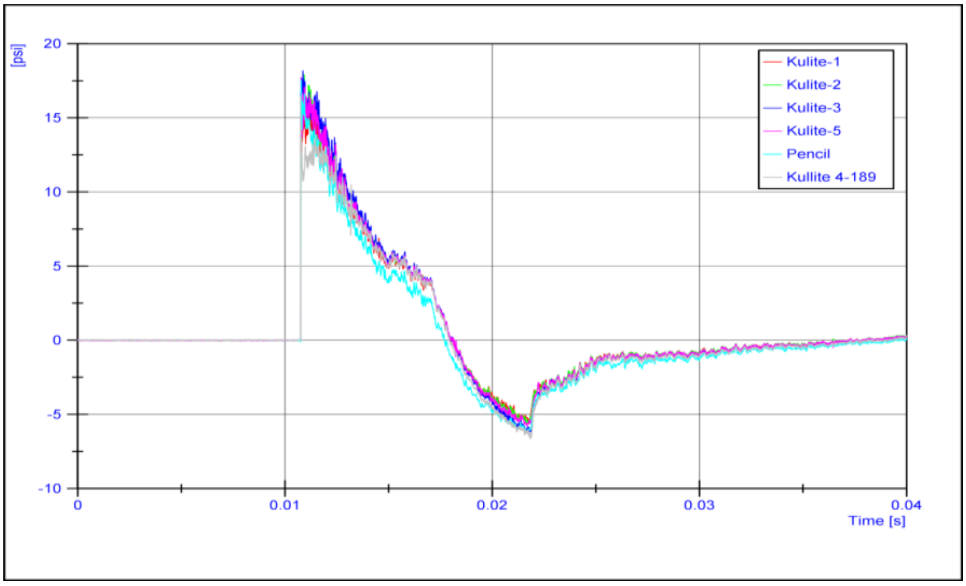

Figure 3-1: An example of calibration on kullite sensors. The newly calibrated pencil sensor was used as a reference.

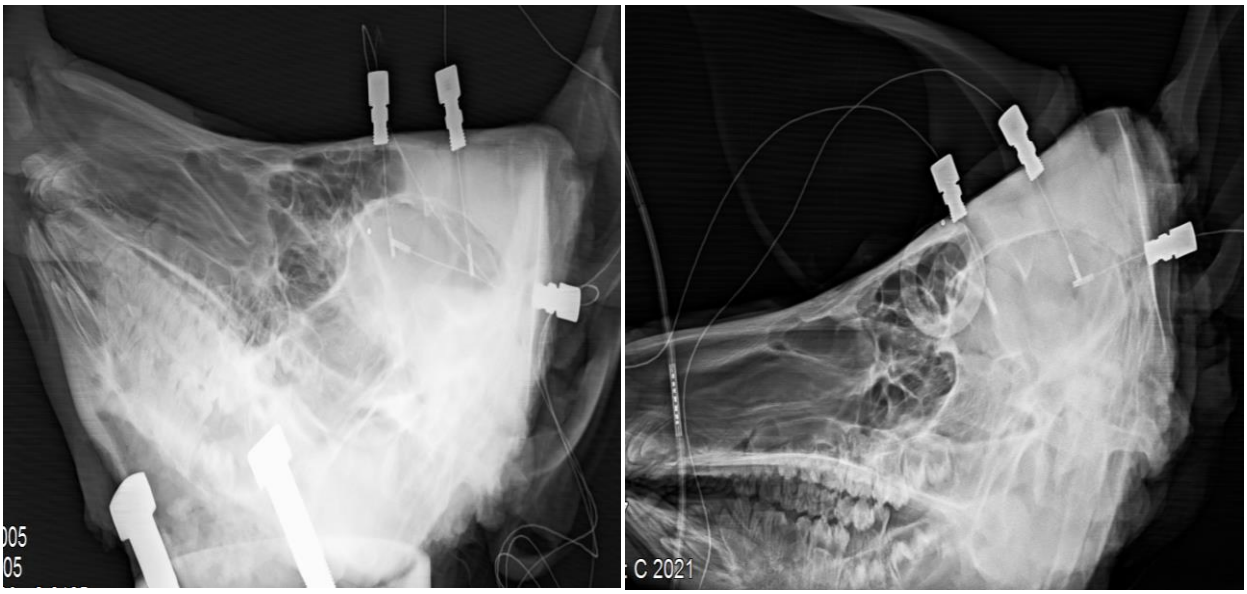

Figure 3-2: Left shows the sensors alignment in the first set-up. The frontal sensor, Occipital sensor in face-on and side-on direction; Right shows the sensor alignment in the second set-up: the Frontal sensor in faced-on and side-on direction and occipital sensor.

Then the pig' head was sealed and stabilized on a platform within the shock tube and performed blast tests. It was found that there was not much difference between ICPs facing different directions. (Figure 3-1).

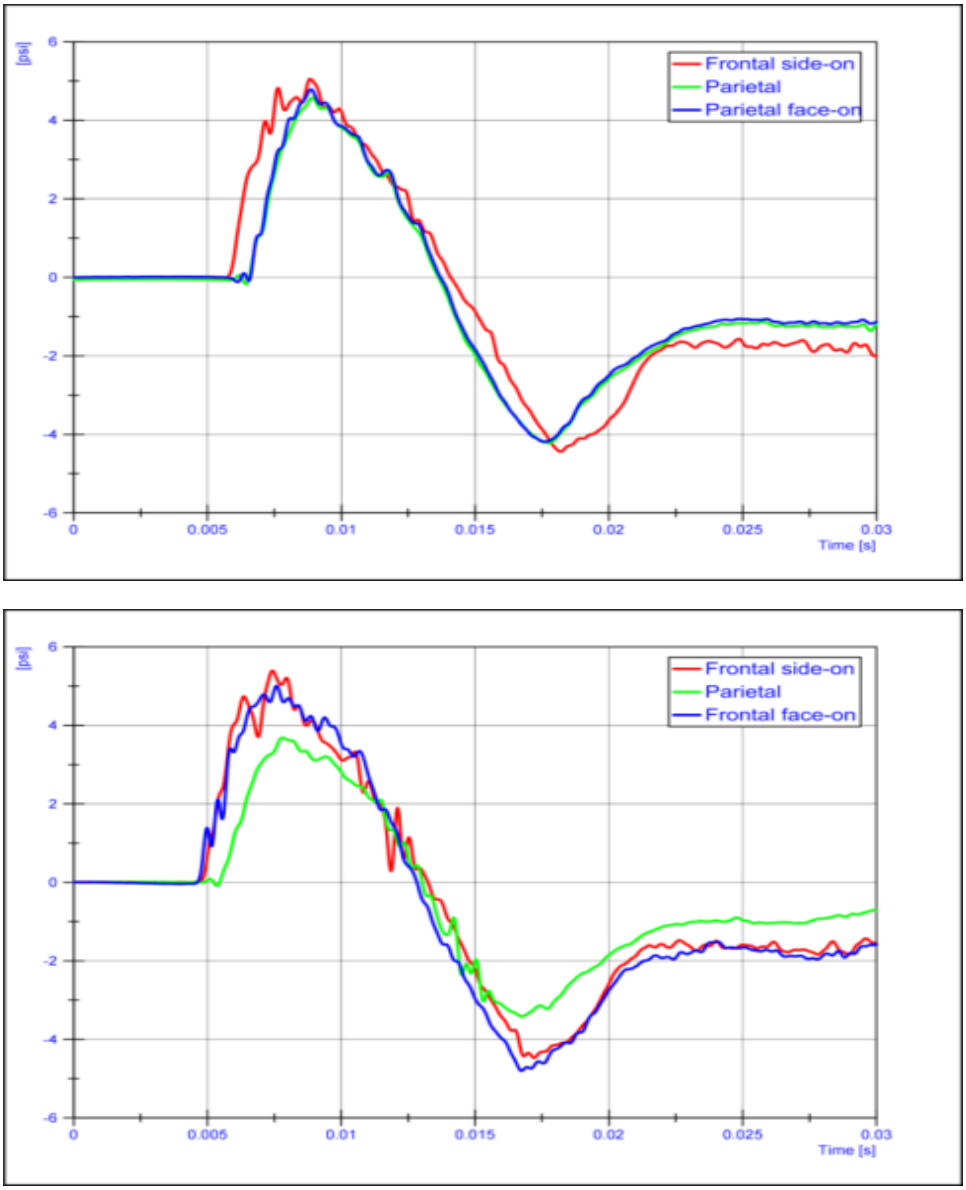


Figure 3-3: The top figure shows a representative figure of sensor readings at frontal and occipital face-on/side-on location. The bottom figure shows a representative figure of sensor readings at frontal face-on/side-on and occipital location.

### 3.1.4 Sensor instrumentation and data acquisition

Before installing the sensors, the scalp was opened from just in front of the nuchal crest to a point in front of the level of the eyes. The periosteum is scraped from the bone and any bleeding

is stopped with diathermy. ICP transducers (XCL-072-100A, Kulite, CA) were installed in the in the frontal, occipital, left and right temporal and parietal lobe and at the center of the brain.

ICP transducers (XCL-072-100A, Kulite, CA) were installed in the in the frontal, occipital, left and right temporal and parietal lobe and at the center of the brain. The vertical distance between the brain surface and the tip of frontal, parietal, temporal, and occipital ICP transducers was 5-7 mm. The depth of the center ICP transducer was 10-12 mm. The diameter of the pressure transducers was 1.9 mm. The three linear accelerometers (7264D-2KTZ-2-360, Meggitt's Endevco, CA) and the three angular rate sensors (ARS-50K-HG, DTS, CA) were fastened to a single aluminum block (ARS HG Triax block, DTS, CA) and installed on top of the skull to monitor the motion of the head. To ensure rigid attachment of the accelerometer block, a 4 × 4-cm of scalp was removed from the posterior of the head to the lambda. Its location is shown in Figure 2 which also shows the approximate locations of the six ICP transducers.

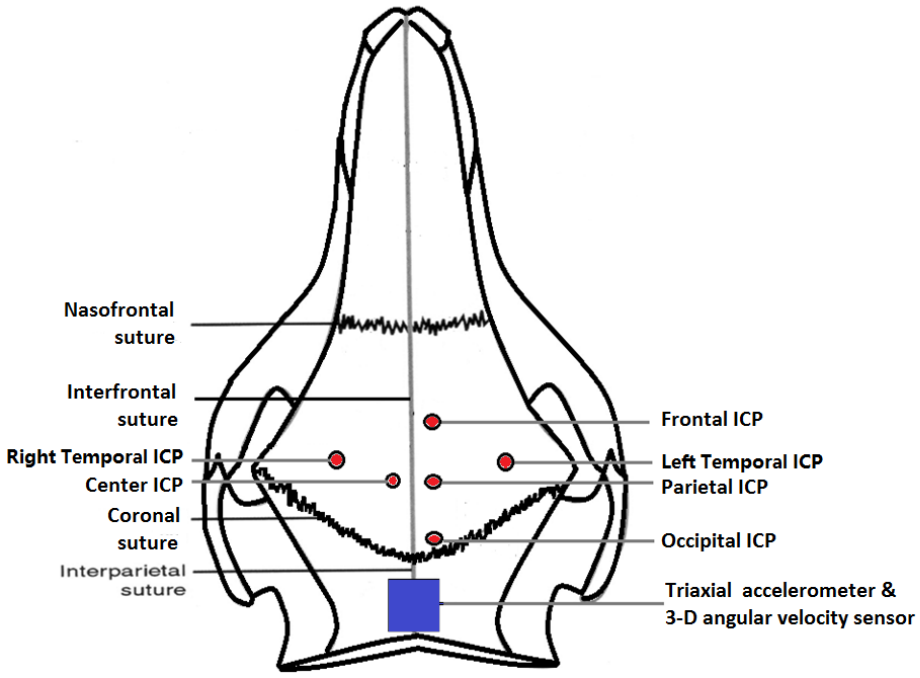


Figure 3-4: Top view of the location of ICP sensors relative to the skull of the swine.

The X-axis was defined as the axial direction of the blast, the Y-axis was defined as being perpendicular to the sagittal plane of swine's head, and the Z-axis was normal to the transverse surface of the swine's head at the location of the sensor block. The detailed sensor locations are presented in Table 3-1. After all the tests were done, the instrumented animal was euthanized at the blast site with an overdose of sodium pentobarbital (120 mg/kg, intraperitoneally). A parallel group of non-instrumented animals also underwent similar blast tests for histological and biomarker studies. Results of these studies are reported separately.

Table 3-1: Summary of the location of all sensors.

| Sensor | Location |
|---|---|
| Frontal ICP | 2.5 cm anterior to Bregma, 0.5 cm left of midline. |
| Parietal ICP | At the level of Bregma, 0.5 cm left of midline. |
| Center ICP | At the level of Bregma, 0.5 cm right of midline. |
| Left temporal ICP | 0.5 cm anterior to Bregma, 1.0 cm left of midline. |
| Right temporal ICP | 0.5 cm anterior to Bregma, 1.0 cm right of midline. |
| Occipital ICP | 1.5 cm posterior to Bregma, 0.5 cm left of midline. |
| Accelerometer block | 2.5 cm posterior to Bregma, on the midline. |

The IOP and the biomechanical responses of the head, including the ICP, head linear acceleration, and head angular velocity were acquired at a sampling rate of 1,000,000 Hz using the DeweSoft (SIRUS, Dewe Soft LLC.,OH) and DEWETRON data acquisition system (Dewe-3020, DEWETRON Inc. RI). Two high-speed digital camera systems (GX-8, HX-1, NAC Image, MN,) were set up to record high-resolution videos of the blast event. One of the cameras was focused on the head of the instrumented swine and ran at 20,000 frames/second (fps). The other camera provided an overall view of the blast wave propagation from the charge to the swine test subject and ran at 10,000 fps. Data acquisition of all the sensors and both cameras were synchronized for each test.


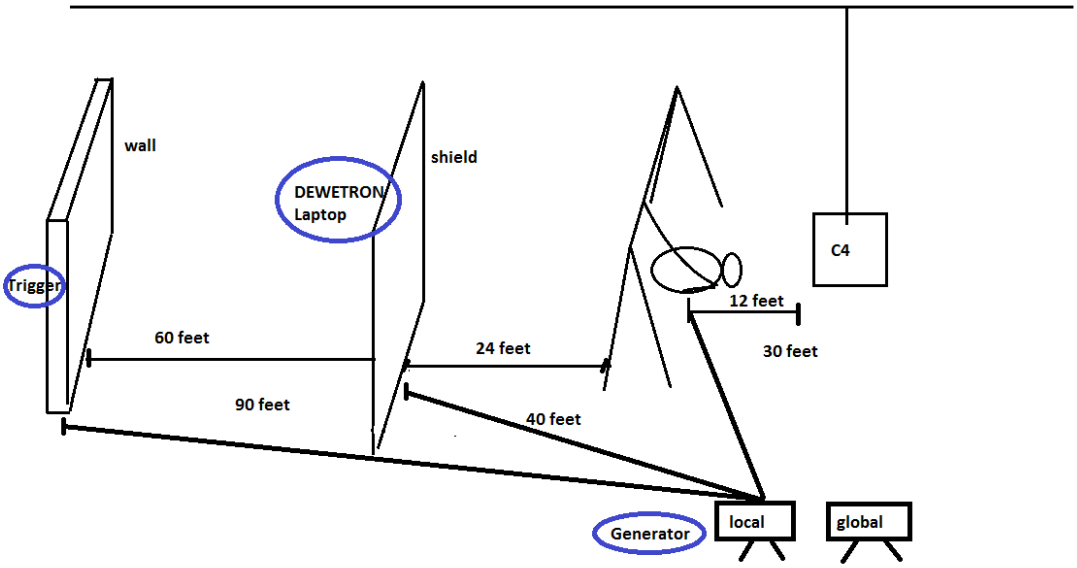


Figure 3-5: Experimental setup. Above is the photo of the blast site. Below is the Schematic diagram of the experimental set-up.

### 3.1.5 Data processing and analysis

IOP and ICP data were filtered with a 100 kHz and 10 kHz Butterworth low pass filter, respectively. Linear acceleration and angular velocity data were filtered with a 2 kHz Butterworth low pass filter. All post data processing and statistical analysis were performed using DIAdem 2012 software (National Instruments Corporation, Austin, TX) and IBM SPSS Statistics (Version

22.0. Armonk, NY). All data were grouped into three IOP levels according to the recorded IOP by the pencil probe located next to the head of the swine. The duration of the blast wave was defined as the time the IOP stayed above ambient pressure and, was determined using Diadem. IOP impulse was defined as the area of the positive phase of the IOP wave and was obtained through integration. Peak ICP values were determined for each blast for statistical analysis. Linear regression models were constructed to predict the relative relationship between ICP readings within groups. ICP Box plots were drawn to show the distribution of pressure within each group. Paired t-tests were performed between IOP and ICP at each location in the same blast level. One-way analysis of variance (ANOVA) tests were performed to compare the mean peak ICP readings between various locations at the same blast level and the peak ICP readings at the same location in different blast levels. Average Peak ICP readings for each test were correlated with their peak IOP values.

The peak resultant acceleration was calculated based on the data measured by the three accelerometers. Similarly, the resultant angular velocity was calculated from results acquired by the three angular rate sensors. Linear regression models were used to describe the relationship between the peak resultant acceleration, peak resultant angular velocity and the peak IOP. One-way ANOVA test of peak resultant acceleration was performed between low, medium, and high blast levels. No data at high blast level was collected due to sensor cable failure and signal anomalies. Independent t-tests were performed to compare the resultant angular velocities between the low and medium pressure levels.

## 3.2 RESULTS

### 3.2.1 Intracranial pressure response

The results of 19 frontal blasts were reported in this study, using five swine. Plots of a typical set of IOP and ICP curves are shown in Figure 3.

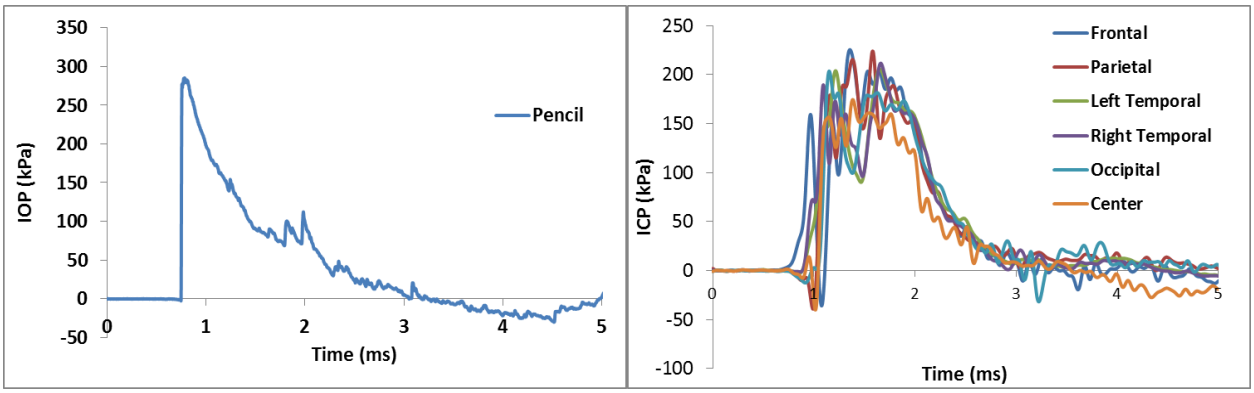


Figure 3-6: Pencil reading from a medium level blast (left) and the ICP results in the swine brain from the same blast. The positive phase duration of the IOP was 2.30 ms, and the impulse of the IOP was 207.7 Pa-s.

The peak IOP, duration, and IOP impulse of each test are summarized in Table 2. In our study, peak IOPs ranged from 143 to 461 kPa. The impulses ranged from 156 to 239 Pa-s. The test results were then divided into three pressure level groups based on the IOP results (Table 3-2). The average peak IOP values were 149, 279, and 409 kPa respectively, for the low, medium, and high blast levels tested. The average peak ICP at various locations of the brain were in the range of 79-144 kPa at the low blast level, 209-282 kPa at the medium blast level, and 312-415 kPa at the high blast level.

Table 3-2: Summary of IOPs in this study: peak values, duration of the first positive wave and the impulse of the first positive waveform. ** indicates test in which swine had already expired during testing.*

| Test ID | Peak IOP(kPa) | Duration (ms) | Impulse (Pa-s) |
|---|---|---|---|
| *1 | 150.3 | 2.8 | 170.3 |
| *2 | 142.7 | 2.9 | 155.7 |
| 3 | 150.3 | 2.9 | 158.3 |
| 4 | 148.2 | 2.9 | 160.3 |
| 5 | 152.4 | 3.1 | 161 |
| 6 | 218 | 2.1 | 193.9 |
| 7 | 253.4 | 2.2 | 195.7 |
| 8 | 255.2 | 2 | 194.9 |
| 9 | 324.2 | 2.3 | 194.1 |
| *10 | 285.5 | 2.3 | 207.7 |
| *11 | 284.1 | 2.1 | 198.1 |
| 12 | 285.4 | 2 | 196.4 |
| 13 | 325.4 | 2 | 204 |
| 14 | 366 | 1.6 | 205.4 |
| *15 | 441.3 | 1.7 | 225.2 |
| *16 | 413.7 | 1.6 | 229.6 |
| *17 | 460.6 | 1.7 | 239.2 |
| *18 | 341.3 | 2.4 | 228.8 |
| 19 | 432.3 | 2.4 | 222.9 |

Table 3-3: IOP peak values vs ICP peak values at low, medium, and high IOP levels

| Test | ICP peak values, mean±SE | | | | | | |
|---|---|---|---|---|---|---|---|
| | IOP | Frontal | Parietal | Left Temp | Right Temp | Occipital | Center |
| Low | 148.8±1.7 | 97.6±19.7 | 144.2±18.0 | 142.8±0.0 | 147.9±0.0 | 78.9±13.4 | 93.7±17.0 |
| Medium | 278.9±13.9 | 236.5±30.7 | 276.0±62.4 | 281.6±35.0 | 253.1±46.8 | 209.1±34.5 | 228.1±29.5 |
| High | 409.2±18.9 | 311.7±29.1 | 414.6±0.0 | 386.4±7.1 | 325.5±8.6 | 328.2±26.7 | 327.2±17.0 |

Scatter plots show that peak ICPs increased with peak IOP at every instrumented location (Figure 3-7).

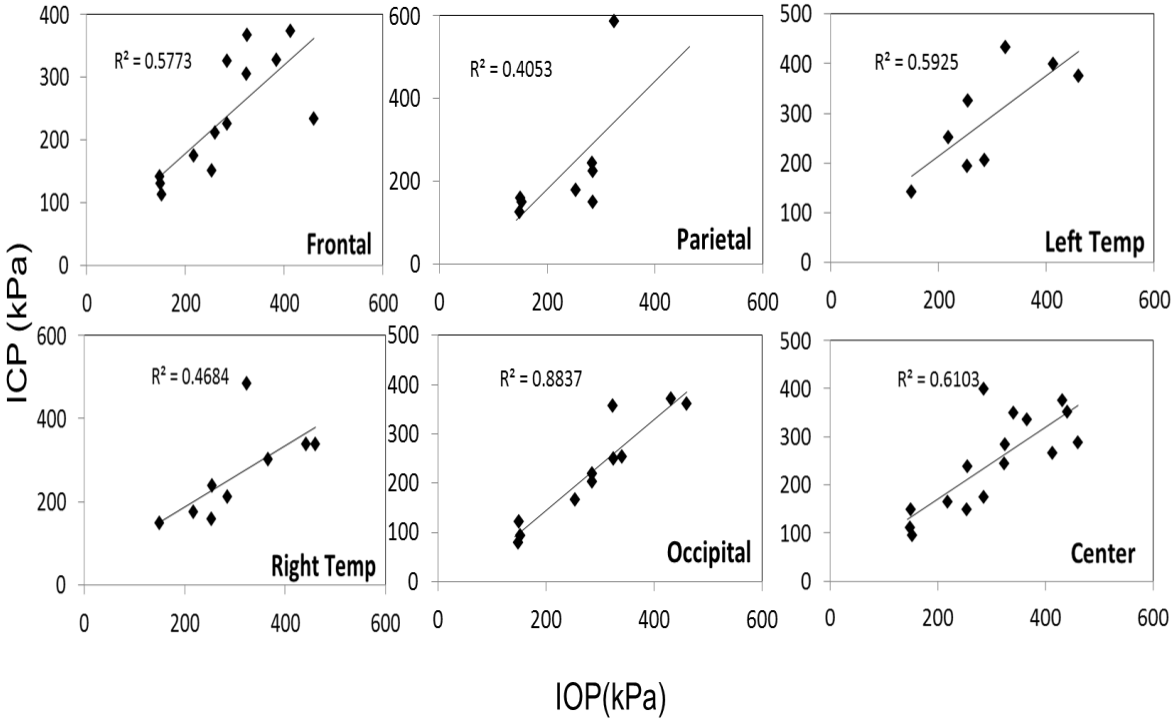


Figure 3-7: Scatter plots of ICP vs IOP at different locations of the brain. The x axis is the IOP and the y axis is the ICP, both in units of kPa. A linear regression model and $R^2$ values are shown in each plot.

More specifically, ICP peak values correlated well with peak IOP in all the three blast pressure levels using linear regression models. The overall ICP responses were close or lower than its IOP at each blast level. At the low blast level, peak ICP responses of occipital and center regions were significantly lower than the peak IOPs (paired *t-test, $p < 0.05$*), with no significant differences in other regions of the brain (paired *t-test*, $p > 0.05$). At the medium blast level, no significant difference was found between peak ICP responses and peak IOP (paired *t-test, $p > 0.05$*). At the high blast level, peak ICPs were not significantly different from the peak IOPs (paired *t-test, $p > 0.05$*), except that in the center regions where the peak ICPs were significantly lower compared with the peak IOPs (paired *t-test, $p < 0.05$*) (Figure 5).

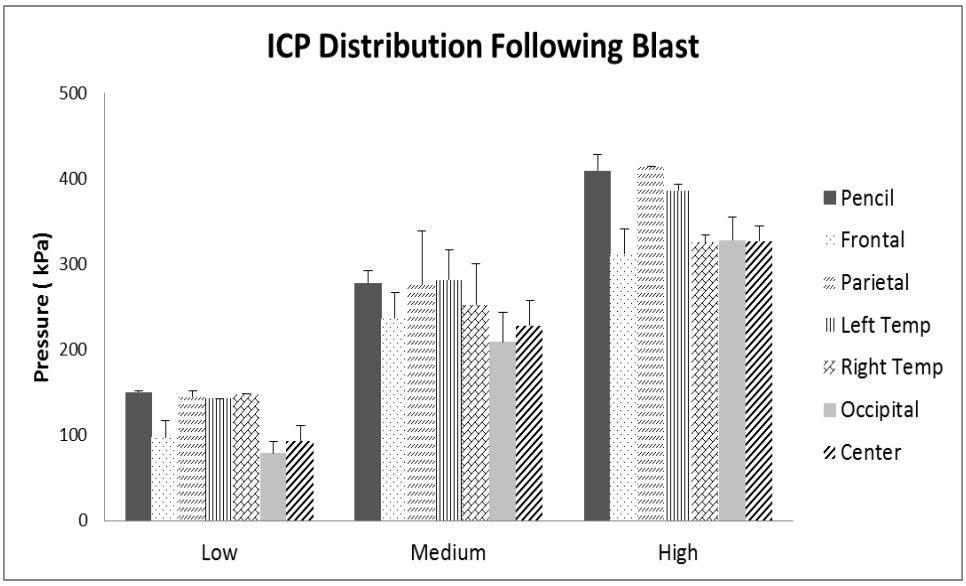


Figure 3-8: Peak ICP readings for different levels of blast. Peak ICPs in different regions of the brain within each blast level group were not statistically different from each other.

There was no statistically significance difference in peak ICPs between various locations at the low, medium and high levels (ANOVA, *$p > 0.05$*). The frontal ICP at the low blast level was significantly lower than that at the medium and the high blast level (ANOVA, PostHoc LSD,

$p < 0.05$). However, there was no significant difference of the peak frontal ICPs between the medium and the high blast level (ANOVA, PostHoc LSD, $p > 0.05$). Similarly, the occipital ICP at low blast level was lower than that at the medium and the high blast level (ANOVA, PostHoc LSD, $p < 0.05$). No significant difference was found with the occipital ICPs between the medium and high blast level (ANOVA, PostHoc LSD, $p > 0.05$). The peak center ICP values at the medium and the high blast level were both significantly higher than that at the low blast level (ANOVA, PostHoc LSD, $p < 0.05$). Statistical analysis also showed significant differences of the peak ICP between the medium and the high blast levels (ANOVA, PostHoc LSD, $p < 0.05$) (Figure 6).

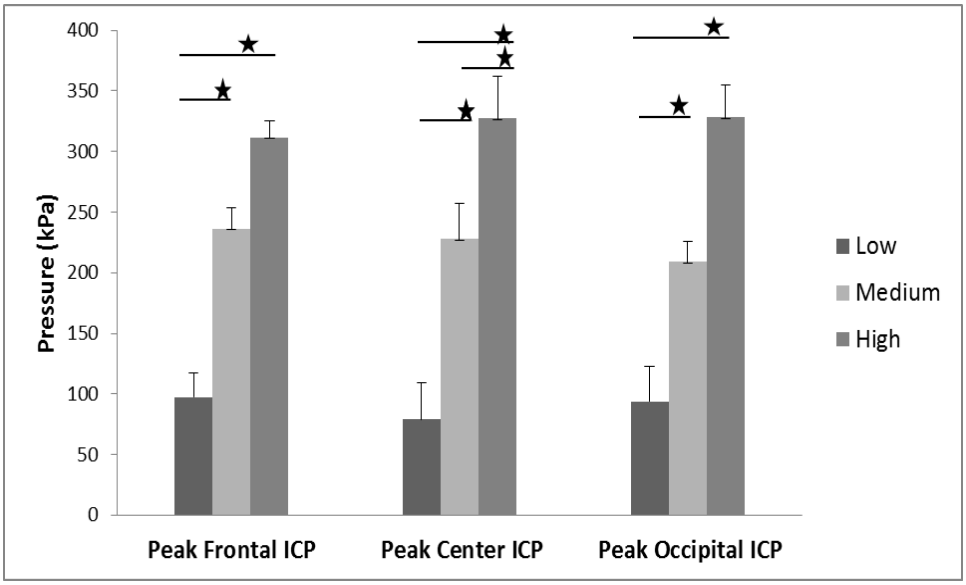


Figure 3-9: ICP peak values in the frontal, central and occipital regions of the brain showed a significant increase with increasing blast levels. Student's t-tests indicated a significant difference between blast levels. (* $p<0.05$)

Average peak ICP peak values in each test correlated well with peak IOPs (Figure 3-11).

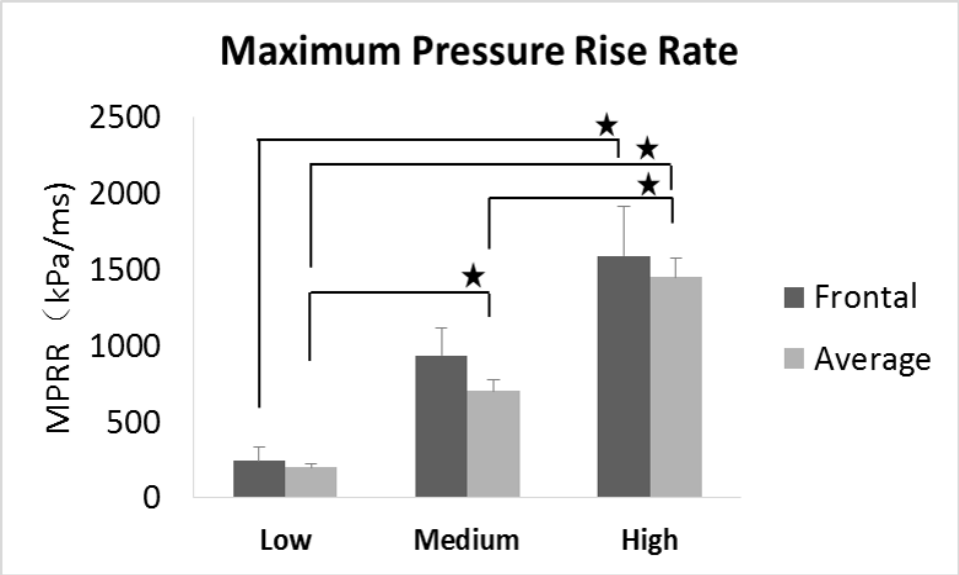


Figure 3-10: Maximum pressure rise rate values show significant increase with IOP levels at frontal and average reading of ICPs and different locations.

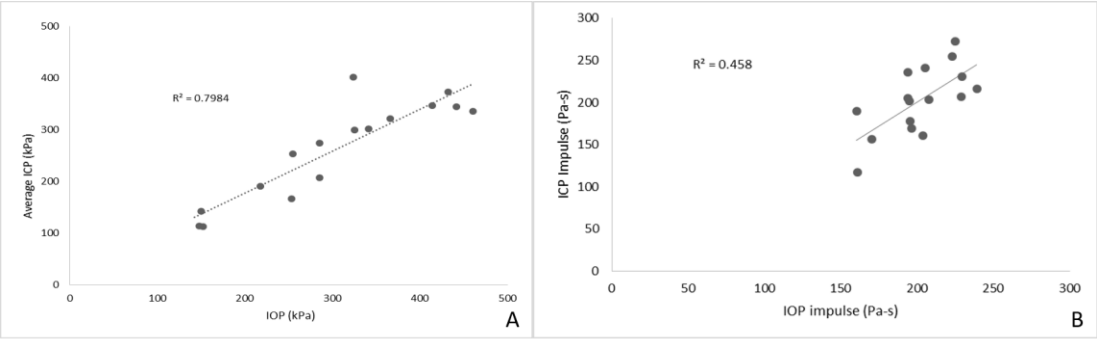


Figure 3-11: Sample time-history plots of the acceleration and angular rate measured on the swine head with instrumentation mounted to the skull. The left plot shows linear acceleration (g) in the x, y and z directions. The right plot shows angular velocity (rad/s)

3.2.2 Head kinematics

In this study, we characterized the head motion with its linear acceleration and angular velocity. Typical time histories of the three linear accelerometers and the three angular rate sensors are shown in Figure 3-12A and 3-12B respectively.

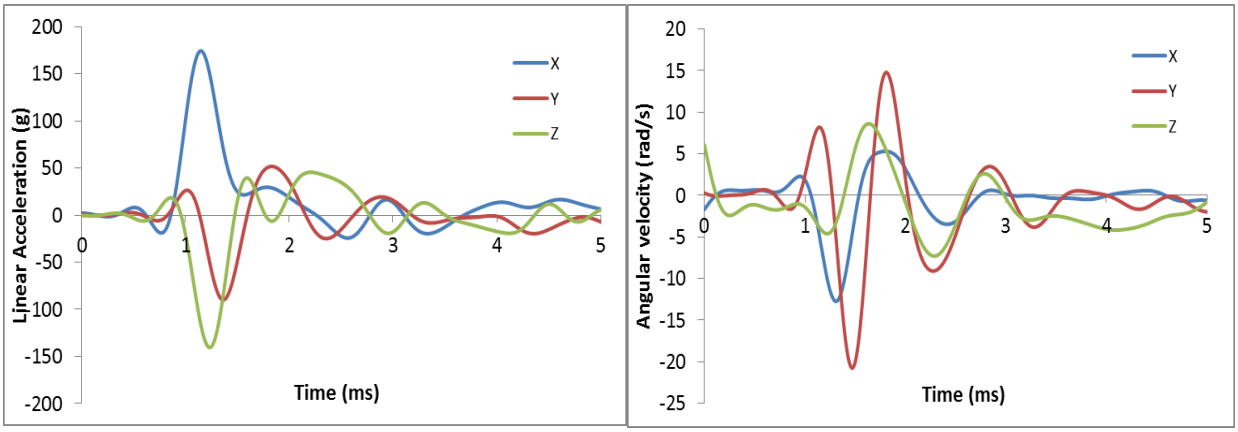


Figure 3-12: Sample time-history plots of the acceleration and angular rate measured on the swine head with instrumentation mounted to the skull. The left plot shows linear acceleration (g) in the x, y and z directions. The right plot shows angular velocity (rad/s) in the x, y and z directions.

The resultant linear accelerations and the resultant angular velocities increased linearly with IOP (Figure 3-13A and B). Additionally, correlations between ICP peak values and head motions were depicted in Figure 3-14 A and B.

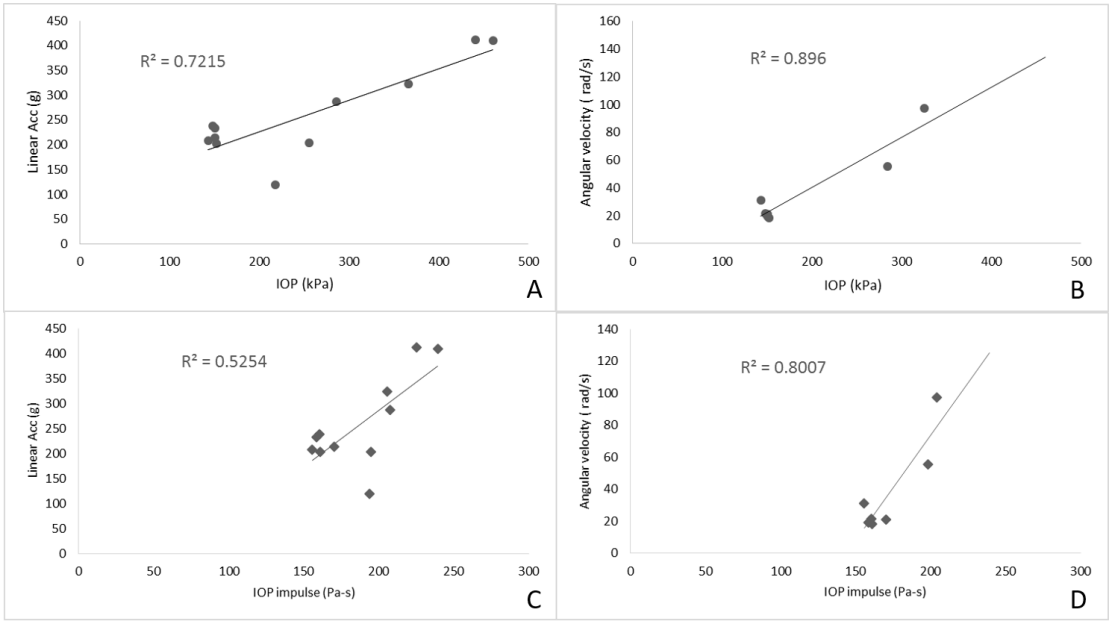


Figure 3-13: Scatter plots of the motion of the head, showing the relationship between the peak IOP (abscissa) and the resultant linear acceleration (ordinate, left graph), or the resultant angular velocity (ordinate, right graph). These variables correlated well with the peak IOP in linear regression models.

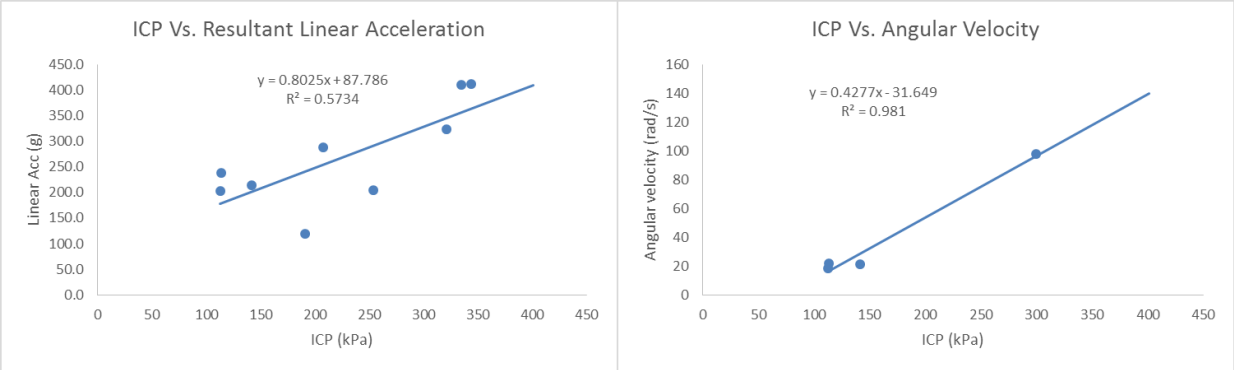


Figure 3-14: Linear relationship were shown between peak ICP and resultant linear acceleration (A), and with resultant angular velocity (B).

The resultant accelerations at high blast levels were significantly higher than that at low and medium blast levels (ANOVA, PostHoc LSD, $p < 0.05$), but there was no statistical significance between the low and the medium blast levels (ANOVA, PostHoc LSD, $p > 0.05$). The resultant angular velocity at the medium blast level was significantly higher than that at the low blast level (independent *t-test*, $p < 0.05$). The durations of the linear acceleration were typically less than 3 ms, indicating that there was little translational movement of the head during primary blast.

3.2.3 Change in sensor array to streamline instrumented swine testing procedure

The original test plan was to instrument the brain of each swine with six miniature ICP sensors (Figure 3-16). Then we would expose the swine to 9 blasts (three forward, three lateral and three backward) on a single test date. Due to the extensive surgery and repeated blasts on the swine head, the survival rate of the anesthetized instrumented animals was very low. Among the first ten tests performed on instrumented pigs, only the first two tests were performed on live pigs; the remaining tests were performed after the pigs had expired. Also, time was very limited to prepare and perform nine tests in one day. Thus, a revised sensor array for the remainder of the

instrumented swine testing was used. In this new instrumentation plan, we used four ICP sensors in each swine (Figure 3-5, 3-16). Instead of exposing each pig to blasts in all three directions, we only tested in the front/rear or side direction. This method resulted in less brain damage to the swine's brain from pressure transducer placement, increased survival rate and allow for the higher probability of completion of the proposed set of blasts in one day. The detailed plan was approved by the COR.

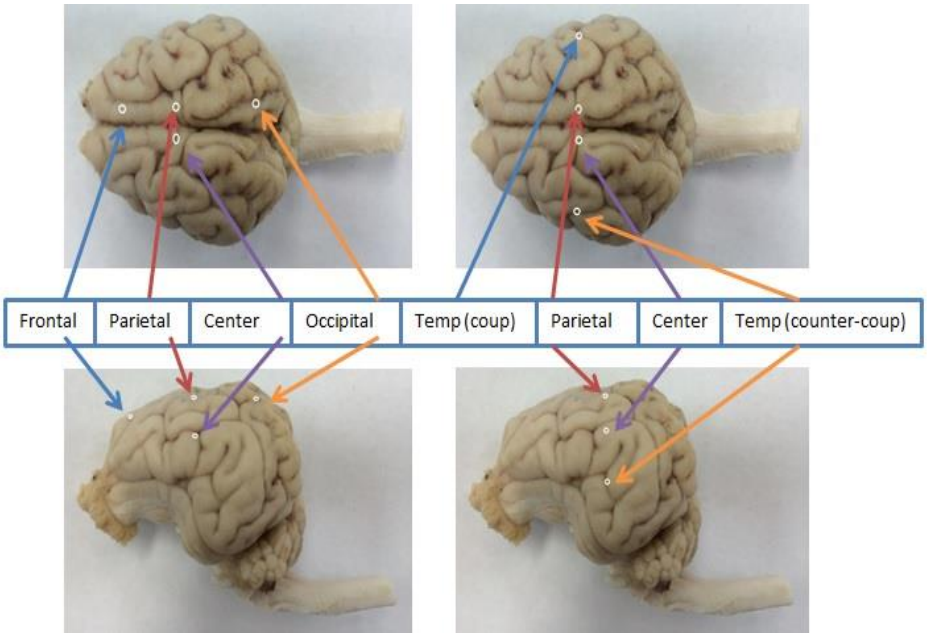


Figure 3-15: Revised locations of ICP sensors in 2014. Total numbers of ICP sensors were reduced from 6 to 4. Two types of set-up were utilized in front-back and side blasts.

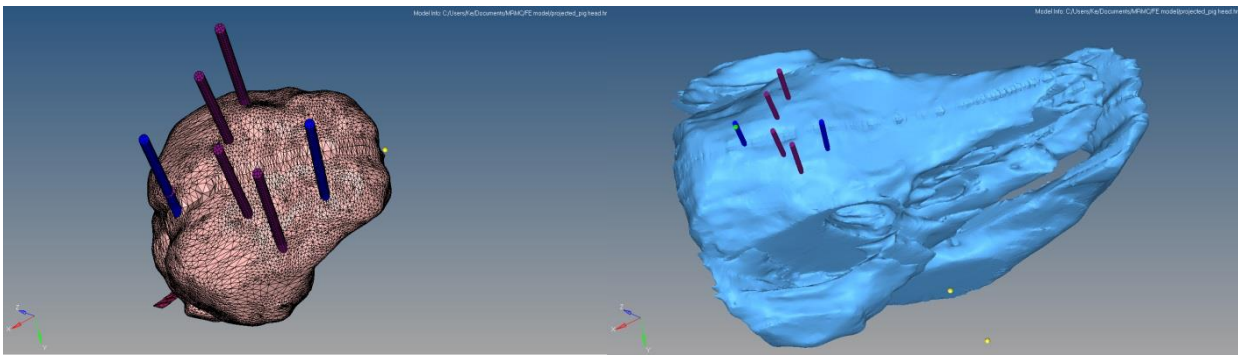

Figure 3-16: Standard ICP locations on the brain and skull in a 3D view.

3.2.4 Location of ICP sensors

The locations of the ICP sensors were set based on pre-designed relative distances to the landmarks on the skull: bregma and lambda (Figure 3-5). The standard locations of these sensors are shown below (Figure 3-17). The locations of ICP sensors were verified with 3D model.

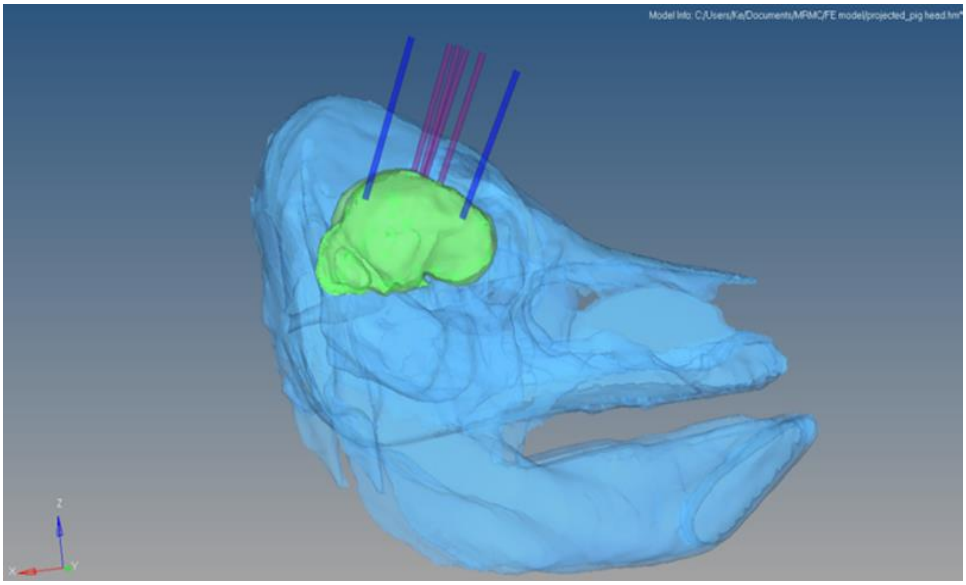

Figure 3-17: Demonstration of ICP sensors in 3D model.

**3.3 DISCUSSION**

Animals are commonly used to study traumatic brain injury (TBI).(Cernak, 2014; Risling and Davidsson, 2012) In this study, we chose Yucatan pigs as the body mass and skull thickness

are closer to those of the human. Also, with a larger body size, biological tolerance level of air-filled organs to blast is believed to be higher.

This study exposed live swine subjects to free-field blast loading at various pressures and durations by changing the standoff distance between the charge and the swine. Of the five swine tested, two expired just before the blast testing, and one died during the tests. This resulted in 8 of the 19 blasts being performed on expired animals. However, the ICP responses showed little difference between expired animals and live animals. The potential causes of death could be related to complications from anesthesia and surgical procedure to insert ICP sensors.

Based on our knowledge of blast physics, the blast wave produces highly variable pressures both spatially and temporally (Ngo et al., 2007) To fulfill this goal of defining mechanical response of the brain to blast, we analyzed the ICP in different regions of the brain at various blast IOP levels. All previous studies have addressed the mechanical responses of the brain to blast with post-mortem human subjects (PMHS),(Bir, 2011) rats,(Chavko et al., 2007; Goldstein et al., 2012; Gullotti et al., 2014; Huber et al., 2013; Leonardi et al., 2011) and swine (Bauman et al., 2009; Saljo et al., 2008; Shridharani et al., 2012; Zhu et al., 2013) models using compressed-gas shock tubes in a laboratory environment or enclosed space. Although some of these models provided crucial information on the correlation between IOP levels and injury responses, challenges with shock tube tests still exist, including animal positioning, orientation, and interpretation of the effect of the relatively longer duration of the blast.(Needham et al., 2015) One previous animal model placed the animal head right outside of shock tube.(Shridharani et al., 2012)It brought dramatic

changes to the IOP characteristics including the formation of a strong vortex flow and elevated dynamic blast pressure and impulse, which deviated significantly from the free-field blast scenario. Data from rat blast models tested in shock tubes recorded positive phase durations in the range of 4-18 ms,(Chavko et al., 2007; Goldstein et al., 2012; Huber et al., 2013; Leonardi et al., 2011) which would render the equivalent human duration much longer than that of a free field blast. Hence, shock tube test results need to be carefully investigated and compared with free-field explosive detonations. In this study, all experiments were performed in an open field blast environment. To minimize multiple waveforms from ground reflections, we placed the animal below the triple point and exposed it to the Mach stem.(Bass et al., 2012) The IOPs were typical free-field Friedlander blast waves in the Mach stem region based on our analysis of the IOP data.

This study provided detailed ICP response in the swine brain subjected to free-field blasts. Historically, some animal tests have been designed and carried out in an attempt to investigate the mechanism of shock interaction with the brain, but only a few animal studies recorded direct pressure within the brain tissue during exposure to blast.(Chavko et al., 2007; Leonardi et al., 2011; Shridharani et al., 2012; Zhu et al., 2013) In our study, the results have demonstrated that ICP followed a trend of increasing magnitude with increased blast severity. However, the shape of ICP curves were different than IOP, this could be explained by the combined results of shock waves and reflection waves from the complex structures of the swine brain and the different materials within the skull.

The relationship between peak ICP and IOP has been determined in several animal blast studies. We showed that, at different locations in the brain, peak ICP values were close to or lower than the IOP. One similar observation was made by another group investigating the mechanical response of the swine brain subjected to left-sided blasts in a shock tube.(Shridharani et al., 2012)The peak IOPs ranged from 110 to 740 kPa with scaled durations from 1.3 to 6.9 ms. ICPs ranged from 80 to 390 kPa and were lower than the IOPs and notably lower than the reflected pressures of 300-2830 kPa. Another swine study by Bauman (Bauman et al., 2009) was performed in both a shock tube and in a simulated building with frontal blasts.(Bauman et al., 2009) The recorded IOP data showed that the test animal was exposed to multiple shock waveforms. Fiber-optic pressure transducers were used to record pressure from within the forebrain, thalamus, and hindbrain of the swine without specifying details related to the locations of transducers. The ICP results showed that for IOP levels of 100-250 kPa, the peak ICP values at the three locations were lower than the IOPs.(Zhu et al., 2013)

In addition to the use of swine, smaller animals like rats have also been used. In a rat study, an optic fiber pressure sensor was used to record shock tube generated ICPs. The animals were exposed to a low level blasts of about 40 kPa and the recorded peak ICPs were close to but lower than the IOP in both the frontal and lateral regions of the brain.(Chavko et al., 2007) However, this study only used one ICP sensor in each test, and the results of the study were not statistically analyzed. There were also some discrepancies between findings in the peak ICP values compared to the peak IOP values in rat models. Leonardi et al. reported that peak ICPs in rats were larger

than the peak IOPs and suggested that skull flexure due to an immature skull suture could be the source of the pressure increase.(Leonardi et al., 2011)One recent study with cadaver rats also showed a higher peak ICP compared to the peak IOP values at different IOP levels.(Skotak et al., 2013)However, the location of the ICP sensor in the brain was not described, and the torso was not properly shielded from the shockwave. Also, the impulse produced in this study was in the range of 165- 497 Pa-s, larger than what we used in this study (160-240 Pa-s).

Blast studies have also been performed on PMHS. In one PMHS study, using a shock tube, four fiber optic sensors were implanted in the right frontal cortex, right lateral ventricle, right parietal lobe and right occipital lobe with the respective depths of the tip of the sensors from the outer surface of the skull being 30, 30, 65, and 30 mm.(Bir, 2011) At each IOP level, the peak ICP values in the frontal lobe were higher than its peak IOP value. This observation was not seen at other locations of the brain. Also, most of the computer models indicated higher peak ICP compared with IOP readings.(Chafi et al., 2010; Zhang et al., 2013), (Moore et al., 2009; Taylor and Ford, 2009; Zhu et al., 2010; Zhu et al., 2013)

The discrepancy between measured and model predicted ICP and IOP readings could be due to several causes. One would be the highly nonlinear relationship between ICP at various locations and the IOP wave.(Zhu et al., 2013) Due to the impedance mismatch between the skull and the brain, ICP peak values tend to be higher at the boundaries and lower in the central region.(Meyers, 1994) With respect to the location of transducers, computer models can precisely pinpoint the coup and countercoup regions of the brain. The location of the ICP sensors in animal

experiments was limited by surgical techniques. The depths of sensors below the skull in all experimental tests were different or not described in detail. Therefore, the ICP readings vary in the published literature as described above. Another reason for ICP differences seen in rats and pig is possibly due to the morphological differences between species. Compared to rats, pigs have a much thicker skull with a complex diploe layer that is full of voids (Figure 3-17). Computer models, on the other hand, may have oversimplified the skull and yielded predictions that did not match experimental data.

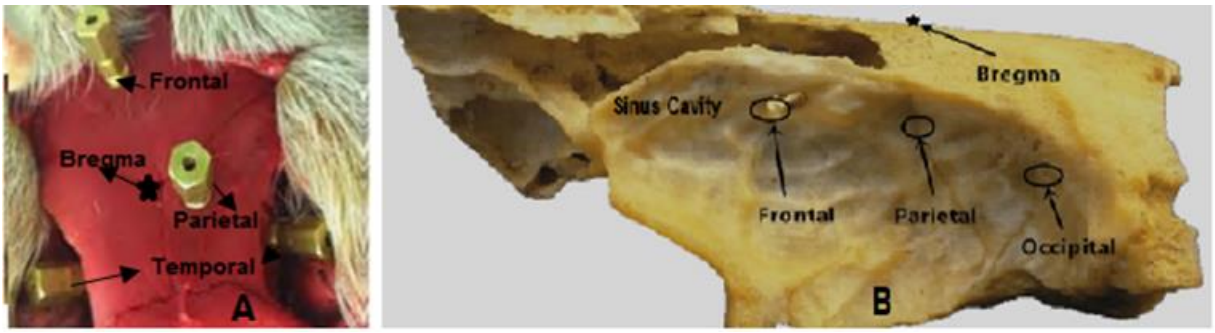


Figure 3-18: (A) A snapshot showing the locations of installed mounts for pressure transducer installation and (B) A sectional view of a skull which shows the frontal sinus cavity along with corresponding frontal sensor location.

Both linear and angular motions of the head were acquired in our tests. The arrival of the ICP wave is almost simultaneous with head motion. Thus the motion is due to the primary blast wave (Figure 3-18).

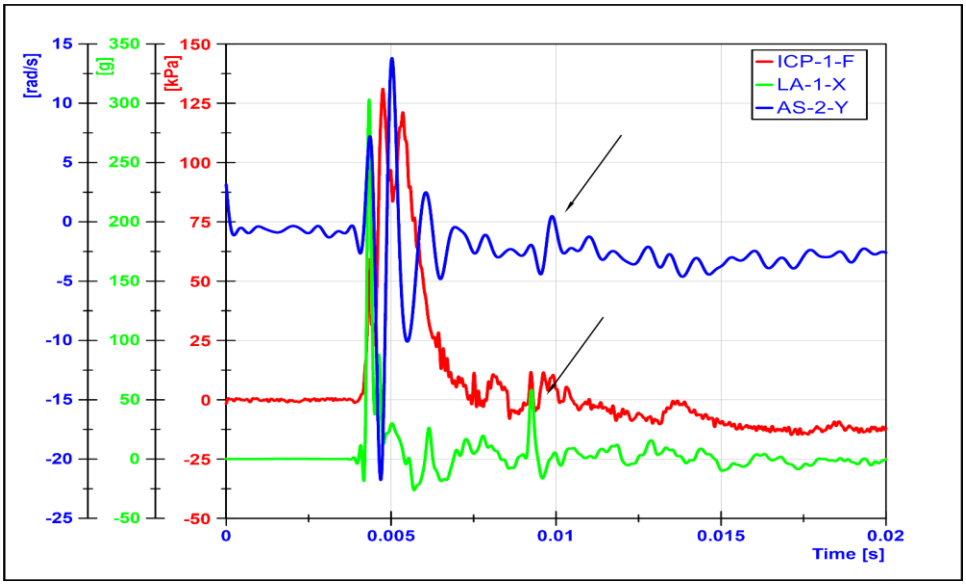


Figure 3-19: The relationship between ICP and head motion (resultant linear head acceleration and angular velocity) demonstrated that primary blast imparted a severe acceleration to the head, albeit the duration was very short.

However, the duration of the motion is relatively short (1-2 ms), which resulted in the maximum head displacement around 2 ms by double integrating linear acceleration over time. Similar observations were made by Shridharani et al. also using swine subjects.(Shridharani et al., 2012) They found strong correlations ($R^2 = 0.9$) between peak resultant acceleration and peak IOP in the range of 110 to 740 kPa in a linear model. Their positive phase duration was around 3 ms, and the maximum head displacement was 7.5 mm. Thus, the observed acceleration in these two studies was likely due to the primary shock wave. Well after the passage of the shock wave, we observed inertial global head movement but the head acceleration due to the blast wind or tertiary blast was not significant compared to the initial acceleration due to the primary shock wave.

We also collected ICP and accelerometer data from side and rear blasts. Due to sample size and the modifications of the sensor locations, we don't have a conclusive statement here. The results of ICP distribution in different oriental blasts are shown in Appendix C.

## 3.4 CONCLUSIONS

The data reported here were acquired from live, anesthetized swine exposed to primary blast waves. This is the first large animal model exposed to free-field blasts in which detailed internal pressure measurements were made at various locations. Head motion due to primary blast waves was also measured. The mechanical responses of swine need to be scaled to the human head to determine human response. However, due to the morphological differences between the two species, scaling laws can be difficult to develop. Also, the limited sample size should also be taken into consideration. Due to time limitations to complete nine blast tests on a single animal in 8 hours and failure of the data acquisition system on one occasion, data were available from 19 tests on 5 animals. Additional testing of more animals should improve the statistical significance of the results.

In summary, the results of this study provided a set of detailed biomechanical response data of swine skull and brain during exposure to primary blast waves, with the peak IOPs ranging from 143 to 461 kPa, and the impulses ranging from 156 to 239 Pa-s. The overall ICP responses were close or lower than its IOP at each blast level. More specifically, peak ICP values at the frontal, parietal, and temporal were statistically the same as its IOP values. Peak ICP values at the frontal, central, and occipital regions were significantly elevated at the medium and high blast levels

compared with the low blast levels. Furthermore, only at central location, was the ICP significantly different between the medium and high pressures tests. Both the linear acceleration and the angular velocity increased with blast levels. Although the head acceleration was high, its duration was less than 2 ms. It is unlikely that the brain would be able to respond to this type of acceleration input. The experimental data can be used to validate computer models.

# CHAPTER 4. NEUROPATHOLOGICAL FINDINGS ON SWINE BRAIN SUBJECTS TO PRIMARY OPEN-FIELD BLASTS

## 4.1 INTRODUCTION

The neuropathology pathways of TBI results from the explosive blast is not as yet fully understood. During the global war of terror, bTBI resulting from exposure to an explosive blast is associated with significant neurobehavioral outcomes. The consequences range from subtle mild cognitive impairment, affecting the ability of a person to perform under demanding conditions, to severe disruption of brain function as serious as coma. These effects can be temporary or chronic(Ling and Ecklund, 2011). Diffusion tensor imaging (DTI) reveals that dose-dependent diffuse axonal injury (DAI) that is different from concussive impact DAI. Opposed to blunt impact TBI, which cerebral edema develops several hours or even days after the trauma event, the brain of bTBI grows much faster, on the order of an hour or so (Armonda et al., 2006).

Currently, due to the complexity nature of bTBI, little is known about the real neuropathological consequences of primary blast wave to the human brain. Edema, intracranial hemorrhage, and vasospasm are the most prominent pathophysiologic characteristics of bTBI(Bauman et al., 2009). In clinical study, Gill J et al recently published data of acute peripheral cytokine levels collected from soldiers who went through singular blast wave in the range of 41-83 kPa. Significant elevated IL6 and TNFα levels were observed after the blast, levels were then rebounded back to baseline level(Gill et al., 2017).

The best pathway to characterize the pathological events and identify blast-specific biomarkers is through animal models *in vivo* and *in vitro*. Even though the biology of animals is different than human in many aspects, there are tremendous advantages of animal models on studying the development of pathology of bTBI. Some researchers have used *in vitro* models looked directly into cellular and molecular cascade of events in primary bTBI without confounding *in vivo* factors. The goal is to differentiate the primary and secondary injury events that both possibly play role in the neuronal degeneration and death. Miller et al. utilized organotypic hippocampal slice cultures exposed to low and high blast overpressures. Their histological evaluation shows neuronal death and activation of astrocytes in both blast levels. (Miller et al., 2015) A similar study was carried out by Effgen et al. In this study they found that the hippocampal slice culture exhibits cell death when exposed to a $530 \pm 17.7$-kPa peak overpressure with a $1.026 \pm 0.017$-ms duration and $190 \pm 10.7$ kPa-ms impulse in-air.(Effgen et al., 2012) The research conducted by Ravin et al. put their focus on the impact of shear stresses on brain cells during blast. (Ravin et al., 2012) The increased Calcium activity suggested that shear forces are likely involved in the primary bTBI.

There were some studies utilizing animals to evaluate the functional deficits of CNS from blast exposure. Connell et al. made direct observation of the blast wave impact and the deformation of nervous tissue in response to blast nozzle produced overpressure loading in an ex-vivo model. Quantification results at tissue level were correlated with blast conditions to illuminate the mechanism of injury. It was found that direct exposure to the blast wave compressed the nervous

tissue at high strain rate and led to significant functional deficits(Connell et al., 2011). De Lanerolle et al. used a Yorkshire swine subjected to blast shock tube and evaluated the histological changes afterward. They observed increased astrocyte activation and axonal injury detected with β-amyloid precursor (βAPP) protein immunohistochemistry [14]. Similarly, a study used primate animal model also reported Increased apoptosis appeared to involve astrocytes and oligodendrocytes in the animals following blast exposure (Lu et al., 2012). In another example, hemorrhage and contusional brain injury was observed at high but not low blast over- pressures in a rat model, pointing toward a pressure dependency of blast-induced brain injury (Kato et al., 2007). The lysis of erythrocytes will lead to the generation of oxidative stress via the release of redox-active iron, which participates in reactions that generate ROS. This consequently triggers events like apoptosis and inflammation, further aggravating the injury (Elsayed et al., 1997). A recent study compared postmortem brains from veterans with blast exposure and athletes with histories of concussive injuries and normal control brain (Goldstein et al., 2012). It was found CTE-like tau neuropathology was shown in both the blast exposed the brain and the repetitive concussion brain of athletes. The researchers also performed single controlled blast exposure on mice and revealed similar histological results. However, the researchers did not present additional evidence that would show whether this neuropathology was principally caused by blast exposure alone or by blunt brain trauma caused by blunt trauma to the head.

Another similar study with mice also reported elevation of multiple phosphor- and cleaved-tau species in neurons, as well as elevating manganese superoxide dismutase (MnSOD or $SOD^2$)

levels, a cellular response to oxidative stress, after single mild level of blast overpressure (108.9 kPa peak pressure and 5.87 ms positive phase duration) produced by shock tube (Huber et al., 2013).

A mouse model subjected to low-level free-field blast was developed to identify pathophysiological processes. Besides functional deficits, immunohistochemistry revealed up-regulation of mitochondrial superoxide dismutase two expressions at 72 h post-exposure in the group exposed to a 5.5 psi wave (Rubovitch et al., 2011).

To sum up, neuronal injury studies have shown varies consequences related to primary bTBI. Although these effects on neurons and glial cells were observed following the blast exposure, it is still unclear whether they are formed directly by the blast overpressure or through indirect mechanisms(Miller et al., 2015). Similarly, due to the complex nature of bTBI, no single bTBI-specific biomarker has yet been identified. A combination of immunohistological data with different markers provided in the acute phase will help elucidate the potential mechanism. To clarify the acute impact of primary bTBI on neuronal loss, we did a detailed histological examination with 11 types of immunohistological stains and biomarkers. Here, we reported results on neuronal degeneration and apoptosis of brain cells with cleaved Casepase-3 and Fluoro-jade C stain at 72 hours post blasts.

Table 4-1: Immunohistological evaluations on bTBI animal models.

| Blast type | Immunohistology | Time point | Purpose | findings | Author |
|---|---|---|---|---|---|
| blast tube | neuron specific enolase (NSE) | 0h, 2h,4h,6h,8h,10hr,12h | neuraonal degeneration | significantly increased concentrations of both markers | Saljo et al.(Saljo et al., 2003) |
| | S-100 | | astrocyte | | |
| High speed bullet | myelin basic protein (MBP) | 0h, 2h,4h,6h,8h | neuraonal degeneration | positive finding in hypothalamus and hippocampus | Wang Q et al(Wang et al., 2004) |
| | Evans blue dye | 24h | reative gliosis | levels are injury severity dependent | Wang H et al.(Wang et al., 2016) |
| | Silver | 7 days | neuraonal degeneration | cerebral cortex most prominent | |
| | Fluoro-Jade B | 24 h | | | |
| blast tube | hematoxylin and eosin (H&E) | 72h | | | Nihal C et al(de Lanerolle et al., 2011b). |
| | Fluoro-Jade B | | | | |
| | GFAP | | astrocytes | | |
| | Dako | | | | |
| | b-APP | | | | |
| open field blast | hematoxylin and eosin (H&E) | 24 hours | | apoptosis in white matter and significantly higher | Lu et al (Lu et al., 2012) |
| | Apoptosis detection kit | | apoptosis | | |
| | S100B | | | | |
| | GFAP | | | | |
| | MAB360 | | | | |
| | MBP | | | | |
| | NeuN | | | | |
| | b-APP | | | | |
| | B1086 | | | | |
| | AQP | | | | |
| | IgG | | | | |
| | TUNEL | | apoptosis | | |

In this study, two types of fluorescent staining were utilized to evaluate neuronal cellular injury and apoptosis: Fluorojade C (FJ-C) and Caspase 3. FJ-C is a cationic fluorescent dye empirically demonstrated to bind to degenerating neurons after tissue fixation. FJ-C stains degenerating neuron cell bodies, dendrites, and axons. It provides a quantifiable index for assessing neuronal damage within interior regions of the brain slices. Caspase 3 has been identified as a key mediator of apoptosis in neuronal cells(D'Amelio et al., 2010). Reed et al used a rat model of direct cranial blast injury (DcBI) to evaluate severe brain injury with Fluor jade C and Caspase 3, the results showed high-level DcBI (~515 KPa) can cause significant neurological dysfunction (Kuehn et al., 2011). An ex vivo study also evaluated the situation of neuron degeneration via FJ-C staining. The results of this study showed that the neuronal injuries were much greater than injury associated with the tissue slice paradigm alone (Sarntinoranont et al., 2012). However, neither of these studies showed the correlations between injuries and pressure loading in the brain. Such information is needed for developing the injury tolerance curve for bTBI on animals and humans.

In general, the animal models used for mechanical recording of bTBI in the past varies in shape and physical testing conditions, these studies provided useful information on evaluating the mechanical responses subjects to blast overpressure. We believe more detailed results on large animals in the real-world blast scenario will add crucial information to the process of illustrating the mechanism of bTBI. More importantly, we propose to correlate the mechanical responses of the brain to immunohistological results of acute bTBI at different blast levels. The purpose of this

study is to provide data to ultimately find the injury tolerance curve of the brain by giving a quantitative evaluation on the pathological course of neuronal cells in the brain.

## 4.2 METHODS

### 4.2.1 Experimental set-up

The proper blast level to produce injury is the key factor in this study. One approach is exposed animals to sequentially higher blast levels and to determine whether a threshold could be identified through pathology results(Ahlers et al., 2012). A series of tests on rat showed that blast exposure up to 74.5 KPa lead to no persistent neurological impairments (Elder et al., 2012; Gama Sosa et al., 2014; Sosa et al., 2013). Similar experimental set-ups of mechanical test group were used in the non-instrumented animal group except there were no intrusive sensor placement in the animal's brain. Non-instrumented swine only received one front blast at an open field. The non-instrumented group underwent blasts at medium and high levels. This design ensured the integrity of the brain and will link any histological findings to the mechanical blast findings. The similar experimental set-up will also be performed on six sham animals. The sham animals were exposed to the same location as the tested animals under identical procedures except exposure to the real blast event. The histological comparison between sham animals and non-instrumented animals revealed the consequences of blasts. The incident pressure was recorded with Dewesoft (DEWETRON Inc. Dewe-3020).

### 4.2.2 Termination and fixation

Swine in non-instrumented group were shipped back to WSU under anesthesia. Then the swine was allowed to recover and was monitored for at least 8 hours. Blood samples was collected pre-blast, and at 6, 24, 48 and 72 hours post-blast for assessment of serum biomarker levels that might be indicative of brain injury. At 72 hours after experiments, swine were re-anesthetized with ketamine and euthanized by sodium pentobarbital (fatal plus) followed by rapid opening of the chest by a midline sternotomy exposing the heart and major vessels. The sternotomy was extended to the neck, in order to visualize the trachea and bilateral carotid arteries. Then, a cannula was inserted into each of the carotid arteries, and the pig was flushed with 2 liters of 0.9% sodium chloride solution. The descending aorta, bilateral subclavian and brachial arteries were clamped (a similar approach was used by Fritz et al., 2005). The right atrium was opened and the returning blood and solution was collected directly by suction into a container for later disposal. Once the returned solution is clear, the brain is fixed by 6 liters of 4% paraformaldehyde solution, as described by Browne et al. (2011). Then, the skull is opened, and brain is removed and post-fixed in 4% paraformaldehyde (500 ml) at two weeks.

### 4.2.3 Slides preparations

The perfused brain was frozen before sectioning. The whole brain is cut into blocks at 5mm thickness with a brain matrix mold (Figure 4-1). Then the brain tissue is then further processed into 40μm sections with automatic microtome.

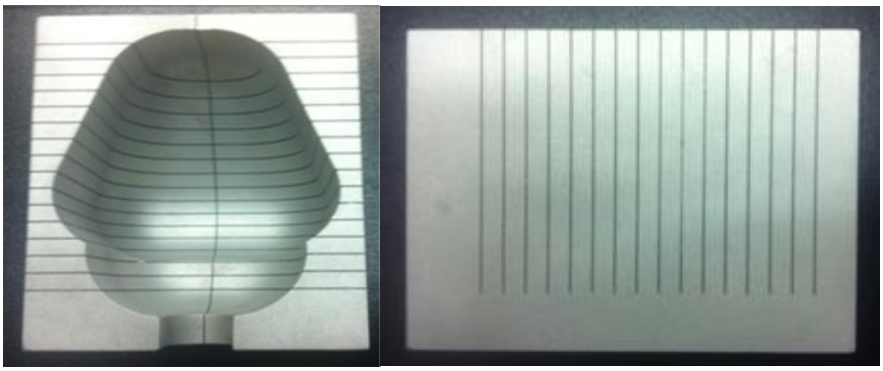

Figure 4-1: Graphs above show the custom-made brain matrix mold. Left graph is the top view of the mold (Zivic Instruments); Right graph shows the grooves of exact 5-mm thickness.

*FJ-C fluorescent staining*: 4 coronal sections were selected according to the ICP sensor locations in the front blast, and are washed thoroughly in distilled water and mounted onto gelled slides. The sections were 20um in thickness encompassing the anterior-posterior aspects of the brain. The gelled slides were prepared by an immersion in a 60 degree C solution of 1% gelatin (Sigma; type A, 300 Bloom) and then oven dried overnight at the same temperature. Then the slides were air dried for 30 minutes on a slide warmer at 50 degree C. The dried slides were then immersed in a basic alcohol solution consisting of 1% sodium hydroxide in 80% ethanol for 5 minutes. Then the slides were rinsed with 70% ethanol for 2 minutes and followed by another 2 minutes in distilled water. Sections are subsequently incubated in 0.06% potassium permanganate solution for 10 minutes. Following a 2-minute water rinse, the slides then were transferred to a 0.0002% solution of FJ-C. In order to quantify the total number of cells within each field of view, the nuclear DNA label 4',6-diamidino-2-phenylindole (DAPI, 0.0001%; Sigma-Aldrich, St. Louis MO) were included in the FJ-C solution in 0.1% acetic acid vehicle. The slides then were washed with three

changes of distilled water for 1 minute per change. After air-drying of the slides, they were cleared in xylene for 2 minutes and then cover slipped with DPX.

*Caspase-3 staining*: another set of brain sections adjacent to those selected for FJ-C staining were chosen for Caspase-3 staining. The staining protocol was developed as follows: All sections are washed three times in PBS, for 5 min at room temperature. Then drain the slide and add 200 µl of blocking buffer (PBS/0.1% Tween 20 + 5% donkey serum). Use of serum from the host species of the conjugate antibody (or closely related species) is suggested. Lay the slides flat in a humidified chamber and incubate for 1-2 hr at room temperature. Rinse once in PBS. Add 100 µl of the active Caspase 3 antibody diluted 1/200 in blocking buffer. Incubate slides in a humidified chamber overnight at 4°C.The following day, wash the slides three times, 10 min each in PBS/0.1% Tween 20 at room temperature. Drain slides and add 100 µl of goat anti-rabbit Cy5® conjugate diluted 1:500 in PBS. Lay the slides flat in a humidified chamber, protected from light, and incubate for 1-2 hr at room temperature. Wash three times in PBS/0.1% Tween 20 for 5 min, protected from light. Drain the liquid, mount the slides in a permanent or aqueous mounting medium and observe with a fluorescence microscope.

4.2.4 Analysis of Fluorescent signal

For each histological stain, 2 sections from each frontal, temporal, parietal, center, and occipital were obtained from previously acquired 5 mm blocks (Figure 4-2). Note that these locations of these five regions were chosen based on the locations of ICP sensors. The range of the slides analyzed here were relatively narrower than the whole brain in the longitudinal direction.

The FJ-C and DAPI stained sections were examined with an epifluorescence microscope (Q-Color3 TM, Olympus, Japan) using proper emission filters. For DAPI signals, the excitation time was set at 100 ms. Exposure time was set at 1 second to capture FJ-C and Caspase-3. In general, 6 randomly-selected images were captured from each section at the similar locations of sensors installed in the instrumented group (Figure 4-3).A total number of 12 images were taken for each region in every animal.

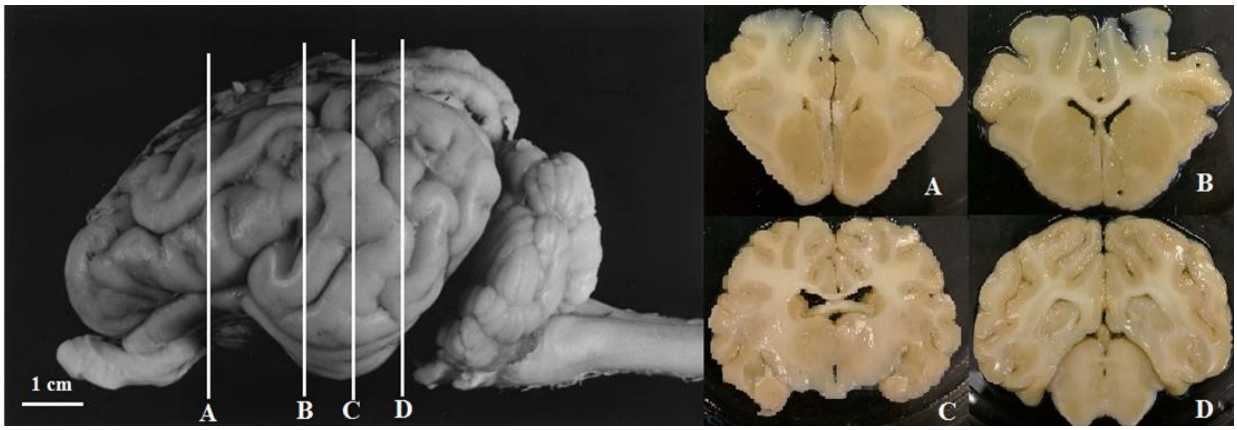


Figure 4-2:Lateral view of the pig brain indicating the sections used to evaluate cellular injury and neuronal degeneration. Four white lines at the left figure show the position of the four coronal sections listed at the right side. They are representative 5 mm blocks from an non-instrumented animal subjected to blast. A) frontal, B) temporal, C) Parietal and Center, D) Occipital.

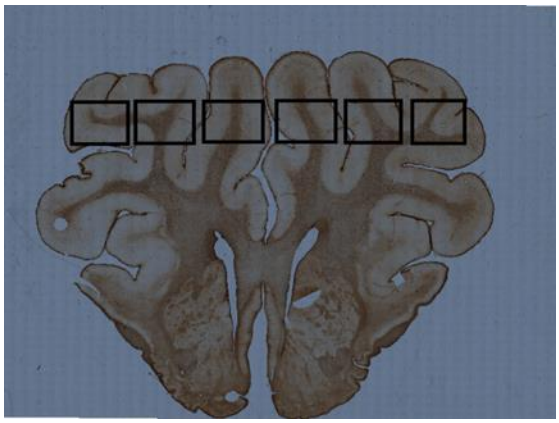

Figure 4-3:Graph shows the imaging methodology on choosing representative pictures at cortical region to quantify FJ-C and Caspase-3 signals.

Image J (Image J, NIH, USA) was used to perform quantitative analysis on Caspase-3 images. The cells (DAPI stains) and the apoptotic cells (Cleaved Caspase-3) were counted following a custom Standard Operating Procedure (SOP) using Image J. DAPI-positive areas were segmented using a pixel intensity threshold. An imaging threshold value of 30% of the background value was determined to identify FJ-C-positive neurons reliably. Background values were calculated from images of the molecular layer of the cortex. The fraction of apoptotic cells labeled by Caspase-3 was determined by dividing the total number of overlapping Caspase-3 and DAPI-positive objects by the total number of DAPI-positive objects in the field. Degenerating neurons (overlapping DAPI and FJ-C stains) were manually quantified in each high-power field (HPF) due to positive signals can come from both the cells and blood vessels. Double-blinded quantification was performed for all the FJ-C slides. Distribution patterns of ICP as mean peak values were used to estimate the likelihood and severity level of injury in different brain regions. Statistical analyses were performed using SPSS software. One-way ANOVA and student t-tests were used to

calculated the *p* values. Results were expressed as mean ± standard error of the mean. A p-value<0.05 was considered as significant.

**4.3 RESULTS**

We have a total number of 11 blasted animals in histological group. We divided them into two blast groups based on their peak pressure levels, the medium blast group (272.7±7.35 kPa) and high blast group (375.3±1.78 kPa). Detailed peak pressure for each blast was listed in table 4-2.

Table 4-2: List of peak IOP in histological blast group.

| Blast No. | Peak IOP (kPa) |
|---|---|
| B1 | 223.5 |
| B2 | 332.3 |
| B3 | 305.4 |
| B4 | 222 |
| B5 | 262.7 |
| B7 | 290.3 |
| B8 | 359.9 |
| B9 | 359.9 |
| B10 | 403.3 |
| B11 | 403.3 |
| B12 | 350.3 |

There was no lethality associated with these blast pressure levels. Our results showed more prominent FJ-C positive-stained zones in the blast groups compared with sham (n=3). (Figure 4-4). A further analysis showed that the number of FJ-C-positive neurons in the high blast group (n=6) were higher than that in the medium blast group (n=5). (student t-test, $p<0.05$) (Figure 4-5). Furthermore, positive stained FJ-C neurons were observed in the cortical regions from frontal to

occipital regions in the blast groups (Figure 4-6). Further analysis showed no difference between different regions of the brain in the same blast level groups.

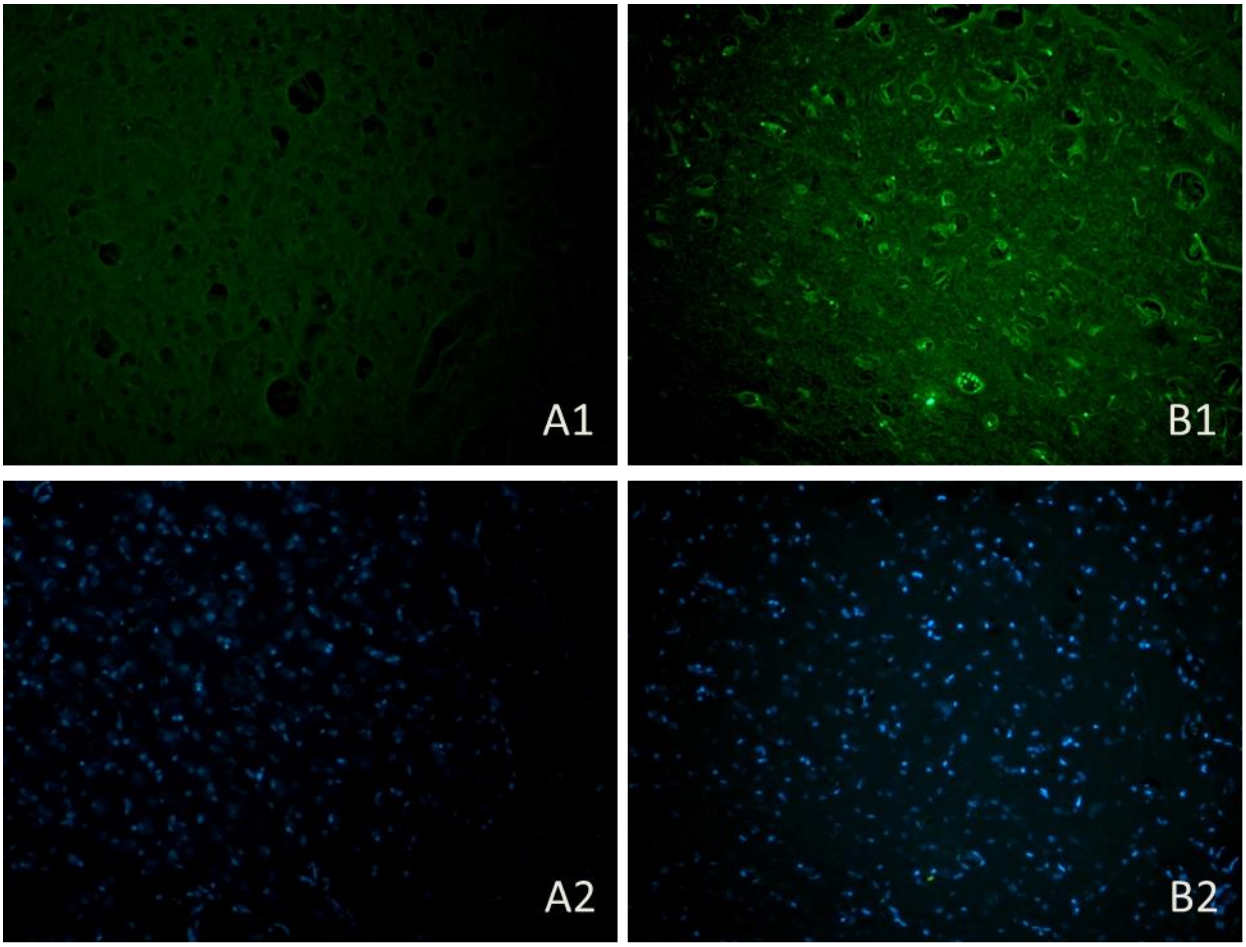


Figure 4-4: Representative images of FJ-C staining in sham (A1,A2) and blast groups (B1, B2). A1 and B1 are FJ-C images, A2 and B2 are counterstained DAPI images in the same region.

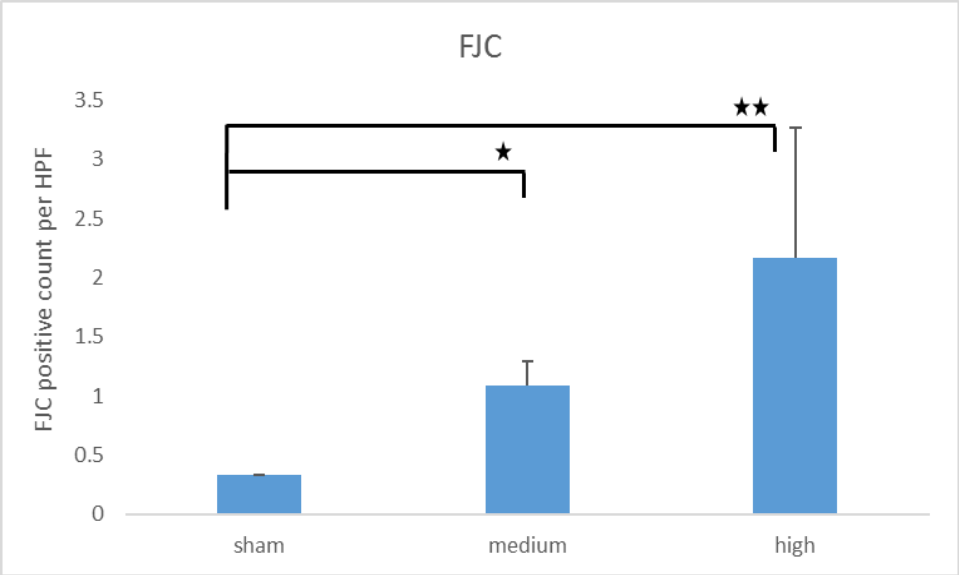


Figure 4-5: FJ-C level in different blast level groups. The medium and high groups are significantly higher than sham group. Additionally, the positive counts of FJ-C in high blast group are significantly higher than medium group. (*P<0.05*)

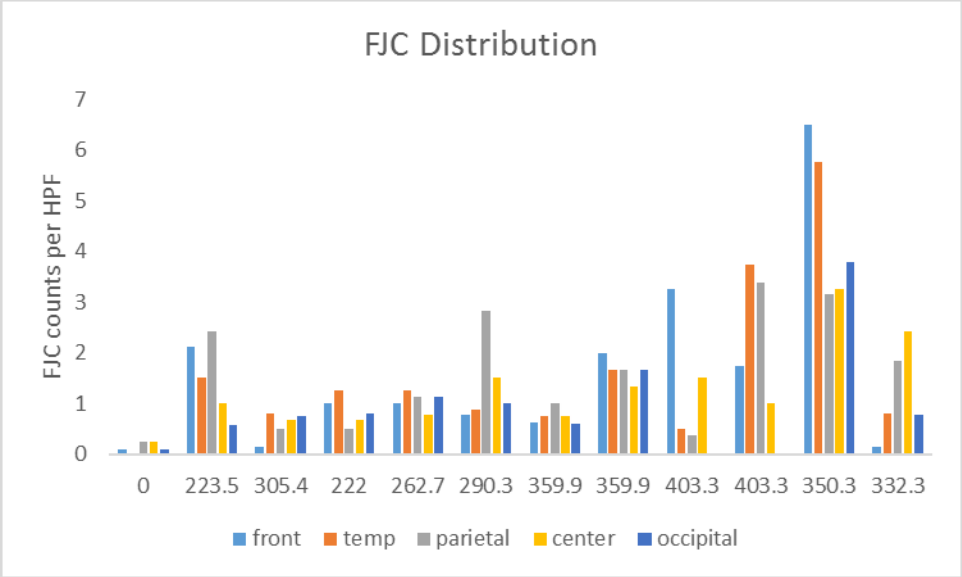


Figure 4-6: FJ-C distributions of the quantified slides from each animal.

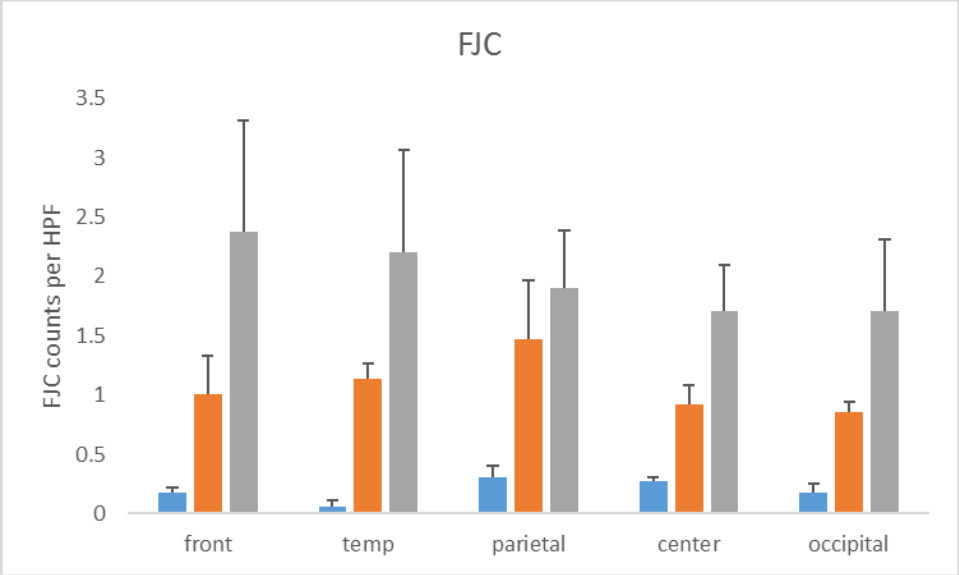


Figure 4-7: One-Way ANOVA showed there was no difference between groups in the same blast level. (p>0.05)

We chose Caspase-3 to identify the level of apoptosis in the brain (Figure 4-7). In brain sections from swine subjected to high blast group (n=3), the apoptosis level was significantly elevated compared with sham group (n=3) and medium blast group (n=6) (*p>0.05*). There was no statistical difference between sham and medium group (Figure 4-8). Apoptotic cells were observed in both white and gray matter in the brain in the blast groups. Caspase-3 stained signals were covered from frontal to occipital regions of the brain (Figure 4-9). One-way ANOVA tests showed there was no difference between various regions of the brain in the same blast level groups (Figure 4-10). In this study, we did not perform the blast to non-instrumented animal paired with instrumented animals due animal availability. Therefore, it would be not accurate to make the statement on the correlation between ICP response with different characteristics and injury outcomes. However, we utilized the relatively high linear correlation equation between IOP and

ICP peak values in the mechanical group to make predictions of the relationship between mechanical responses and the injury outcome (Figure 4-12, Figure 4-13).

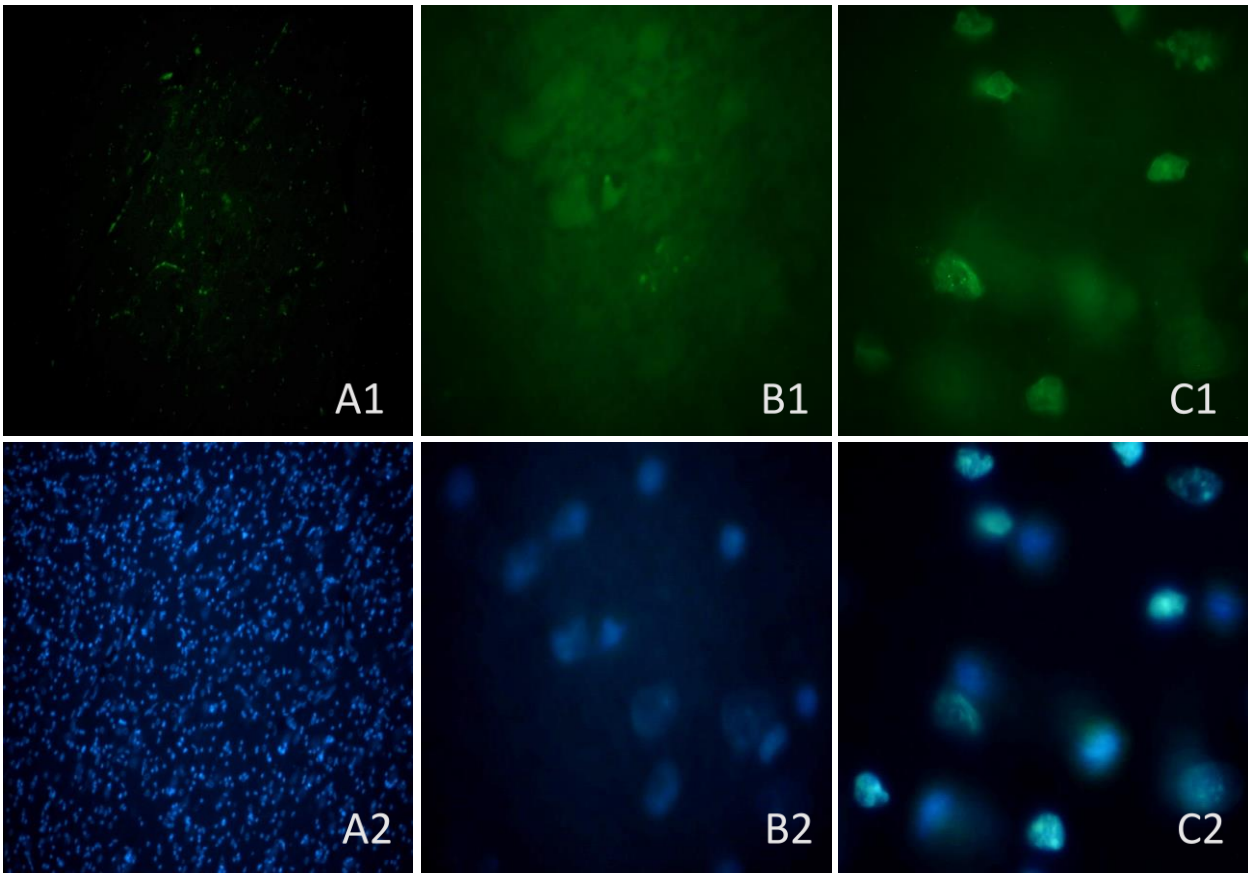


Figure 4-8: Caspase-3 expression. A1and A2 shows positive staining of Caspase-3 with DAPI counterstain. B and C are images at 100x. B shows negative caspase-3 stain, C shows positive Casepase-3 with DAPI.

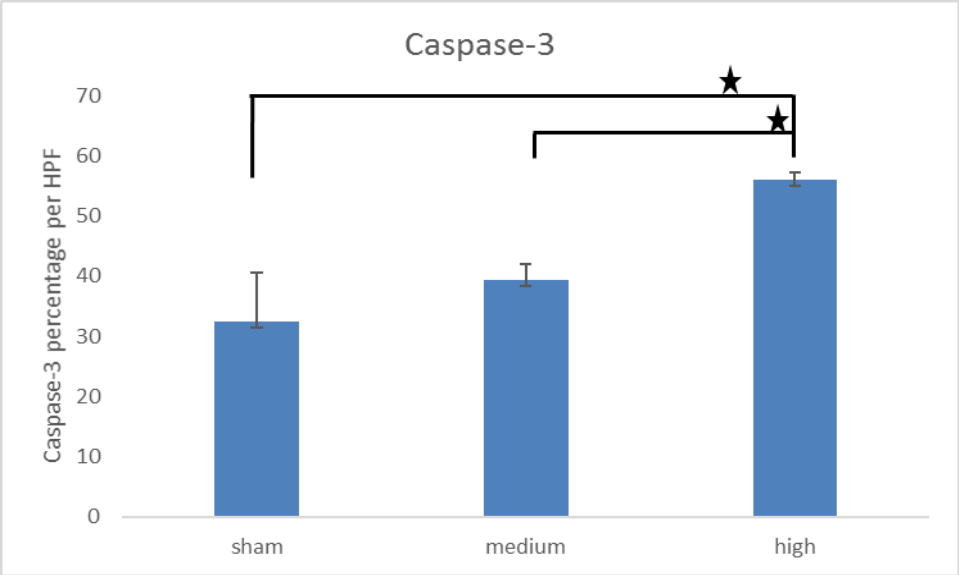


Figure 4-9: The number of Apoptotic cells were significantly higher in the high blast group than sham and medium group. $p<0.05$

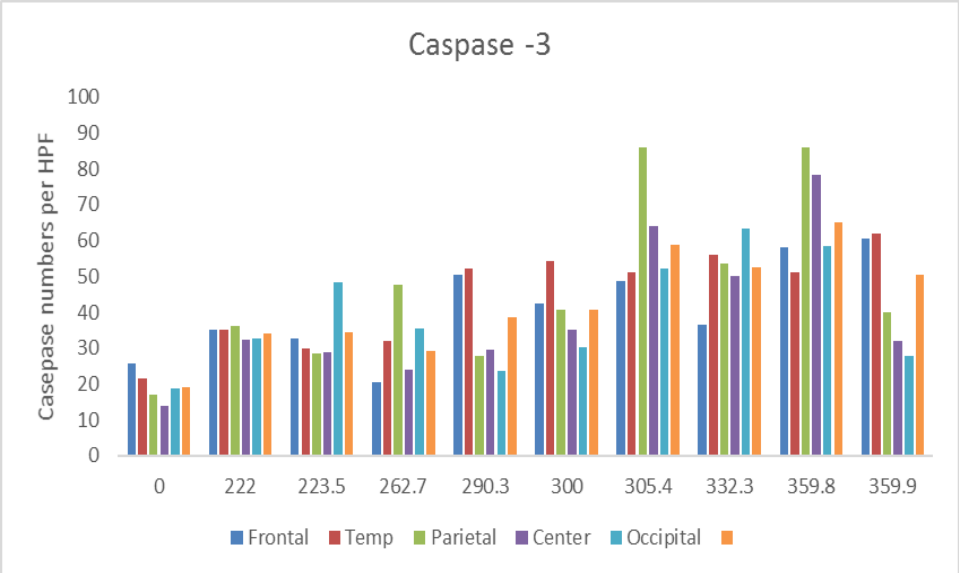


Figure 4-10: Casepase-3 distribution at different locations of the brain in every blast.

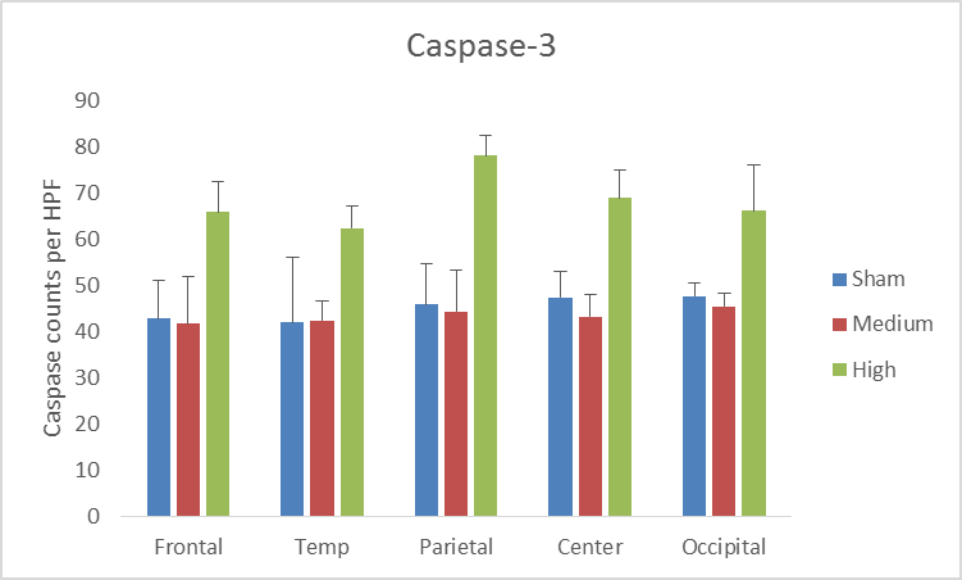


Figure 4-11: Caspase distribution at different regions in each blast level group. Statistics did not show any difference between the different regions. (p>0.05)

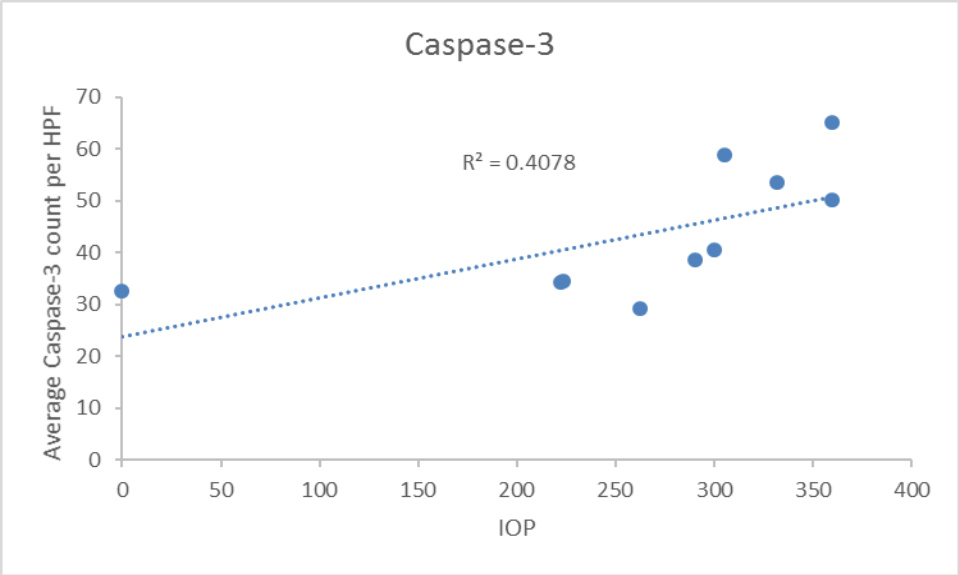


Figure 4-12: Scatter plots shows the correlation between IOP and Apoptotic cells.

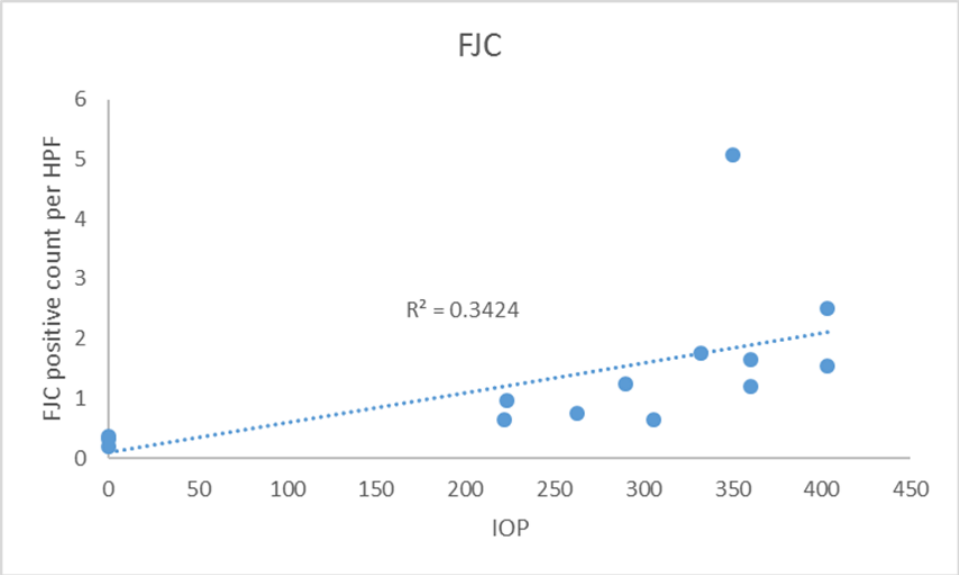


Figure 4-13: Distribution of average FJ-C counts in each test. The data was correlated with linear trend line.

## 4.4 DISCUSSION

### 4.4.1 Neuronal degeneration and apoptosis in the brain

To our knowledge, this study is the first of its kind to attempt to address the fundamental question whether an open field blast exposure causes injurious changes in the gyrencephalic brain. Although there were other studies that attempted to address the same question in a gyrencephalic model using explosives, animals in those studies were exposed to a simulated open field blast by positioning the animal either in a shock tube, high mobility multipurpose wheeled vehicle surrogate or in a four-sided building with no roof using a moderate charge (Bauman et al., 2009; de Lanerolle et al., 2011; Gyorgy et al., 2011). Another previous open field blast study (2.1 kg explosive) positioned the animal on a steel shelf mounted to the concrete wall of the bunker and studied only physiological parameters such as respiration, circulation and cortical activity but no histological analyses of brain for injury changes as in the current study(Axelsson et al., 2000).

Sa¨ljo¨ et al on the other hand, offers some details on the effects of repetitive blast pressure (3 times during a 10–15 minute period) in swine exposed to low level noise produced by various weapons (a howitzer, a bazooka, an automatic rifle) or underwater explosives(Saljo et al., 2008; Saljo et al., 2011). They reported that animals exposed to bazooka (Pmax 42 kPa) and automatic rifle (Pmax 23 kPa) showed significant increase in subarachnoidal and small parenchymal bleedings in cortical regions with occipital lobe and cerebellum being the most predominantly affected structures. Animals exposed to howitzer blasts at 30 kPa although displayed parenchymal and subarachnoid hemorrhages, they were not significantly different from that of controls due to the limitations in the number of animals. Sa¨ljo¨ et al concluded that low levels of blast causes brain edema as indicated by increased bioelectric impedance, an increase in intracranial pressure, small brain hemorrhages and impaired cognitive function(Saljo et al., 2011). In our study the animals were exposed to higher open field blast pressure than these animals and the likelihood of such hemorrhages although possible was not investigated as the focus was to study neuronal injury and glial reactivity changes.

We studied injury changes in the brain following an free-field blast in Yucatan swine suspended in a sling and positioned below the triple point and exposed to a single Friedlander wave form either at medium (range 222 kPa—305 kPa; average 272±5 kPa) or high blast overpressure (range 335–403 kPa; average 380±3 kPa). Our lowest medium blast overpressure of 222 kPa was similar to the mean shock tube blast pressure (241±8 kPa) reported by de Lanerolle et al (2011) in Yorkshire swine. Besides, the shock tube pressures reported by de Lanerolle et al

ranged from 131–365 kPa(de Lanerolle et al., 2011) with their lowest pressure range far lower than in our study. In our experience there were no mortalities in both the medium and high blast overpressure groups. These pressures were very close to those utilized by de Lanerolle et al (2011) who reported shock tube and vehicular blast pressures in the range of 255–365 kPa with potentially long durations that may be a contributing factor for the observed mortality. Furthermore, the medium and high blast overpressures used in our study are higher than those used by Gyorgy et al (2011) who used three different blast overpressures of <152 kPa, 138–276 kPa and >276 kPa respectively on Yorkshire swine and reported time dependent changes in serum biomarkers (Gyorgy et al., 2011).

Animal models suggest that primary blast injury can be associated with neural injury, although the underlying mechanism is not yet clear (Cernak et al., 2001a, b). In this paper, we made efforts on evaluation of the degenerating neurons and apoptotic cells in the frontal, temporal, parietal, center and occipital of the brain 72-hours post the blast test with immune-fluorescent histology. We found that, the degenerating neurons were significantly more in blast groups than that in sham animals. The level of degeneration also increased with the incident blast levels. These findings were consistent with our recent immunohistological data, acquired from frontal lobe of the brain from the same study(Kallakuri et al., 2017). The level of βAPP, NF-L, and NF-M all showed significant increase compared with that in the sham animals. On the other hand, the apoptosis level in the high blast group was significantly higher compared with that in the medium

group and the sham animals, indicating that the high blast level (380 kPa) induced apoptosis within the brain at the acute stage of the swine brain.

The evaluation of brain pathology of TBI are time sensitive(Masel and DeWitt, 2010). The evaluation on TBI also should cover the whole chronic time periods of secondary injury. Smith M et al utilized rat hippocampal slice cultures to study the neuronal degeneration of primary bTBI.(Smith et al., 2016) Fluoro-Jade B staining found no indication of degenerating neurons in the pyramidal fields of hippocampal slices in either single of repeated blast tests. Abdul-Muneer PM et al found that a single incident pressure with a peak value of 123 kPa caused brain injury on rats. Caspase-3 expression at 24-hour post-test was much higher than control group. Repeated blast resulted in higher caspase -3 level than single blast.(Abdul-Muneer et al., 2013) However, the characteristics of its incident pressure was not described in this study. Additionally, Wang et al. developed a mice model of single and repeated blast exposure. Fluoro-Jade B positive staining was observed in the group with 3 repeated blasts at 142 kPa 24-hour posttest.(Wang et al., 2011).Several studies have evaluated Caspase-3 levels at various time point post blast. A underwater blast study showed subtle pathological changes of the brain 1-28 days after blast. No elevation of apoptotic cells were observed in 300, 2700,140000 kPa blast groups.(Sawyer et al., 2017). Miller AP et al. utilized rat organotypic hippocampal slice cultures (OHCs) as an in vitro system to model bTBI(Miller et al., 2017) They characterized the astrocytic response to a blast overpressure at 2 hours following injury. Quantification of the number of dead astrocytes per counting area in the hippocampal cornu Ammonis 1 region (CA1), demonstrated a significant

increase in dead astrocytes in the low- and high-blast, compared to sham control OHCs, but majorly from necrosis. A recent research studied the apoptosis-related protein expression in rabbits exposed to blasts. Immunohistochemistry was performed 1, 6, 12, 24 hours, and 3, 7, and 14 days post blasts. Caspse-3 expression was elevated 1 hour after the blast. The level was peaked at 24 hours, then gradually decreased and restored to normal by day 14(Xu et al., 2012). If Caspase -3 expression follows the same expression trend in our study, it could mean the apoptosis level at the medium blast group were the same as sham group or it was decreased and restored back to normal by day 3.

We also noticed that there was no statistical difference between various regions of the brain at the same blast level. This finding is consistent with our observations on peak ICPs at different regions of the brain. The slides represented the regions of the brain were selected based on the locations of ICP sensors. Even we name them frontal and occipital slides, they were not located in the most anterior or posterior part of the brain. It could be the reasons why we were not observing differences of injury level at the coup and counter coup region at the same blast level.

4.4.2 Correlation between mechanical responses and histological findings on bTBI

Appropriate animal models of blast-induced TBI will not only assist the understanding of physical characteristics of the blast, but also help to address the potential mechanisms. Information on the relationship between measured mechanical responses on swine head and the quantified axonal changes and other neuronal changes subjected to a free-field blast has not been published. The long-term goal of this study is to establish accurate injury tolerance curves for bTBI that can

be used to guide assessment and targeted treatment. In the current study, quantitative and qualitative neuron cell injury findings in specific locations in the brain was correlated with the mechanical responses using an open-field blast swine head injury model. Since the peak IOP were different between instrumented and non-instrumented group, we utilized the linear correlation equation developed by IOP and its corresponded ICP to replace the IOP in the non-instrumented group. Scatter plots of FJ-C and Casepase-3 level with predicted ICP were developed (Figure 4-10, 4-11). They indicated that the expression level of FJ-C and Casepase-3 are pressure level dependent. The relationship was not linear. In addition, we hypothesize that the swine brain injury threshold of mTBI from open-field blast could lie in the range of 275-380 kPa.

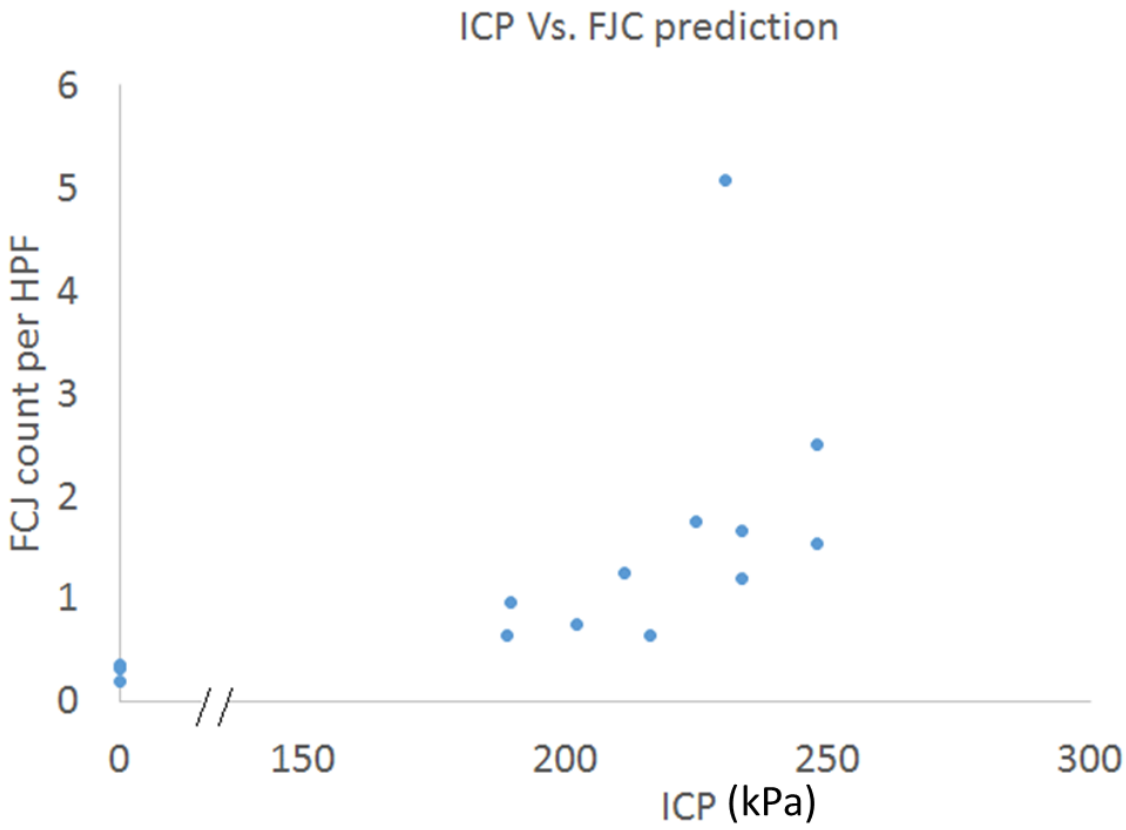


Figure 4-14: FJ-C level and its predicted ICP readings in the swine brain.

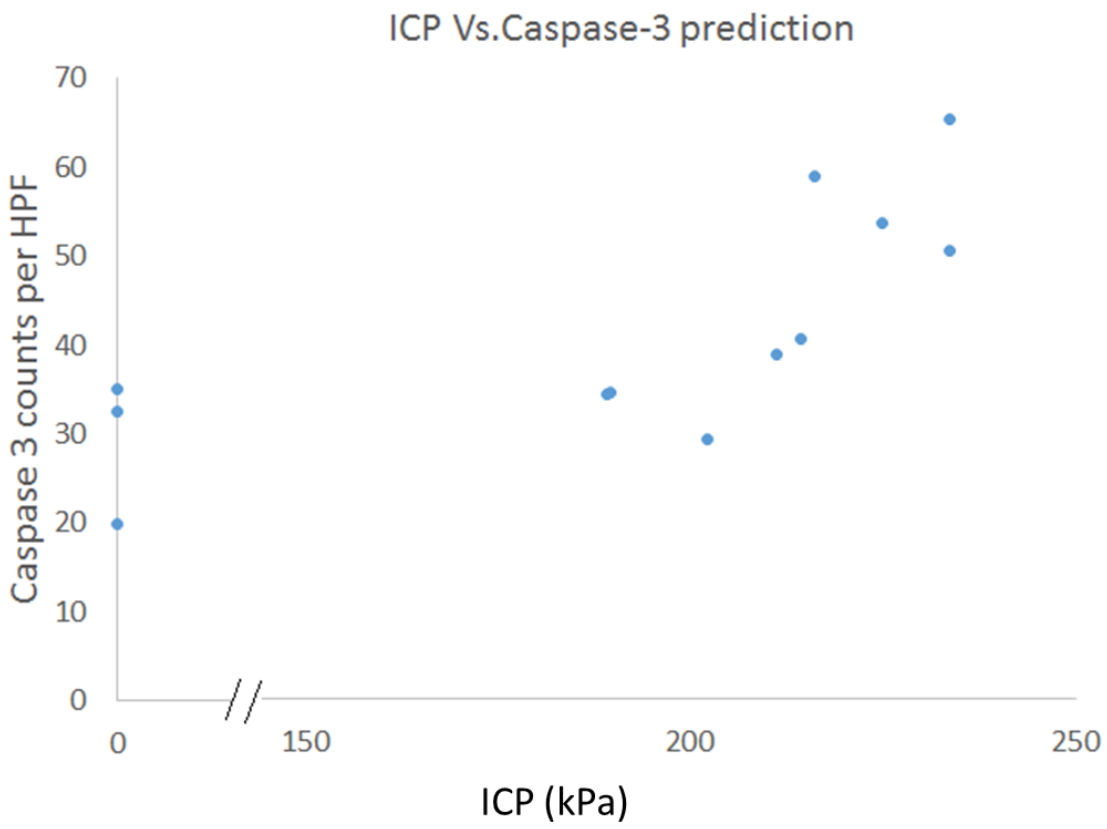


Figure 4-15: Caspase-3 level and its predicted ICP in the swine brain.

# CHAPTER 5. FUTURE WORK

## 5.1 LIMITATION OF THIS STUDY

Potential limitations including areas of biology, sample size, fixation technique and image processing exist for the study. As mentioned in Chapter 2 and 4, we have biological limitation by using the swine instead of humans. This is standard limitation of animal models and is well acknowledged by the research community.

Biomechanical responses were recorded during the open-field blast event. While we selected sturdy sensors with strengthened coating, there were some sensor failures in the tests due to the strong blast wind, limiting the sample size of ICP and acceleration data of the swine brain.

For the immunohistological quantification of the swine brain, we harvested the brain 72 hours post experiment. As we discussed earlier, some of the neuropathological changes occur within 72 hours. Therefore it is possible that some of the metabolic changes were back to baseline and was not captured by the analysis.

## 5.2 SUMMARY AND FUTURE DIRECTIONS

This project has developed an experimental model to investigate the mechanisms of primary bTBI. There are a variety of ways in which this work can be extended and improved upon to expand our understanding the mechanisms of bTBI. Some of the possible extensions of this work are listed here:

Extending the time frame post experiment. Instead of singular time point after blasts, setting a series of investigate time points to evaluate brain injury at the cellular level would help us to identify the timelines for each specific physiological disruption.

Labeling multiple forms of neuronal injuries within the same brain sections. With various aspects of quantification, it would improve the ability to assess how the trauma cascades at cellular level.

The underlying neuropathology of primary bTBI remains incomplete. More studies at the cellular, subcellular and physiologic levels will help elucidate generation of primary bTBI. With comprehensive characterization of the pathology, the degenerating neurons and axons as well as cell death can be used as markers for measuring the severity of brain damage and target for the repair strategies. In future, coordinated experiments and mathematical modeling research can shed light into the mechanisms of mild bTBI. Validating computer models based on the experimental data acquired in this study. In this experiment, we physically acquired and analyzed mechanical responses of the brain at several brain locations. However, computer models are the only way to fully understand the complex loading conditions with validation. In the future, validated computer models will not only provide detailed distribution of ICP, but also other physical premasters that can demonstrate the propagation of primary blast wave in the brain. The long-term goal of this research is ultimately finding the best protective device for blast-induced brain injuries. Besides what is presented here, behavior study and clinical research should be combined to elucidate the mechanism of bTBI better in the future.

## 5.3 CONCLUSIONS

In conclusion, we developed a swine model in open field blast to study primary bTBI. We evaluated the mechanical responses of the swine brain and its injury level three days after blast exposure. 1) Mechanically, we found ICP had linear relationship with IOP. 2) No difference was found in different regions of the brain in the same blast level. 3) Little head movement was observed during the primary blast. 4) Our non-instrumented group showed results supported the presence of a robust neuronal injury in the brain. The severity of the observed neuronal degeneration appeared to be proportional to the level of blast exposure. 5) Significant apoptosis level was observed in the high blast group. 6) The injury levels were not different between different regions of the brain in the same blast level. These finding indicate that mild to moderate primary blast exposures result in changes, the functional implication of these observed acute changes may be related to neuronal, axonal and dendritic degeneration.

## Appendix A: ICP CURVES VALIDATION OF ICP DATA IN FRONTAL BLASTS (LEVEL ORIENTED)

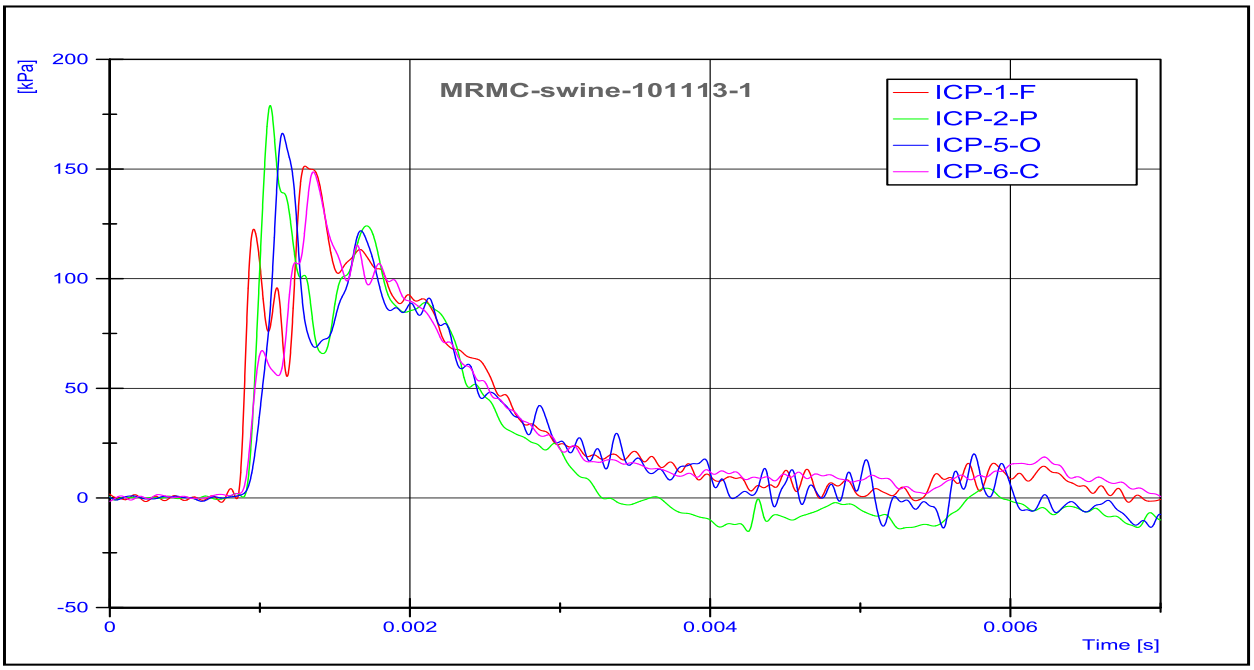


All data looks normal, Peak values are validated.

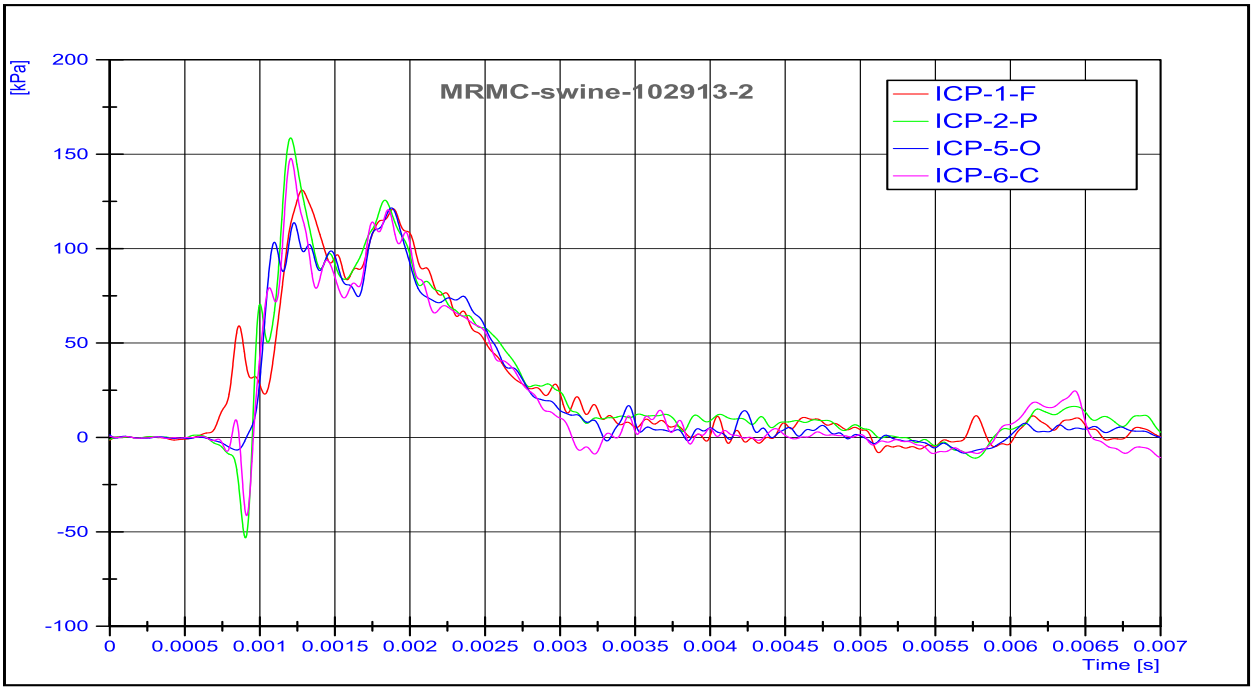


All data looks normal, peak values are validated.

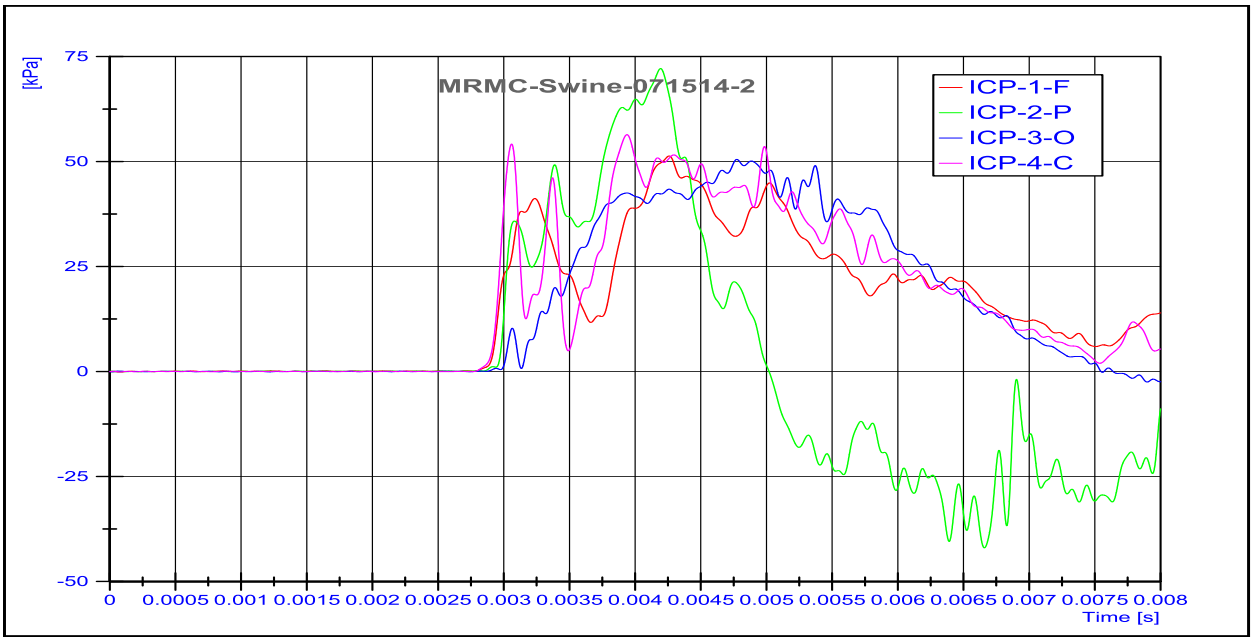


071514 metal bolts used for sealing were fastened by hand, a question of tightness on the sensor wire needs to consider. P readings got questionable after a few milliseconds.

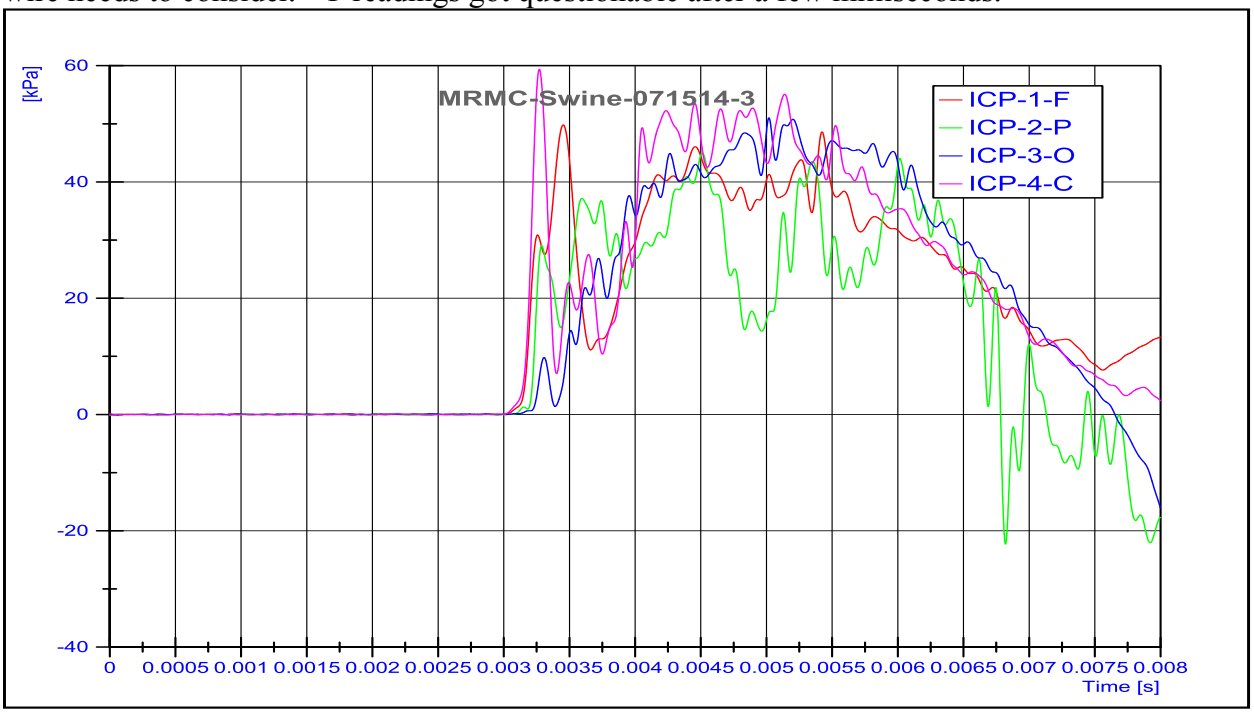


071514 metal bolts used for sealing were fastened by hand, a question of tightness on the sensor wire needs to consider. P readings got questionable after a few milliseconds.

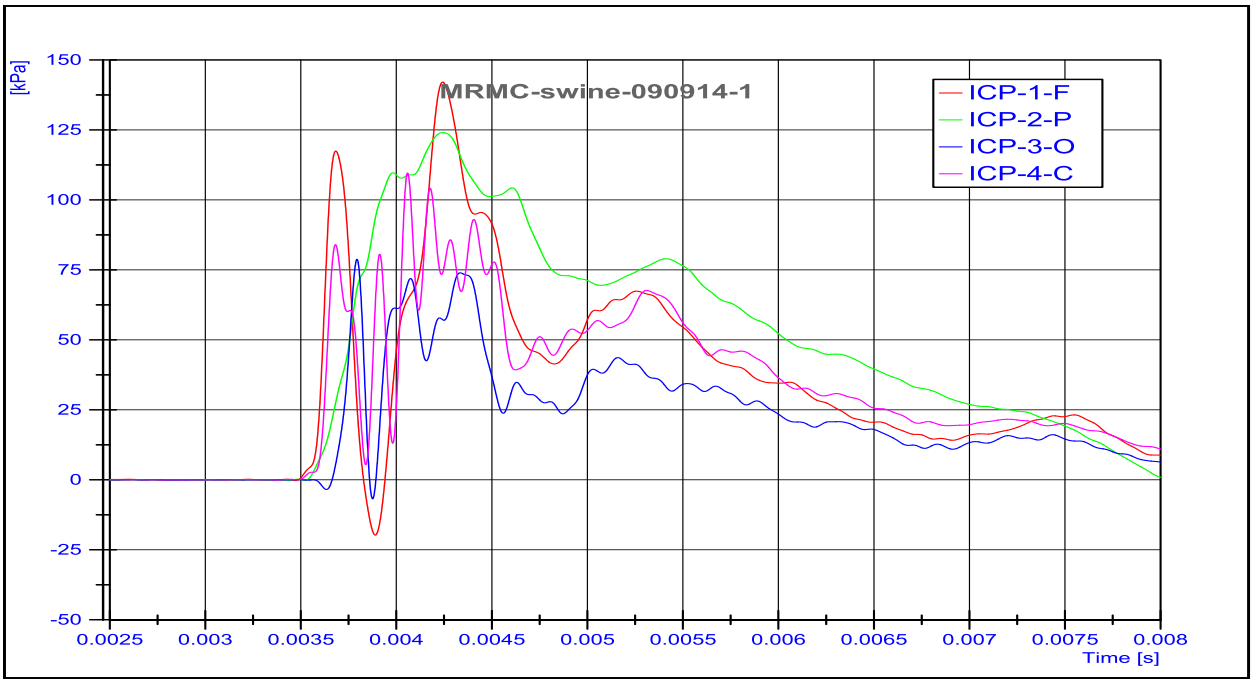


Data looks normal and peak values are validated.

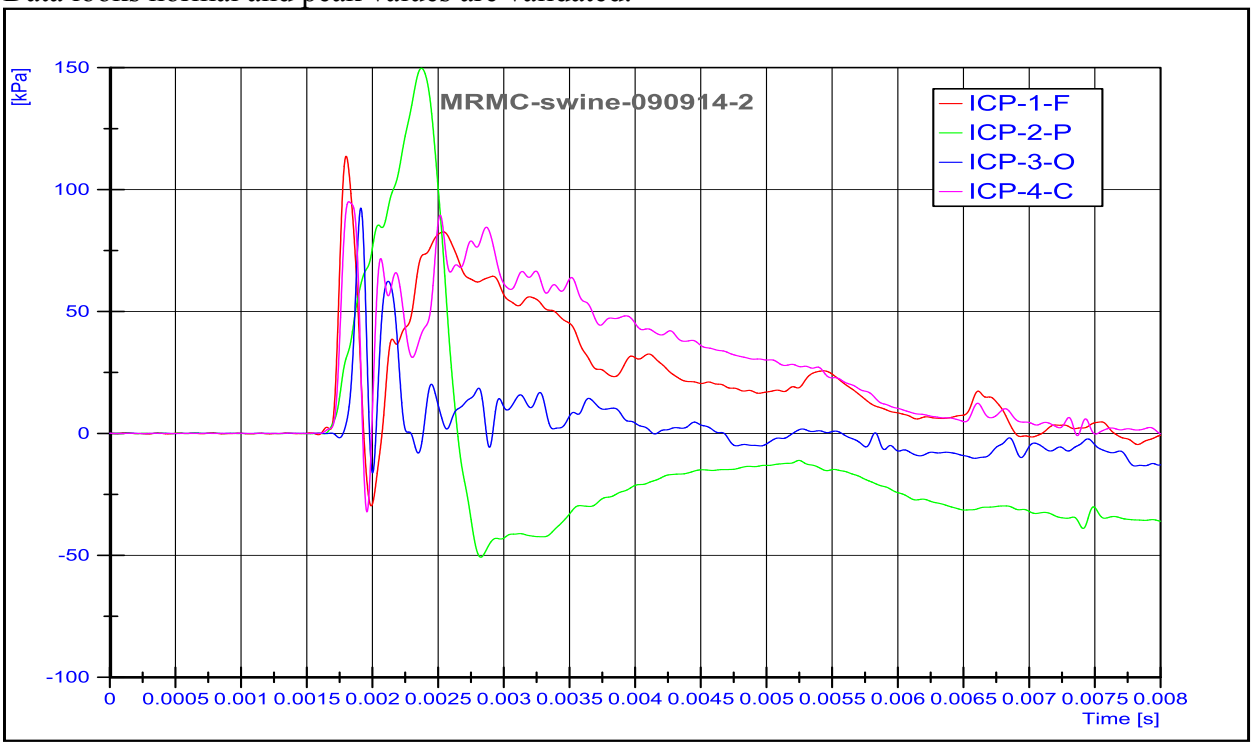


P rise time is delayed but still fell in the same timeline as other sensors. Peak value kept but questionable.

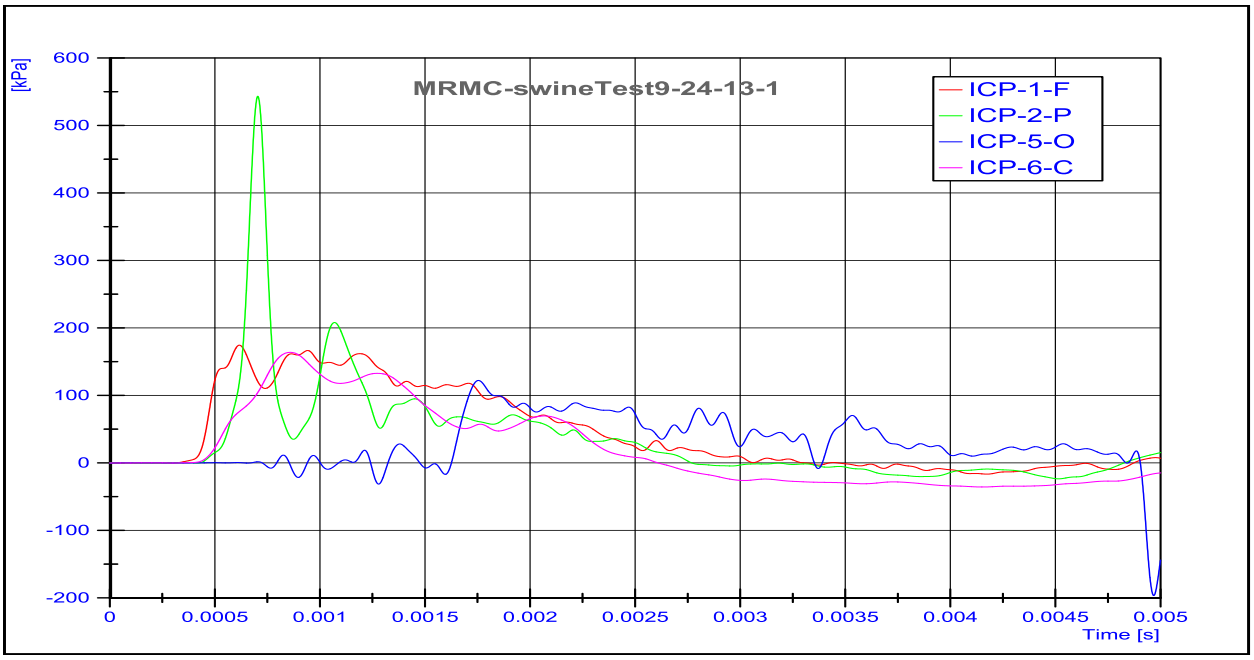


O rise time is significantly delayed and be discarded in this test. P is questionable.

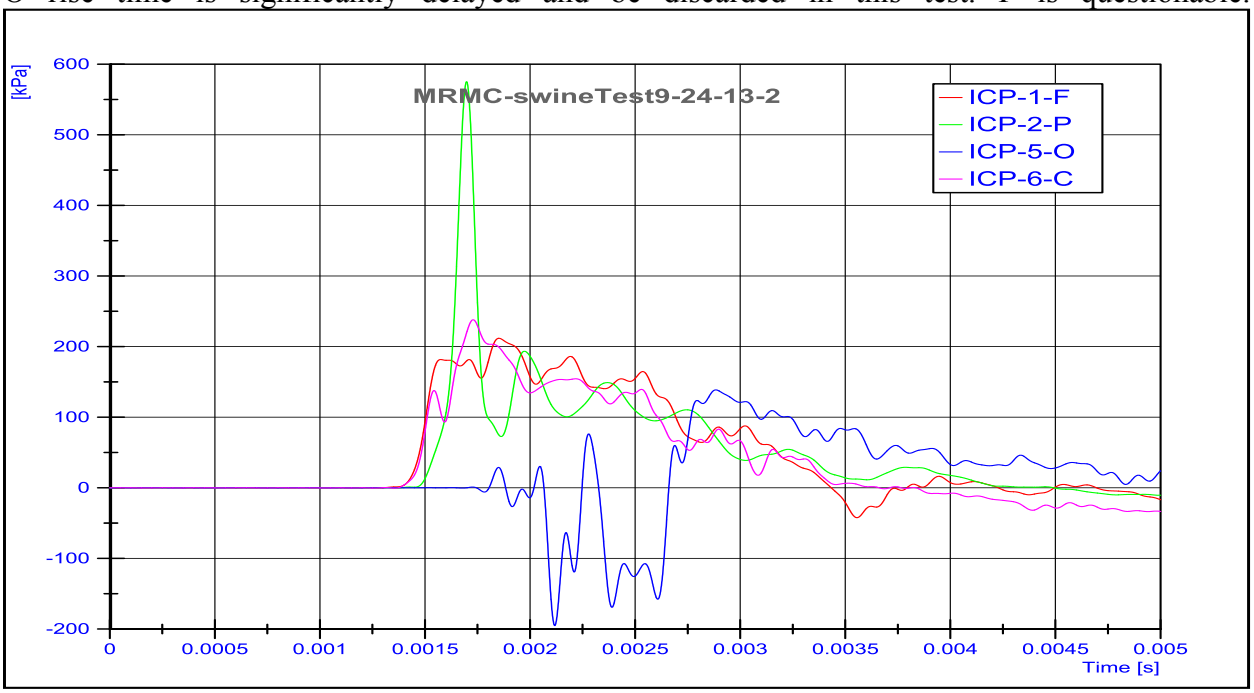


O rise time is significantly delayed and be discarded in this test. P is questionable.

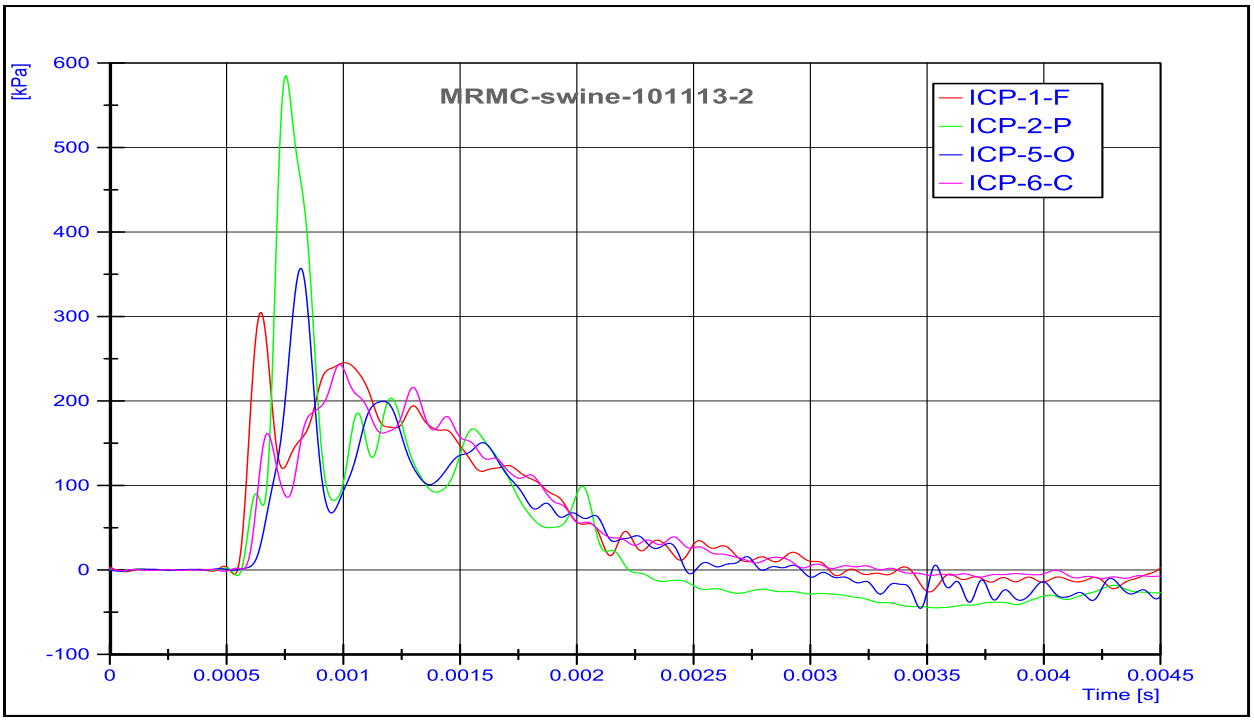


Data looks normal and peak values are validated.

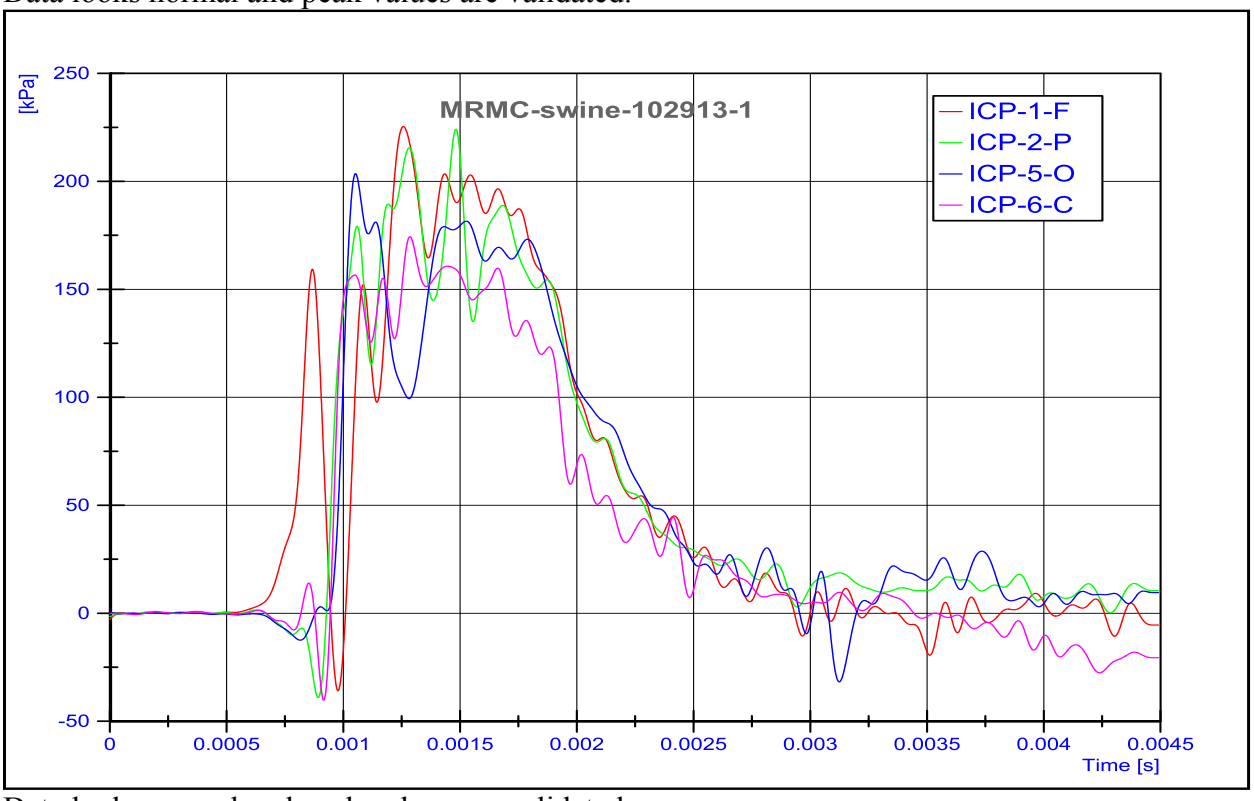


Data looks normal and peak values are validated.

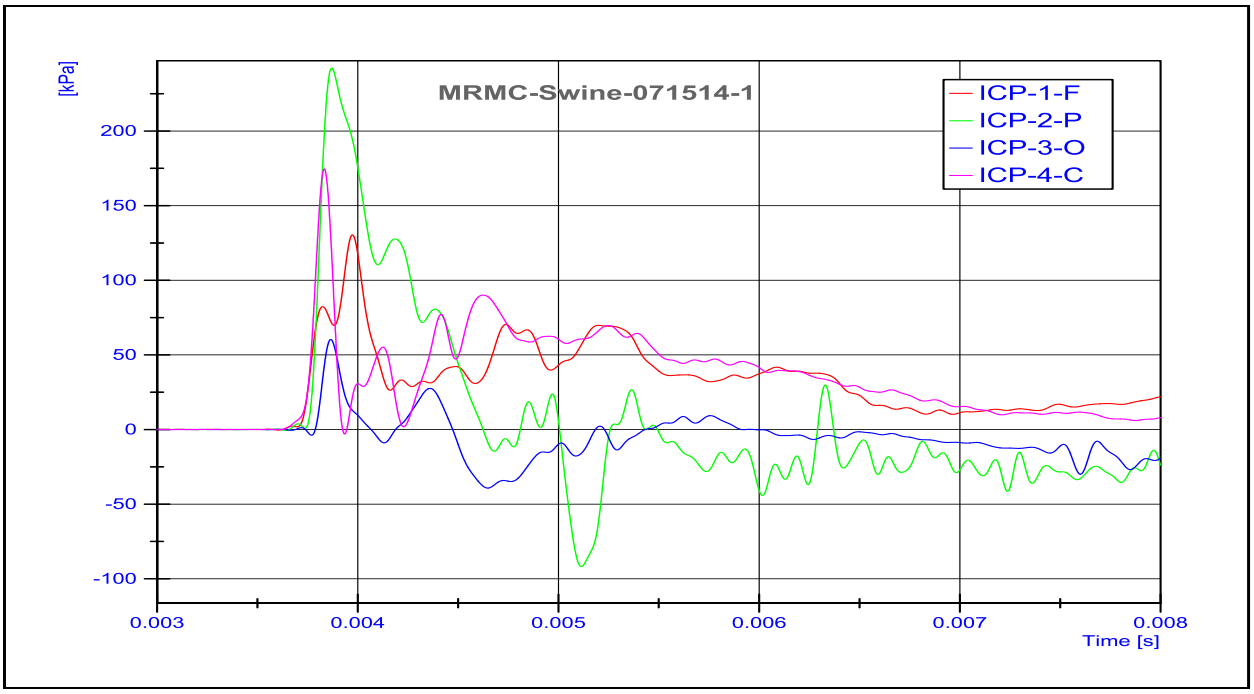


071514 metal bolts used for sealing were fastened by hand, a question of tightness on the sensor wire needs to consider. Data looks normal.

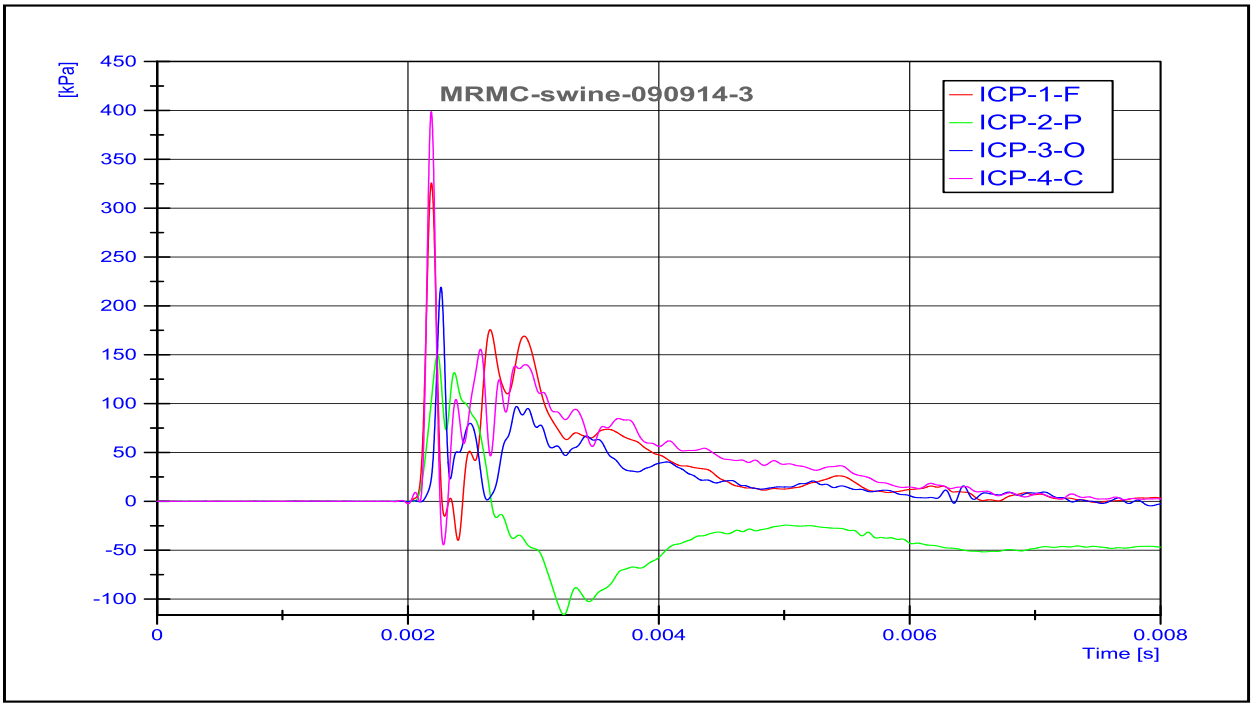


P looks questionable.

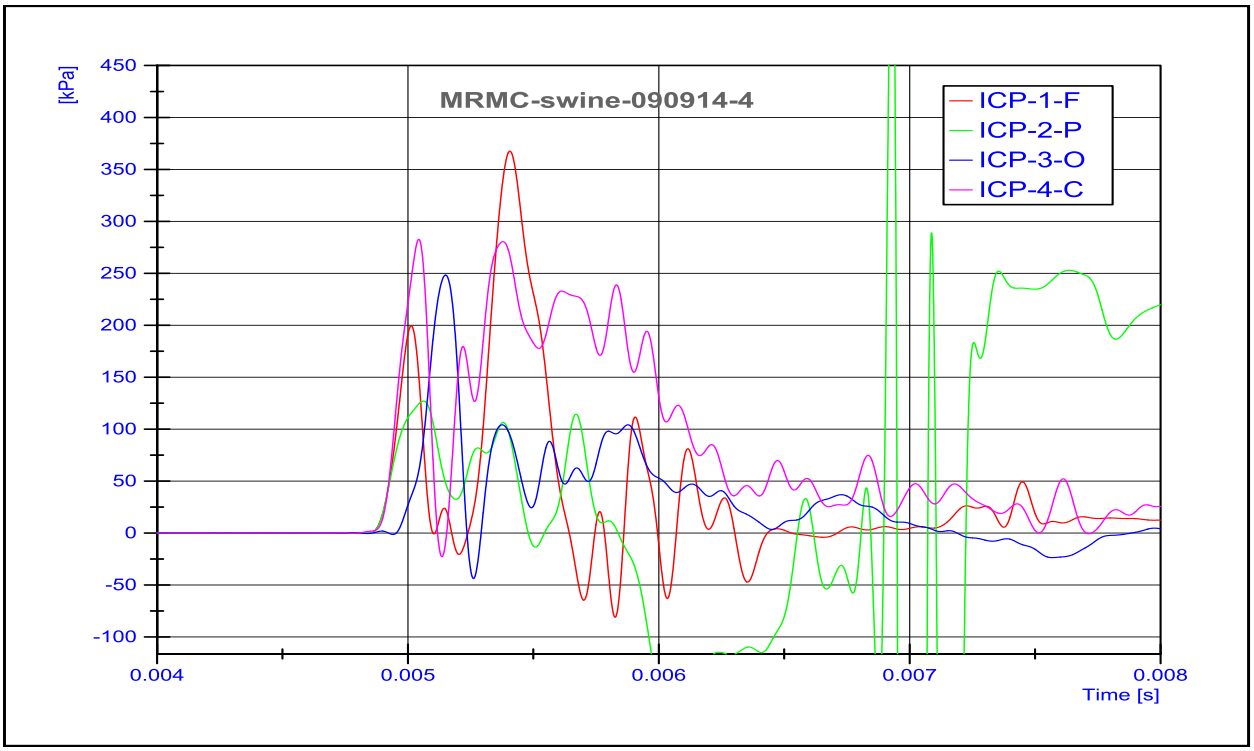


P peak value is discarded.

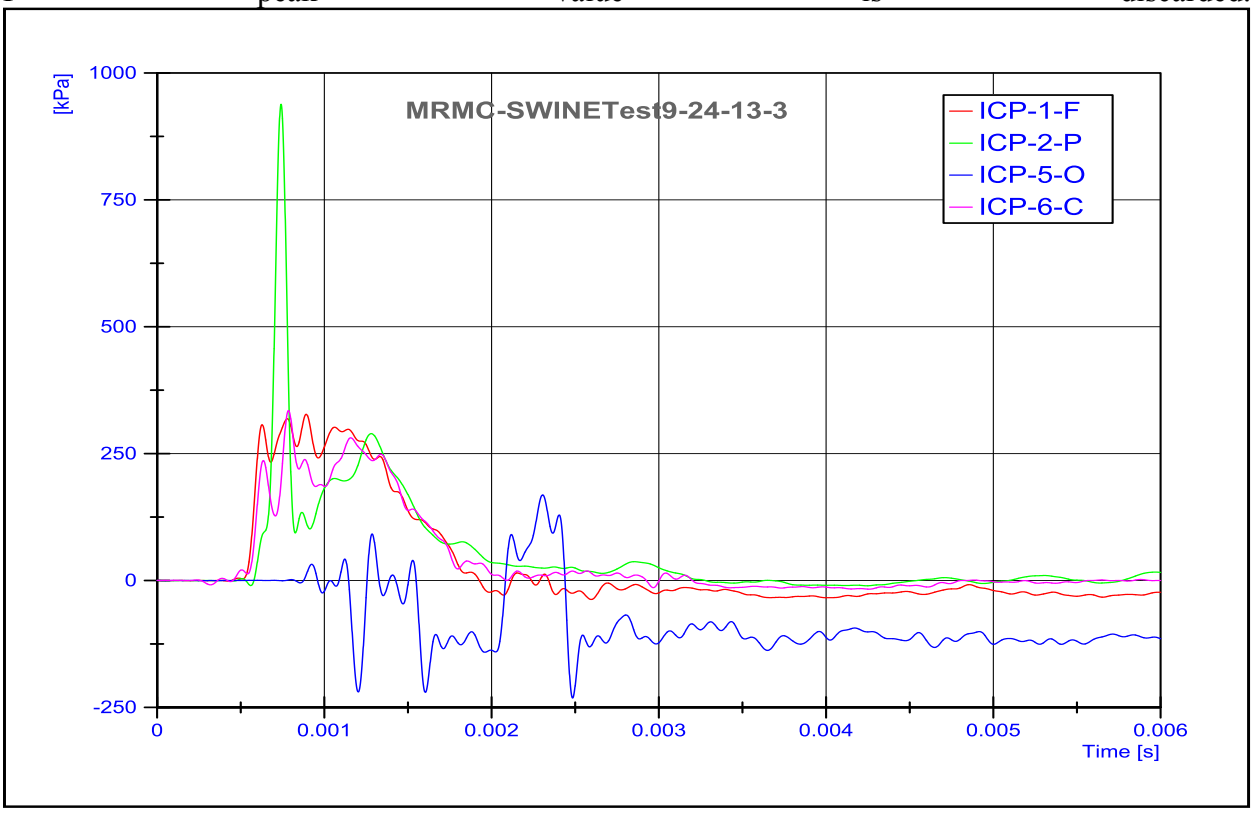


O is discarded. P looks questionable.

O

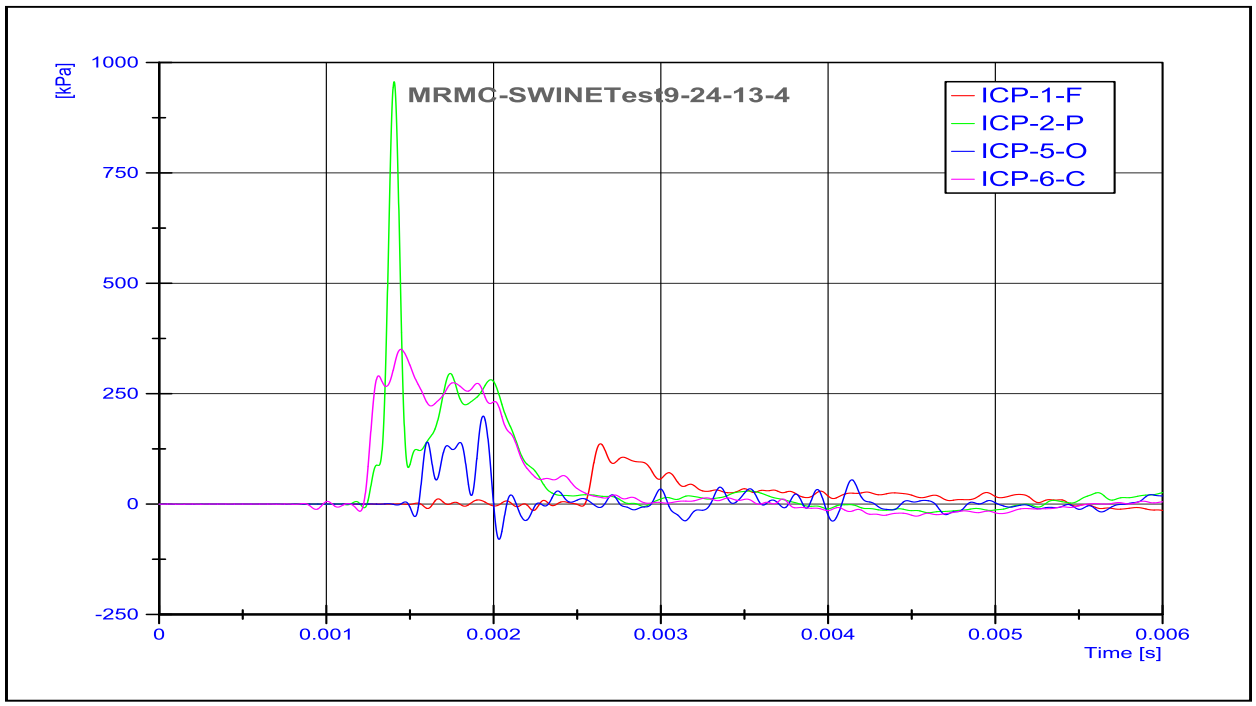


F and O are discarded. P looks questionable.

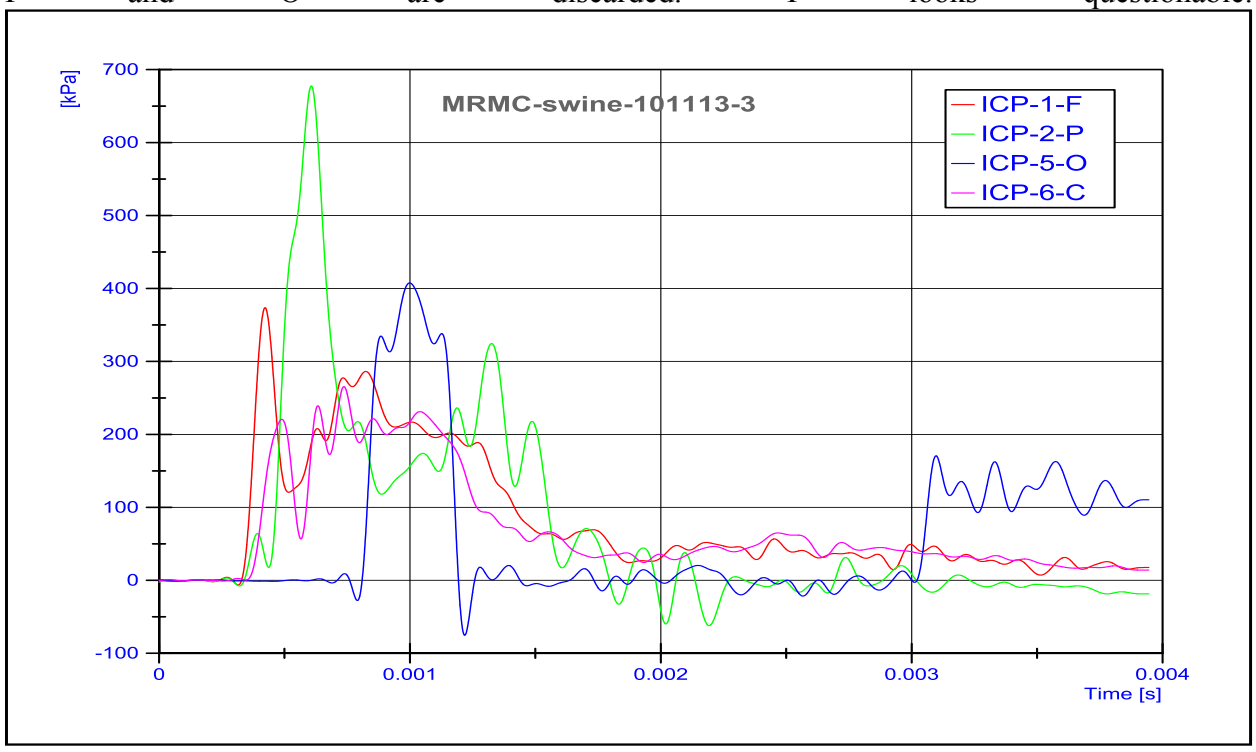


O is discarded due to late rise time. P is questionable.

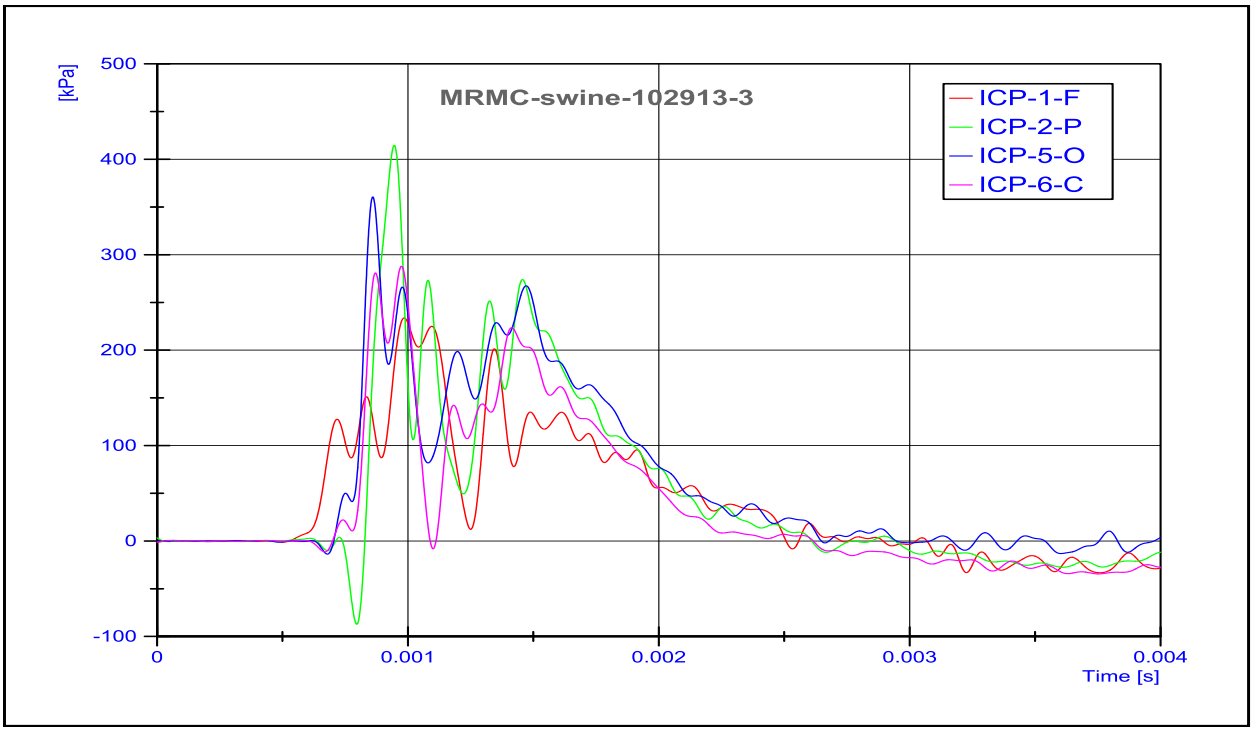


Data looks normal and peak values are validated.

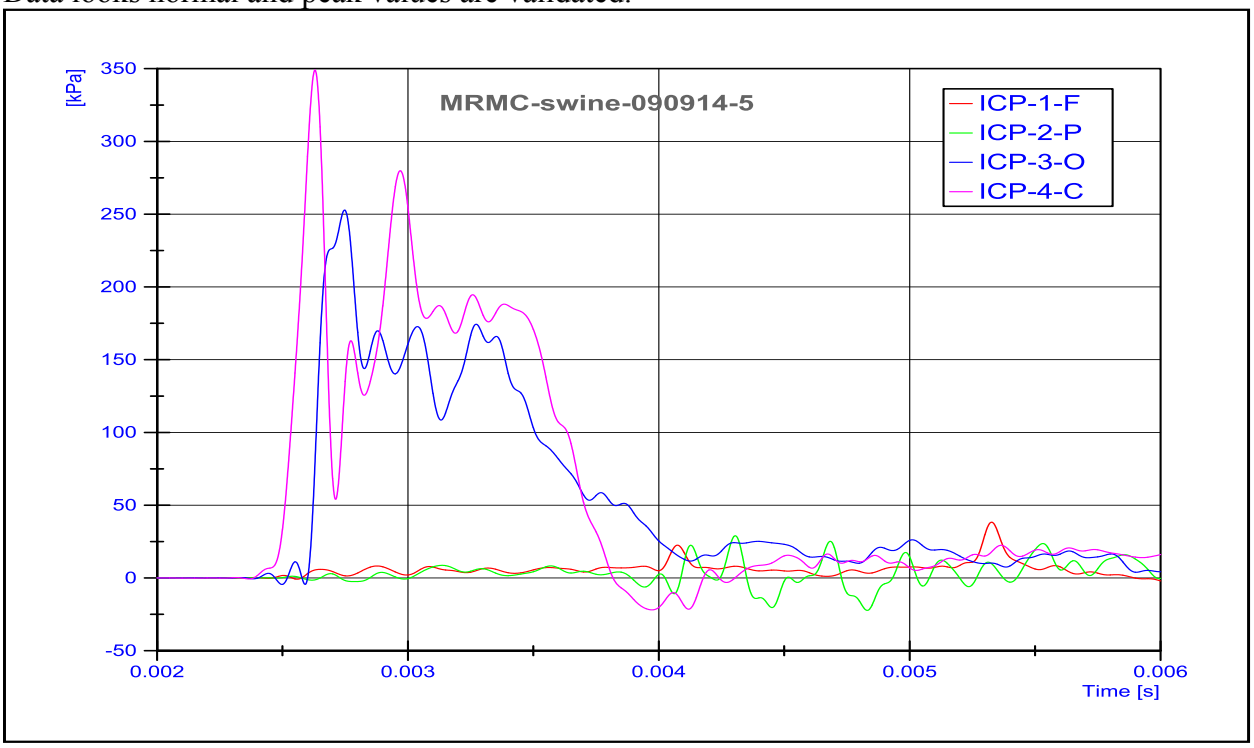


F and P are discarded due to abnormal readings.

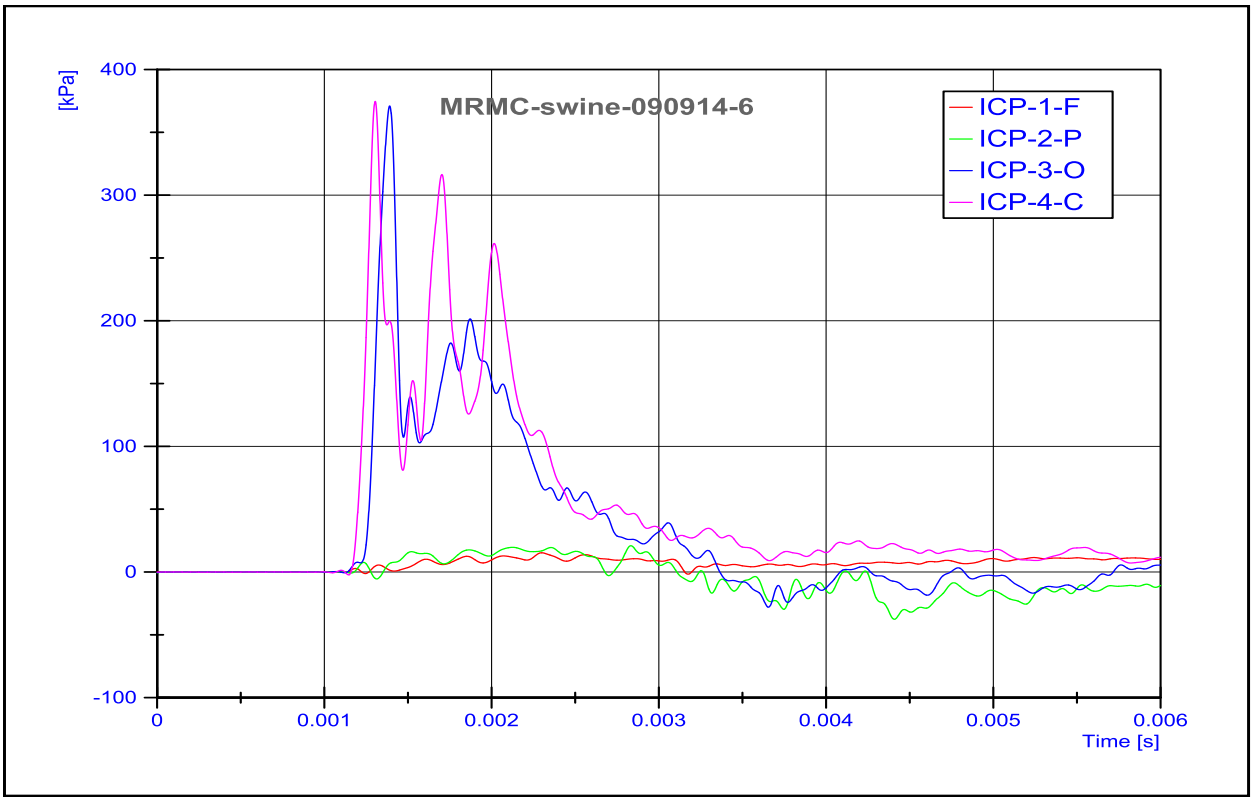


F and P are discarded due to abnormal readings.

## APPENDIX B: ACCELERATION CURVE

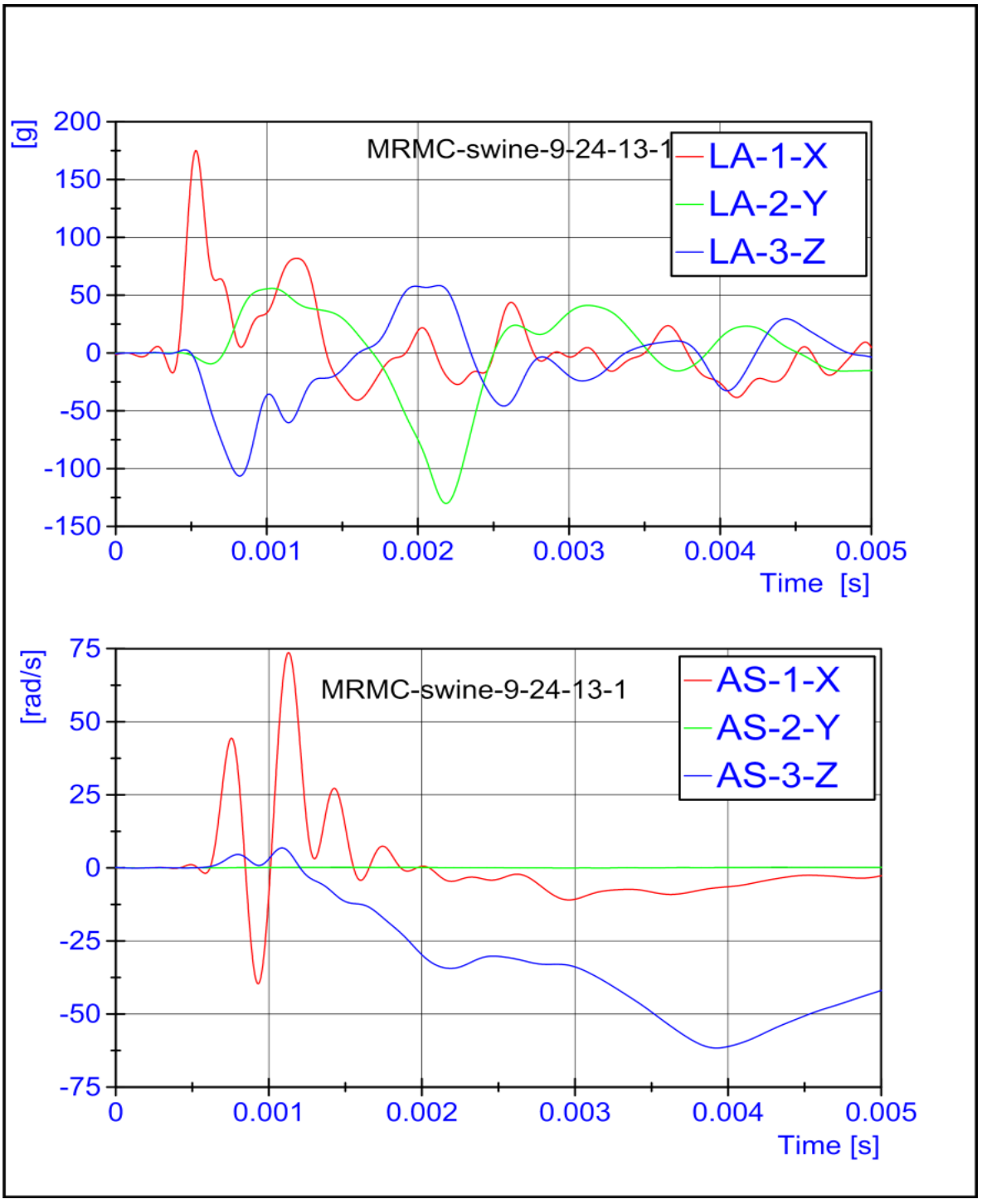

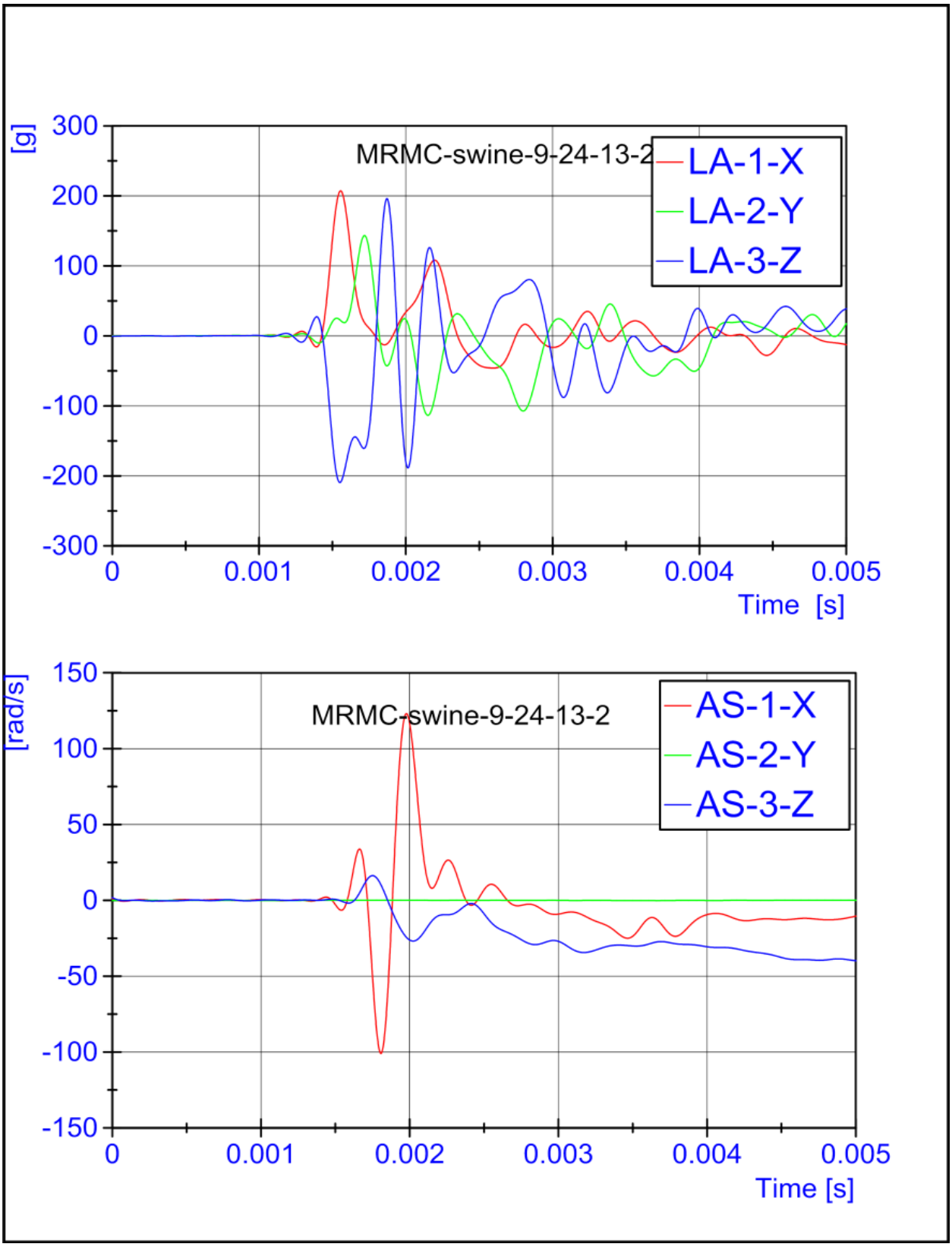
[g]
300
200
100
0
-100
-200
-300
MRMC-swine-9-24-13-2
LA-1-X
LA-2-Y
LA-3-Z
0
0.001
0.002
0.003
0.004
0.005
Time [s]
[rad/s]
150
100
50
0
-50
-100
-150
MRMC-swine-9-24-13-2
AS-1-X
AS-2-Y
AS-3-Z
0
0.001
0.002
0.003
0.004
0.005
Time [s]

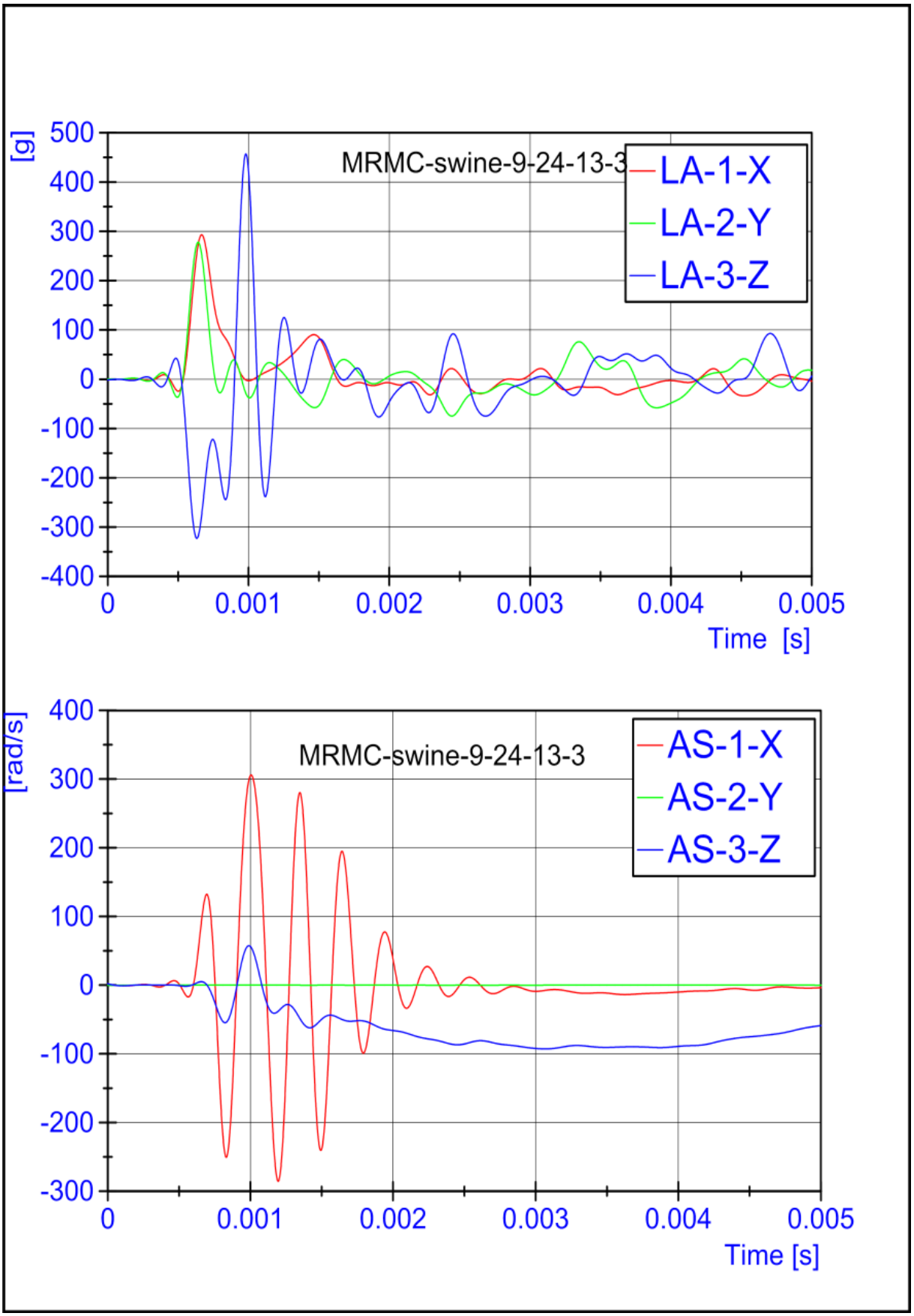
[g]
500
400
300
200
100
0
-100
-200
-300
-400
MRMC-swine-9-24-13-3
LA-1-X
LA-2-Y
LA-3-Z
0
0.001
0.002
0.003
0.004
0.005
Time [s]
[rad/s]
400
300
200
100
0
-100
-200
-300
MRMC-swine-9-24-13-3
AS-1-X
AS-2-Y
AS-3-Z
0
0.001
0.002
0.003
0.004
0.005
Time [s]

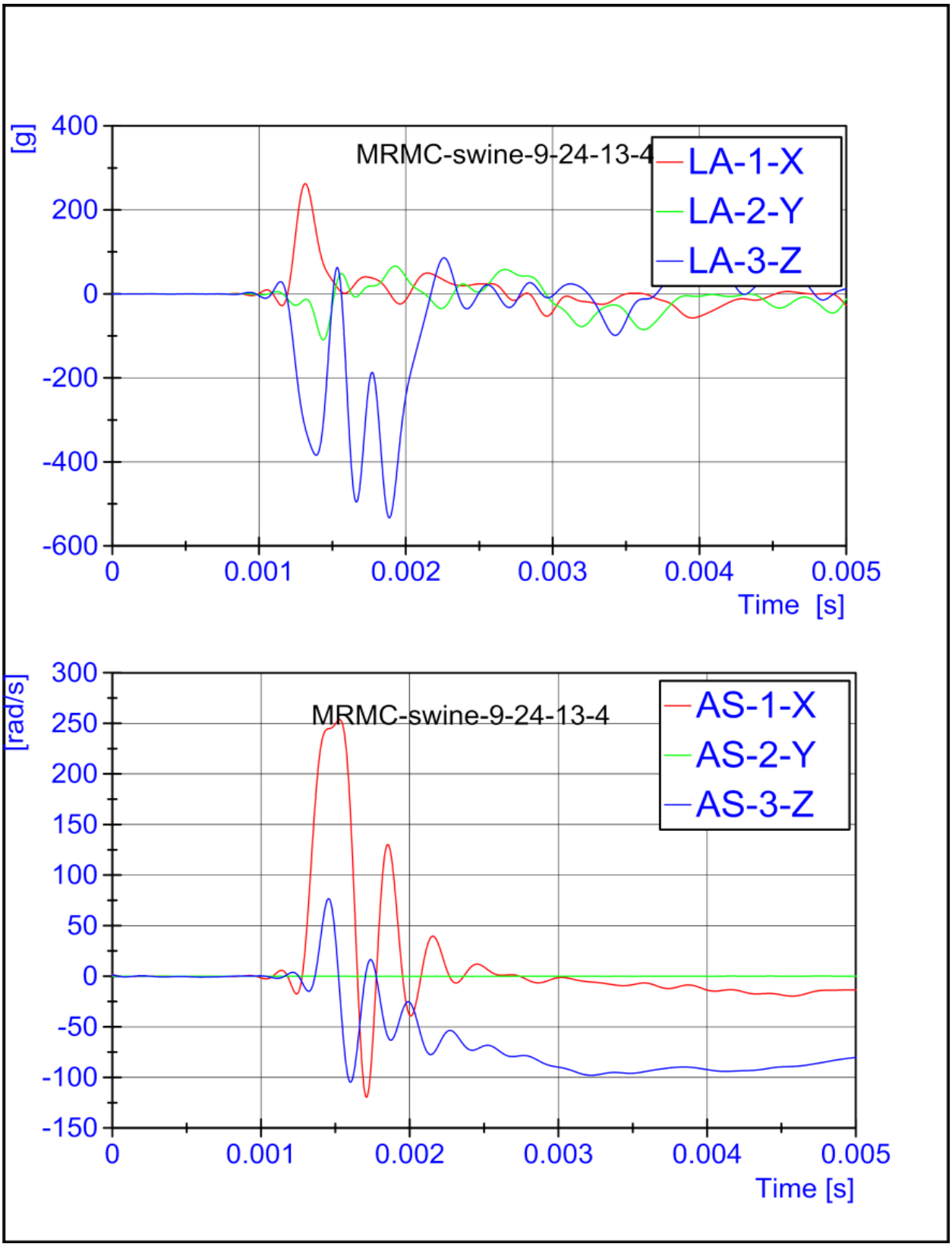
[g]
400
200
0
-200
-400
-600
MRMC-swine-9-24-13-4
LA-1-X
LA-2-Y
LA-3-Z
0
0.001
0.002
0.003
0.004
0.005
Time [s]
[rad/s]
300
250
200
150
100
50
0
-50
-100
-150
MRMC-swine-9-24-13-4
AS-1-X
AS-2-Y
AS-3-Z
0
0.001
0.002
0.003
0.004
0.005
Time [s]

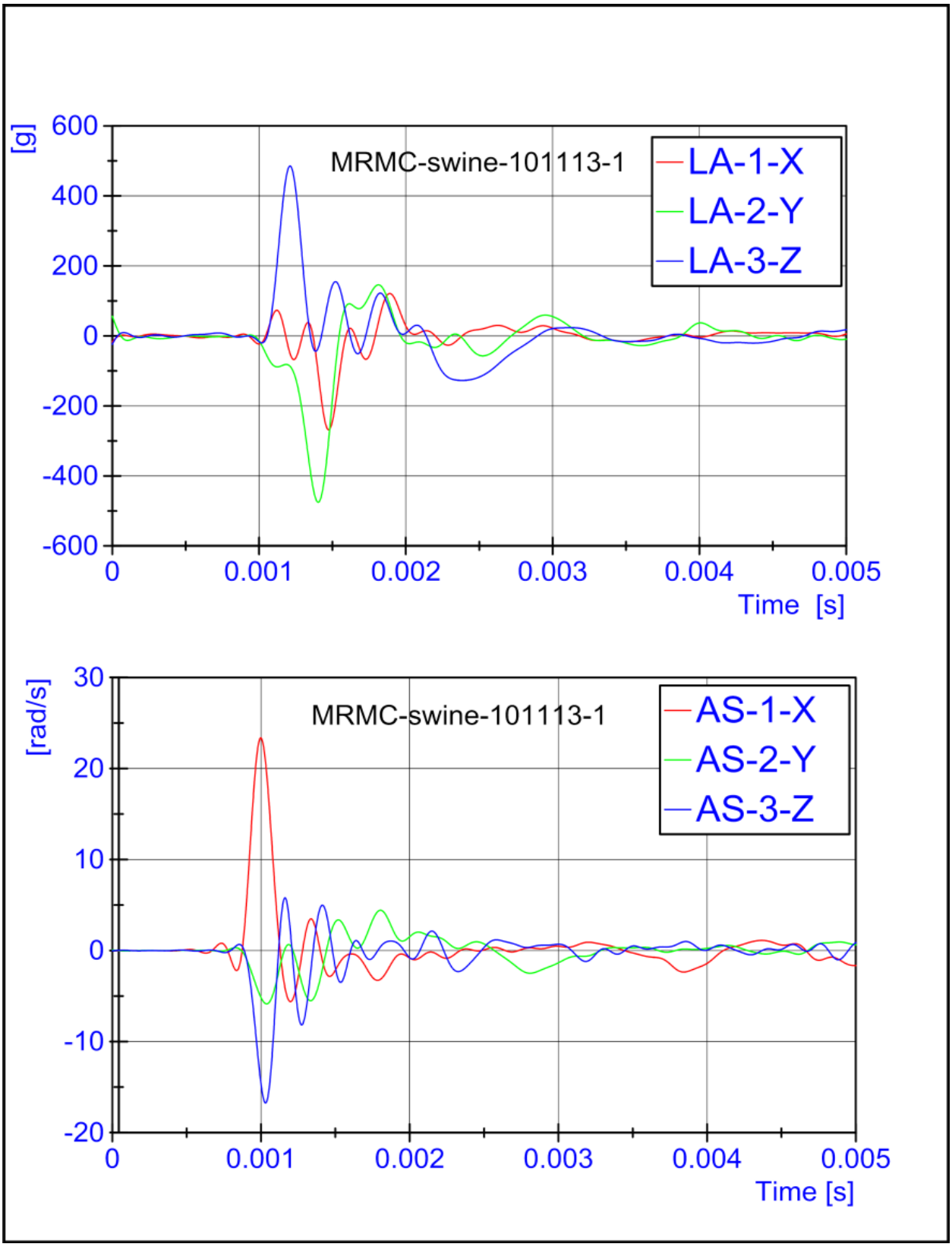
[g]
600
400
200
0
-200
-400
-600
MRMC-swine-101113-1
LA-1-X
LA-2-Y
LA-3-Z
0
0.001
0.002
0.003
0.004
0.005
Time [s]
[rad/s]
30
20
10
0
-10
-20
MRMC-swine-101113-1
AS-1-X
AS-2-Y
AS-3-Z
0
0.001
0.002
0.003
0.004
0.005
Time [s]

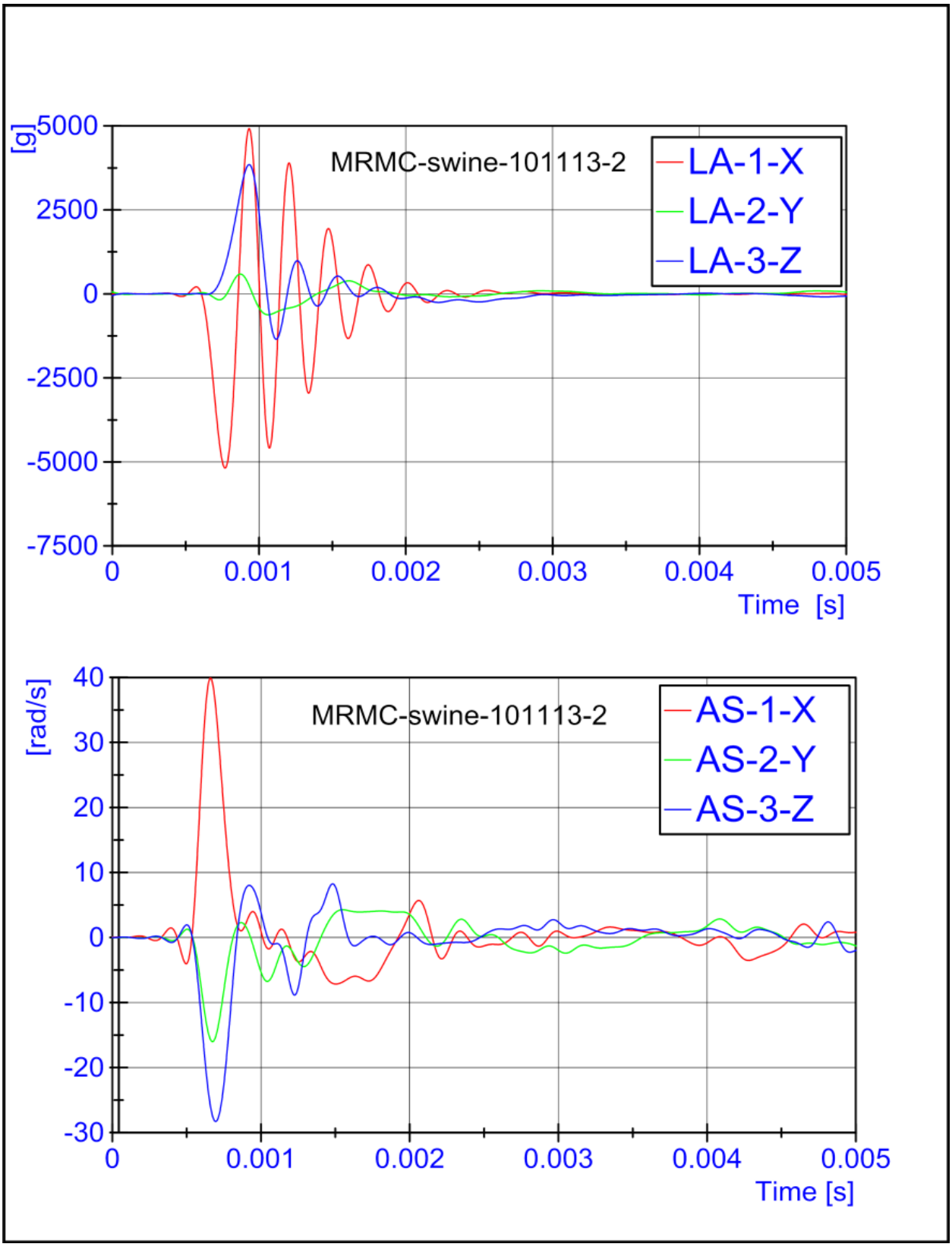
[g]
5000
2500
0
-2500
-5000
-7500
MRMC-swine-101113-2
LA-1-X
LA-2-Y
LA-3-Z
0
0.001
0.002
0.003
0.004
0.005
Time [s]
[rad/s]
40
30
20
10
0
-10
-20
-30
MRMC-swine-101113-2
AS-1-X
AS-2-Y
AS-3-Z
0
0.001
0.002
0.003
0.004
0.005
Time [s]

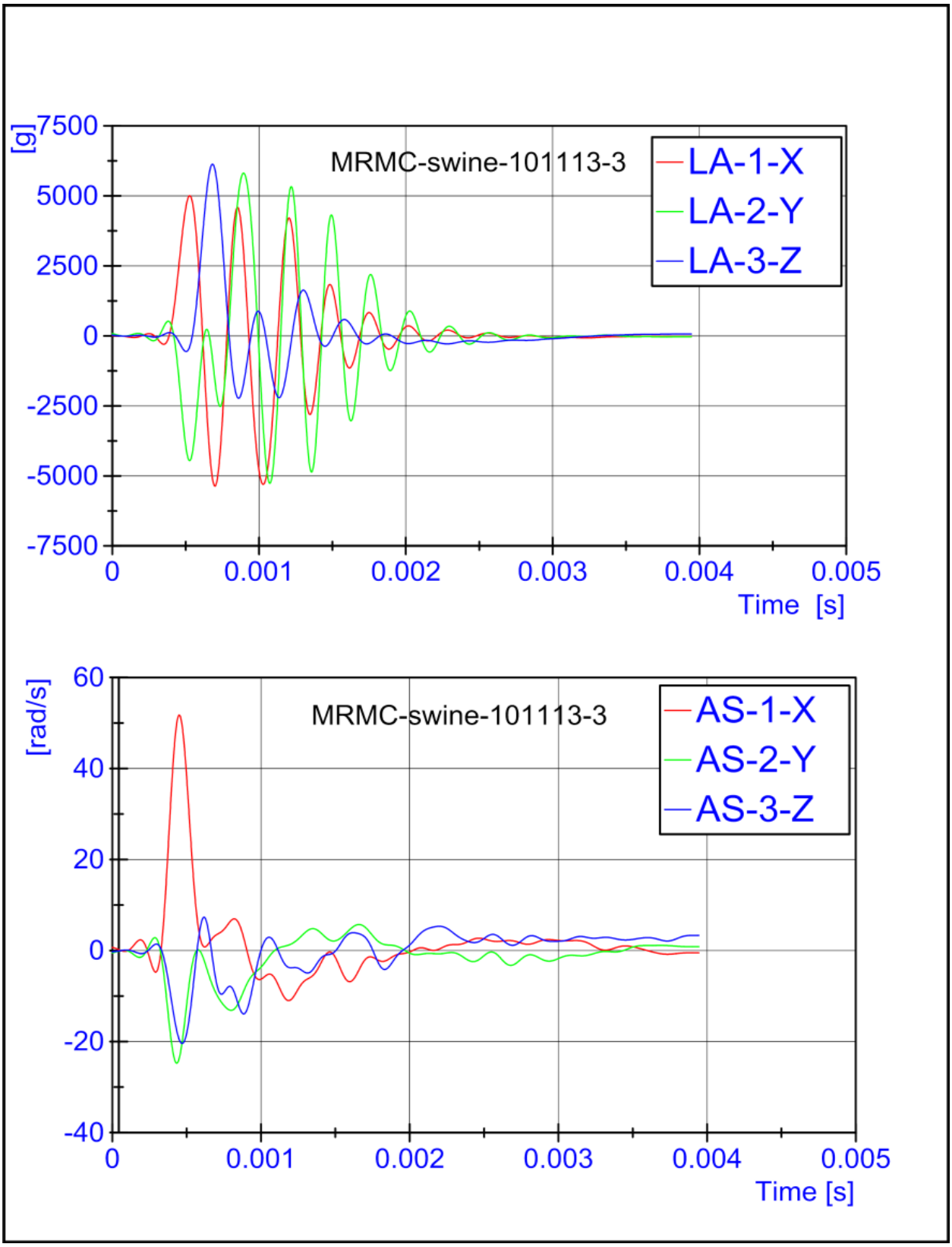
[g]
7500
5000
2500
0
-2500
-5000
-7500
MRMC-swine-101113-3
LA-1-X
LA-2-Y
LA-3-Z
0
0.001
0.002
0.003
0.004
0.005
Time [s]
[rad/s]
60
40
20
0
-20
-40
MRMC-swine-101113-3
AS-1-X
AS-2-Y
AS-3-Z
0
0.001
0.002
0.003
0.004
0.005
Time [s]

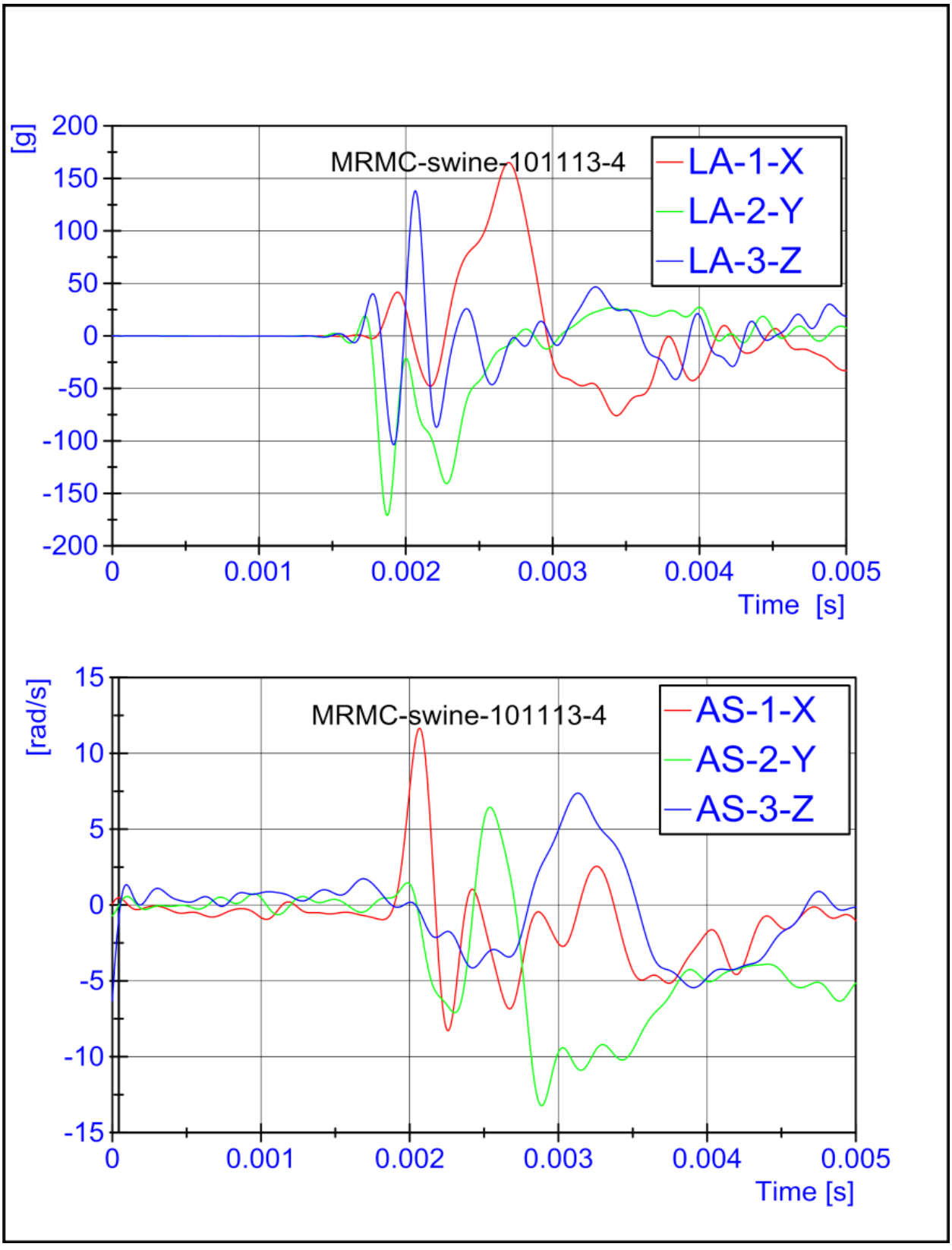
[g]
200
150
100
50
0
-50
-100
-150
-200
MRMC-swine-101113-4
LA-1-X
LA-2-Y
LA-3-Z
0
0.001
0.002
0.003
0.004
0.005
Time [s]
[rad/s]
15
10
5
0
-5
-10
-15
MRMC-swine-101113-4
AS-1-X
AS-2-Y
AS-3-Z
0
0.001
0.002
0.003
0.004
0.005
Time [s]

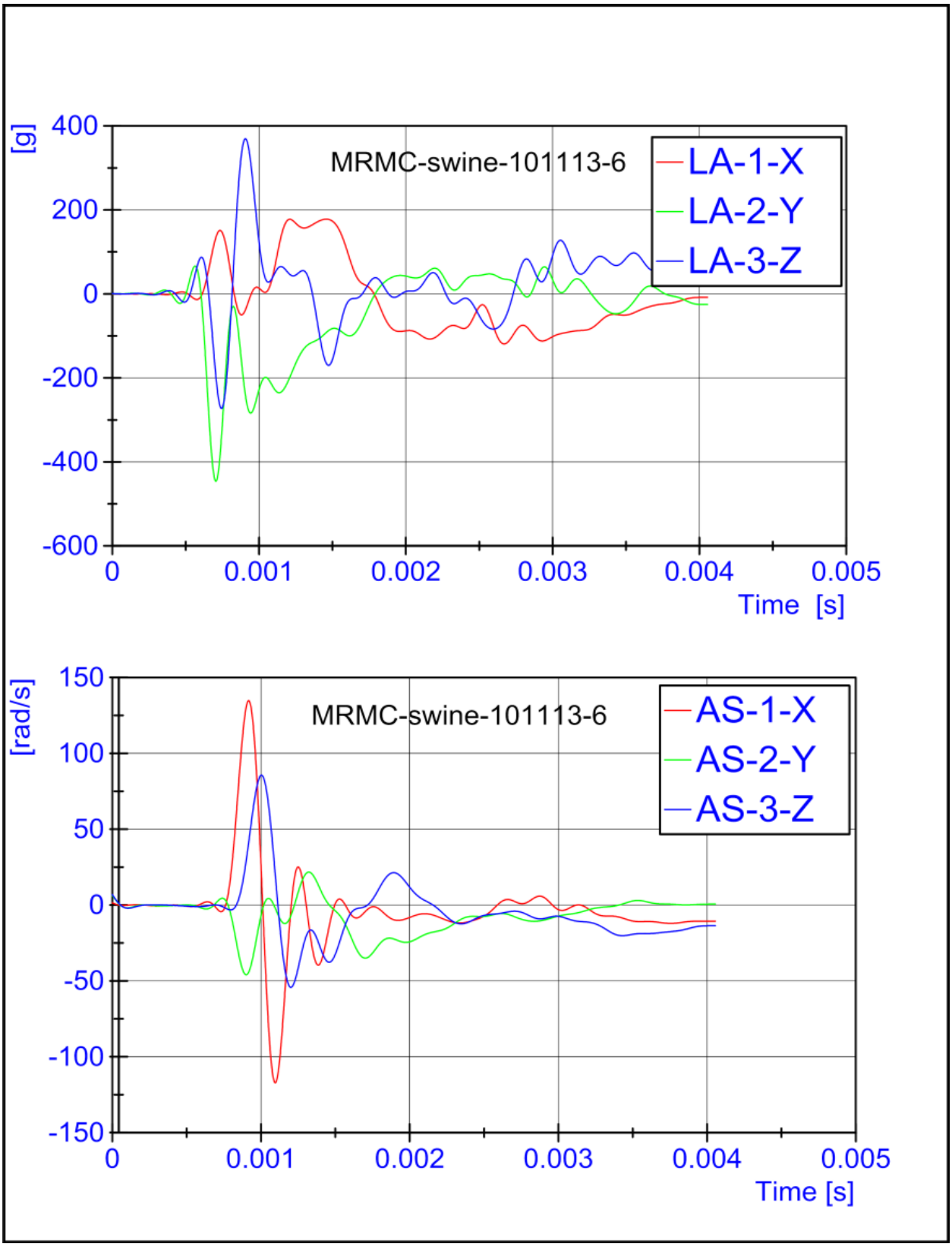
[g]
400
200
0
-200
-400
-600
MRMC-swine-101113-6
LA-1-X
LA-2-Y
LA-3-Z
0
0.001
0.002
0.003
0.004
0.005
Time [s]
[rad/s]
150
100
50
0
-50
-100
-150
MRMC-swine-101113-6
AS-1-X
AS-2-Y
AS-3-Z
0
0.001
0.002
0.003
0.004
0.005
Time [s]

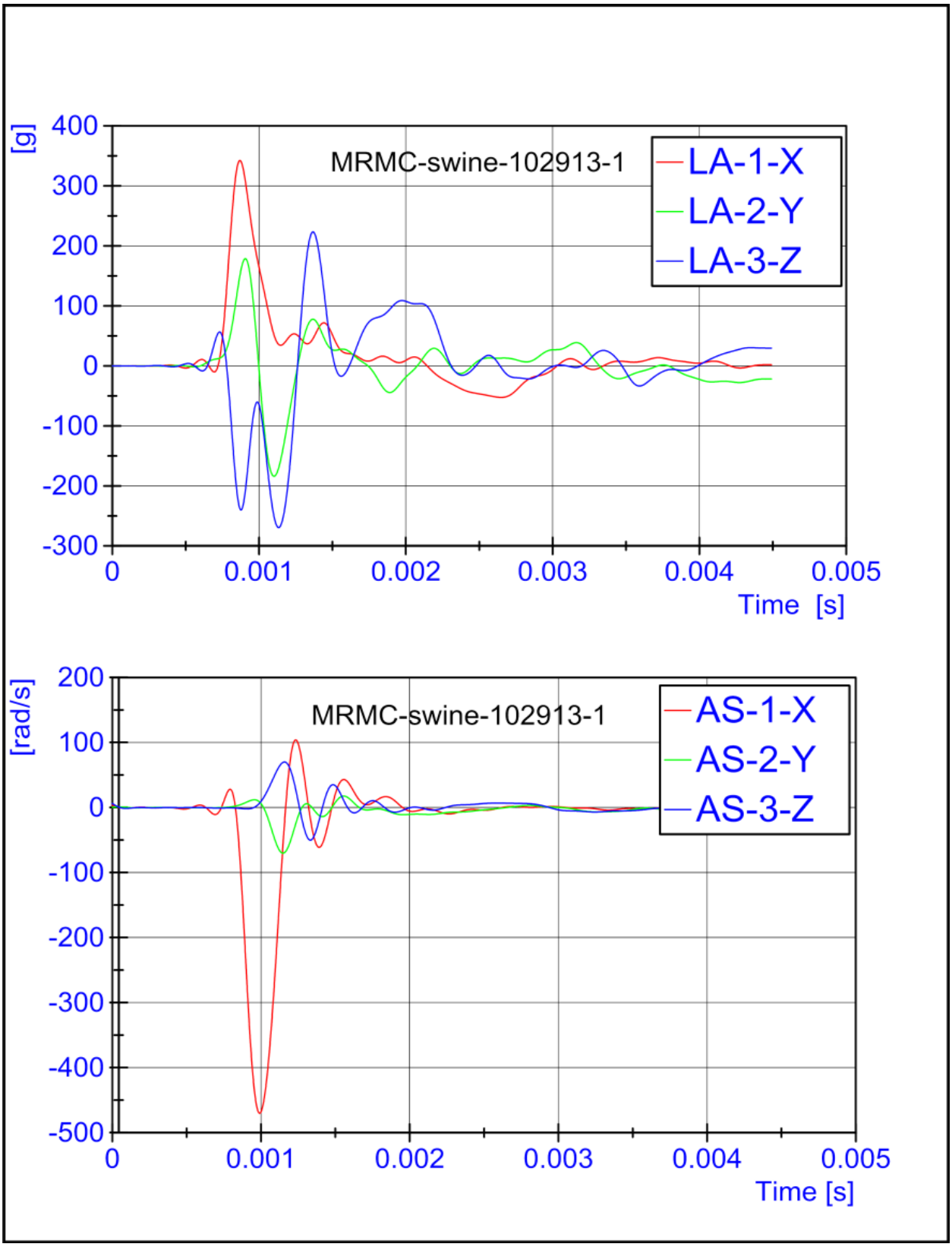
[g]
400
300
200
100
0
-100
-200
-300
MRMC-swine-102913-1
LA-1-X
LA-2-Y
LA-3-Z
0
0.001
0.002
0.003
0.004
0.005
Time [s]
[rad/s]
200
100
0
-100
-200
-300
-400
-500
MRMC-swine-102913-1
AS-1-X
AS-2-Y
AS-3-Z
0
0.001
0.002
0.003
0.004
0.005
Time [s]

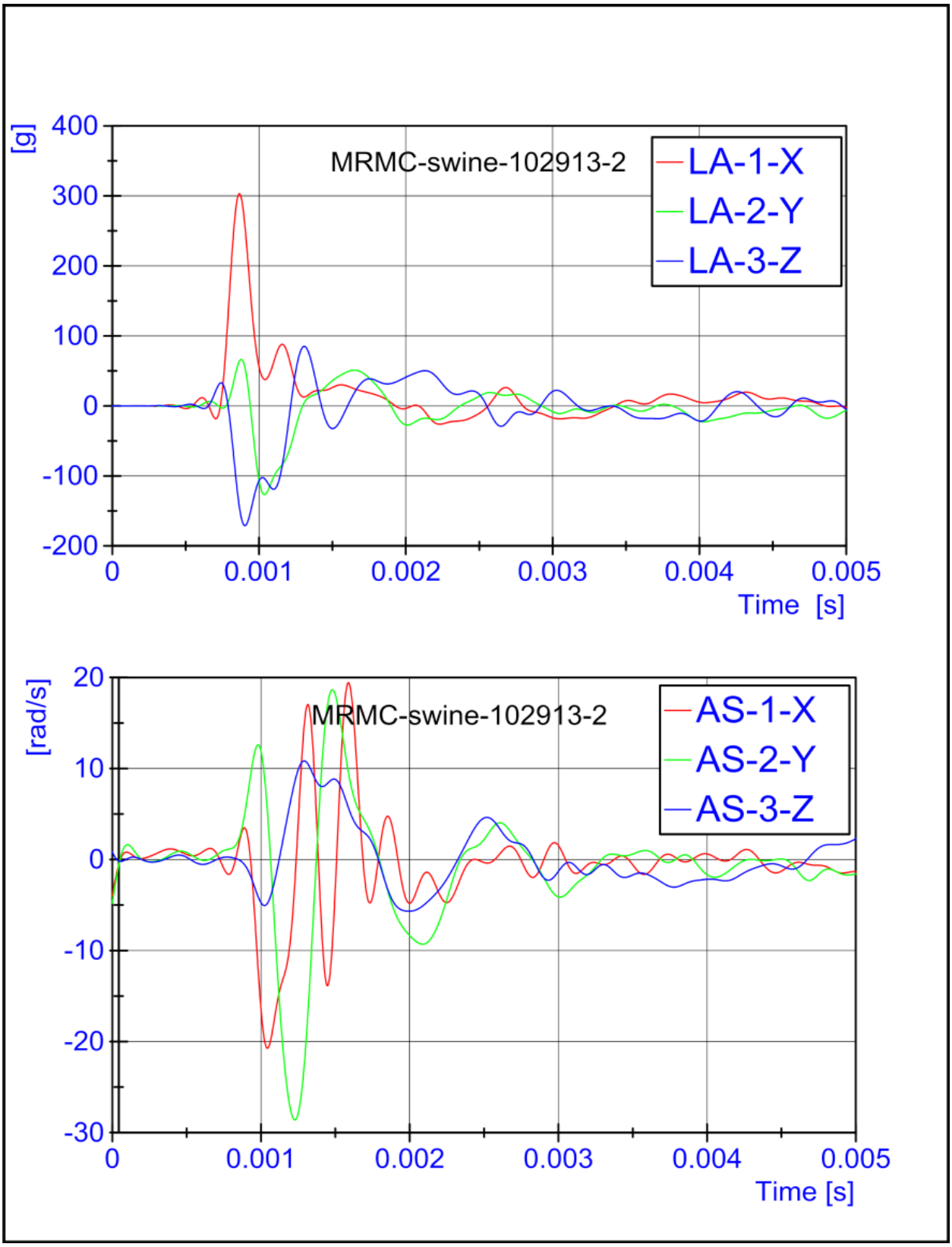
[g]
400
300
200
100
0
-100
-200
MRMC-swine-102913-2
LA-1-X
LA-2-Y
LA-3-Z
0
0.001
0.002
0.003
0.004
0.005
Time [s]
[rad/s]
20
10
0
-10
-20
-30
MRMC-swine-102913-2
AS-1-X
AS-2-Y
AS-3-Z
0
0.001
0.002
0.003
0.004
0.005
Time [s]

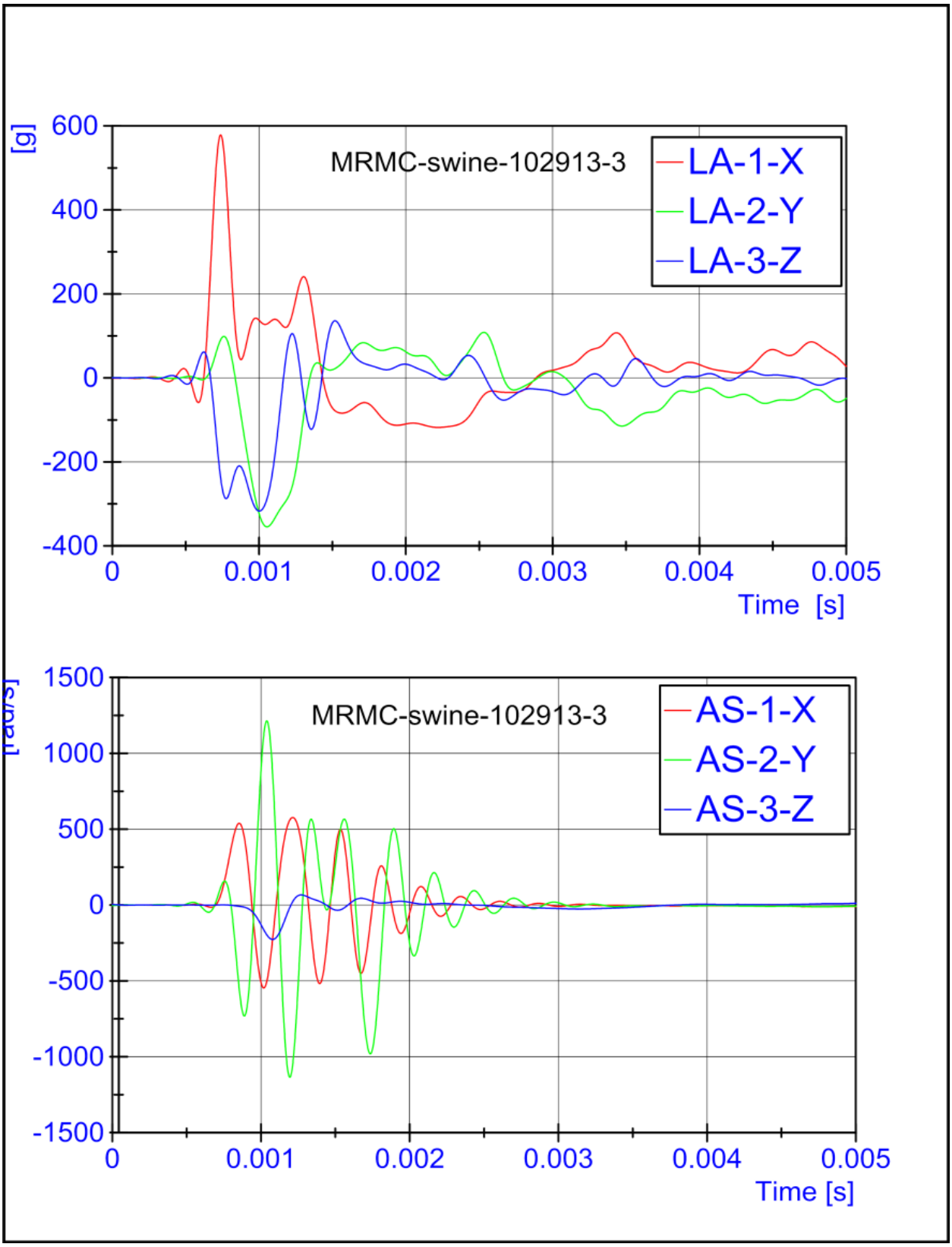
[g]
600
400
200
0
-200
-400
MRMC-swine-102913-3
LA-1-X
LA-2-Y
LA-3-Z
0
0.001
0.002
0.003
0.004
0.005
Time [s]
[rad/s]
1500
1000
500
0
-500
-1000
-1500
MRMC-swine-102913-3
AS-1-X
AS-2-Y
AS-3-Z
0
0.001
0.002
0.003
0.004
0.005
Time [s]

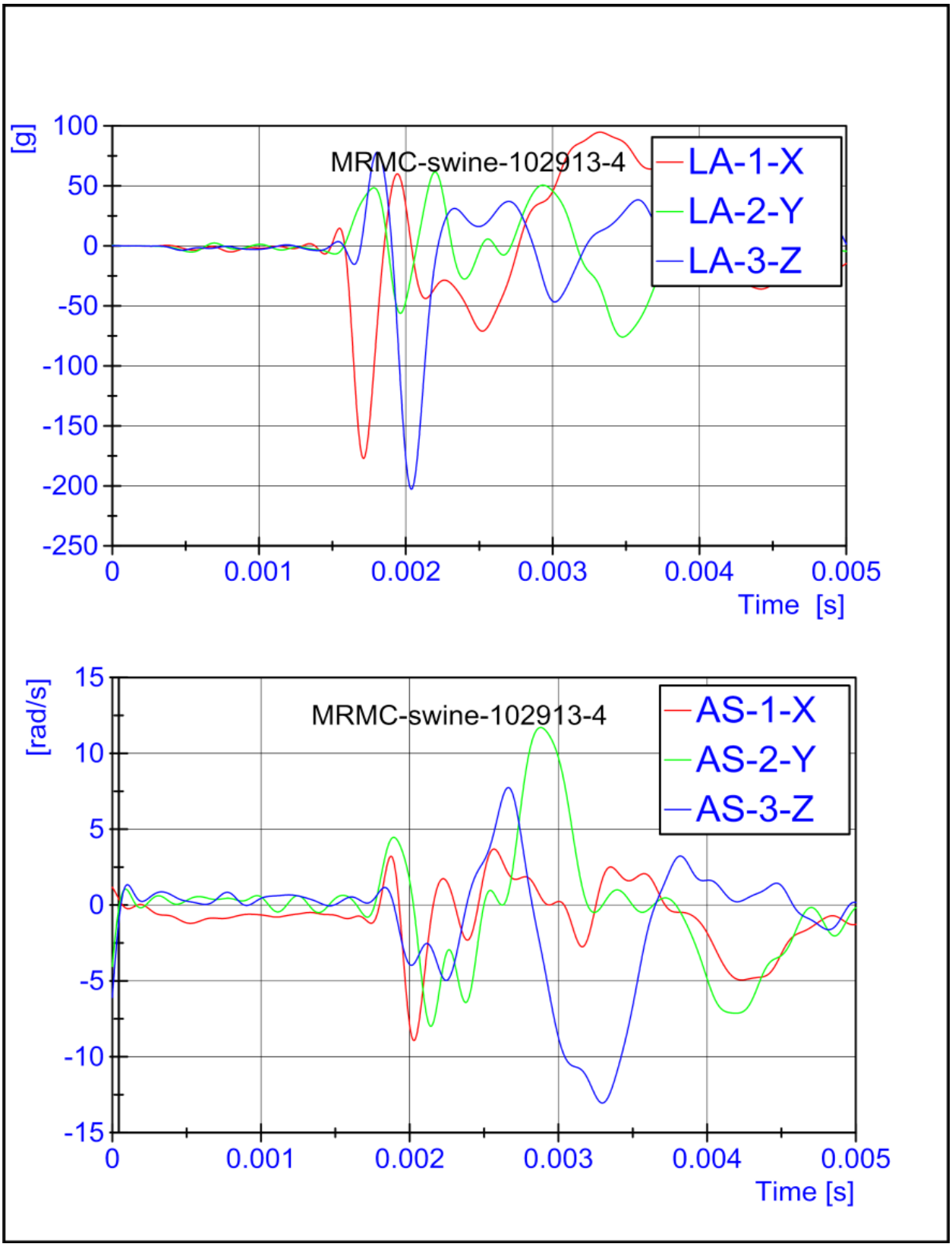
[g]
100
50
0
-50
-100
-150
-200
-250
MRMC-swine-102913-4
LA-1-X
LA-2-Y
LA-3-Z
0
0.001
0.002
0.003
0.004
0.005
Time [s]
[rad/s]
15
10
5
0
-5
-10
-15
MRMC-swine-102913-4
AS-1-X
AS-2-Y
AS-3-Z
0
0.001
0.002
0.003
0.004
0.005
Time [s]

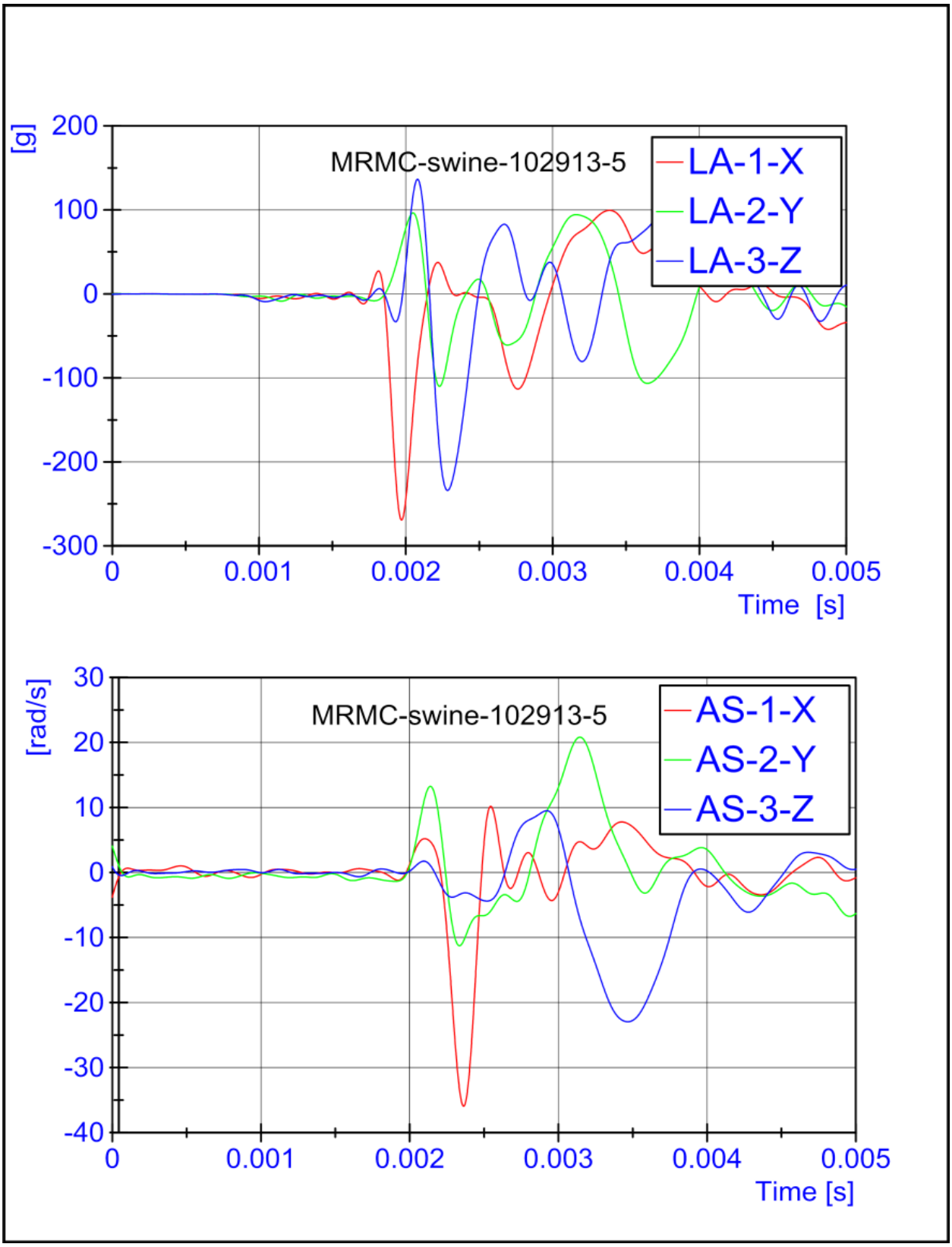
[g]
200
100
0
-100
-200
-300
MRMC-swine-102913-5
LA-1-X
LA-2-Y
LA-3-Z
0
0.001
0.002
0.003
0.004
0.005
Time [s]
[rad/s]
30
20
10
0
-10
-20
-30
-40
MRMC-swine-102913-5
AS-1-X
AS-2-Y
AS-3-Z
0
0.001
0.002
0.003
0.004
0.005
Time [s]

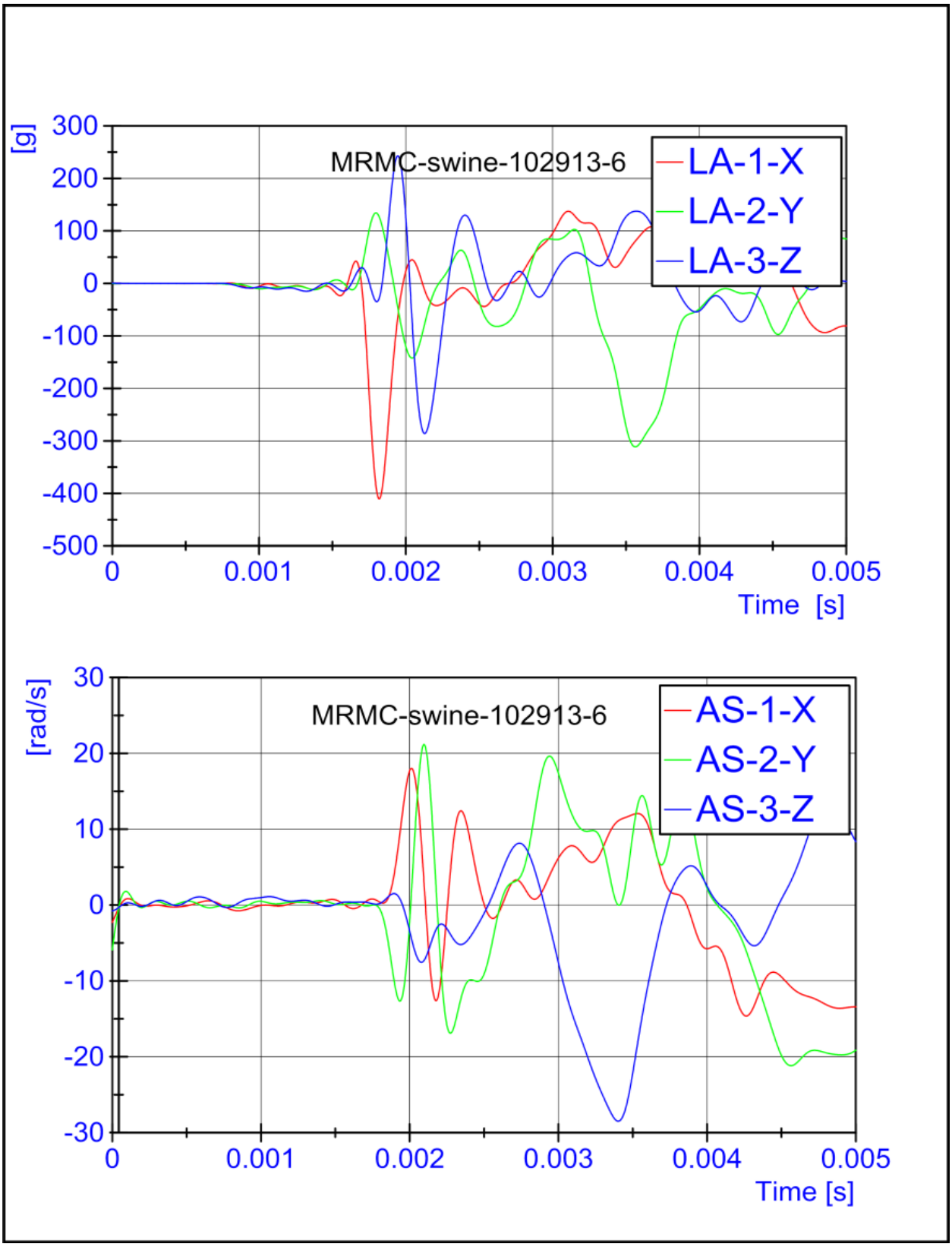
[g]
300
200
100
0
-100
-200
-300
-400
-500
MRMC-swine-102913-6
LA-1-X
LA-2-Y
LA-3-Z
0
0.001
0.002
0.003
0.004
0.005
Time [s]
[rad/s]
30
20
10
0
-10
-20
-30
MRMC-swine-102913-6
AS-1-X
AS-2-Y
AS-3-Z
0
0.001
0.002
0.003
0.004
0.005
Time [s]

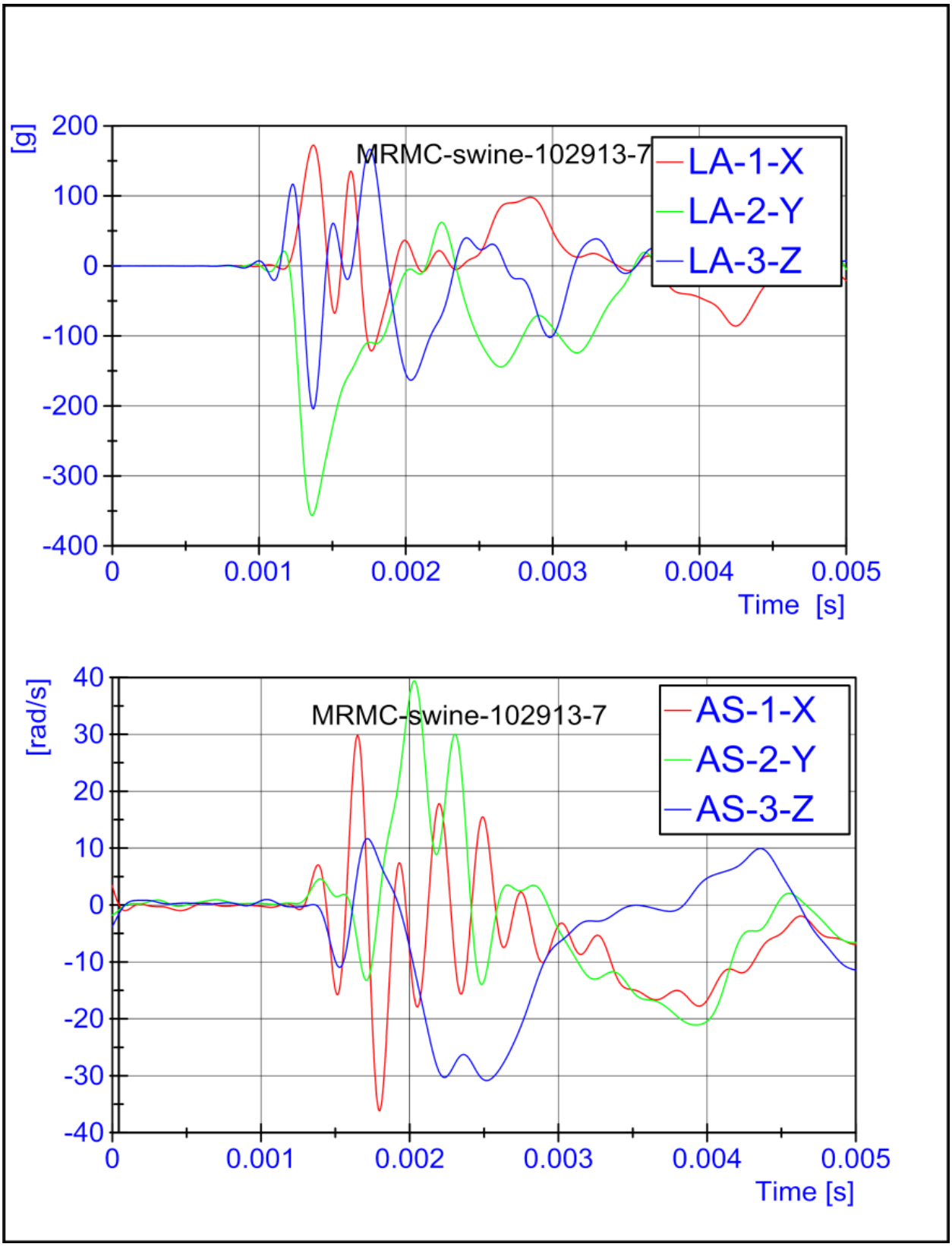
[g]
200
100
0
-100
-200
-300
-400
MRMC-swine-102913-7
LA-1-X
LA-2-Y
LA-3-Z
0
0.001
0.002
0.003
0.004
0.005
Time [s]
[rad/s]
40
30
20
10
0
-10
-20
-30
-40
MRMC-swine-102913-7
AS-1-X
AS-2-Y
AS-3-Z
0
0.001
0.002
0.003
0.004
0.005
Time [s]

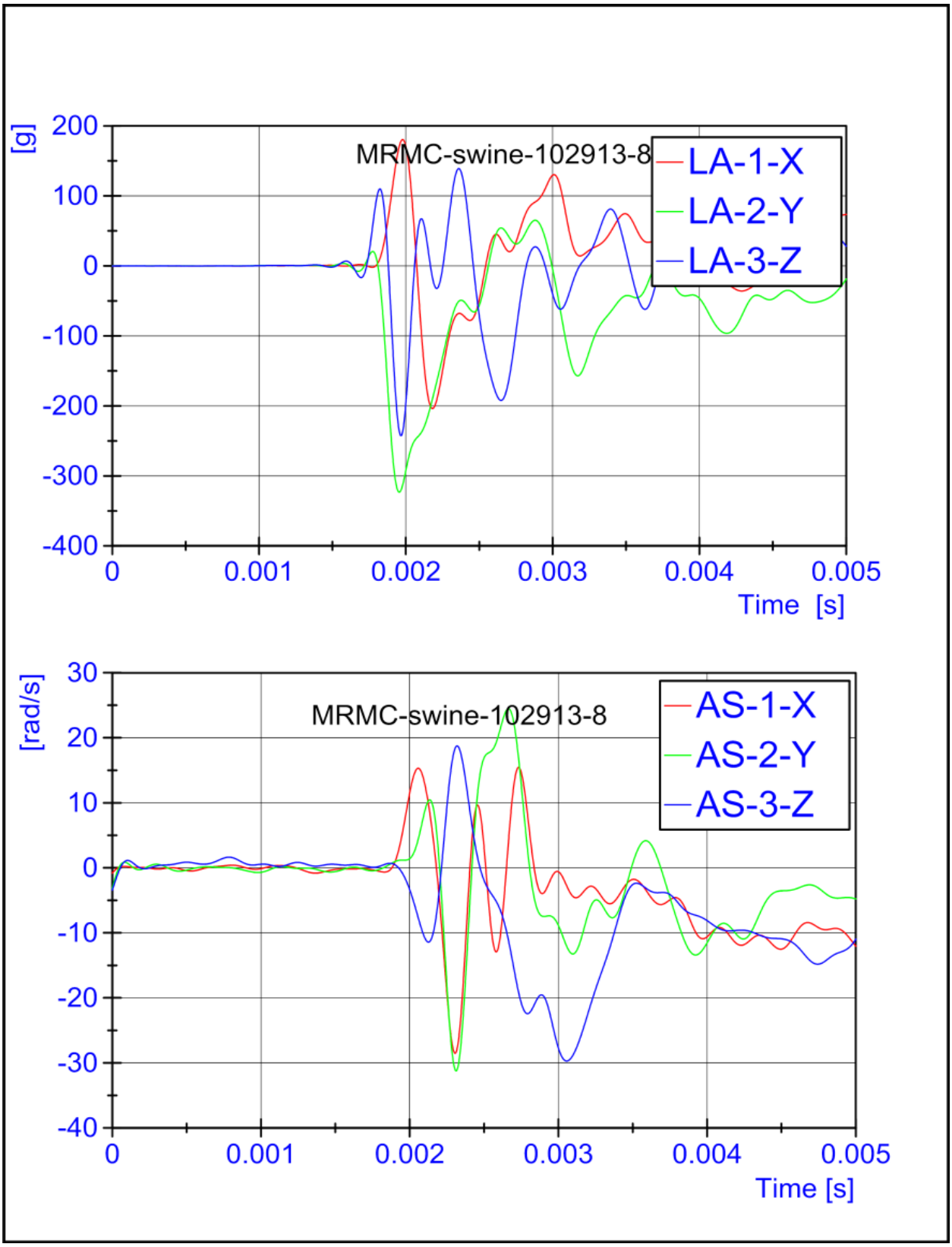
[g]
200
100
0
-100
-200
-300
-400
MRMC-swine-102913-8
LA-1-X
LA-2-Y
LA-3-Z
0
0.001
0.002
0.003
0.004
0.005
Time [s]
[rad/s]
30
20
10
0
-10
-20
-30
-40
MRMC-swine-102913-8
AS-1-X
AS-2-Y
AS-3-Z
0
0.001
0.002
0.003
0.004
0.005
Time [s]

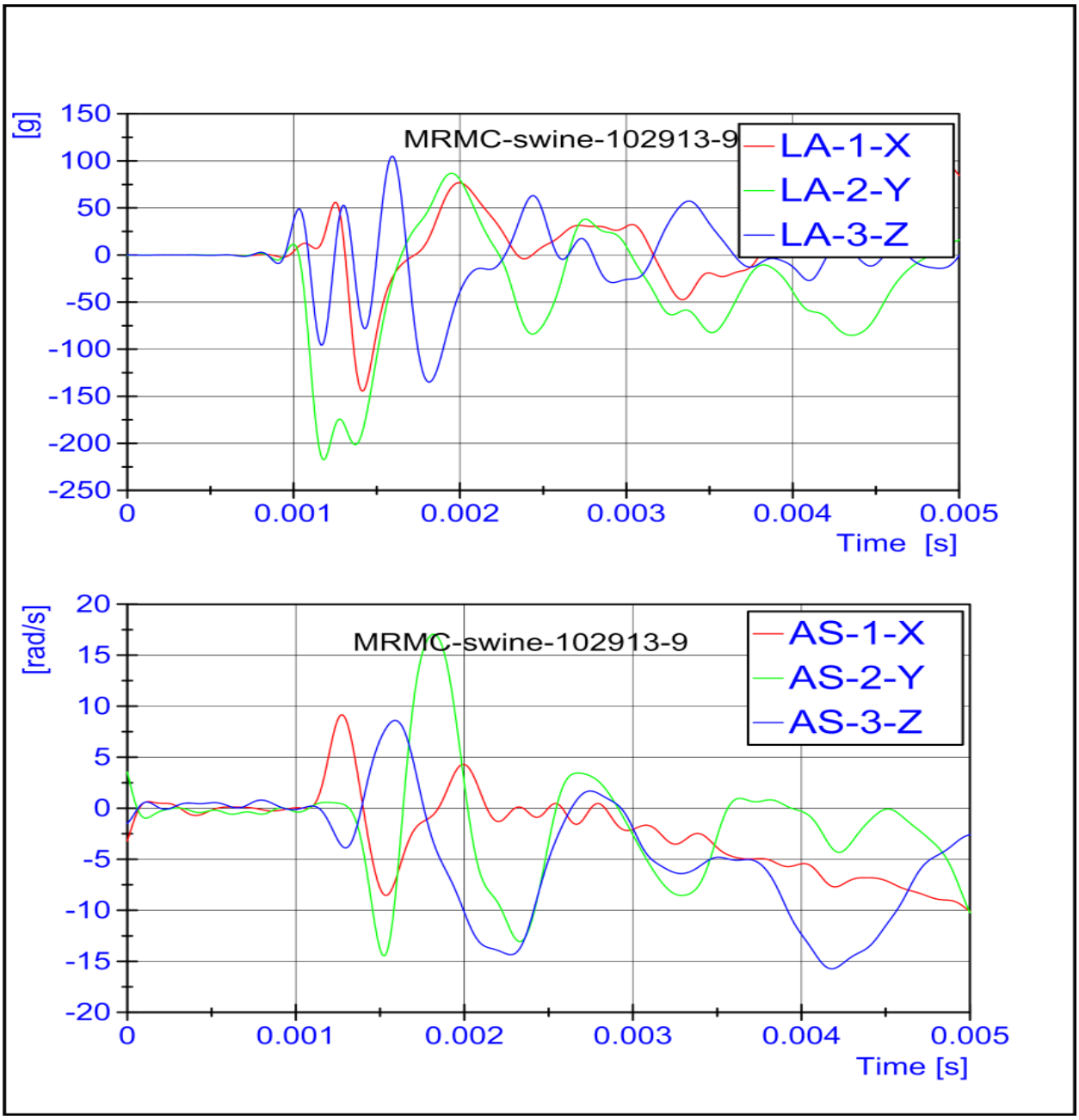
[g]
150
100
50
0
-50
-100
-150
-200
-250
MRMC-swine-102913-9
LA-1-X
LA-2-Y
LA-3-Z
0
0.001
0.002
0.003
0.004
0.005
Time [s]
[rad/s]
20
15
10
5
0
-5
-10
-15
-20
MRMC-swine-102913-9
AS-1-X
AS-2-Y
AS-3-Z
0
0.001
0.002
0.003
0.004
0.005
Time [s]

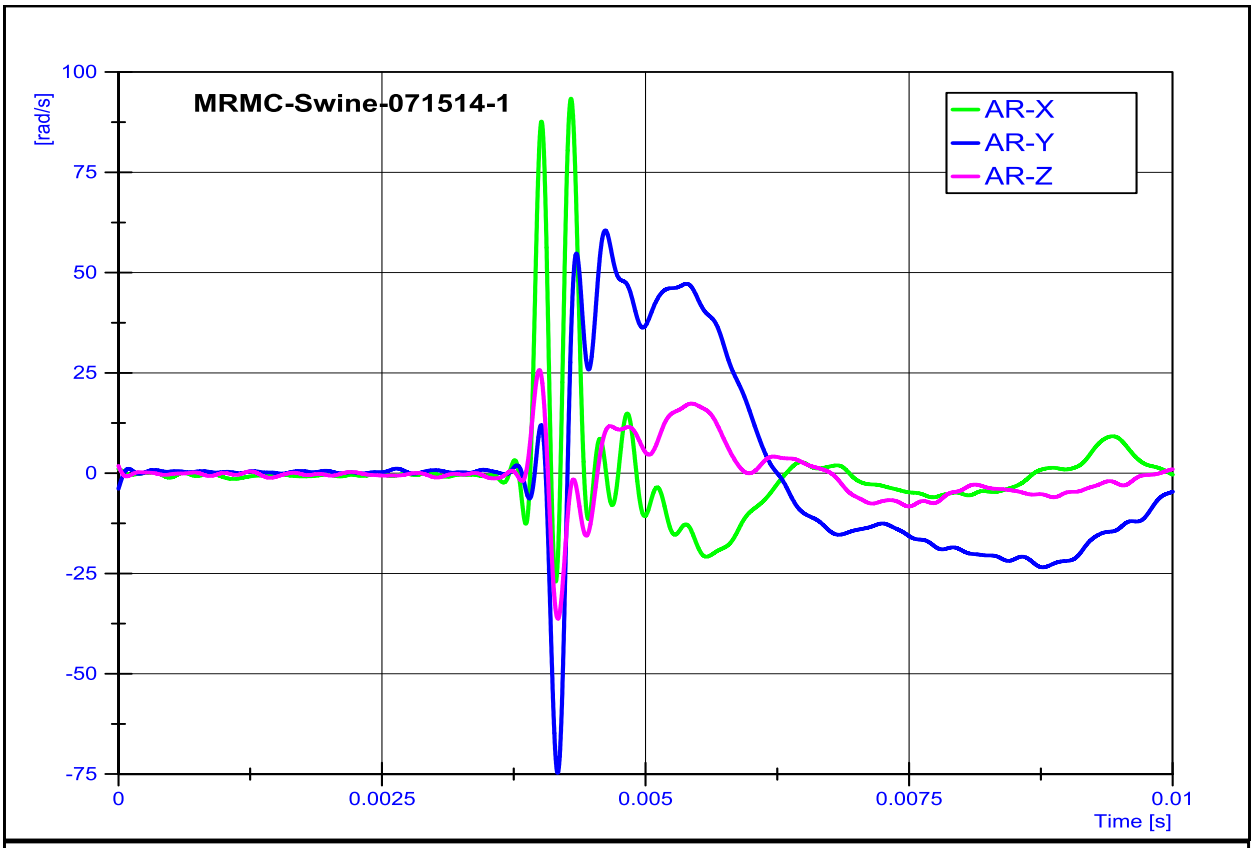
MRMC-Swine-071514-1
AR-X
AR-Y
AR-Z
[rad/s]
100
75
50
25
0
-25
-50
-75
0
0.0025
0.005
0.0075
0.01
Time [s]

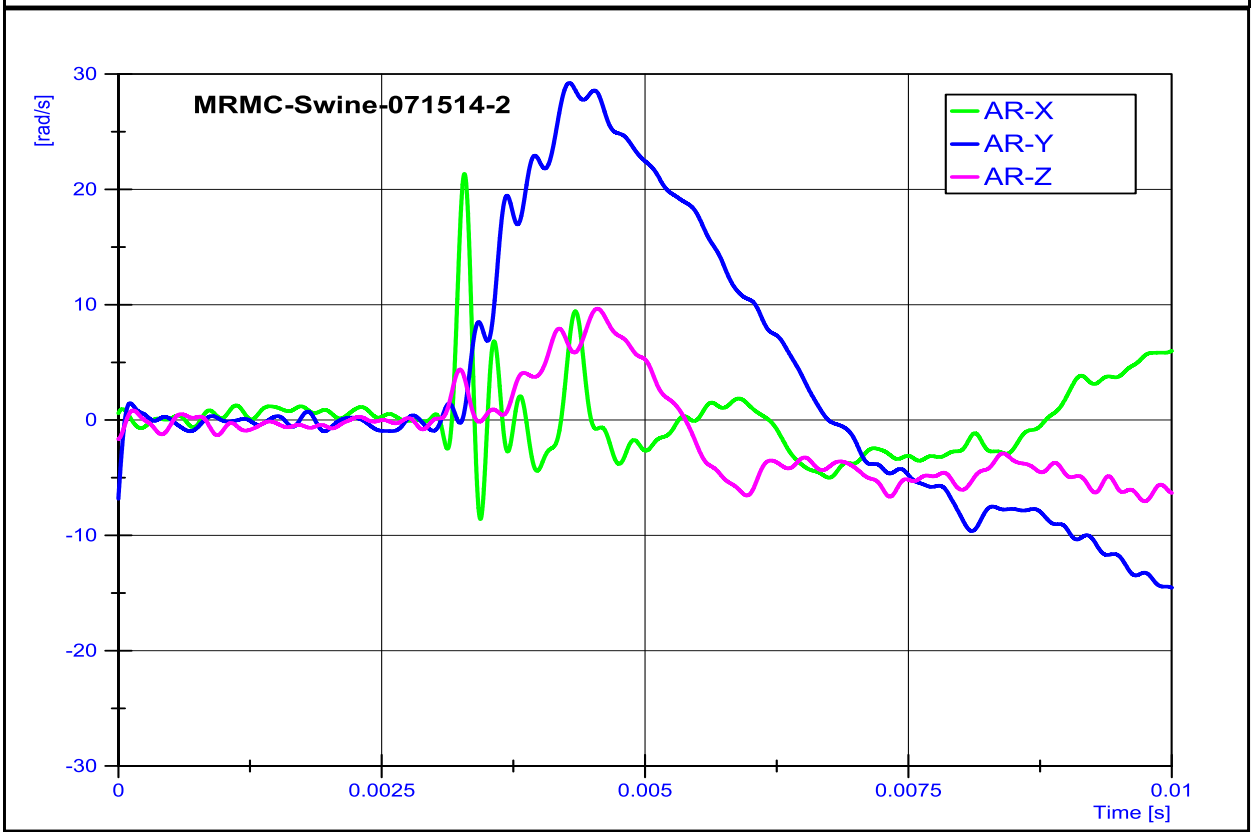
MRMC-Swine-071514-2
AR-X
AR-Y
AR-Z
[rad/s]
30
20
10
0
-10
-20
-30
0
0.0025
0.005
0.0075
0.01
Time [s]

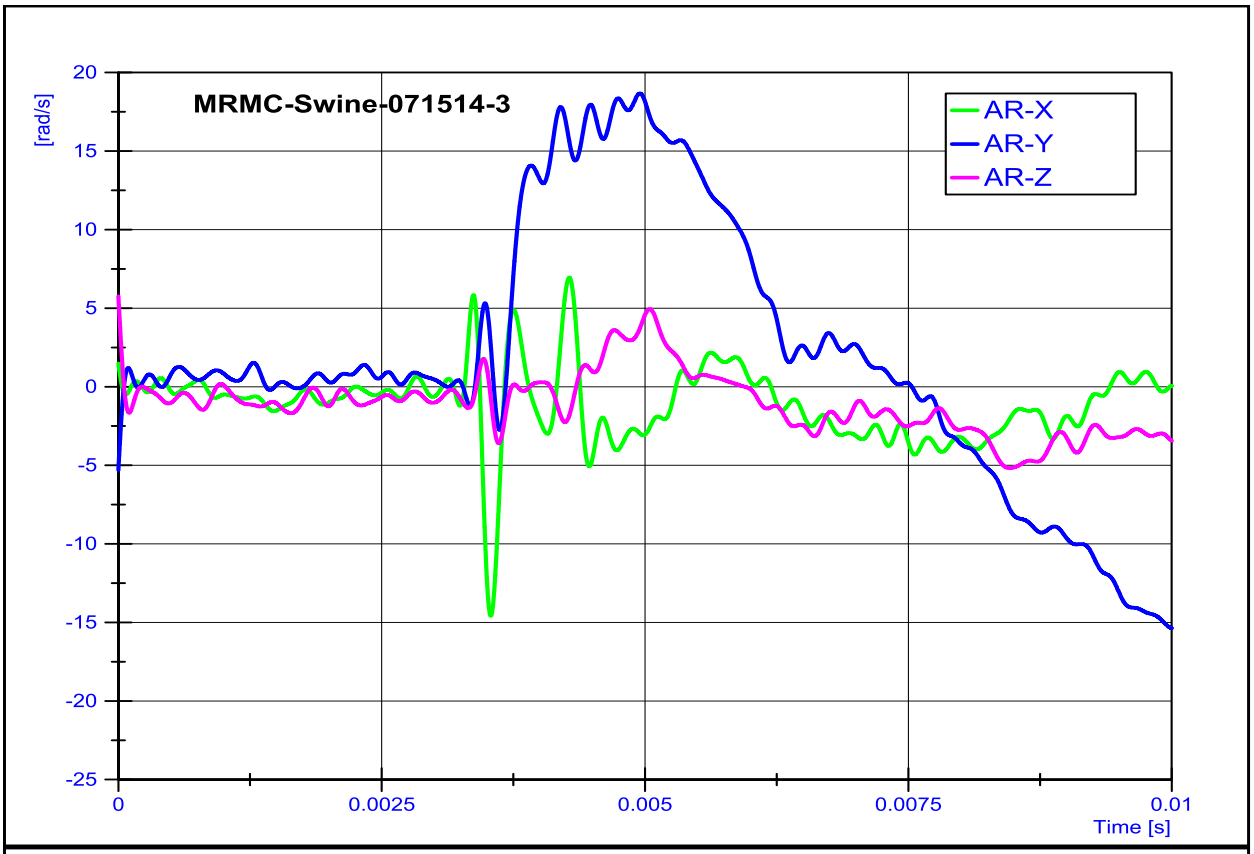
MRMC-Swine-071514-3
AR-X
AR-Y
AR-Z
[rad/s]
20
15
10
5
0
-5
-10
-15
-20
-25
0
0.0025
0.005
0.0075
0.01
Time [s]

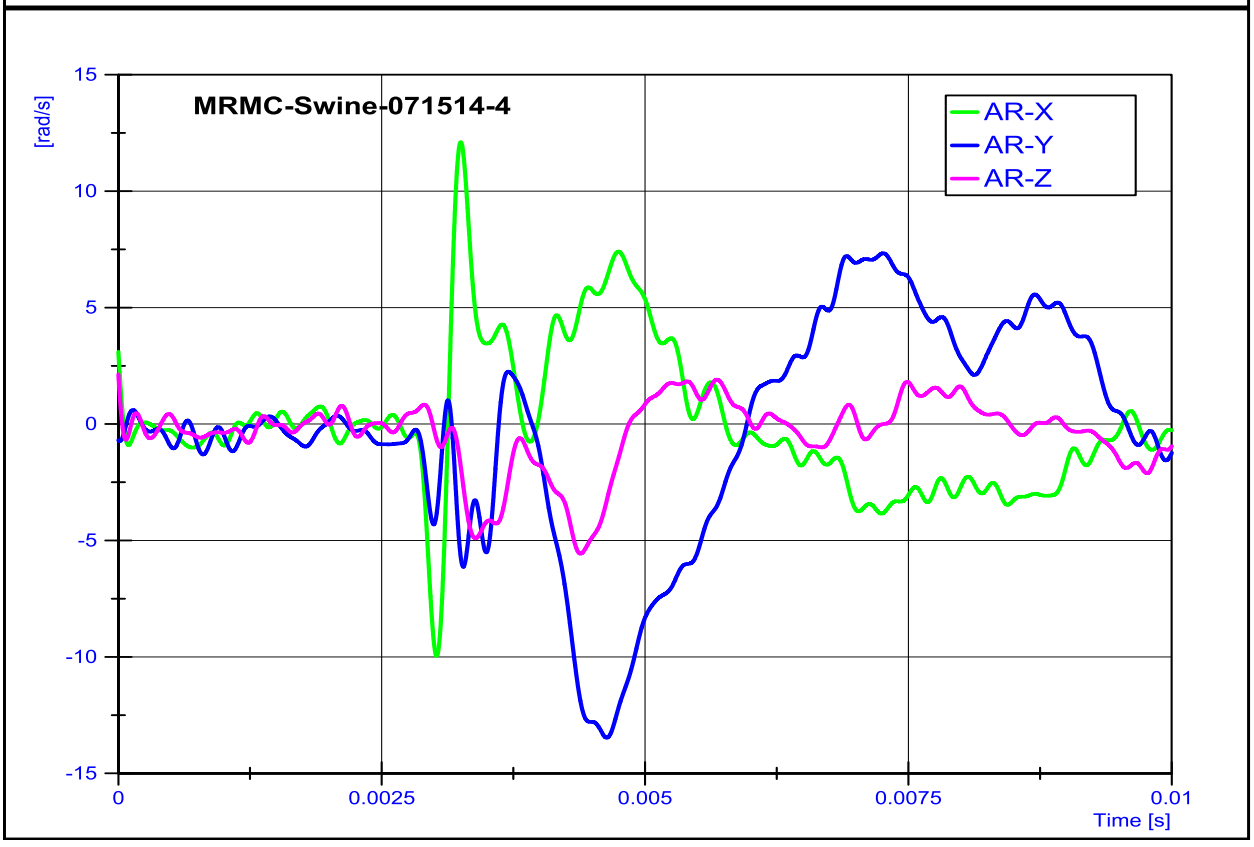
MRMC-Swine-071514-4
AR-X
AR-Y
AR-Z
[rad/s]
15
10
5
0
-5
-10
-15
0
0.0025
0.005
0.0075
0.01
Time [s]

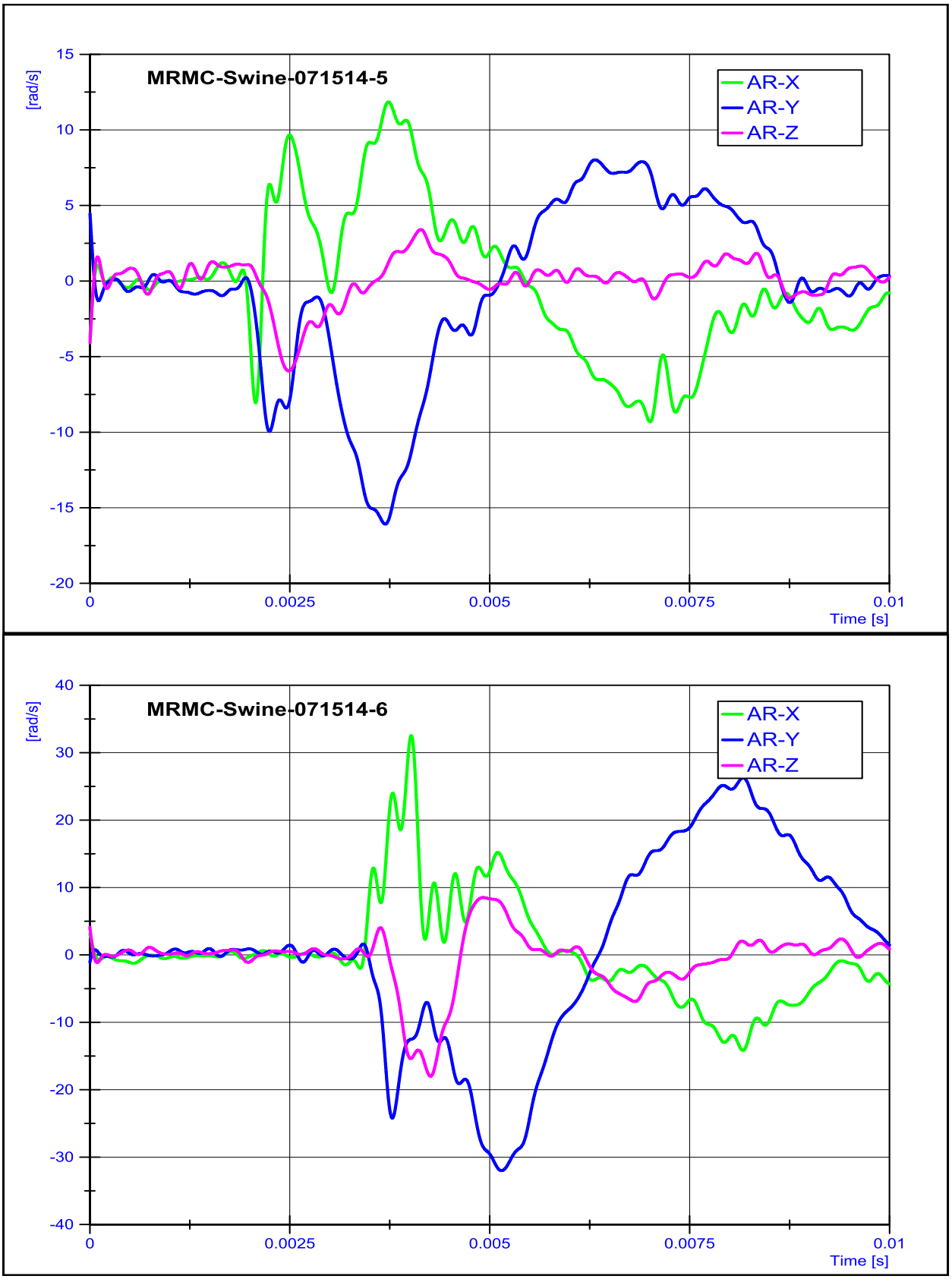
MRMC-Swine-071514-5
AR-X
AR-Y
AR-Z
[rad/s]
15
10
5
0
-5
-10
-15
-20
0
0.0025
0.005
0.0075
0.01
Time [s]
MRMC-Swine-071514-6
AR-X
AR-Y
AR-Z
[rad/s]
40
30
20
10
0
-10
-20
-30
-40
0
0.0025
0.005
0.0075
0.01
Time [s]

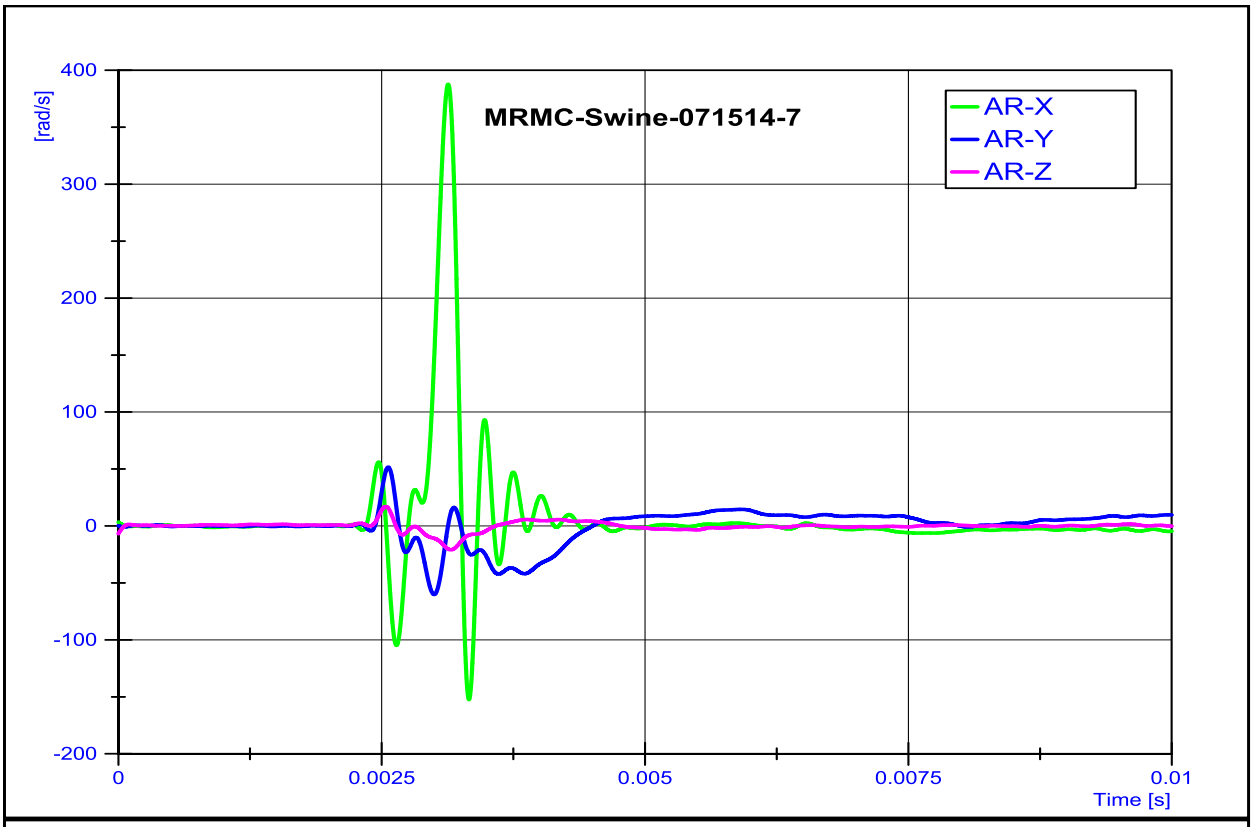
MRMC-Swine-071514-7
AR-X
AR-Y
AR-Z
[rad/s]
400
300
200
100
0
-100
-200
0
0.0025
0.005
0.0075
0.01
Time [s]

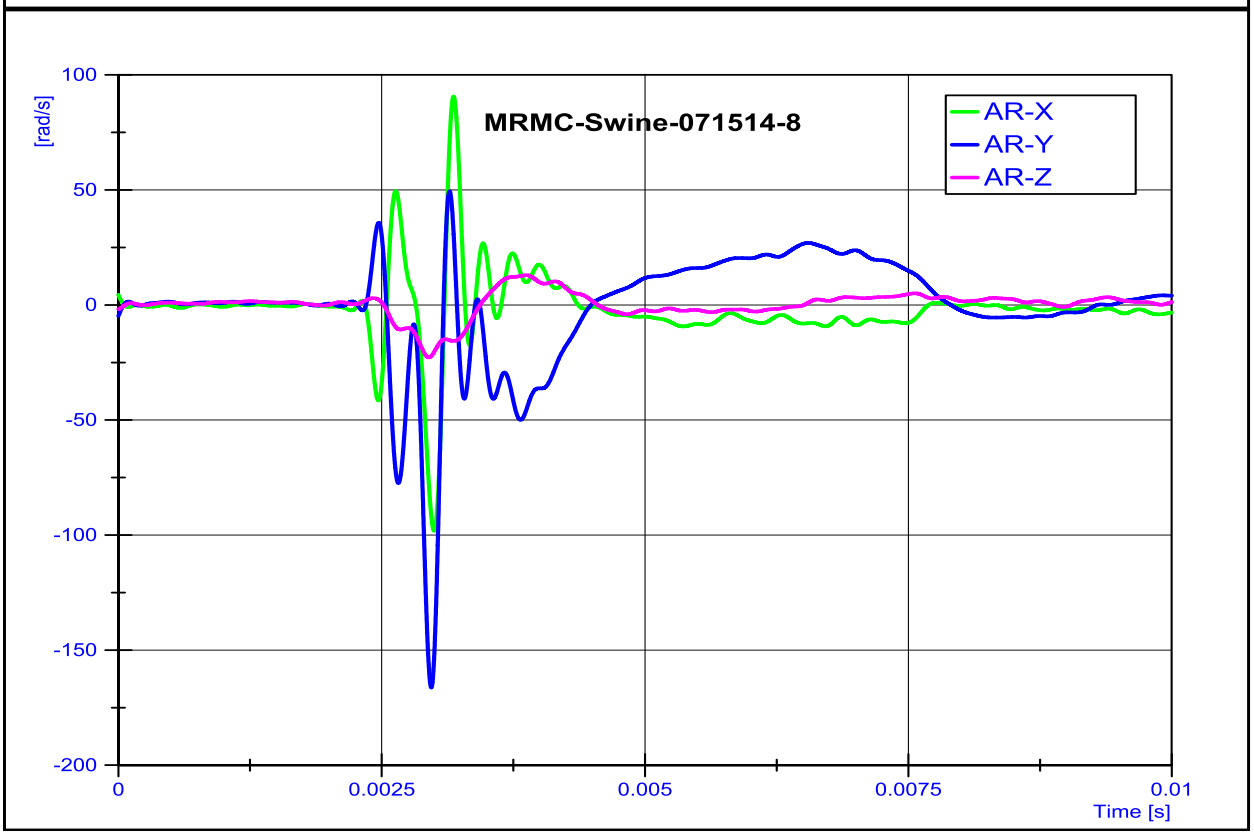
MRMC-Swine-071514-8
AR-X
AR-Y
AR-Z
[rad/s]
100
50
0
-50
-100
-150
-200
0
0.0025
0.005
0.0075
0.01
Time [s]

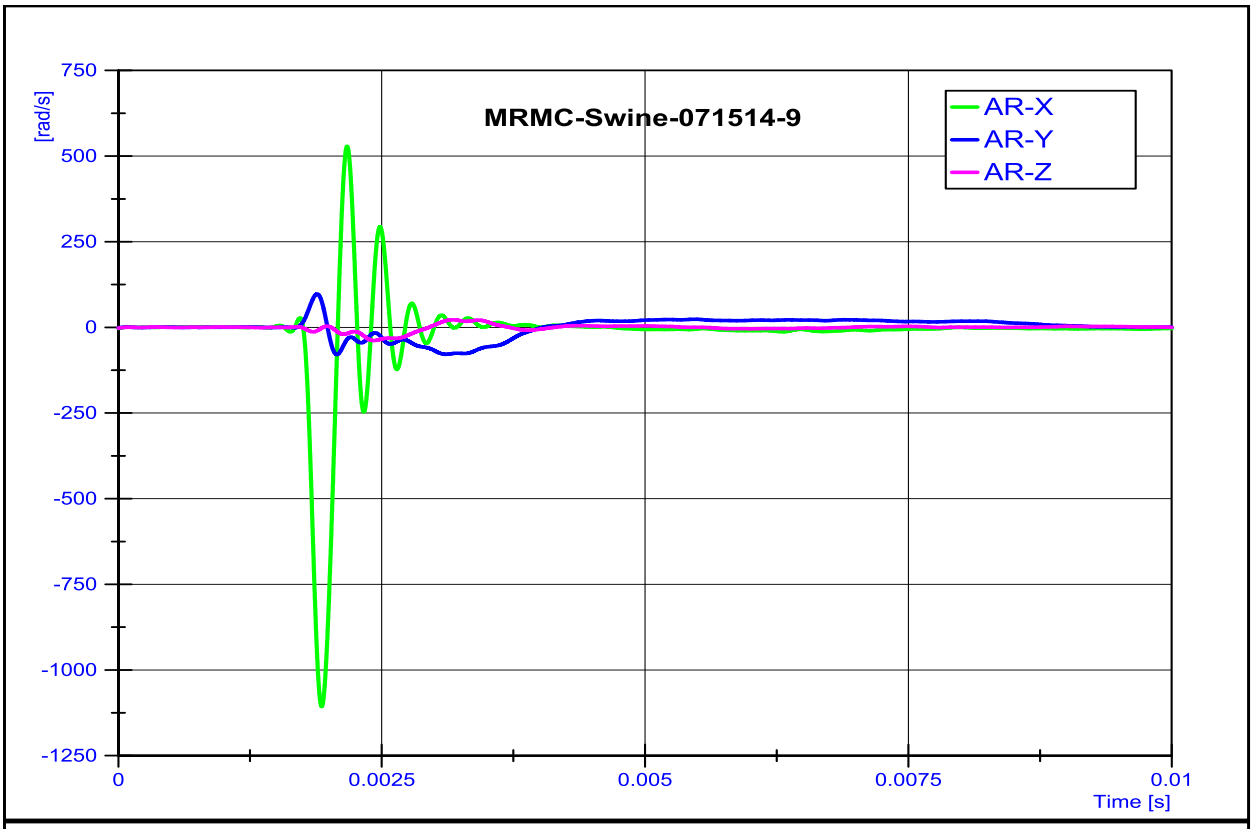
MRMC-Swine-071514-9
AR-X
AR-Y
AR-Z
[rad/s]
750
500
250
0
-250
-500
-750
-1000
-1250
0
0.0025
0.005
0.0075
0.01
Time [s]

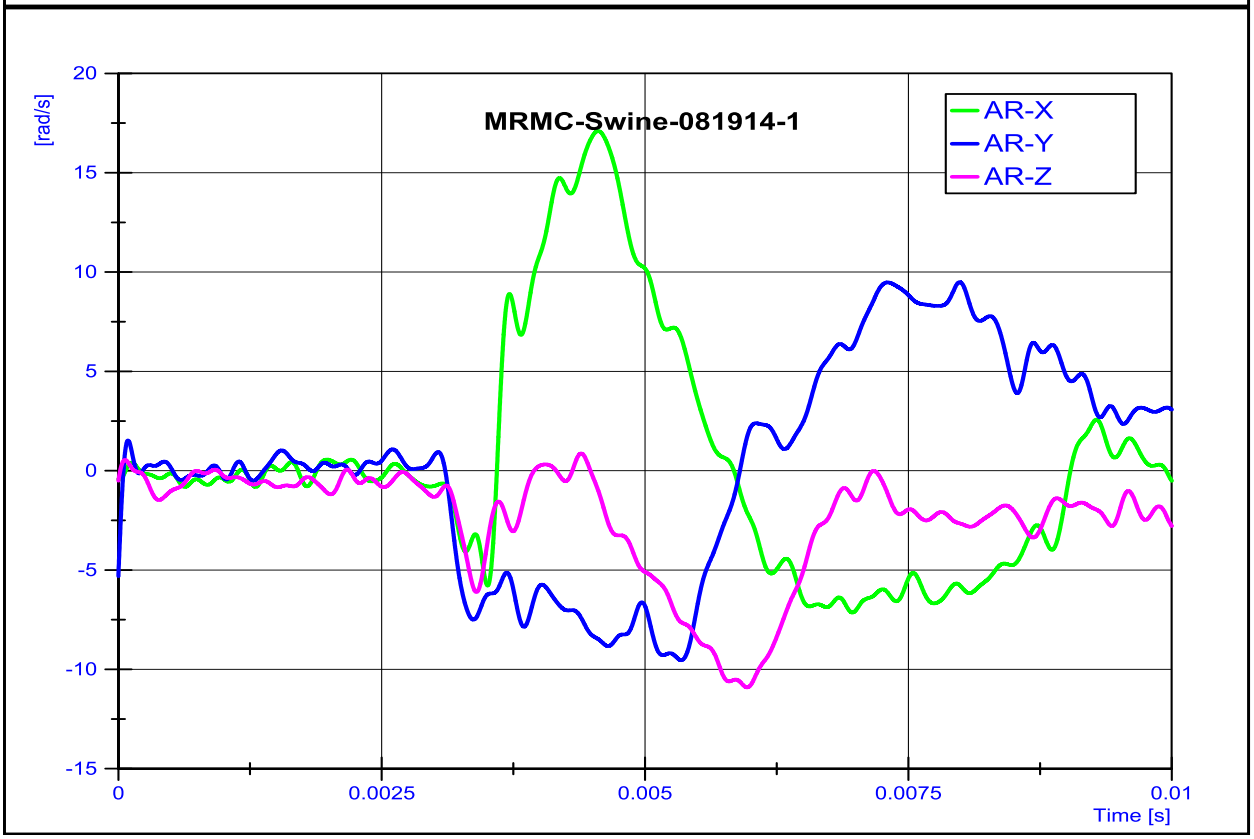
MRMC-Swine-081914-1
AR-X
AR-Y
AR-Z
[rad/s]
20
15
10
5
0
-5
-10
-15
0
0.0025
0.005
0.0075
0.01
Time [s]

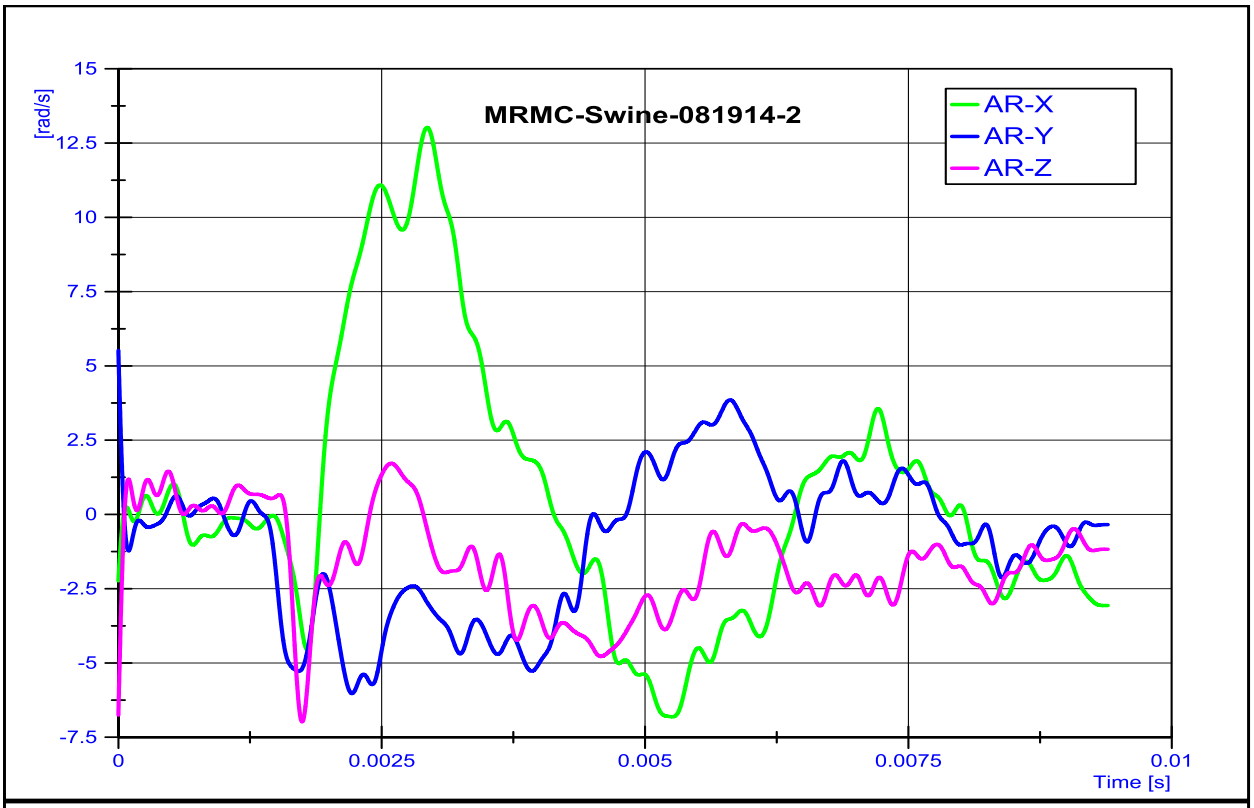
MRMC-Swine-081914-2
AR-X
AR-Y
AR-Z
[rad/s]
15
12.5
10
7.5
5
2.5
0
-2.5
-5
-7.5
0
0.0025
0.005
0.0075
0.01
Time [s]

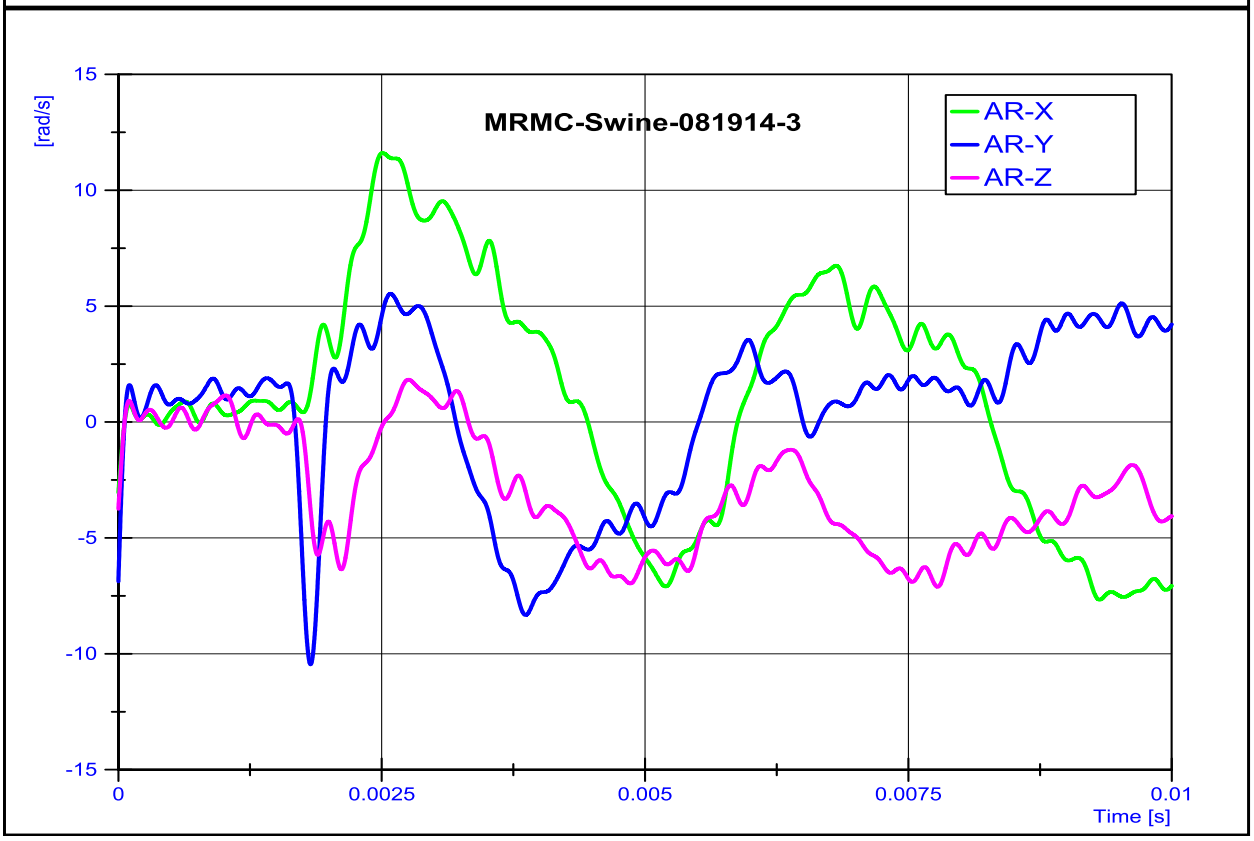
MRMC-Swine-081914-3
AR-X
AR-Y
AR-Z
[rad/s]
15
10
5
0
-5
-10
-15
0
0.0025
0.005
0.0075
0.01
Time [s]

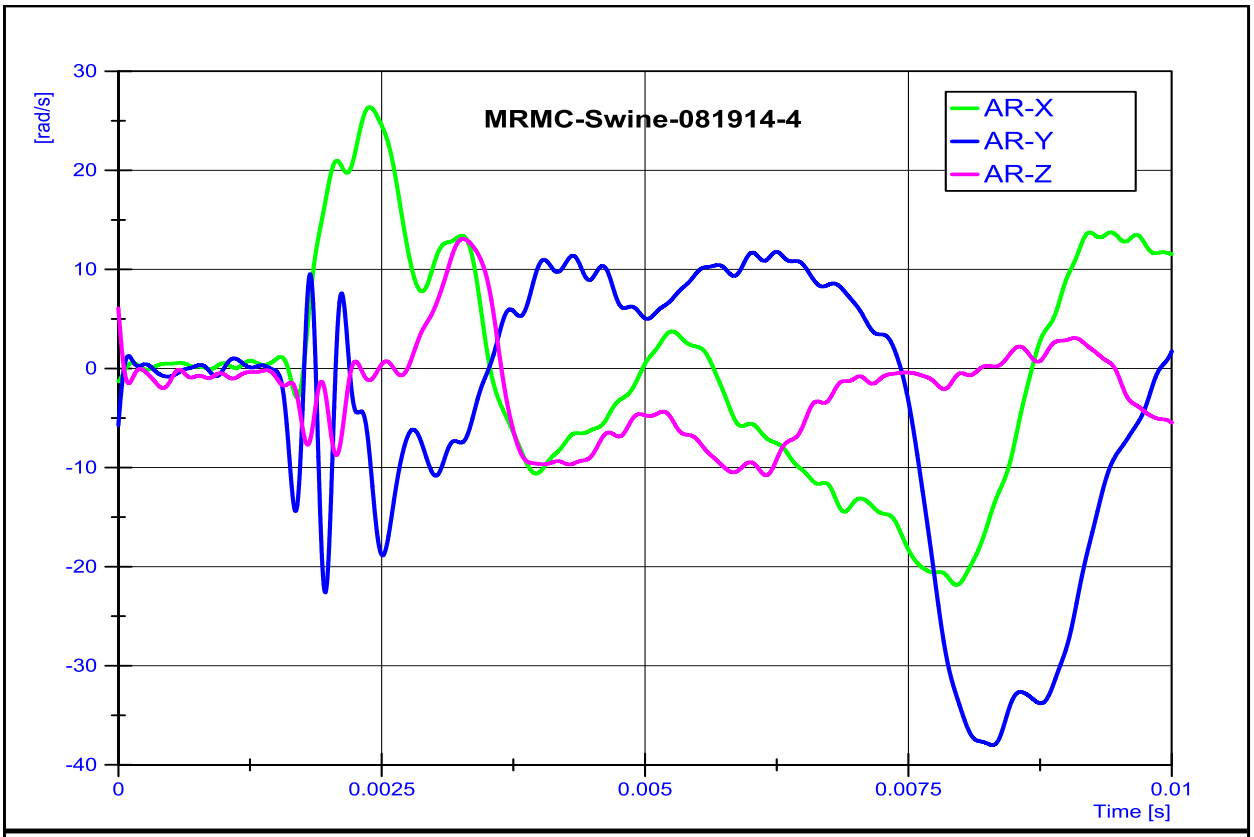
MRMC-Swine-081914-4
AR-X
AR-Y
AR-Z
[rad/s]
30
20
10
0
-10
-20
-30
-40
0
0.0025
0.005
0.0075
0.01
Time [s]

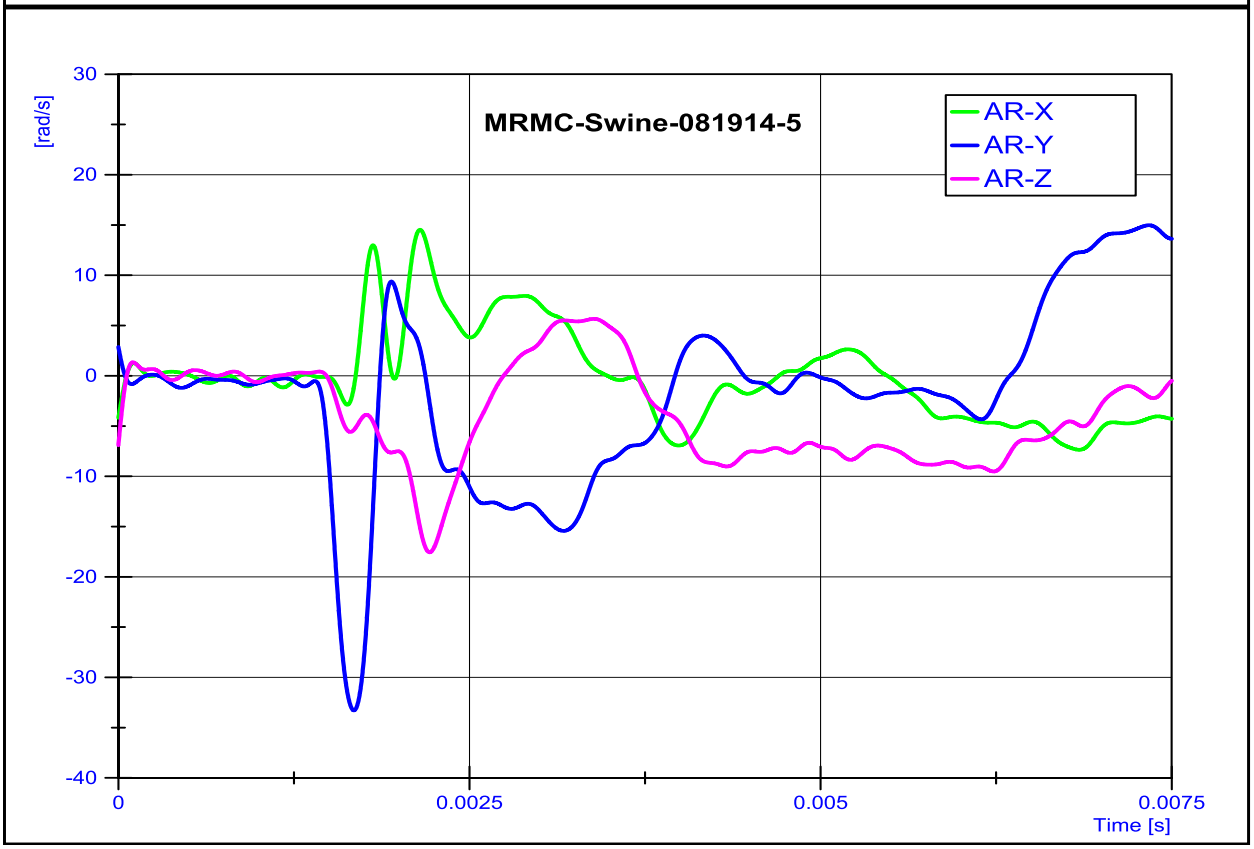
MRMC-Swine-081914-5
AR-X
AR-Y
AR-Z
[rad/s]
30
20
10
0
-10
-20
-30
-40
0
0.0025
0.005
0.0075
Time [s]

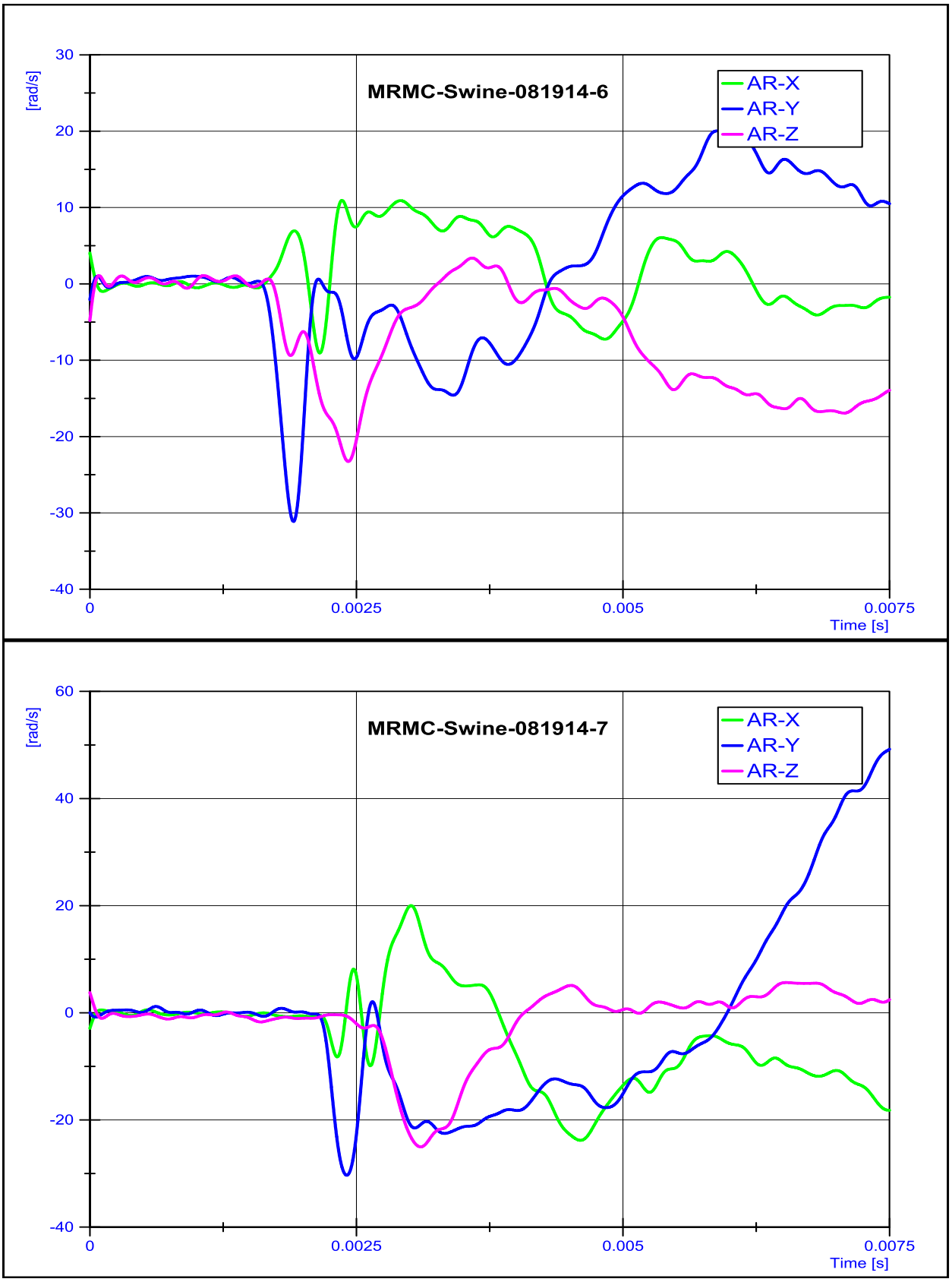
MRMC-Swine-081914-6
AR-X
AR-Y
AR-Z
[rad/s]
30
20
10
0
-10
-20
-30
-40
0
0.0025
0.005
0.0075
Time [s]
MRMC-Swine-081914-7
AR-X
AR-Y
AR-Z
[rad/s]
60
40
20
0
-20
-40
0
0.0025
0.005
0.0075
Time [s]

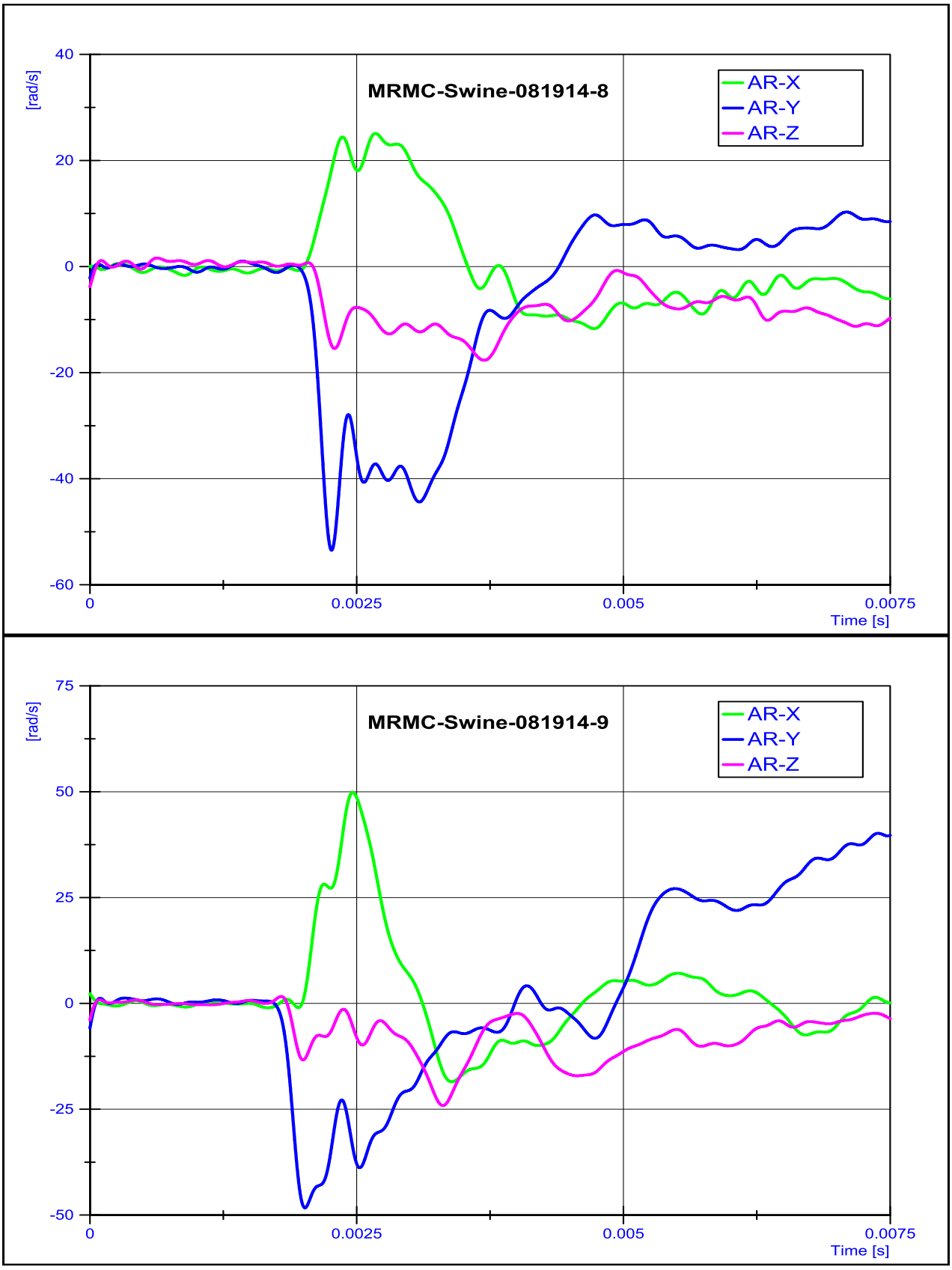
MRMC-Swine-081914-8
AR-X
AR-Y
AR-Z
[rad/s]
40
20
0
-20
-40
-60
0
0.0025
0.005
0.0075
Time [s]
MRMC-Swine-081914-9
AR-X
AR-Y
AR-Z
[rad/s]
75
50
25
0
-25
-50
0
0.0025
0.005
0.0075
Time [s]

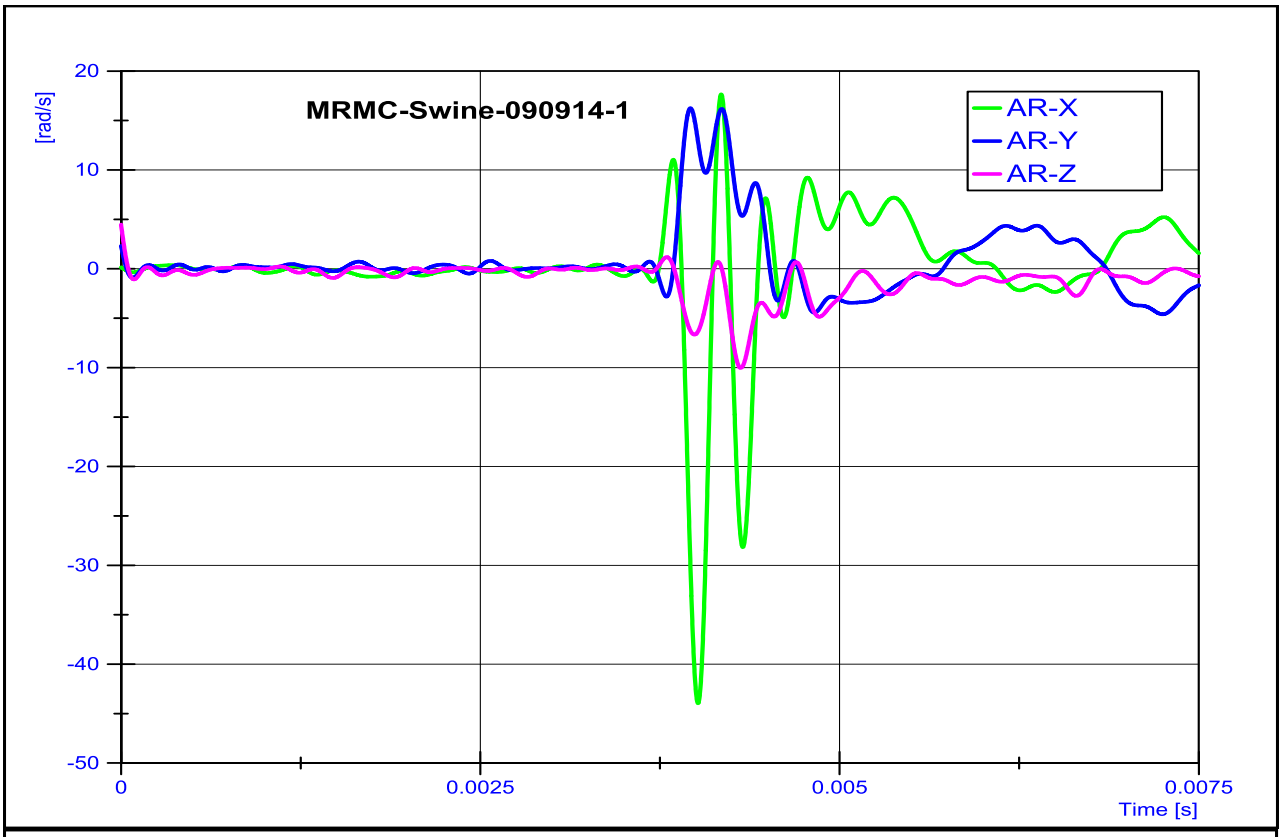
MRMC-Swine-090914-1
AR-X
AR-Y
AR-Z
[rad/s]
20
10
0
-10
-20
-30
-40
-50
0
0.0025
0.005
0.0075
Time [s]

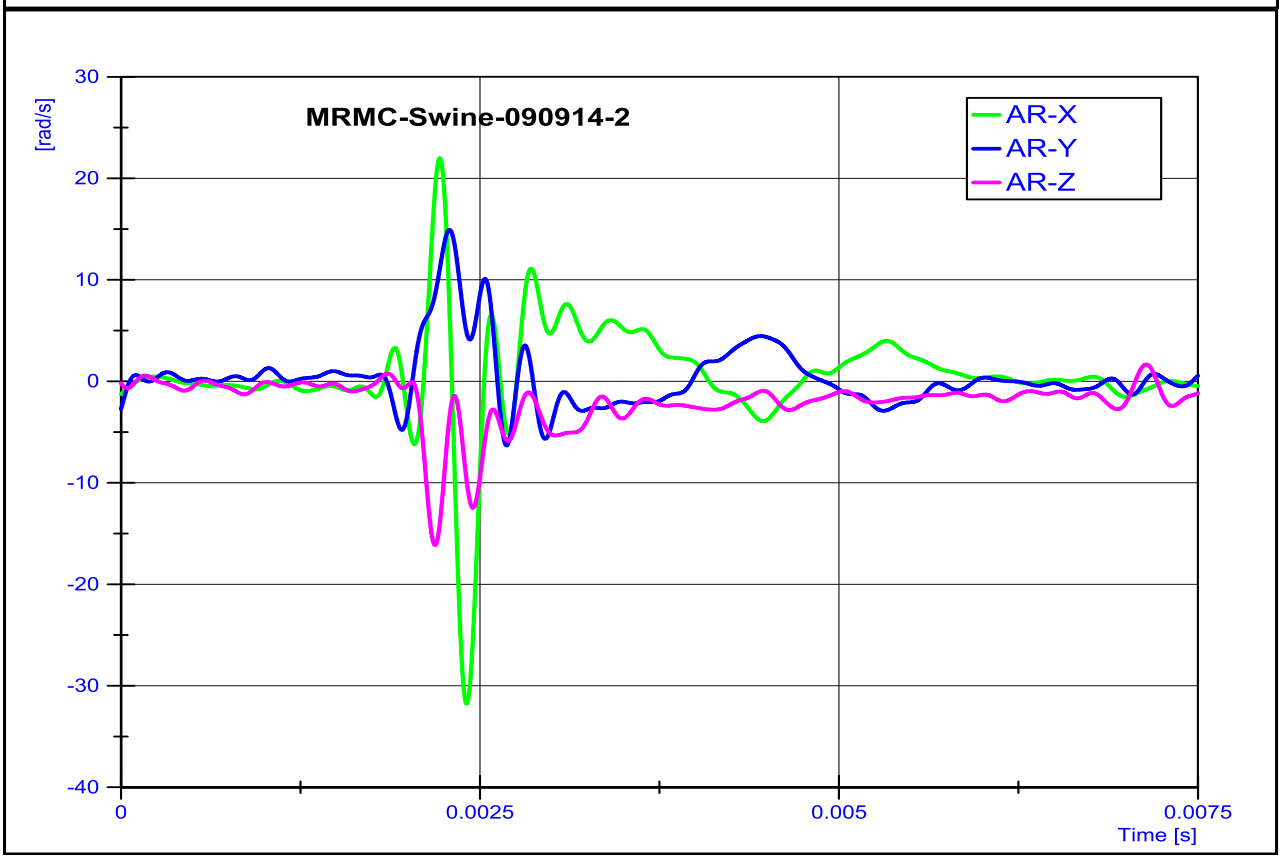
MRMC-Swine-090914-2
AR-X
AR-Y
AR-Z
[rad/s]
30
20
10
0
-10
-20
-30
-40
0
0.0025
0.005
0.0075
Time [s]

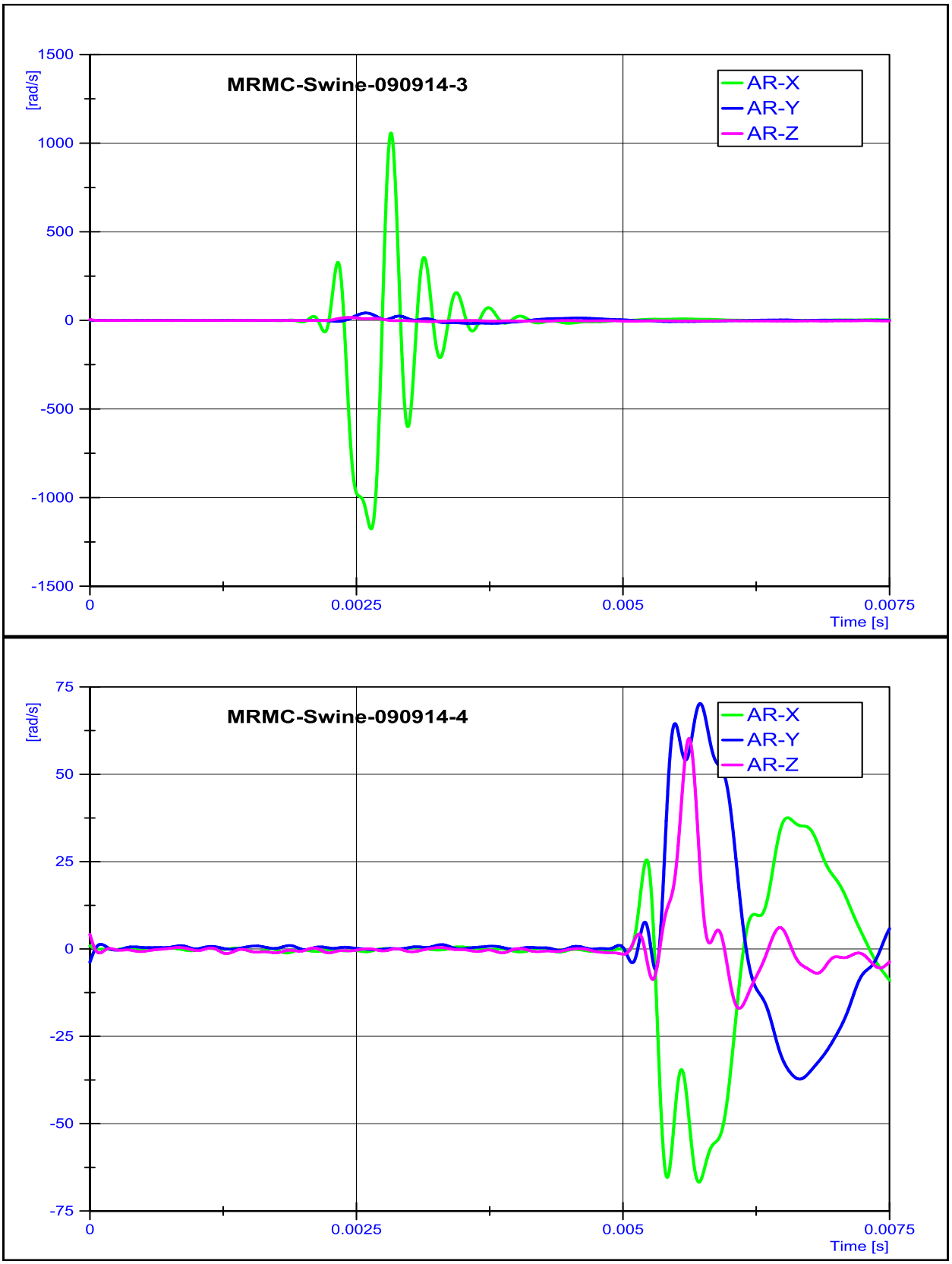
MRMC-Swine-090914-3
AR-X
AR-Y
AR-Z
[rad/s]
1500
1000
500
0
-500
-1000
-1500
0
0.0025
0.005
0.0075
Time [s]
MRMC-Swine-090914-4
AR-X
AR-Y
AR-Z
[rad/s]
75
50
25
0
-25
-50
-75
0
0.0025
0.005
0.0075
Time [s]

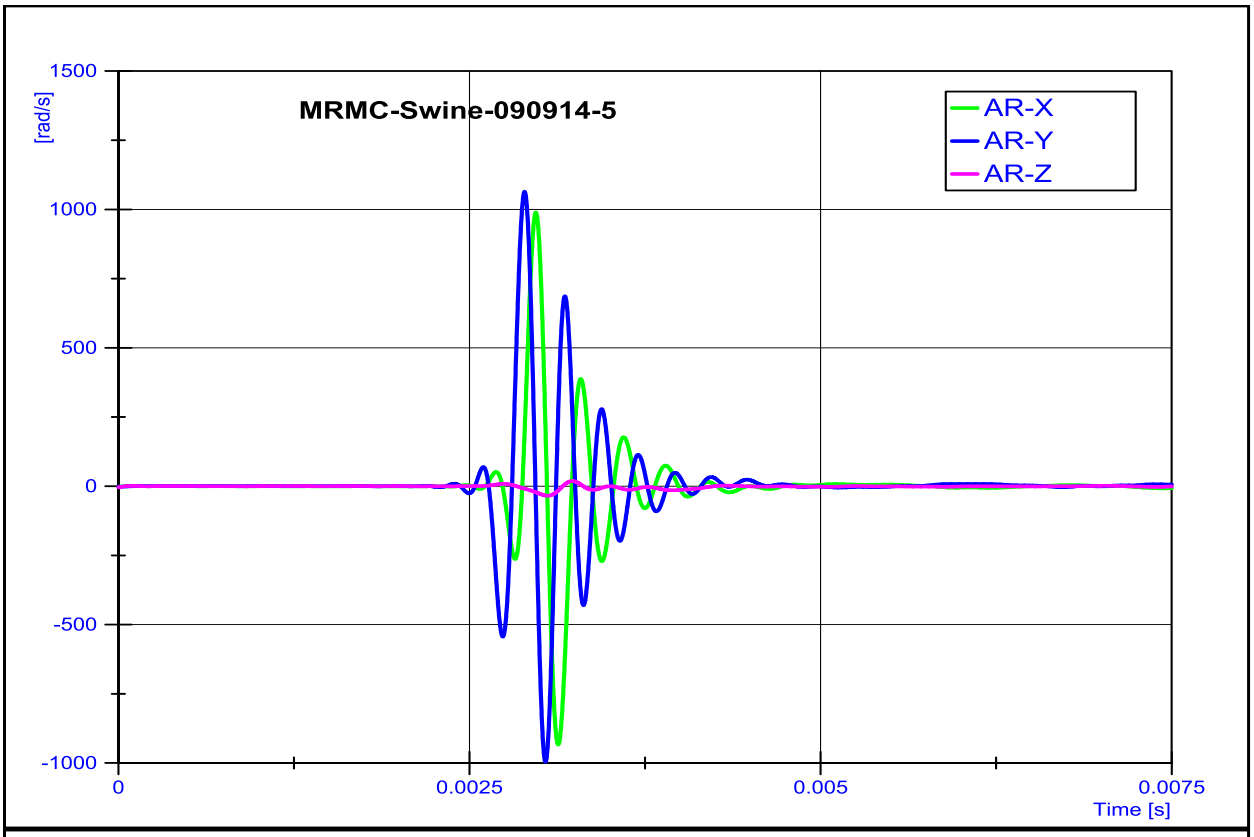
MRMC-Swine-090914-5
AR-X
AR-Y
AR-Z
[rad/s]
1500
1000
500
0
-500
-1000
0
0.0025
0.005
0.0075
Time [s]

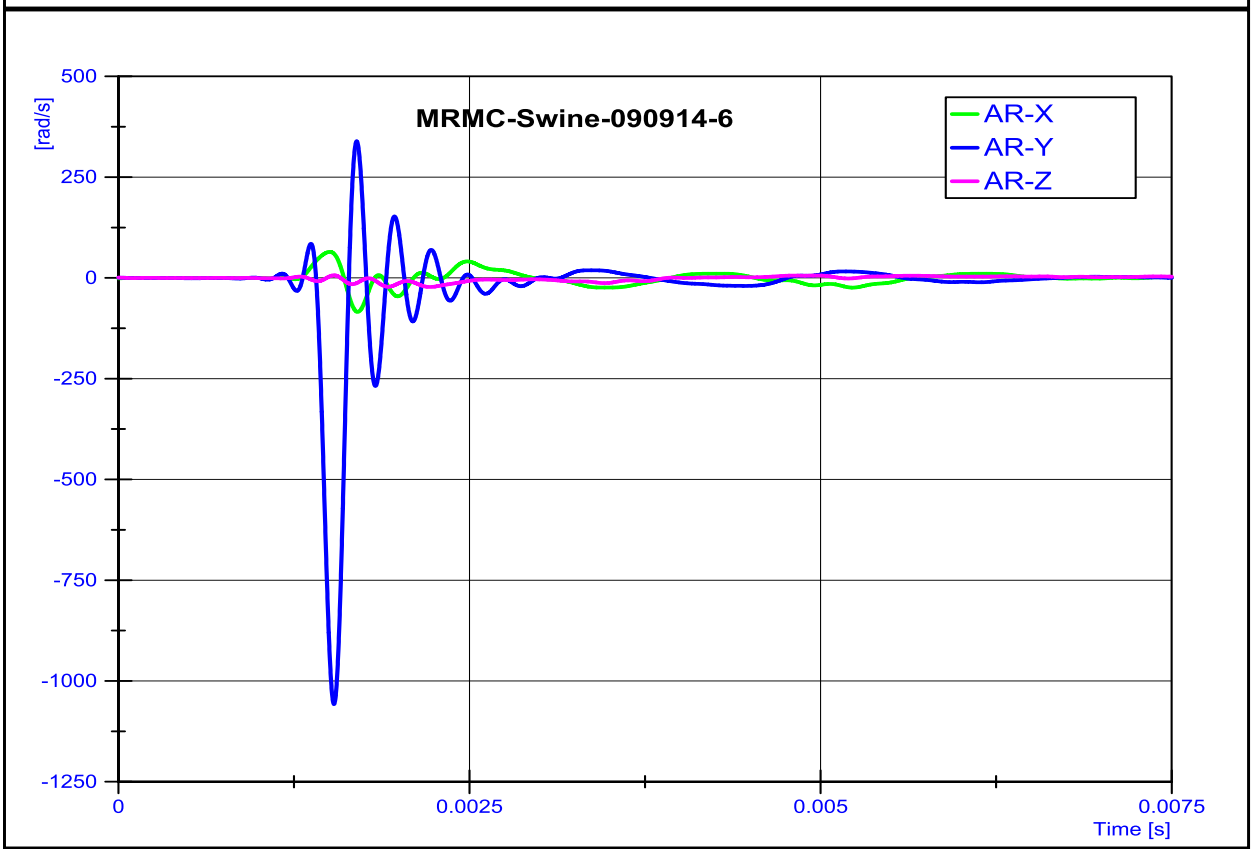
MRMC-Swine-090914-6
AR-X
AR-Y
AR-Z
[rad/s]
500
250
0
-250
-500
-750
-1000
-1250
0
0.0025
0.005
0.0075
Time [s]

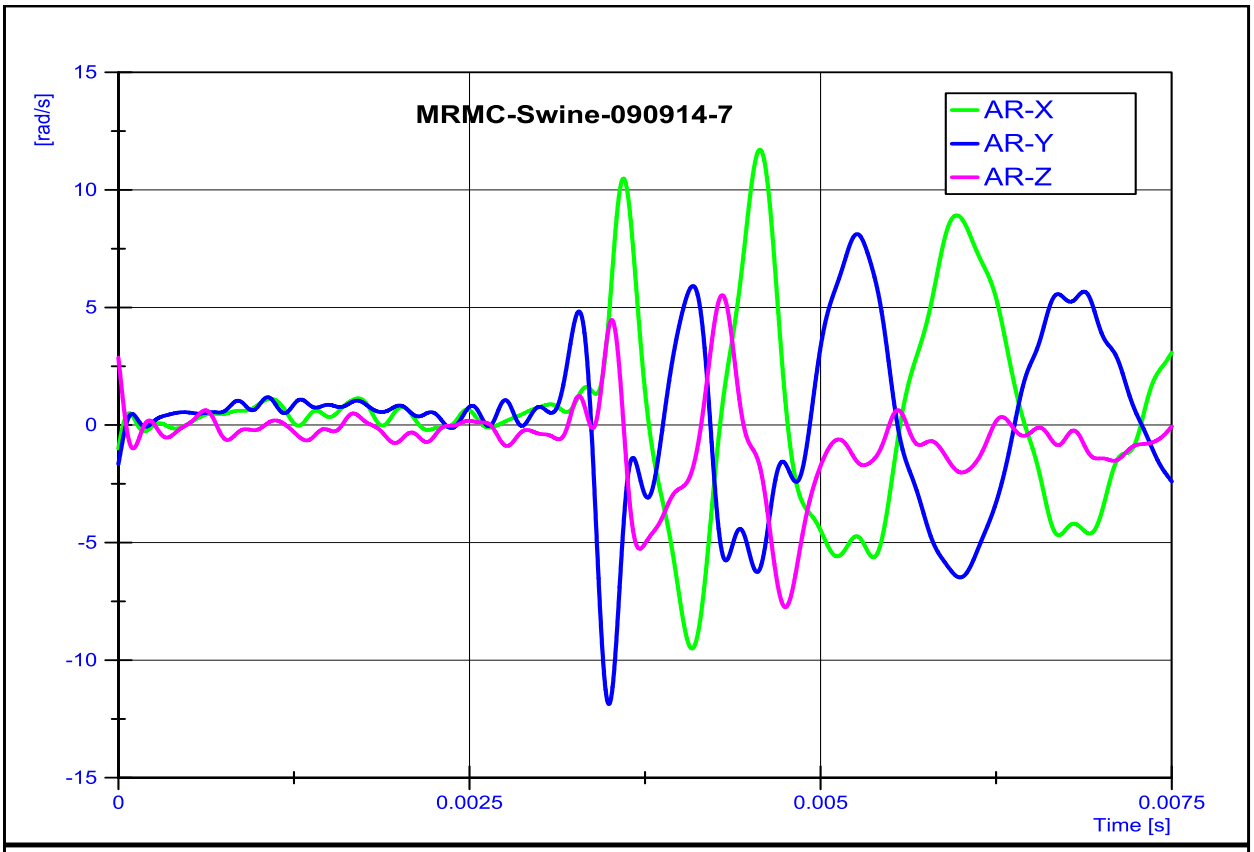
MRMC-Swine-090914-7
AR-X
AR-Y
AR-Z
[rad/s]
15
10
5
0
-5
-10
-15
0
0.0025
0.005
0.0075
Time [s]

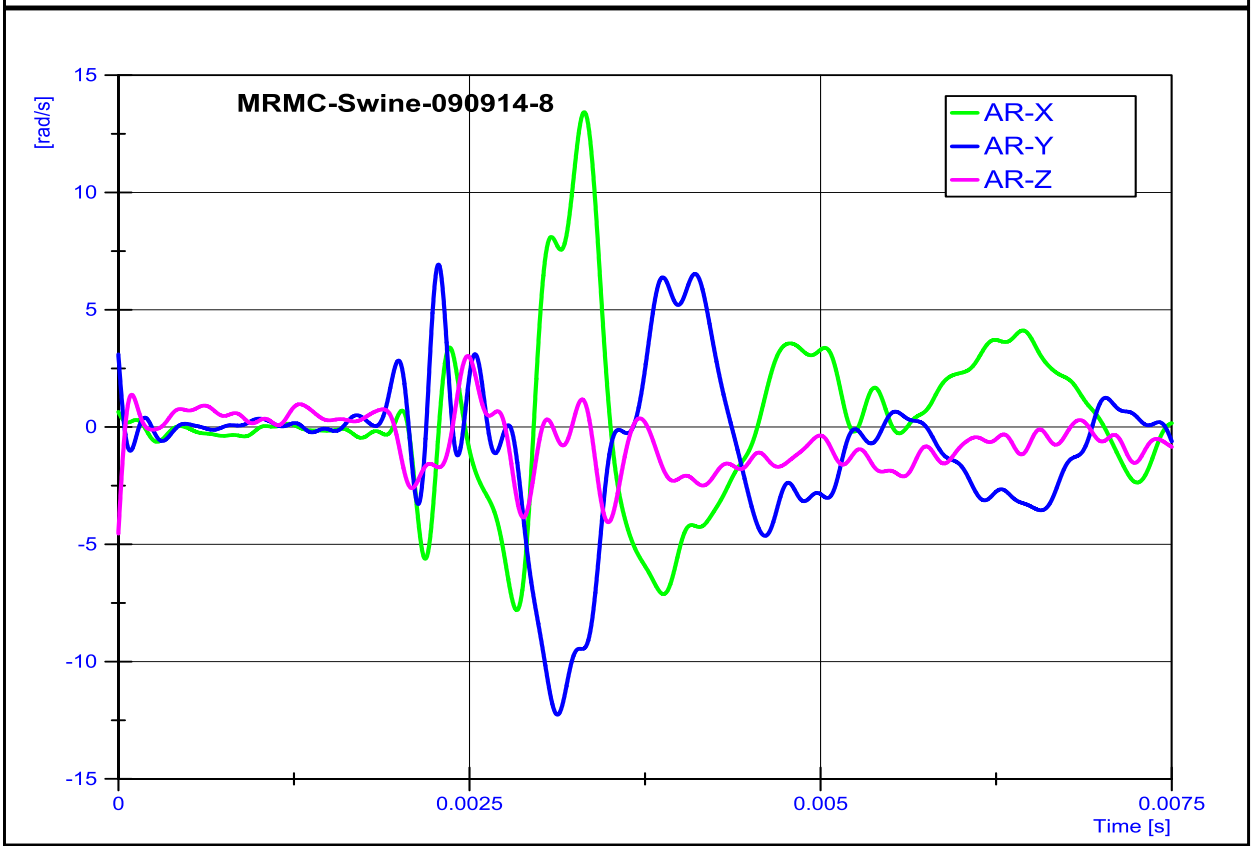
MRMC-Swine-090914-8
AR-X
AR-Y
AR-Z
[rad/s]
15
10
5
0
-5
-10
-15
0
0.0025
0.005
0.0075
Time [s]

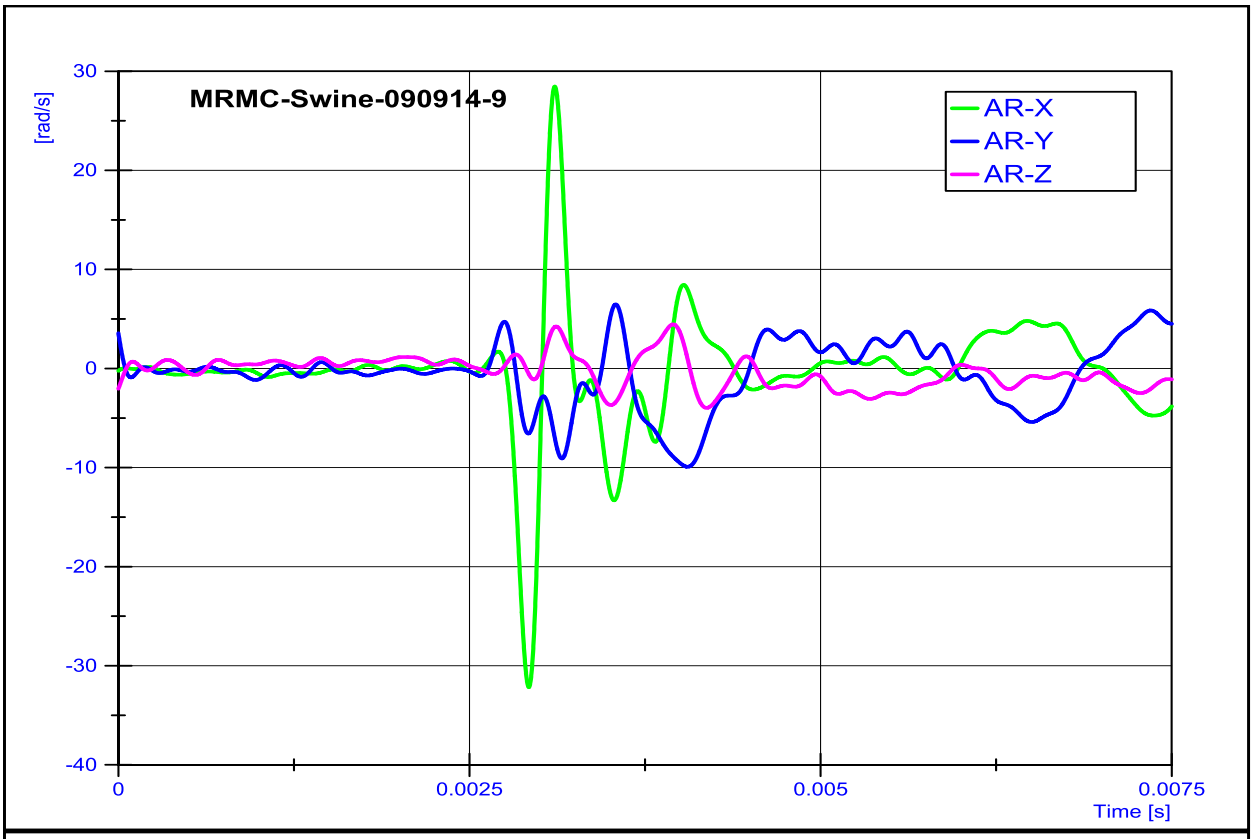
MRMC-Swine-090914-9
AR-X
AR-Y
AR-Z
[rad/s]
30
20
10
0
-10
-20
-30
-40
0
0.0025
0.005
0.0075
Time [s]

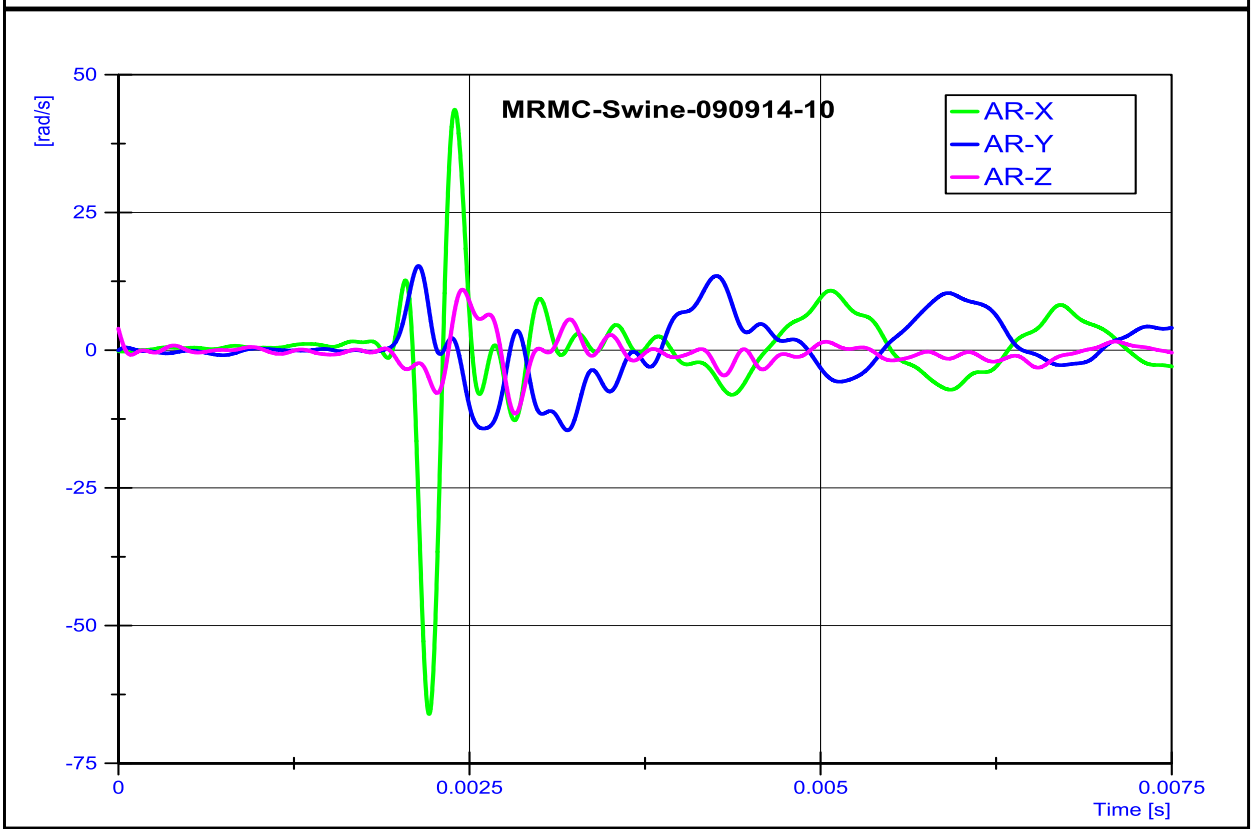
MRMC-Swine-090914-10
AR-X
AR-Y
AR-Z
[rad/s]
50
25
0
-25
-50
-75
0
0.0025
0.005
0.0075
Time [s]

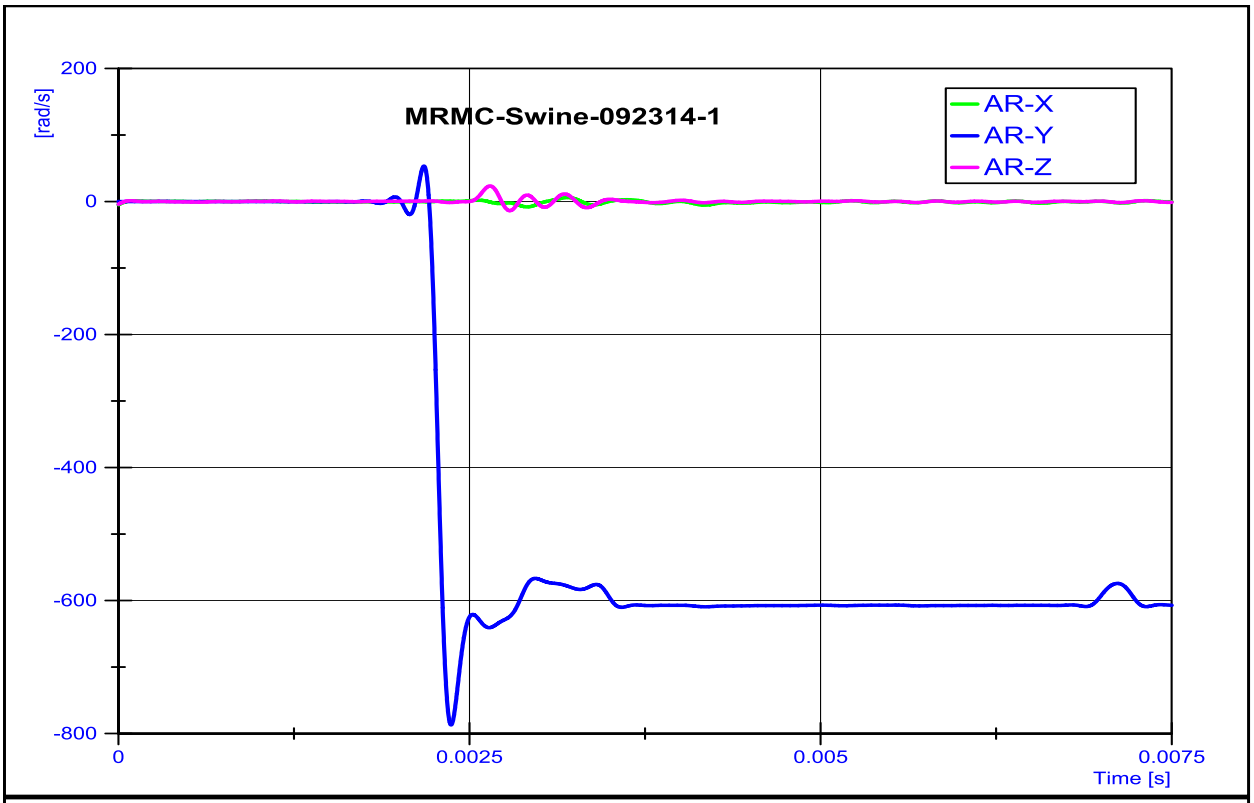
MRMC-Swine-092314-1
AR-X
AR-Y
AR-Z
[rad/s]
200
0
-200
-400
-600
-800
0
0.0025
0.005
0.0075
Time [s]

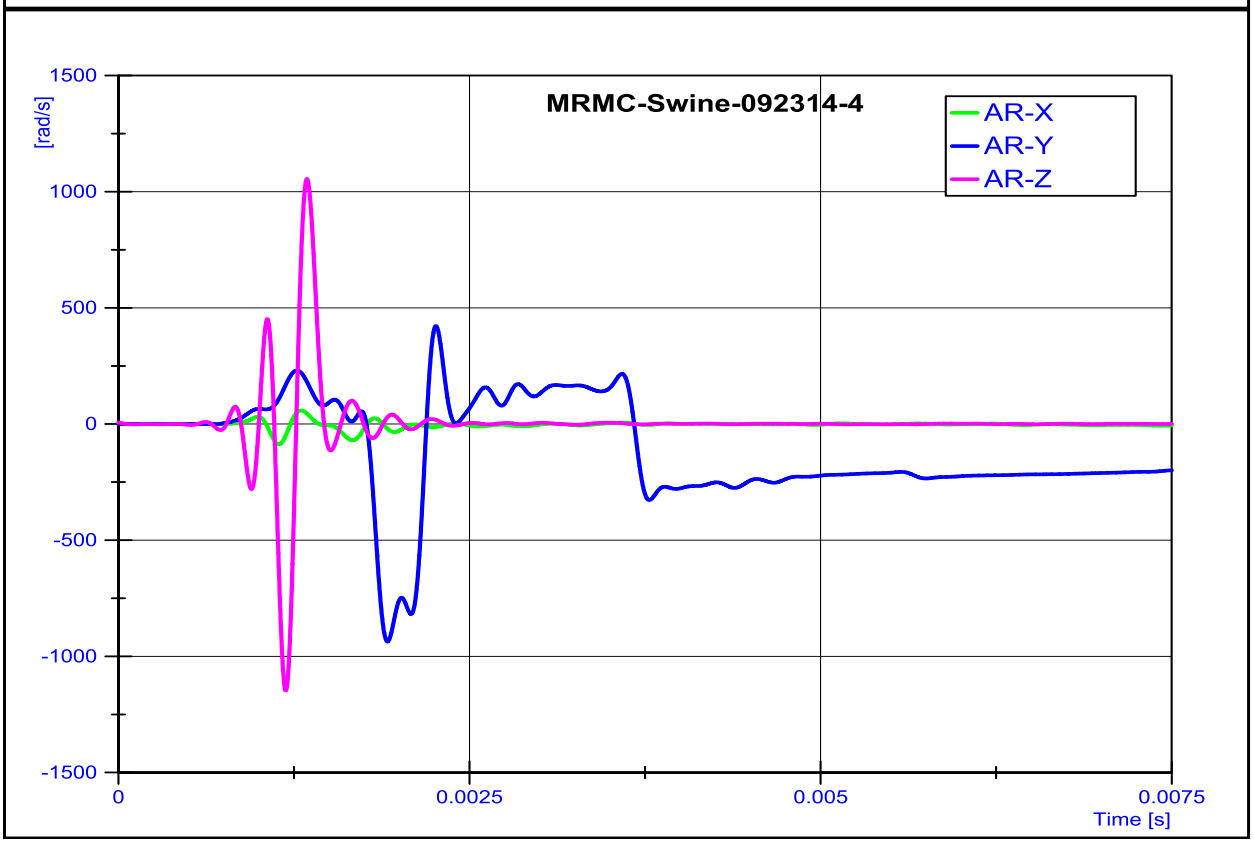
MRMC-Swine-092314-4
AR-X
AR-Y
AR-Z
[rad/s]
1500
1000
500
0
-500
-1000
-1500
0
0.0025
0.005
0.0075
Time [s]

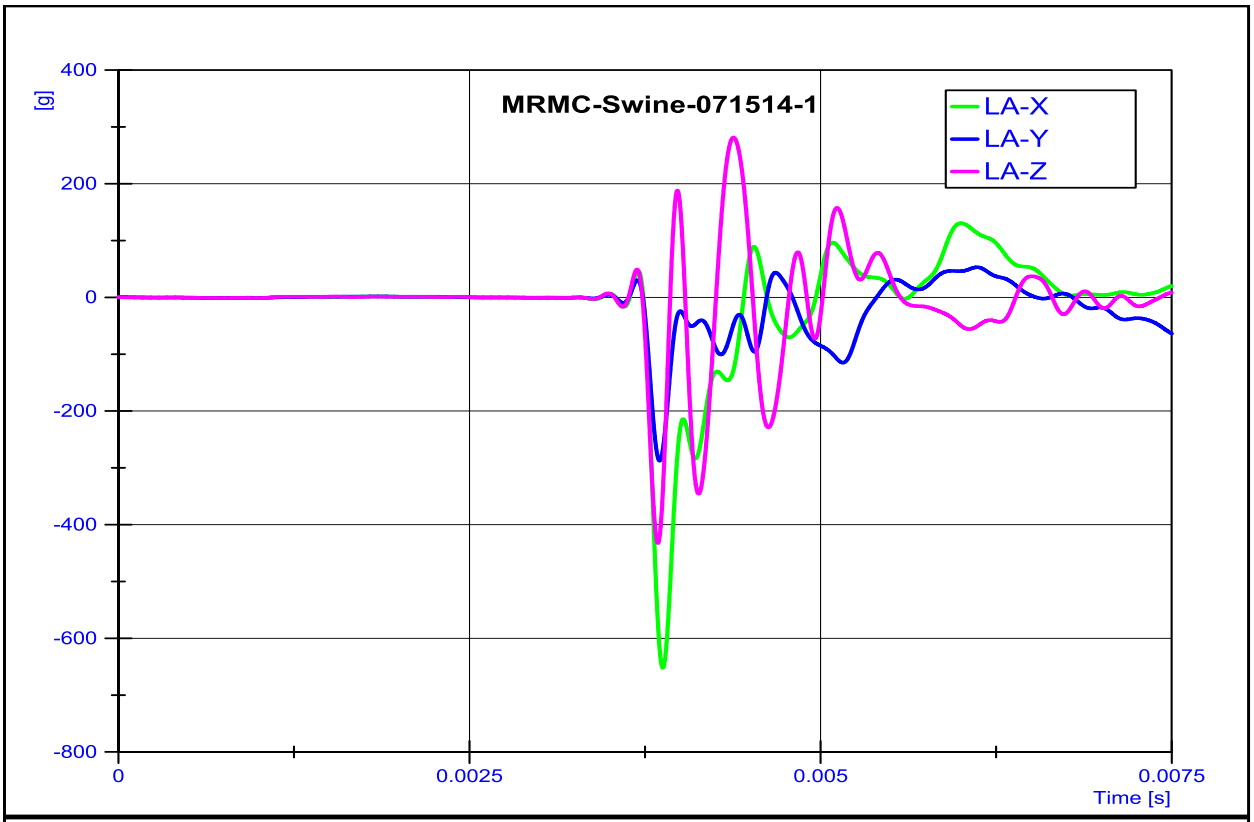
MRMC-Swine-071514-1
LA-X
LA-Y
LA-Z
[g]
400
200
0
-200
-400
-600
-800
0
0.0025
0.005
0.0075
Time [s]

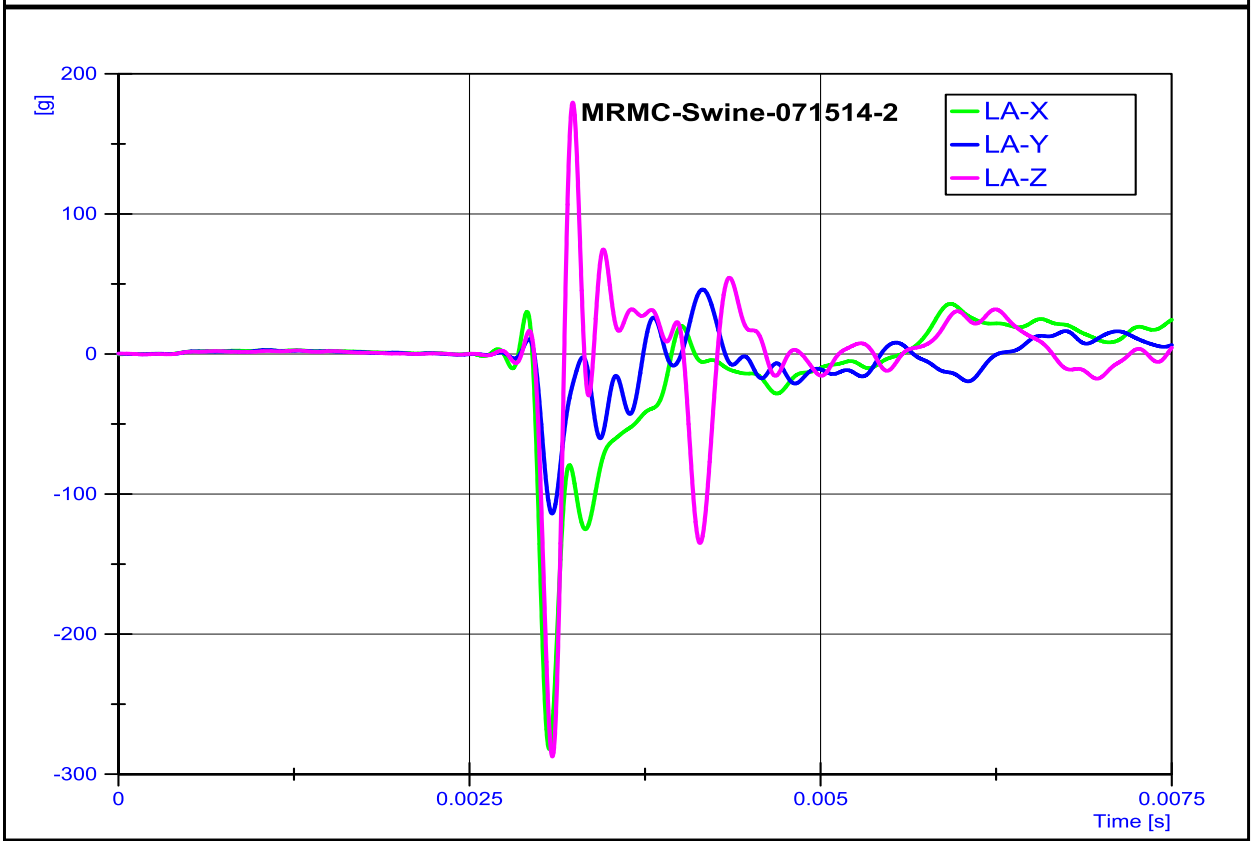
MRMC-Swine-071514-2
LA-X
LA-Y
LA-Z
[g]
200
100
0
-100
-200
-300
0
0.0025
0.005
0.0075
Time [s]

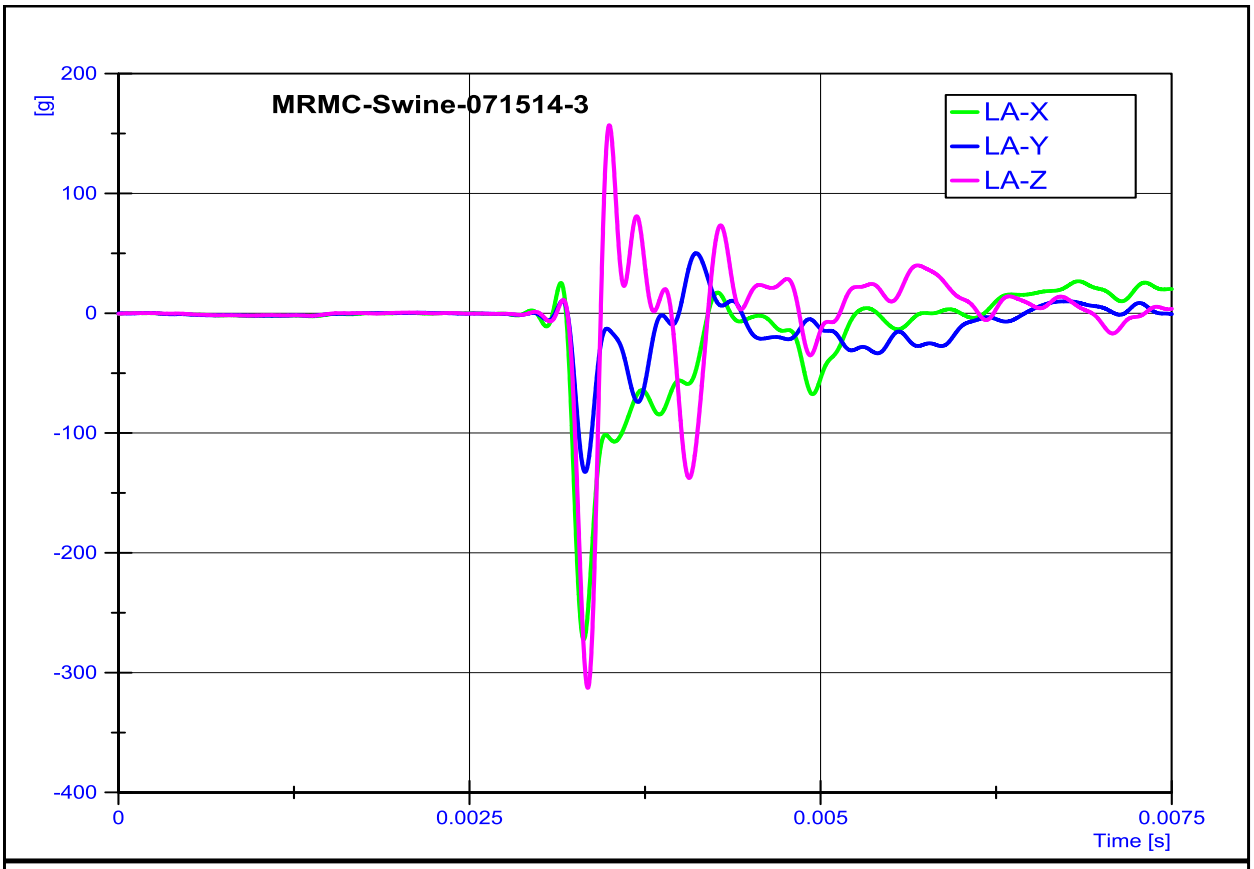
MRMC-Swine-071514-3
LA-X
LA-Y
LA-Z
[g]
200
100
0
-100
-200
-300
-400
0
0.0025
0.005
0.0075
Time [s]

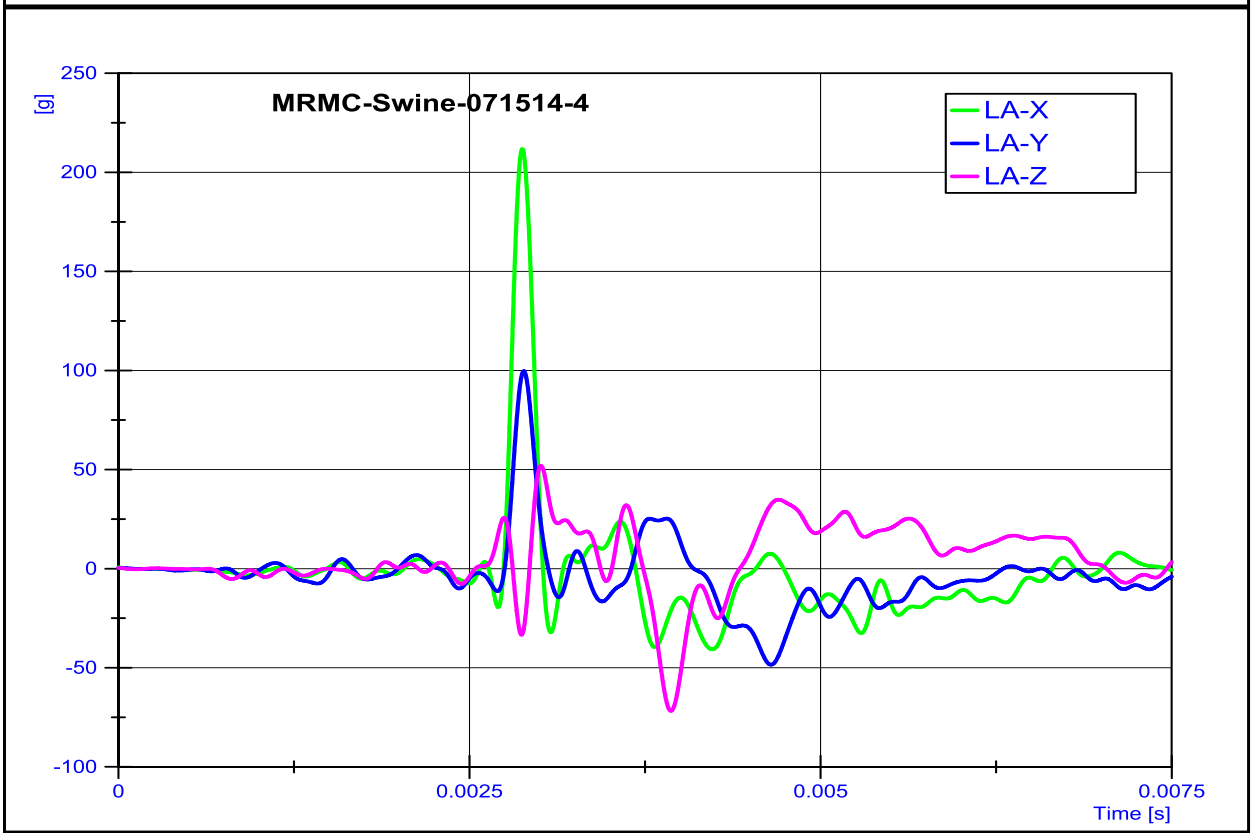
MRMC-Swine-071514-4
LA-X
LA-Y
LA-Z
[g]
250
200
150
100
50
0
-50
-100
0
0.0025
0.005
0.0075
Time [s]

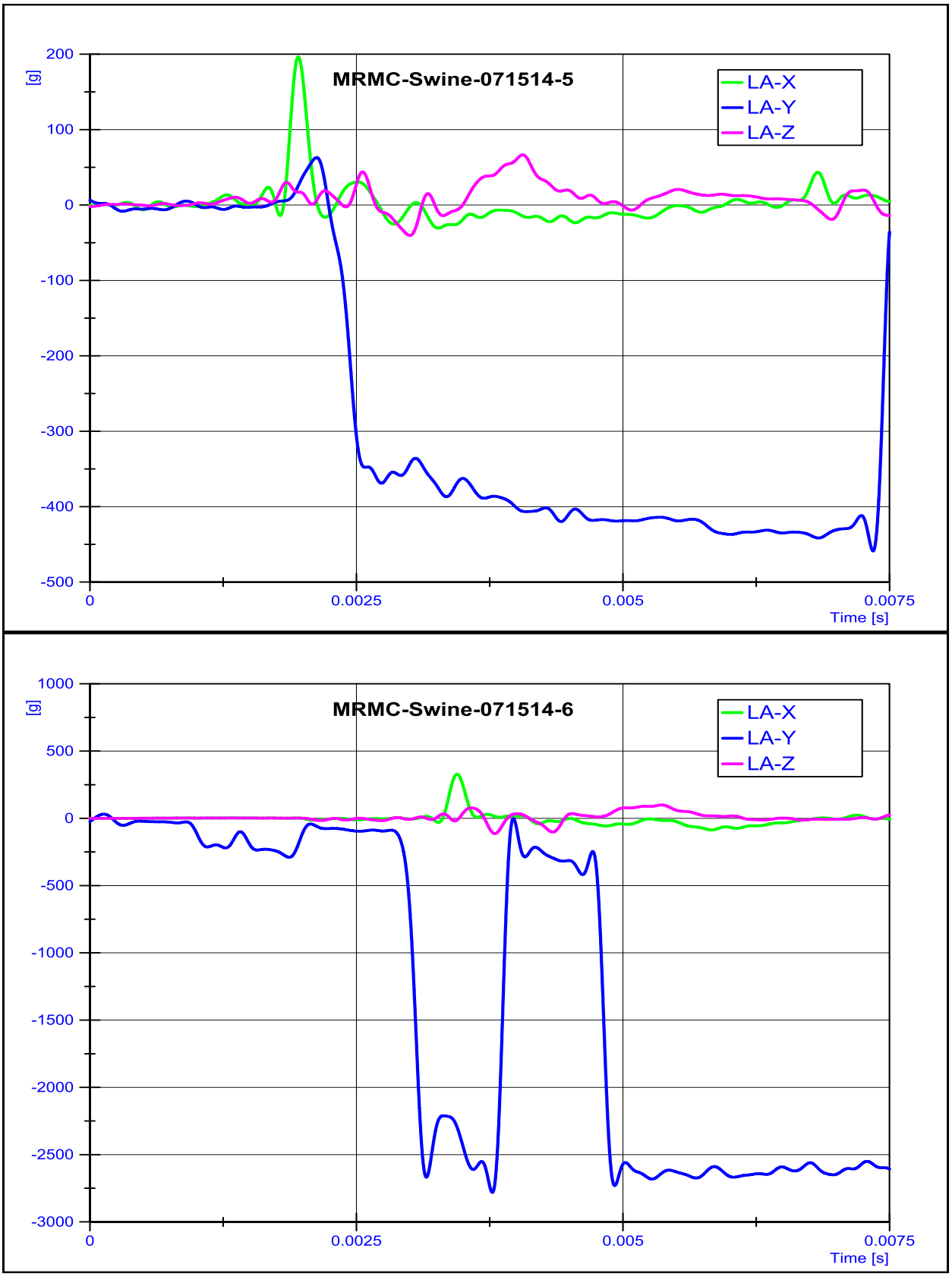
MRMC-Swine-071514-5
LA-X
LA-Y
LA-Z
[g]
200
100
0
-100
-200
-300
-400
-500
0
0.0025
0.005
0.0075
Time [s]
MRMC-Swine-071514-6
LA-X
LA-Y
LA-Z
[g]
1000
500
0
-500
-1000
-1500
-2000
-2500
-3000
0
0.0025
0.005
0.0075
Time [s]

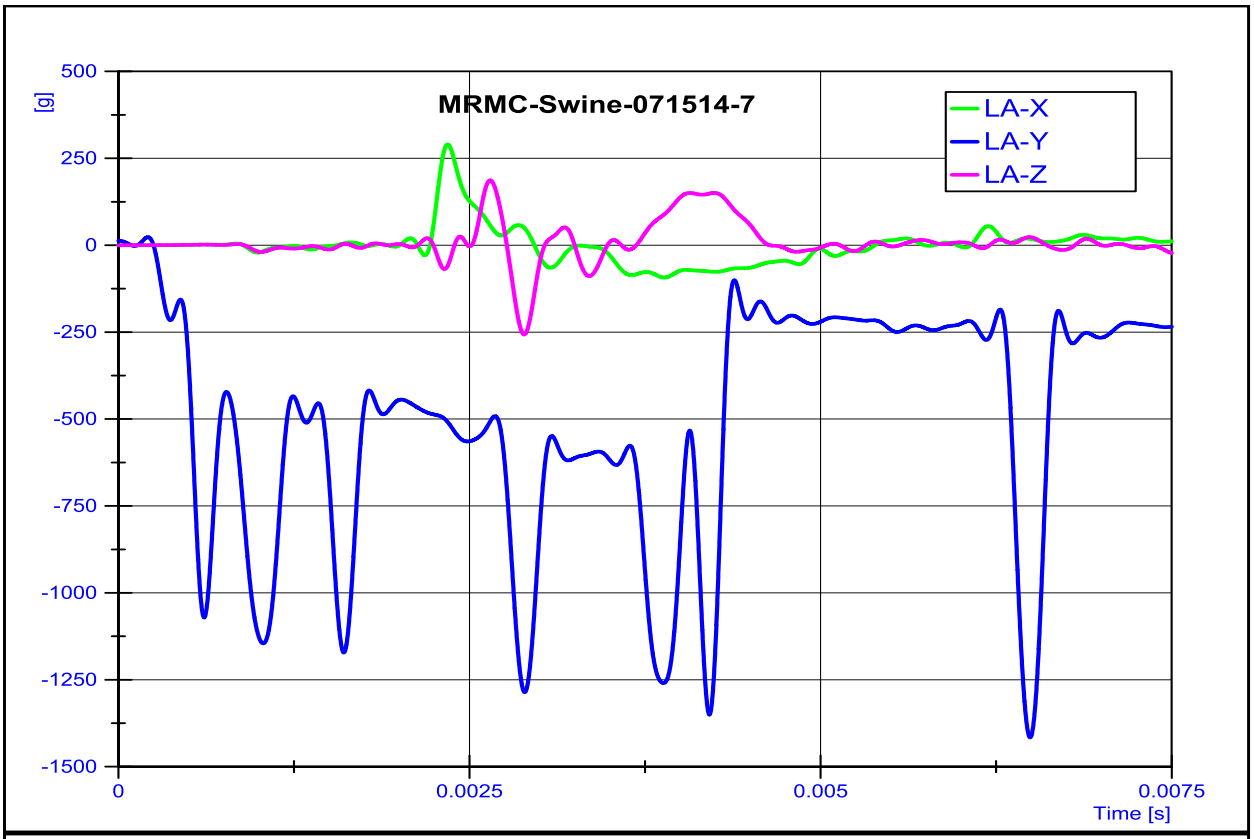
MRMC-Swine-071514-7
LA-X
LA-Y
LA-Z
[g]
500
250
0
-250
-500
-750
-1000
-1250
-1500
0
0.0025
0.005
0.0075
Time [s]

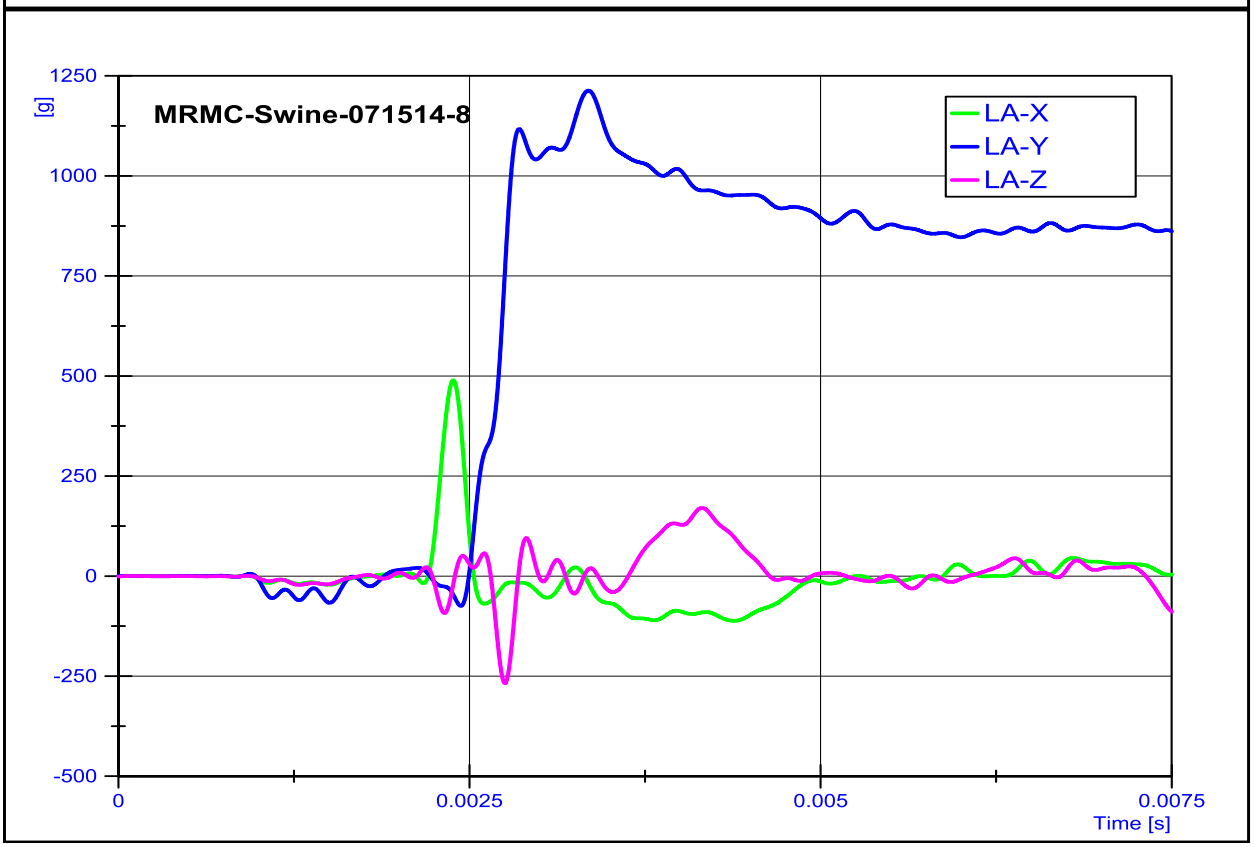
MRMC-Swine-071514-8
LA-X
LA-Y
LA-Z
[g]
1250
1000
750
500
250
0
-250
-500
0
0.0025
0.005
0.0075
Time [s]

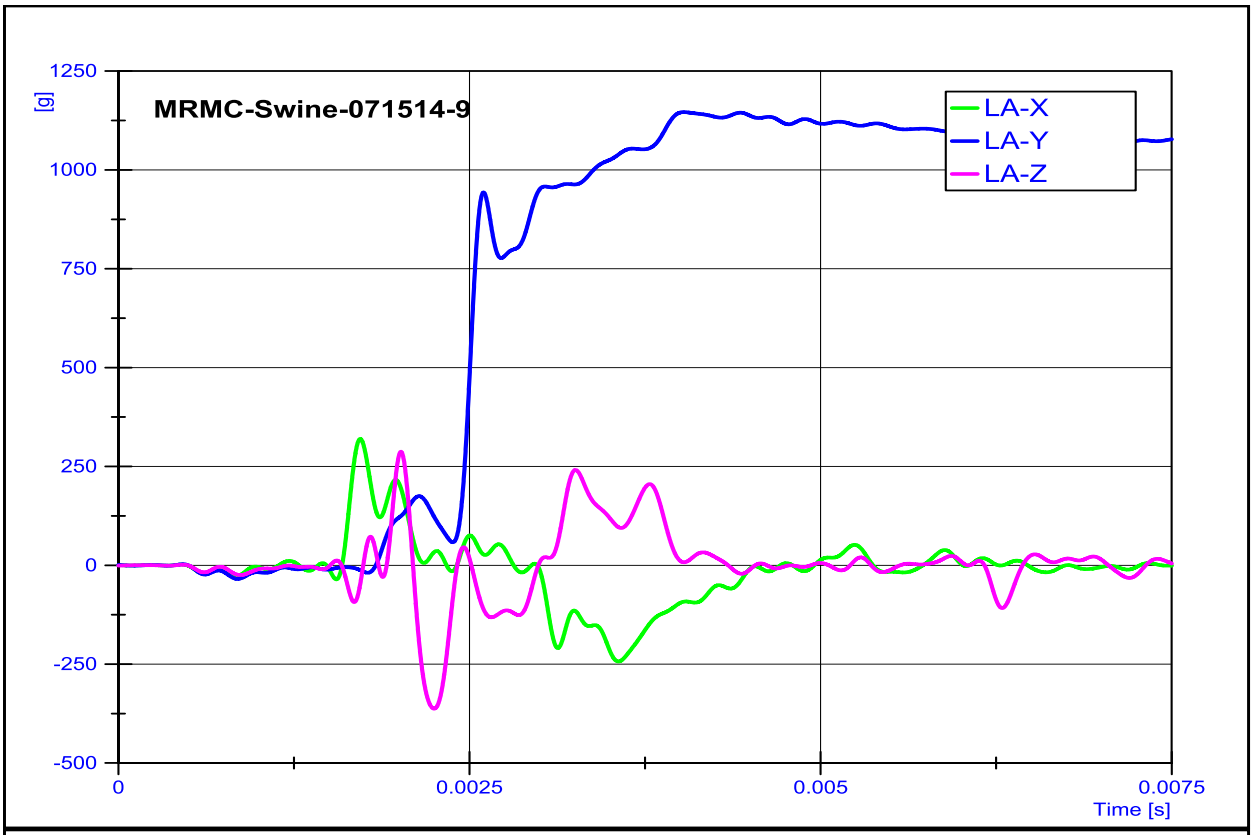
MRMC-Swine-071514-9
LA-X
LA-Y
LA-Z
[g]
1250
1000
750
500
250
0
-250
-500
0
0.0025
0.005
0.0075
Time [s]

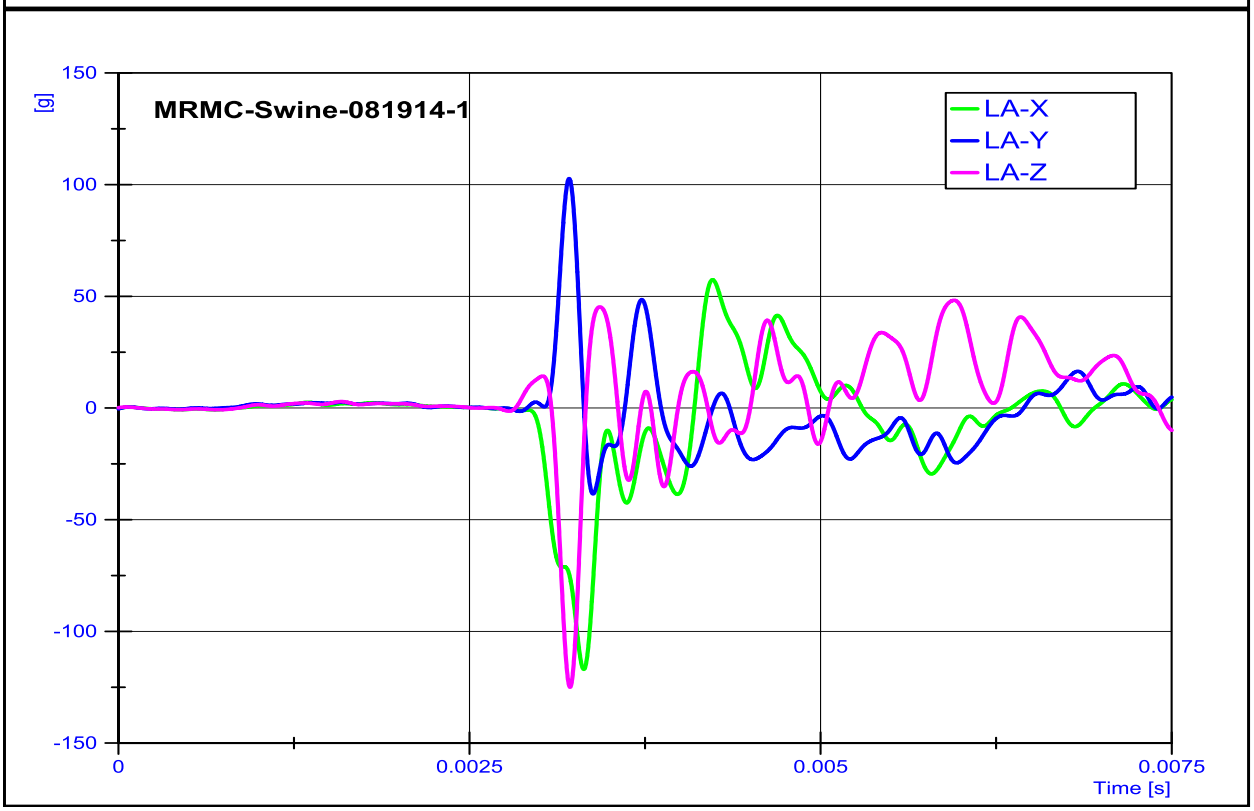
MRMC-Swine-081914-1
LA-X
LA-Y
LA-Z
[g]
150
100
50
0
-50
-100
-150
0
0.0025
0.005
0.0075
Time [s]

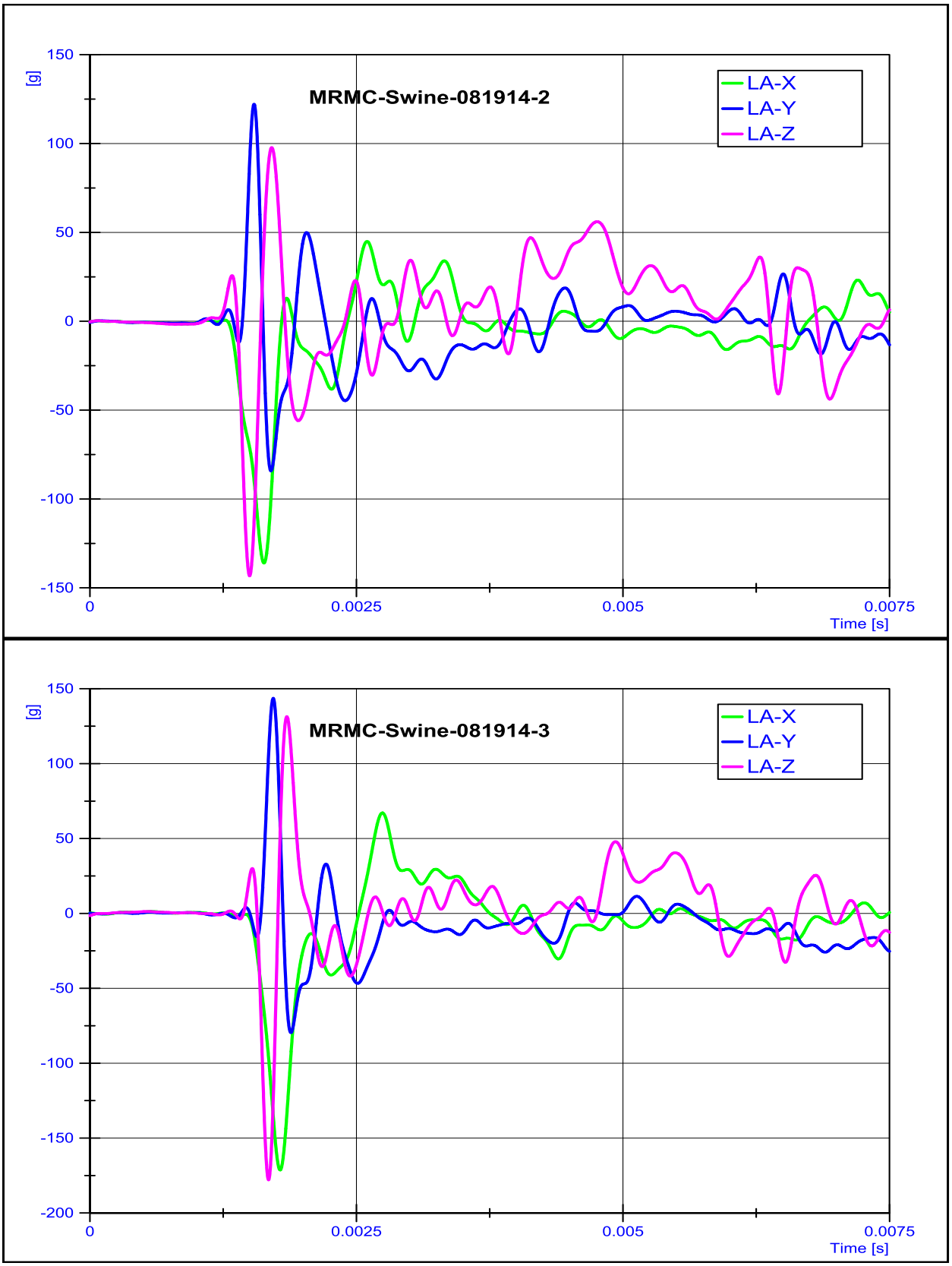
MRMC-Swine-081914-2
LA-X
LA-Y
LA-Z
[g]
150
100
50
0
-50
-100
-150
0
0.0025
0.005
0.0075
Time [s]
MRMC-Swine-081914-3
LA-X
LA-Y
LA-Z
[g]
150
100
50
0
-50
-100
-150
-200
0
0.0025
0.005
0.0075
Time [s]

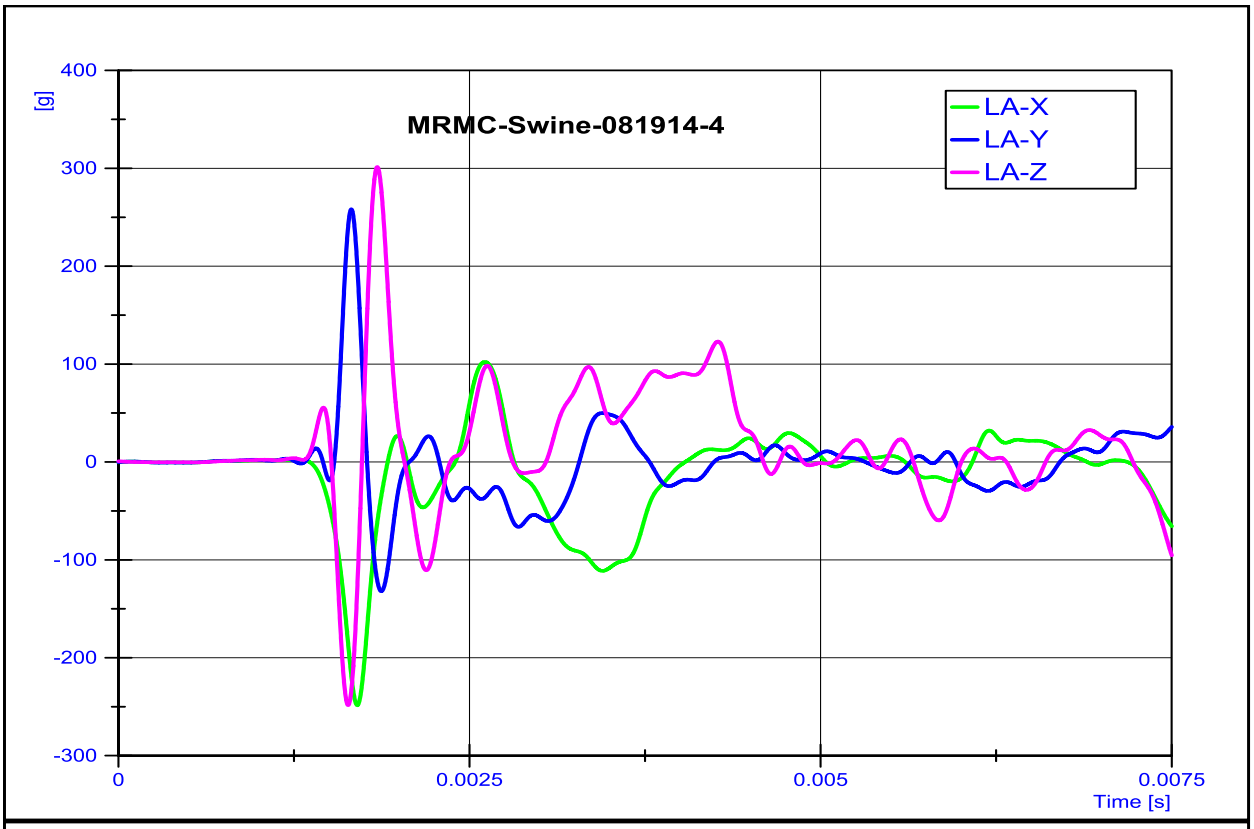
MRMC-Swine-081914-4
LA-X
LA-Y
LA-Z
[g]
400
300
200
100
0
-100
-200
-300
0
0.0025
0.005
0.0075
Time [s]

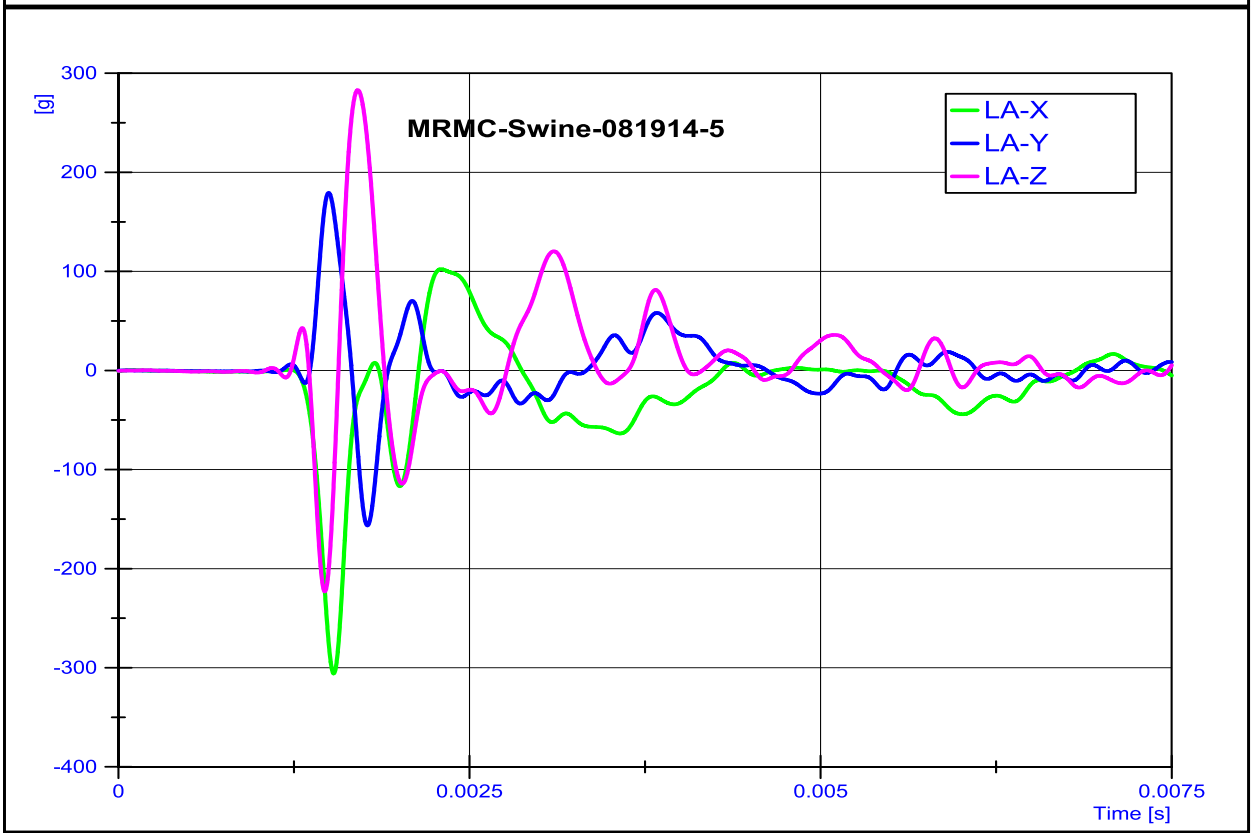
MRMC-Swine-081914-5
LA-X
LA-Y
LA-Z
[g]
300
200
100
0
-100
-200
-300
-400
0
0.0025
0.005
0.0075
Time [s]

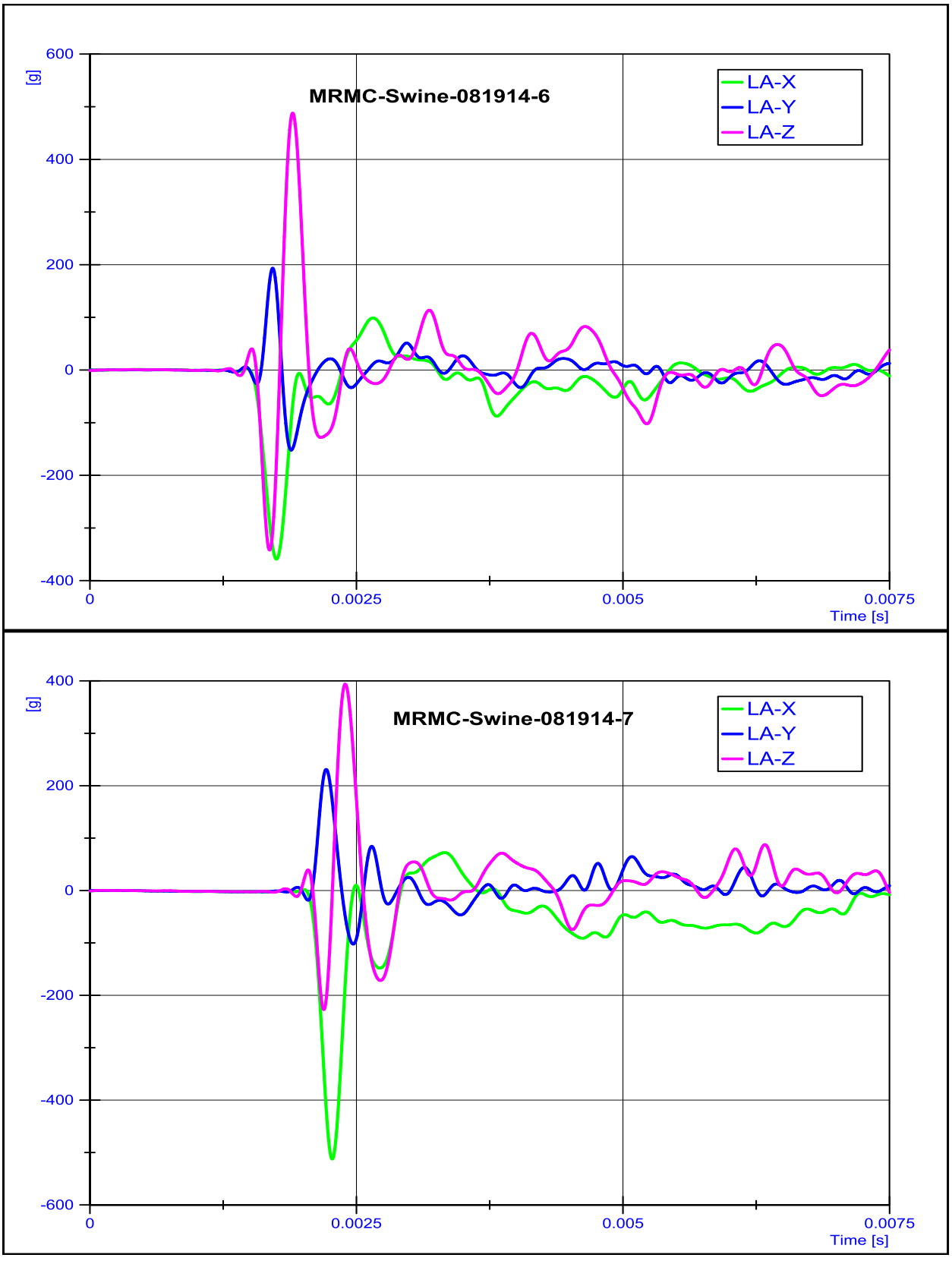
MRMC-Swine-081914-6
LA-X
LA-Y
LA-Z
[g]
600
400
200
0
-200
-400
0
0.0025
0.005
0.0075
Time [s]
MRMC-Swine-081914-7
LA-X
LA-Y
LA-Z
[g]
400
200
0
-200
-400
-600
0
0.0025
0.005
0.0075
Time [s]

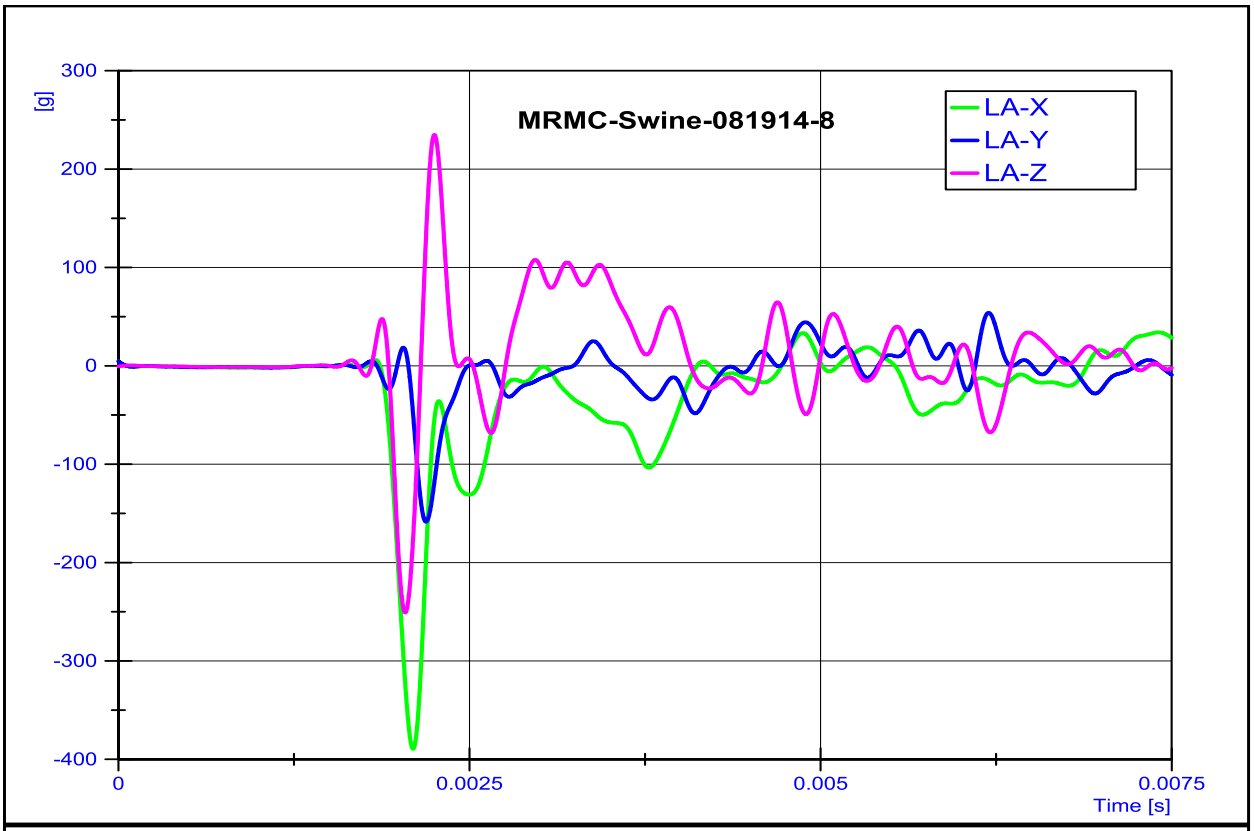
MRMC-Swine-081914-8
LA-X
LA-Y
LA-Z
[g]
300
200
100
0
-100
-200
-300
-400
0
0.0025
0.005
0.0075
Time [s]

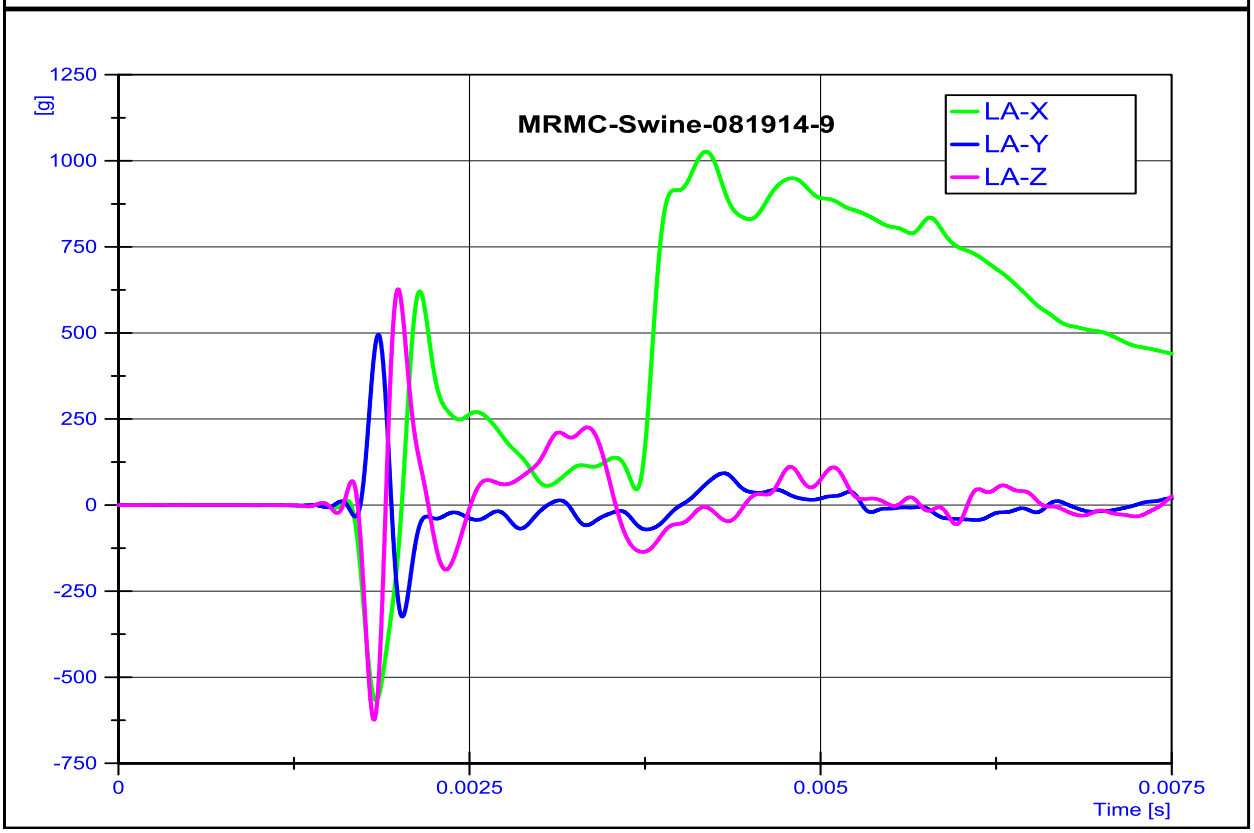
MRMC-Swine-081914-9
LA-X
LA-Y
LA-Z
[g]
1250
1000
750
500
250
0
-250
-500
-750
0
0.0025
0.005
0.0075
Time [s]

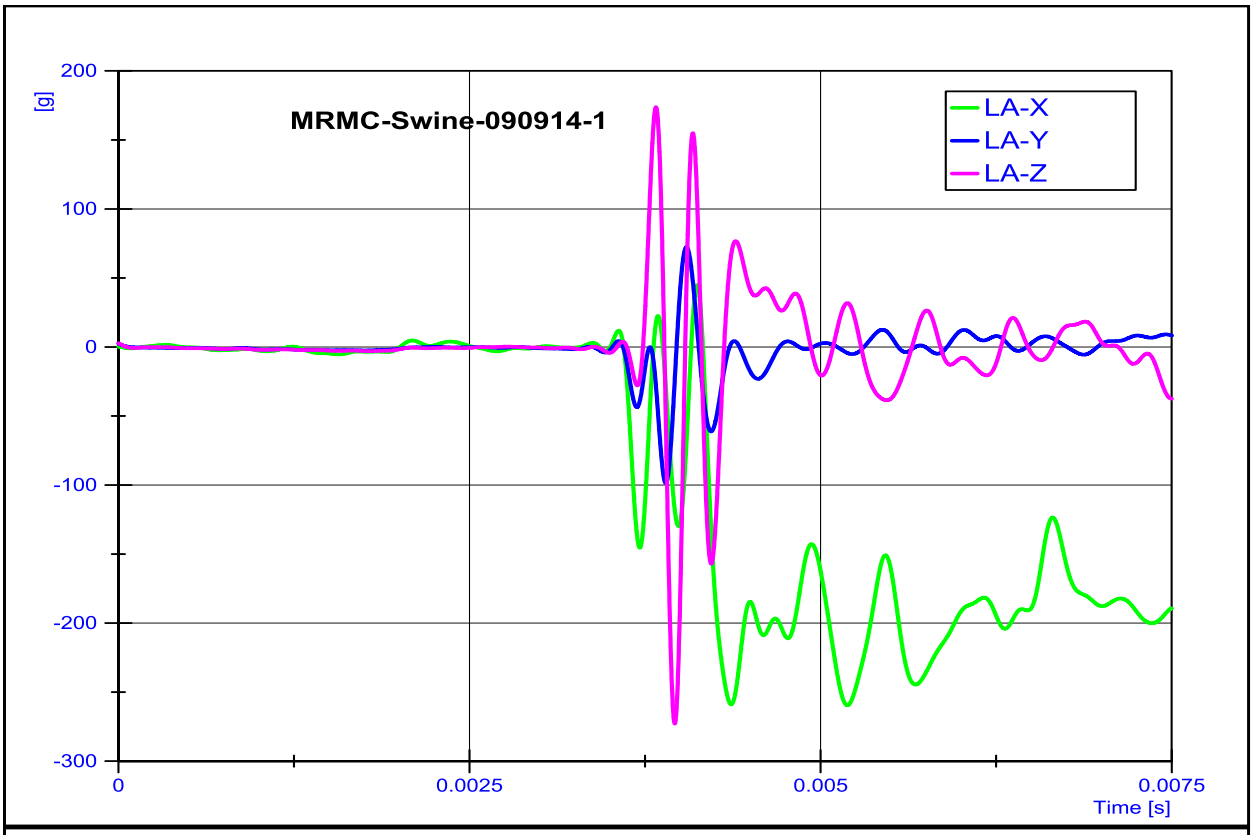
MRMC-Swine-090914-1
LA-X
LA-Y
LA-Z
[g]
200
100
0
-100
-200
-300
0
0.0025
0.005
0.0075
Time [s]

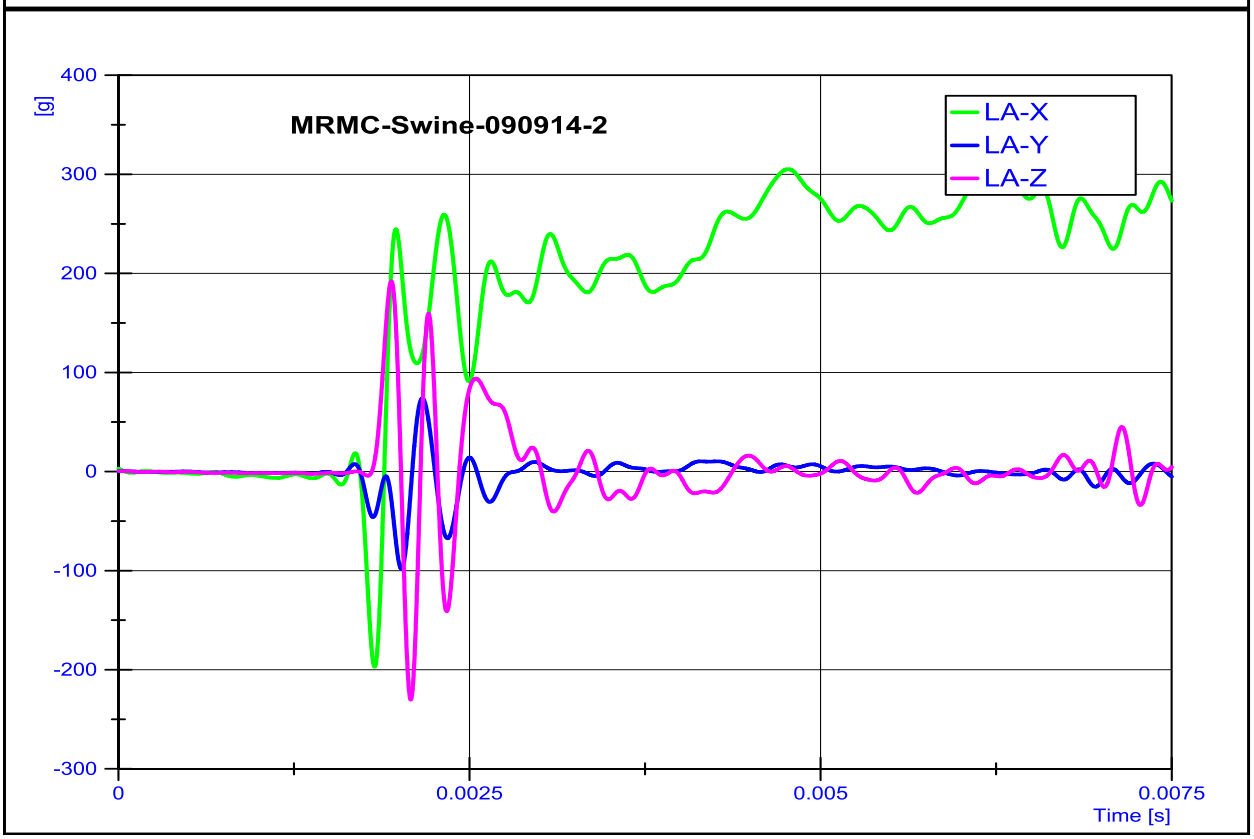
MRMC-Swine-090914-2
LA-X
LA-Y
LA-Z
[g]
400
300
200
100
0
-100
-200
-300
0
0.0025
0.005
0.0075
Time [s]

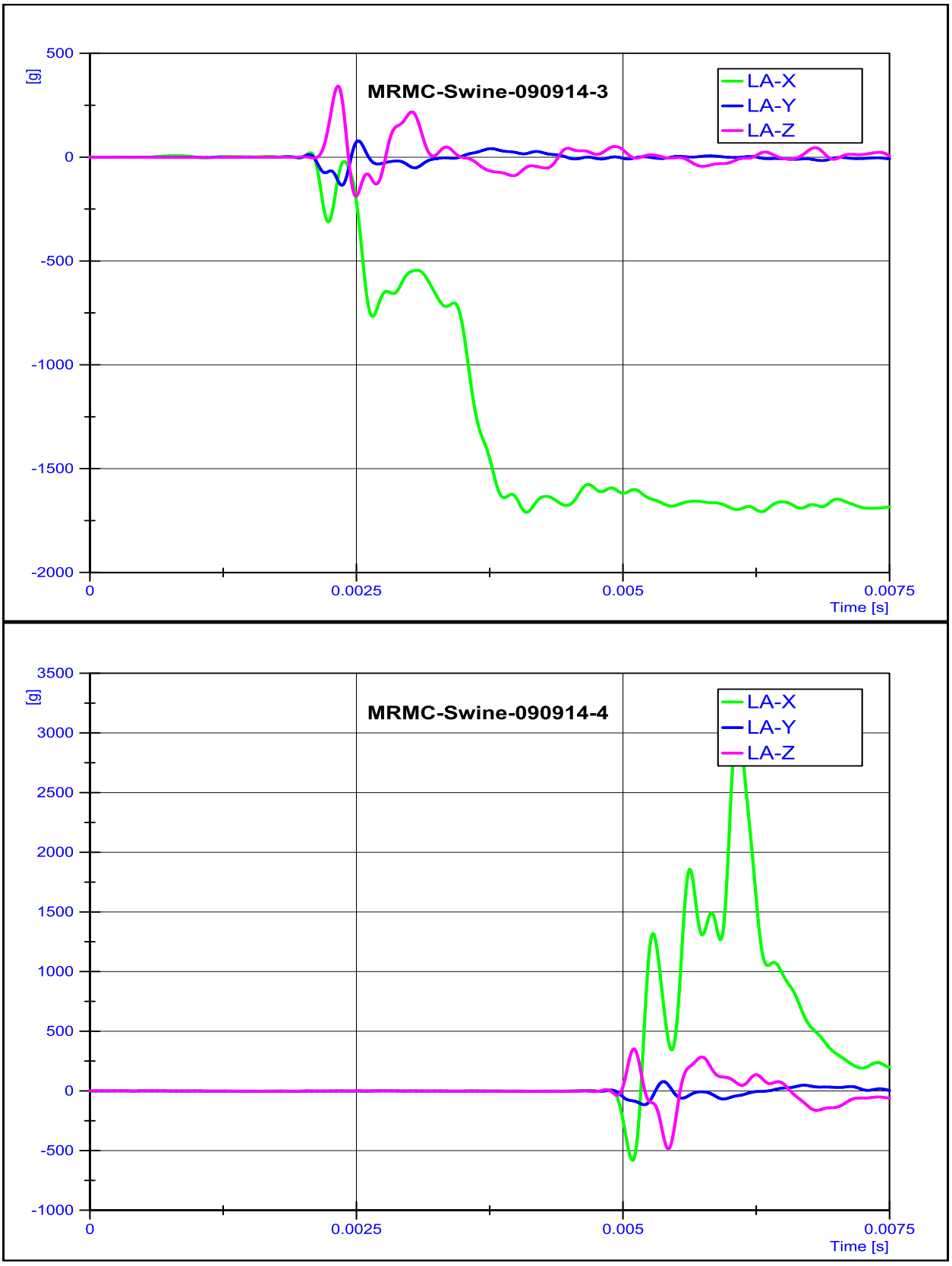
MRMC-Swine-090914-3
LA-X
LA-Y
LA-Z
[g]
500
0
-500
-1000
-1500
-2000
0
0.0025
0.005
0.0075
Time [s]
MRMC-Swine-090914-4
LA-X
LA-Y
LA-Z
[g]
3500
3000
2500
2000
1500
1000
500
0
-500
-1000
0
0.0025
0.005
0.0075
Time [s]

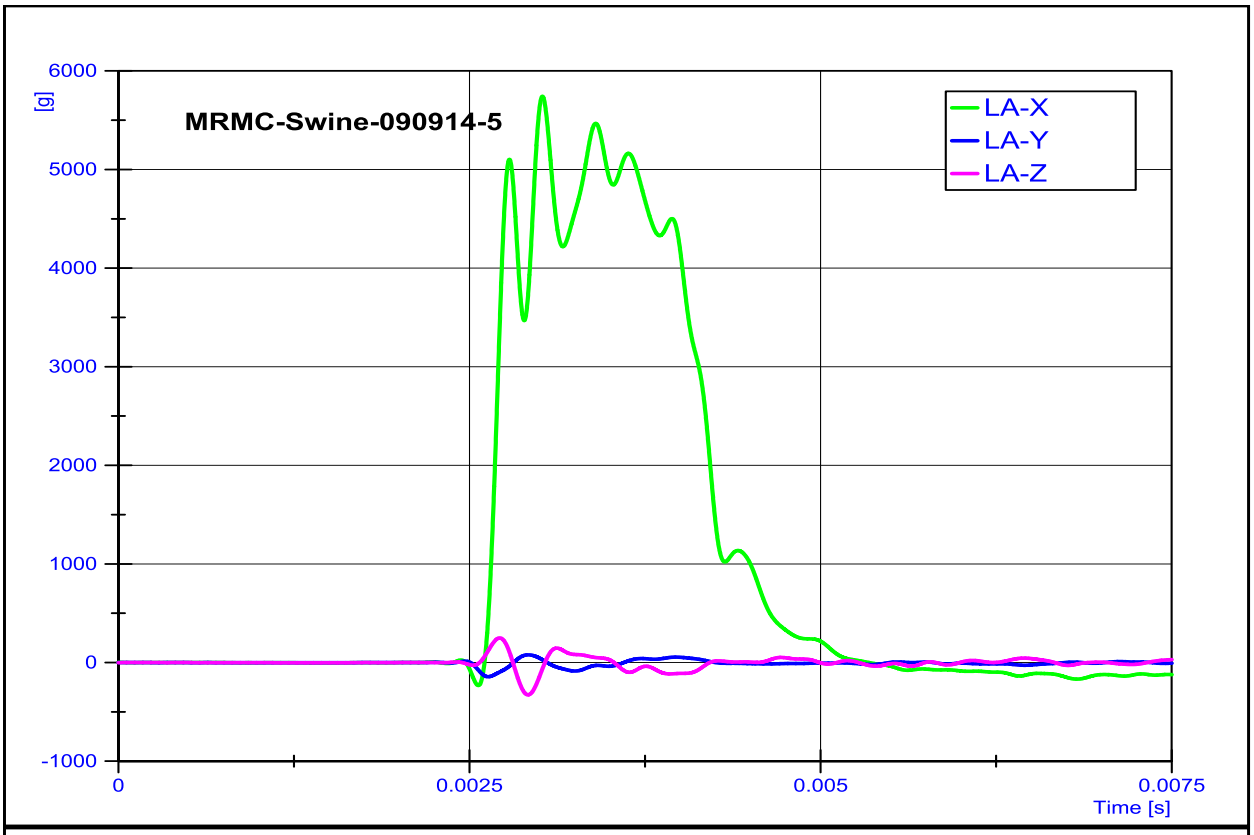
MRMC-Swine-090914-5
LA-X
LA-Y
LA-Z
[g]
6000
5000
4000
3000
2000
1000
0
-1000
0
0.0025
0.005
0.0075
Time [s]

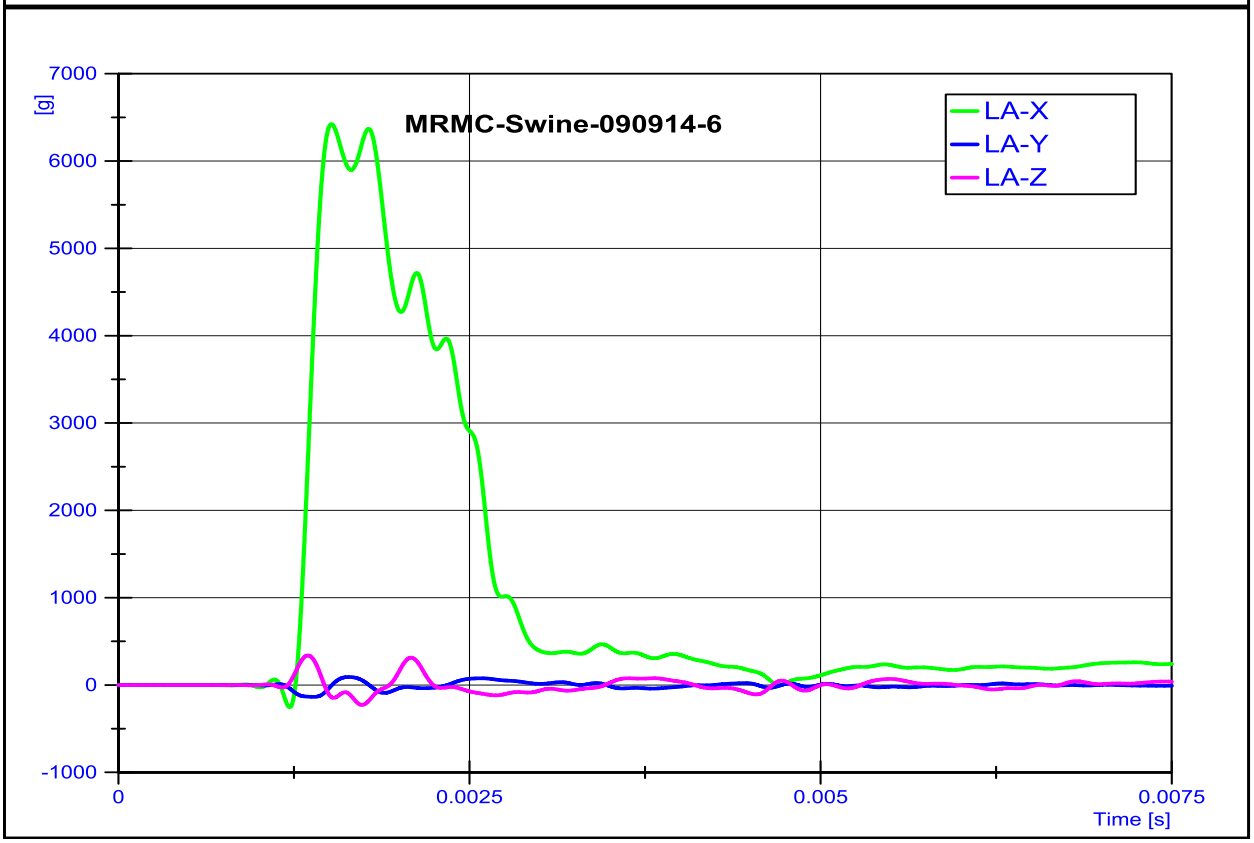
MRMC-Swine-090914-6
LA-X
LA-Y
LA-Z
[g]
7000
6000
5000
4000
3000
2000
1000
0
-1000
0
0.0025
0.005
0.0075
Time [s]

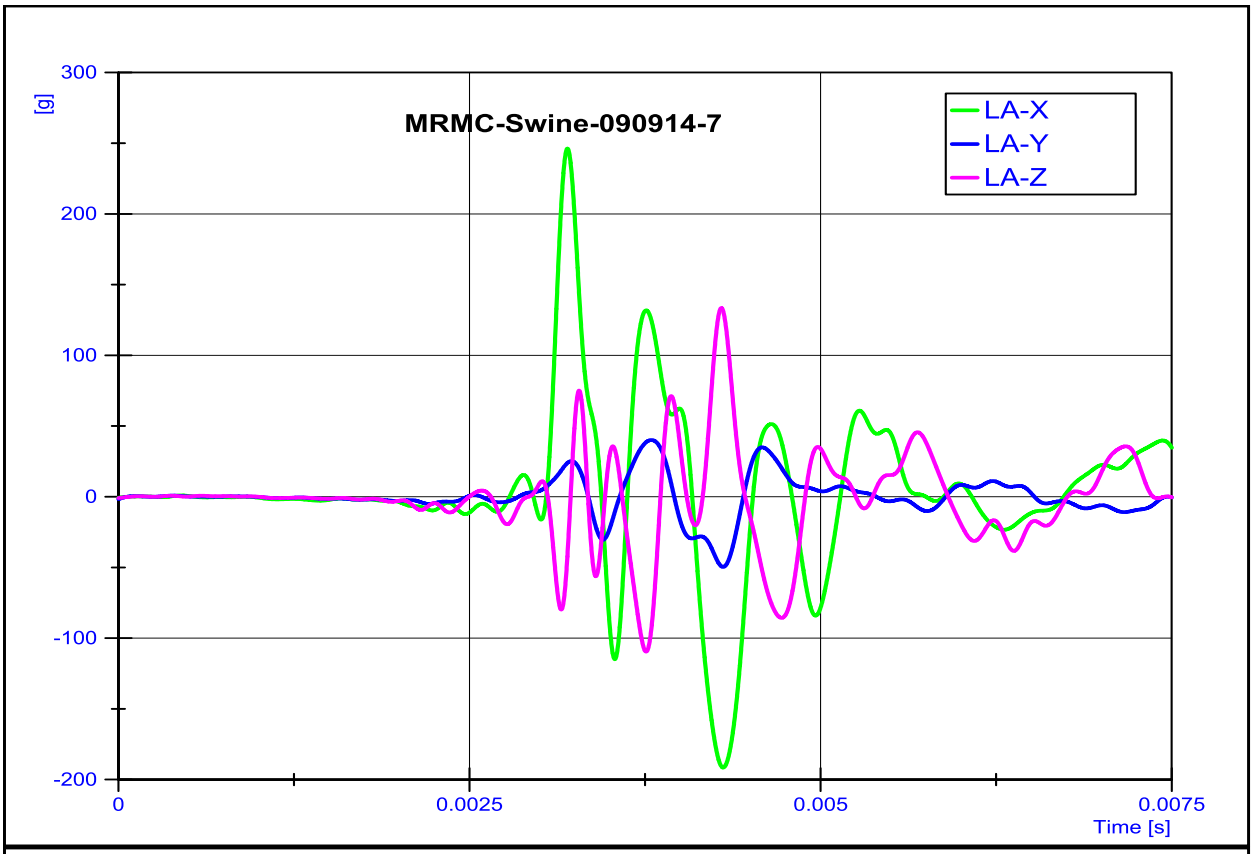
MRMC-Swine-090914-7
LA-X
LA-Y
LA-Z
[g]
300
200
100
0
-100
-200
0
0.0025
0.005
0.0075
Time [s]

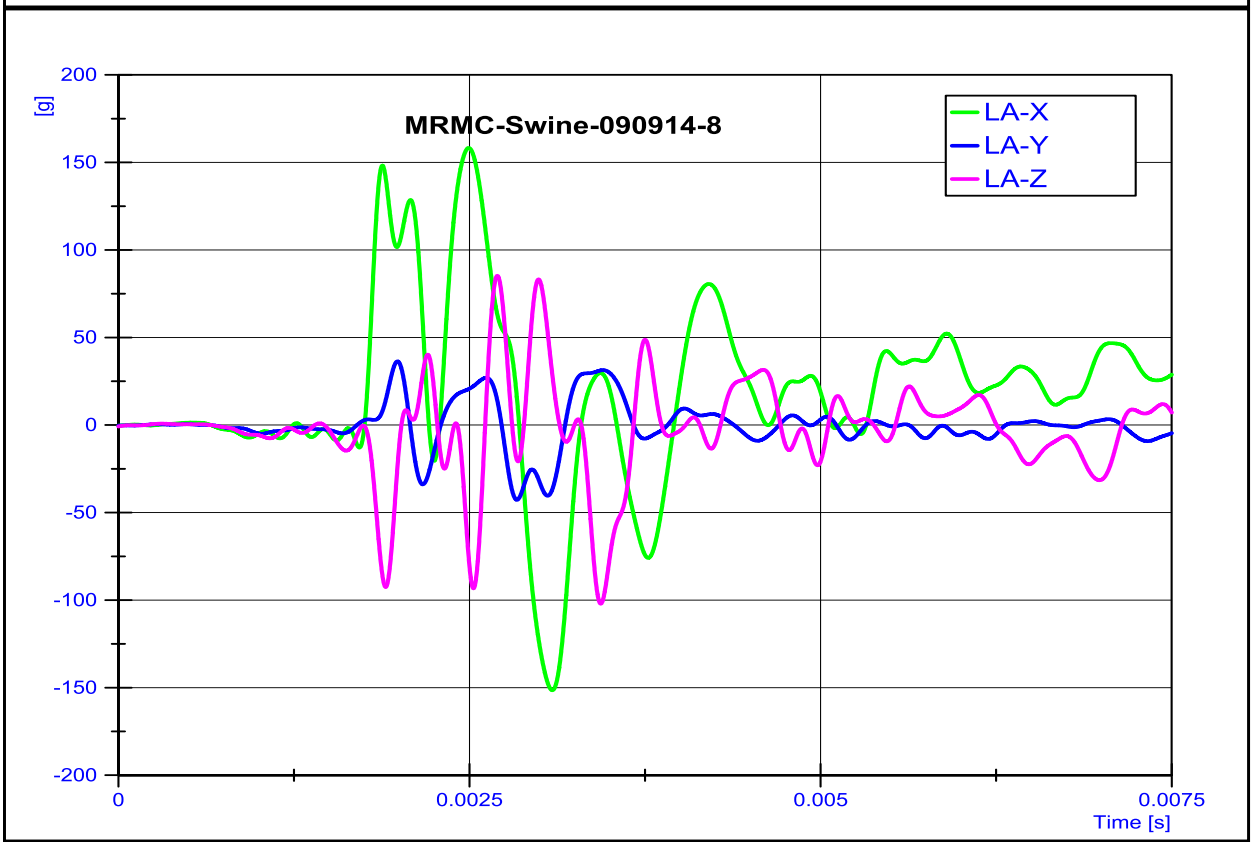
MRMC-Swine-090914-8
LA-X
LA-Y
LA-Z
[g]
200
150
100
50
0
-50
-100
-150
-200
0
0.0025
0.005
0.0075
Time [s]

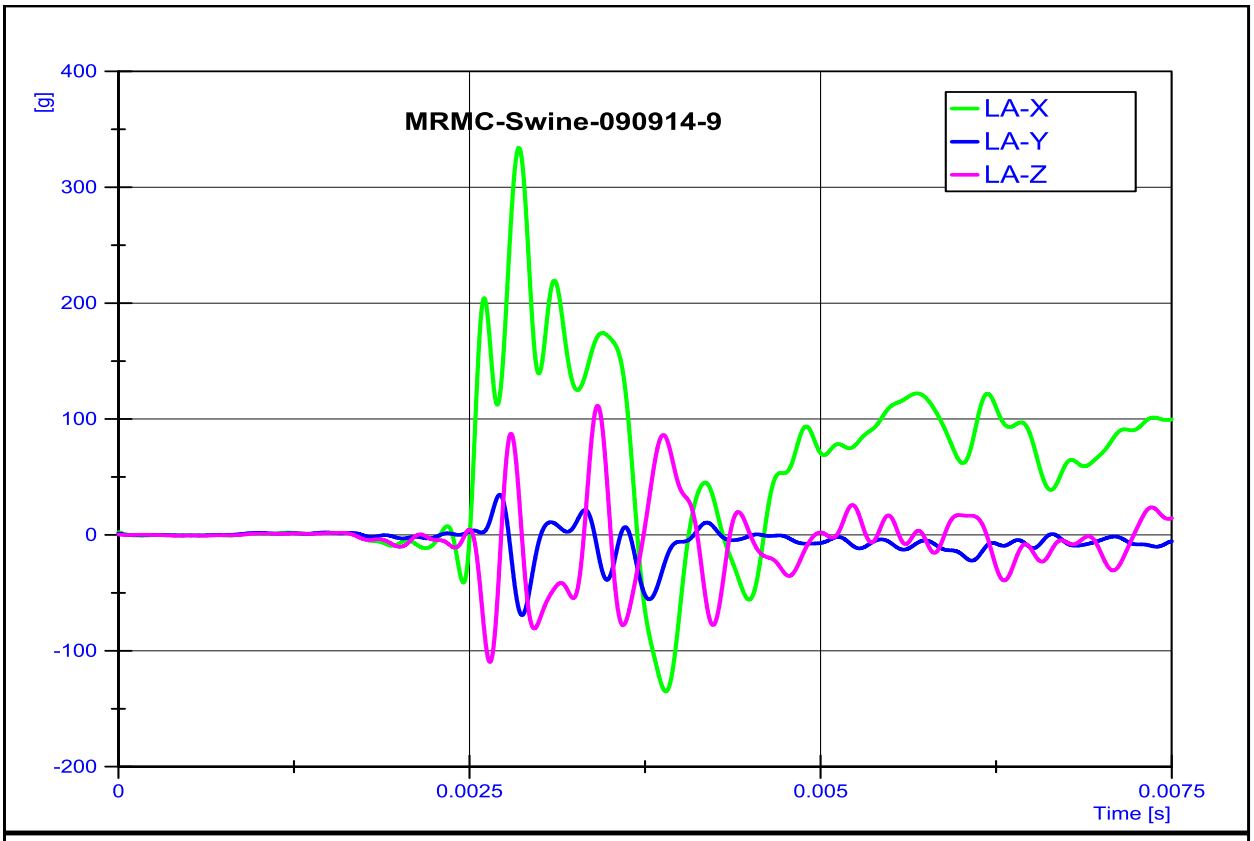
MRMC-Swine-090914-9
LA-X
LA-Y
LA-Z
[g]
400
300
200
100
0
-100
-200
0
0.0025
0.005
0.0075
Time [s]

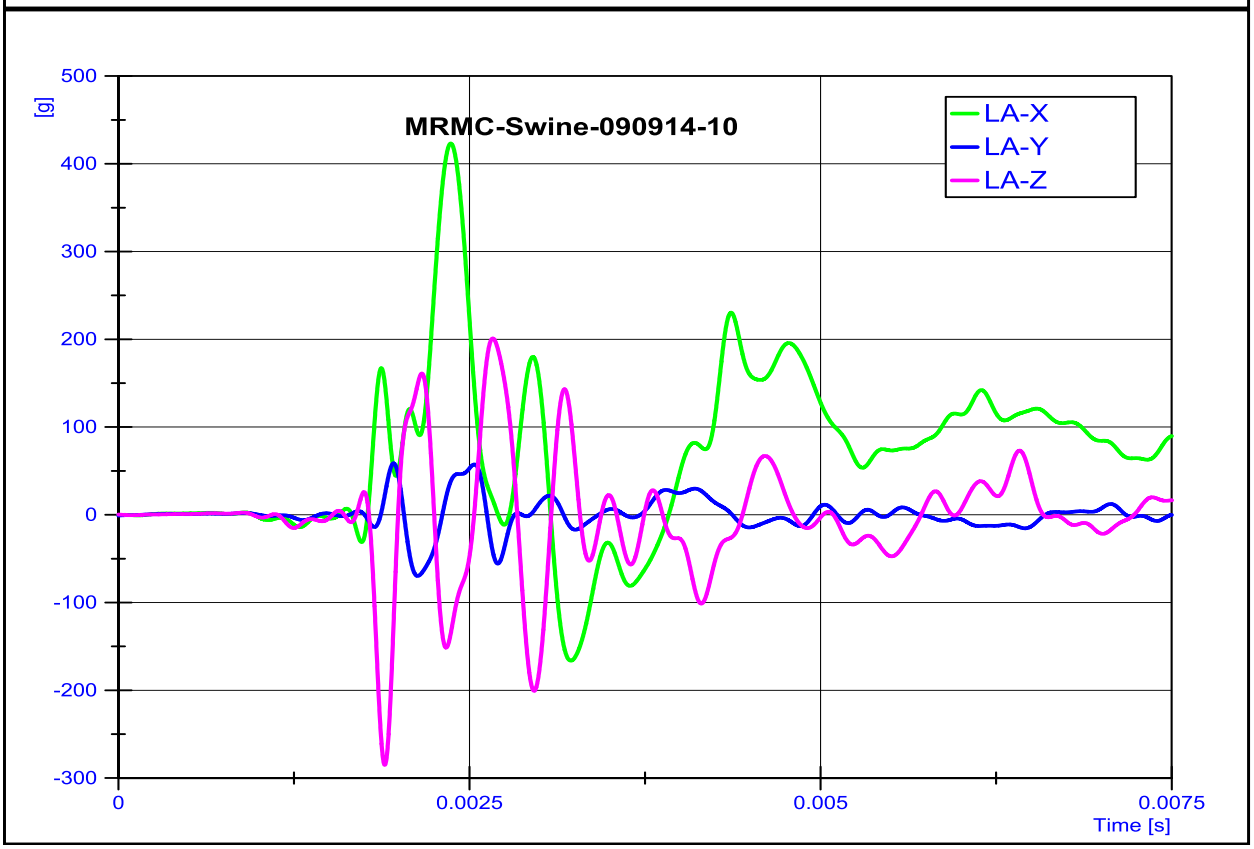
MRMC-Swine-090914-10
LA-X
LA-Y
LA-Z
[g]
500
400
300
200
100
0
-100
-200
-300
0
0.0025
0.005
0.0075
Time [s]

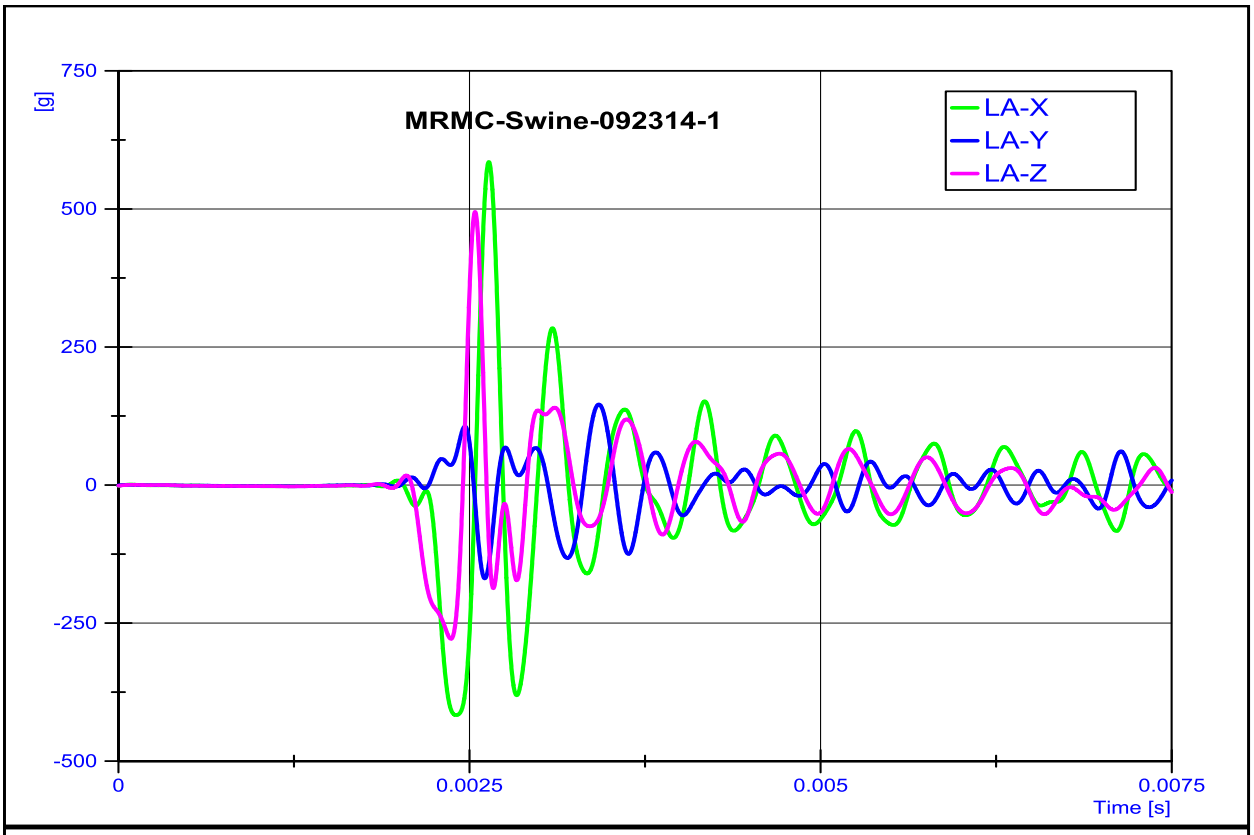
MRMC-Swine-092314-1
LA-X
LA-Y
LA-Z
[g]
750
500
250
0
-250
-500
0
0.0025
0.005
0.0075
Time [s]

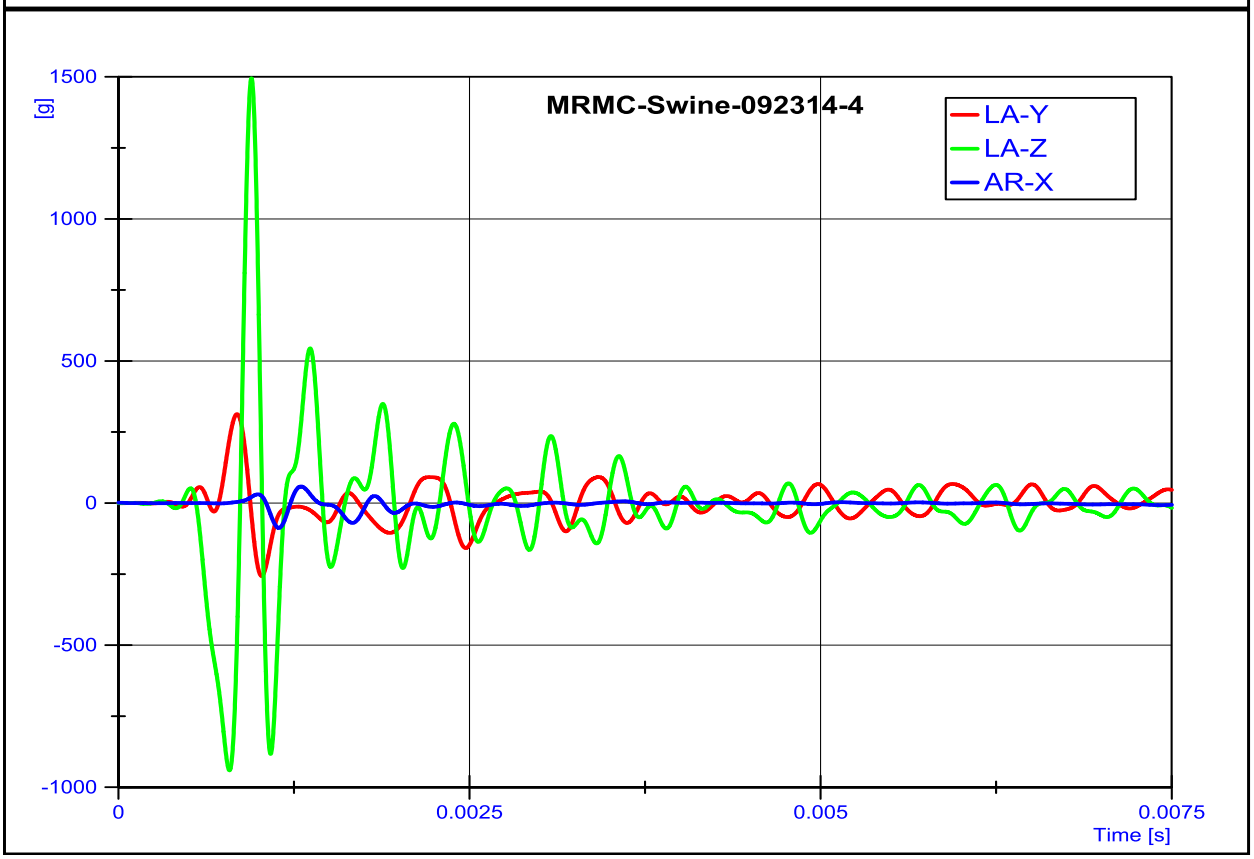
MRMC-Swine-092314-4
LA-Y
LA-Z
AR-X
[g]
1500
1000
500
0
-500
-1000
0
0.0025
0.005
0.0075
Time [s]

# APPENDIX C: SIDE AND REAR BLAST DATA

## 1: REAR AND SIDE BLAST ICP DISTRIBUTION OVERVIEW

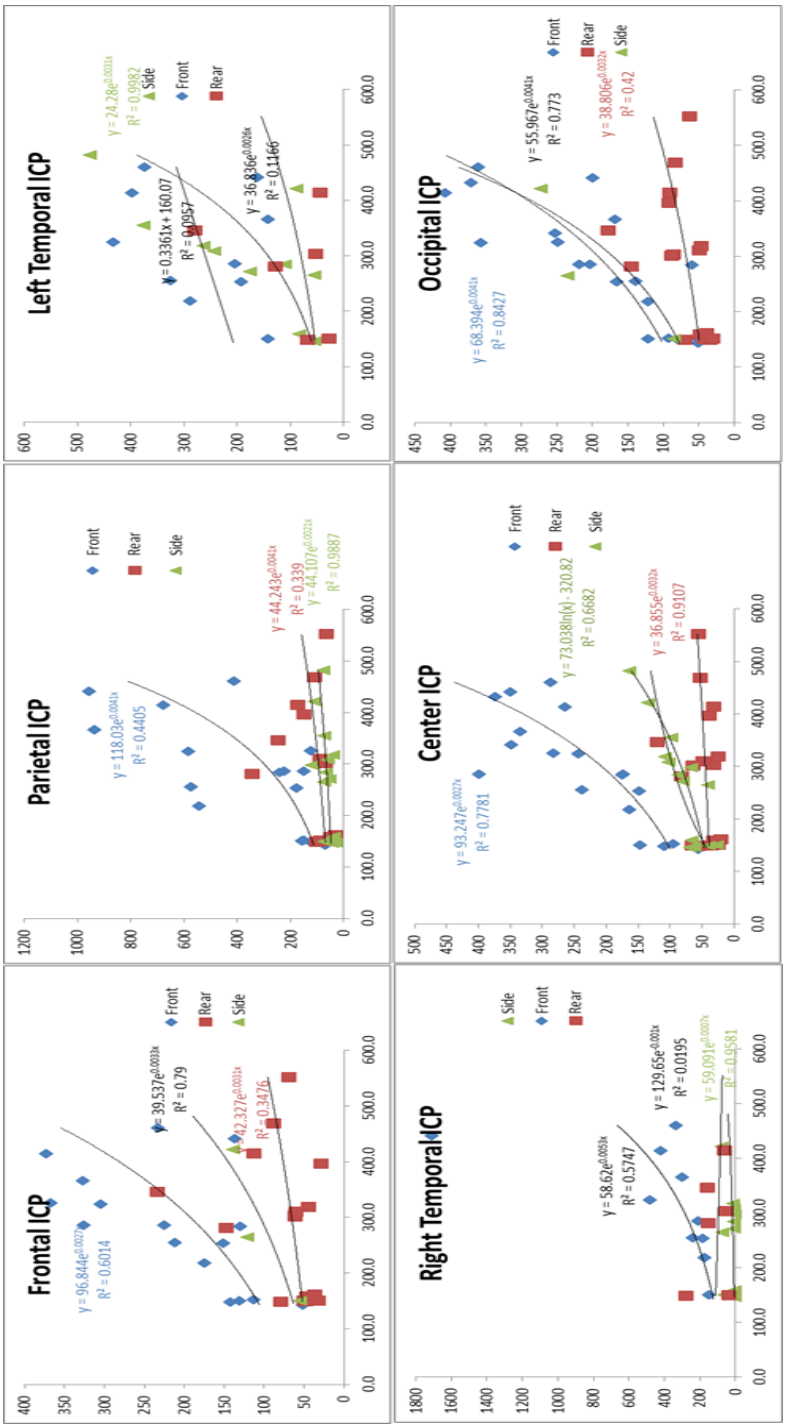

## 2. SIDE BLAST MOTION CURVES

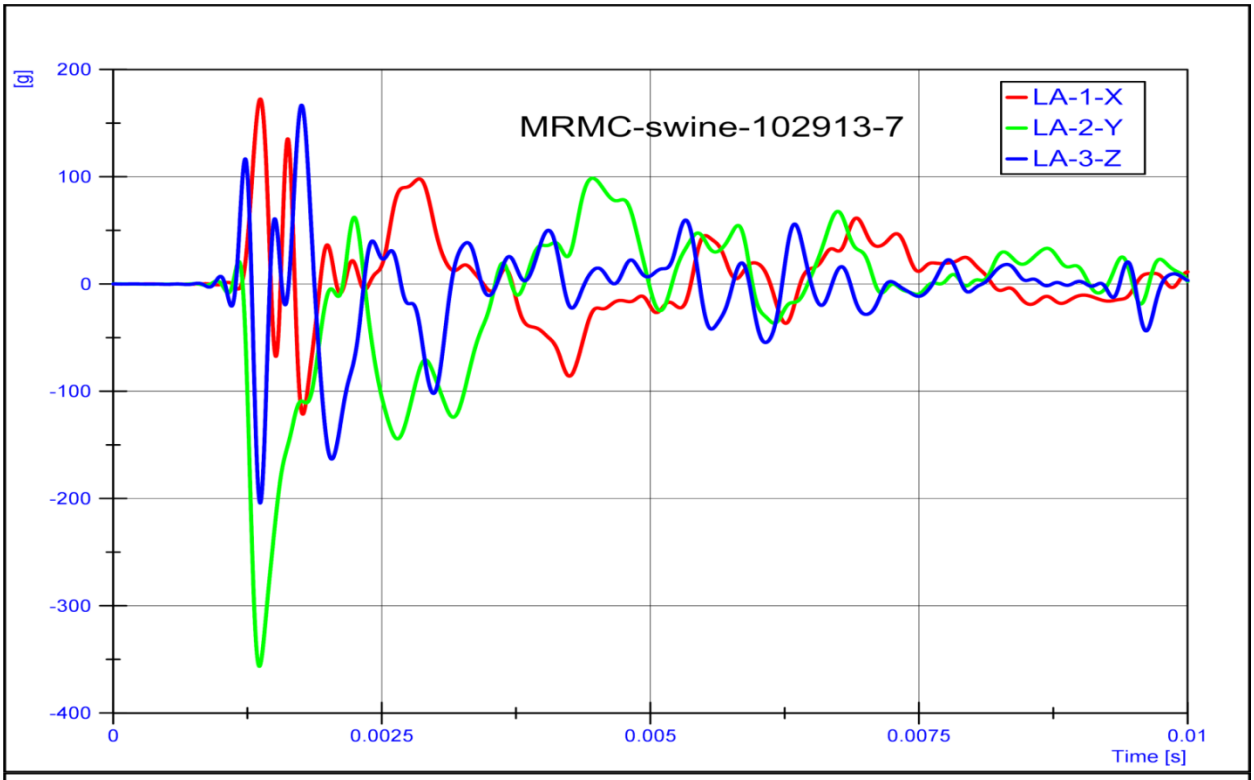


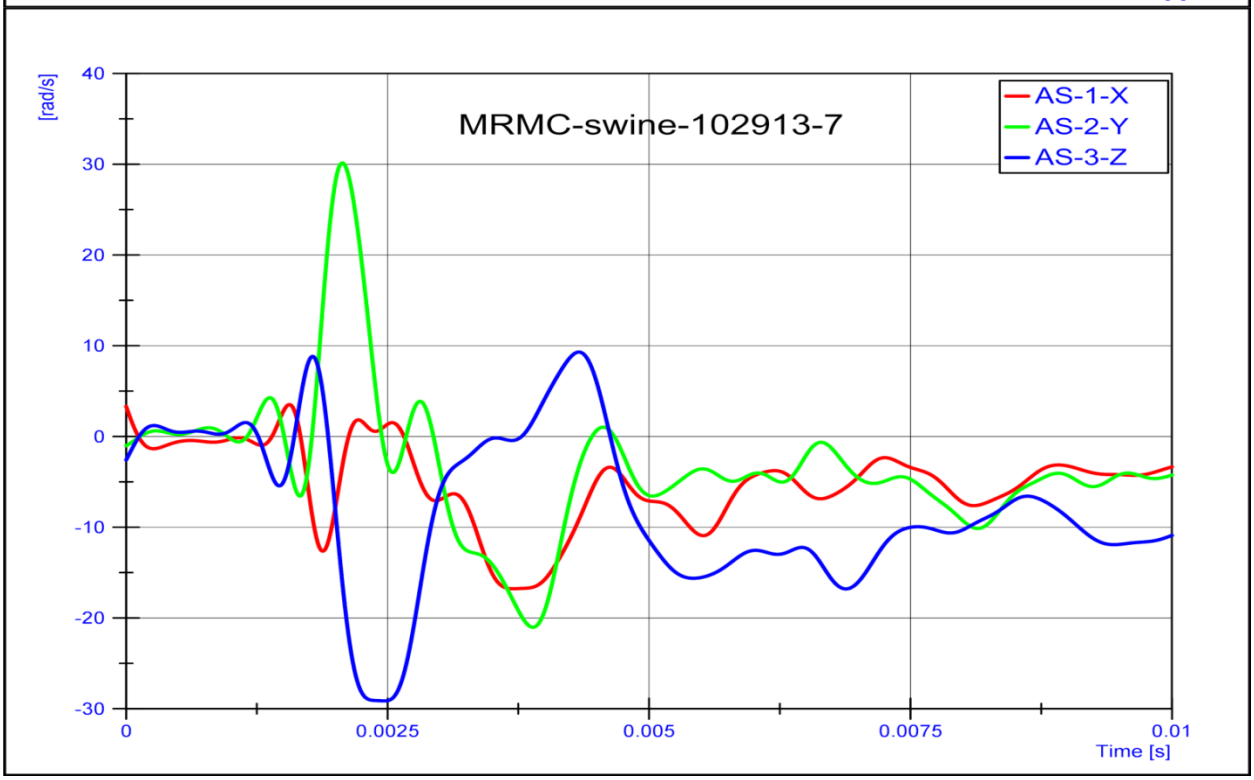

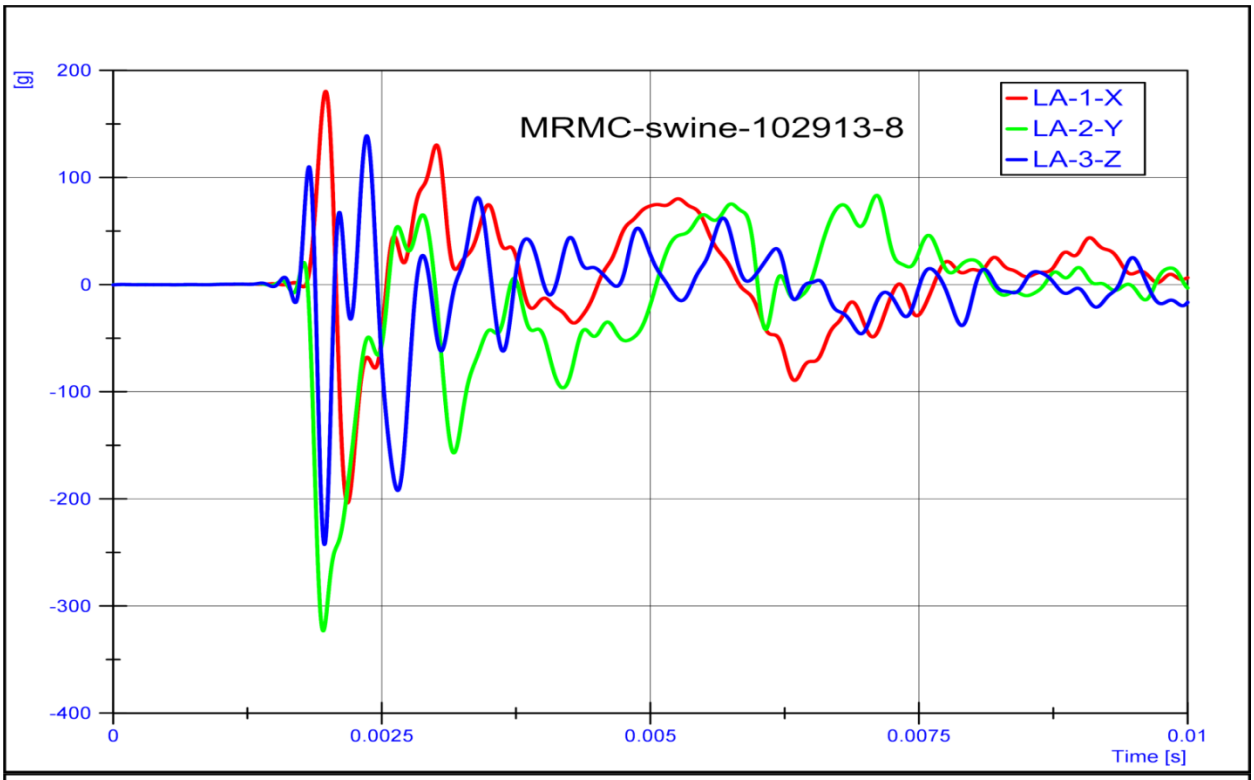
MRMC-swine-102913-8
LA-1-X
LA-2-Y
LA-3-Z
[g]
200
100
0
-100
-200
-300
-400
0
0.0025
0.005
0.0075
0.01
Time [s]

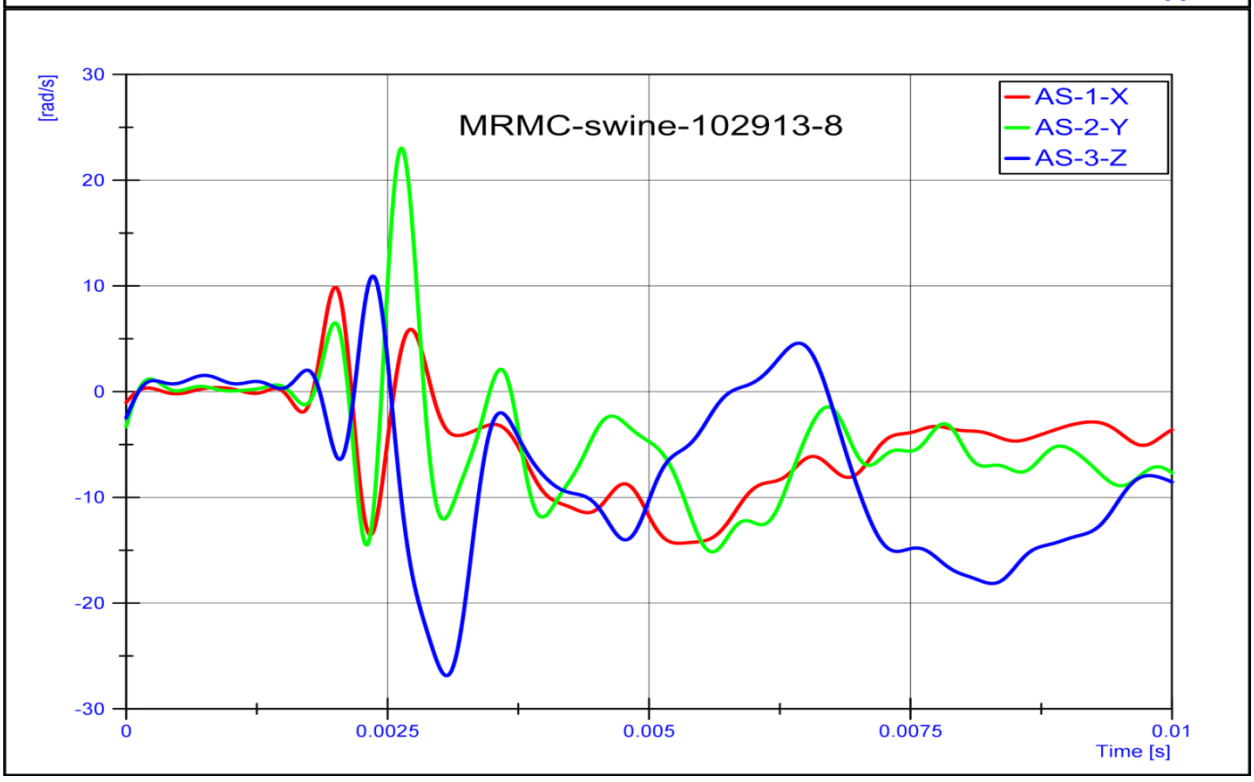
MRMC-swine-102913-8
AS-1-X
AS-2-Y
AS-3-Z
[rad/s]
30
20
10
0
-10
-20
-30
0
0.0025
0.005
0.0075
0.01
Time [s]

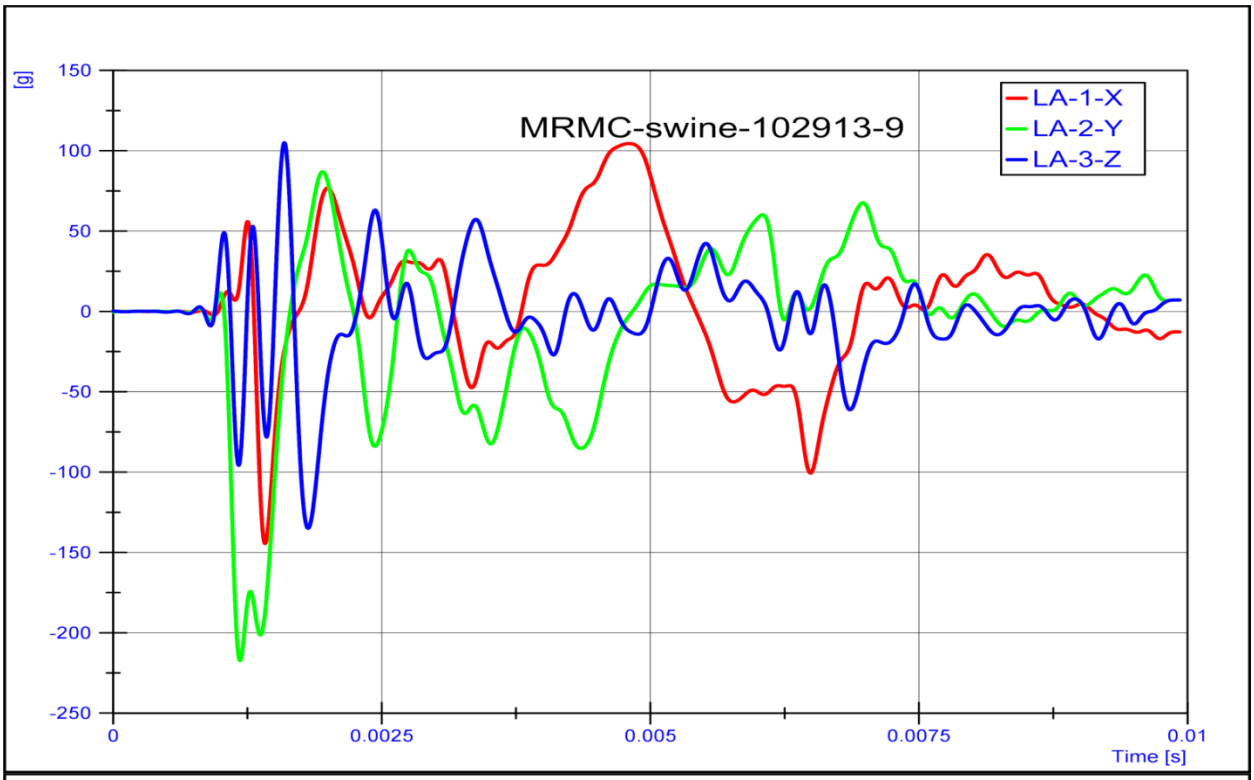
MRMC-swine-102913-9
LA-1-X
LA-2-Y
LA-3-Z
[g]
150
100
50
0
-50
-100
-150
-200
-250
0
0.0025
0.005
0.0075
0.01
Time [s]

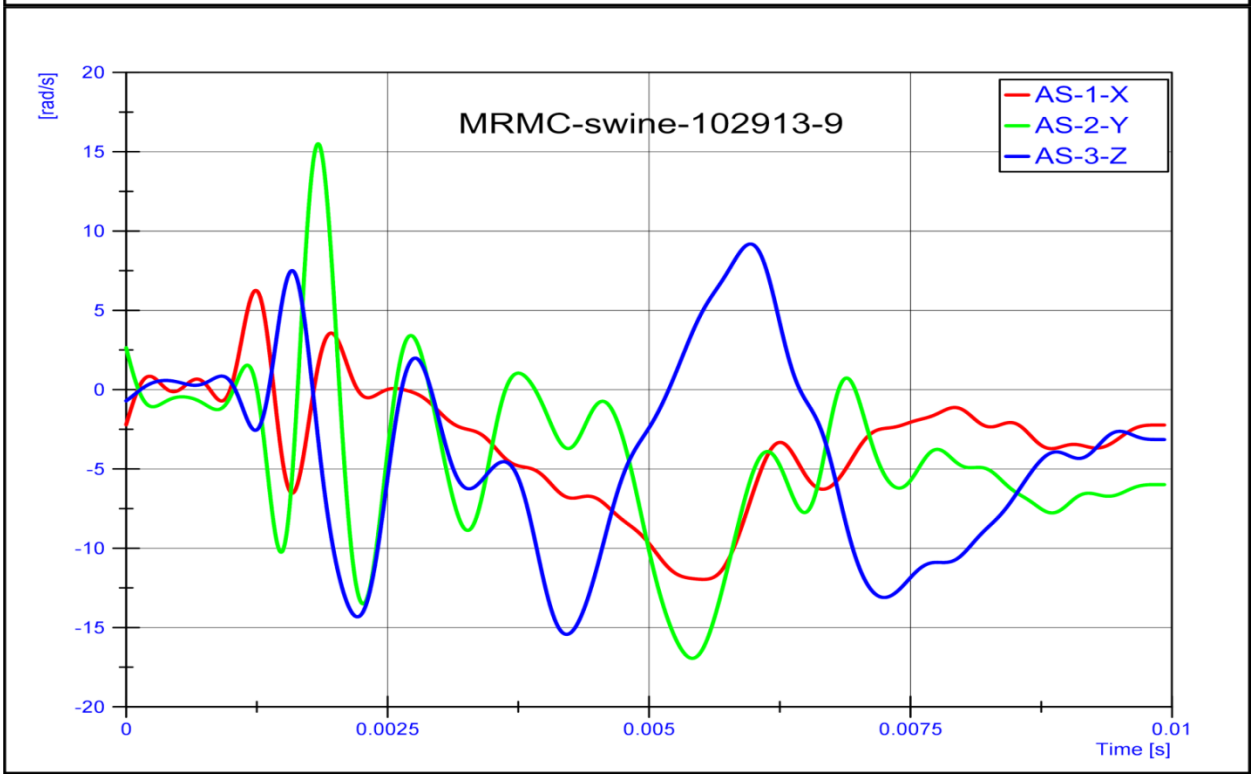
MRMC-swine-102913-9
AS-1-X
AS-2-Y
AS-3-Z
[rad/s]
20
15
10
5
0
-5
-10
-15
-20
0
0.0025
0.005
0.0075
0.01
Time [s]

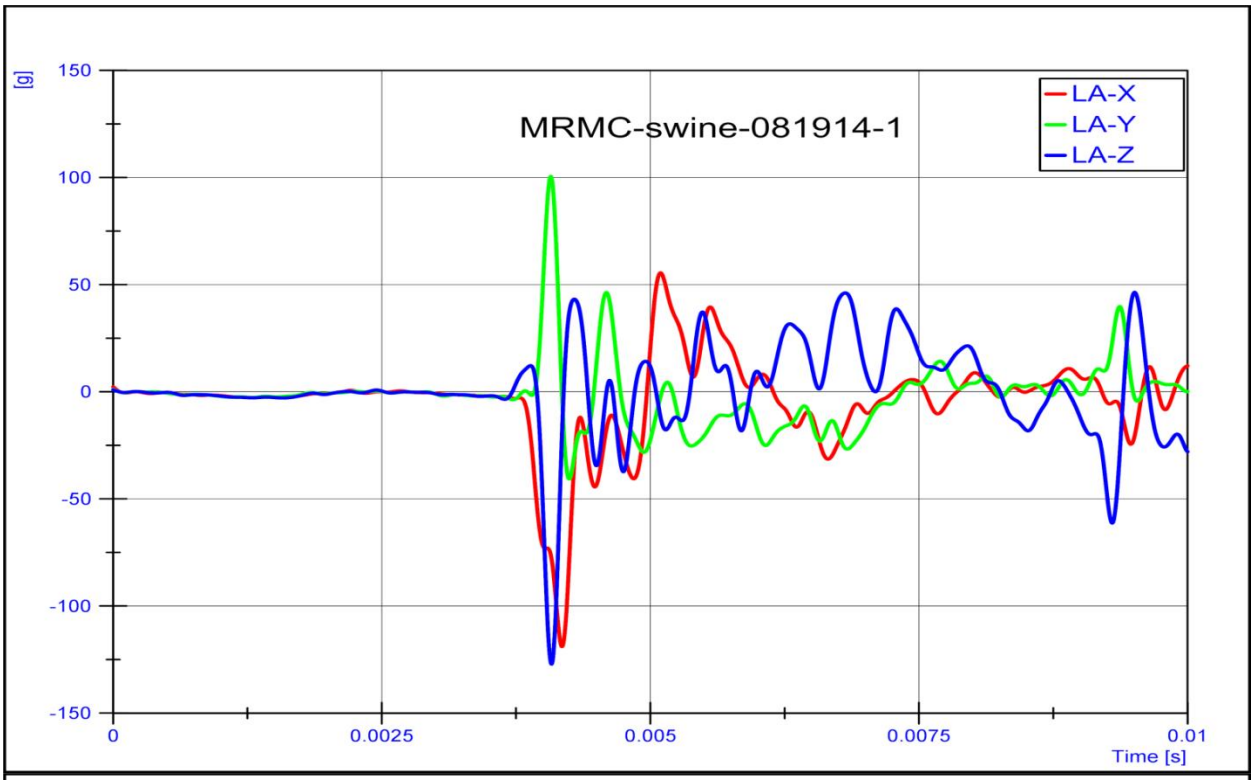
MRMC-swine-081914-1
LA-X
LA-Y
LA-Z
[g]
150
100
50
0
-50
-100
-150
0
0.0025
0.005
0.0075
0.01
Time [s]

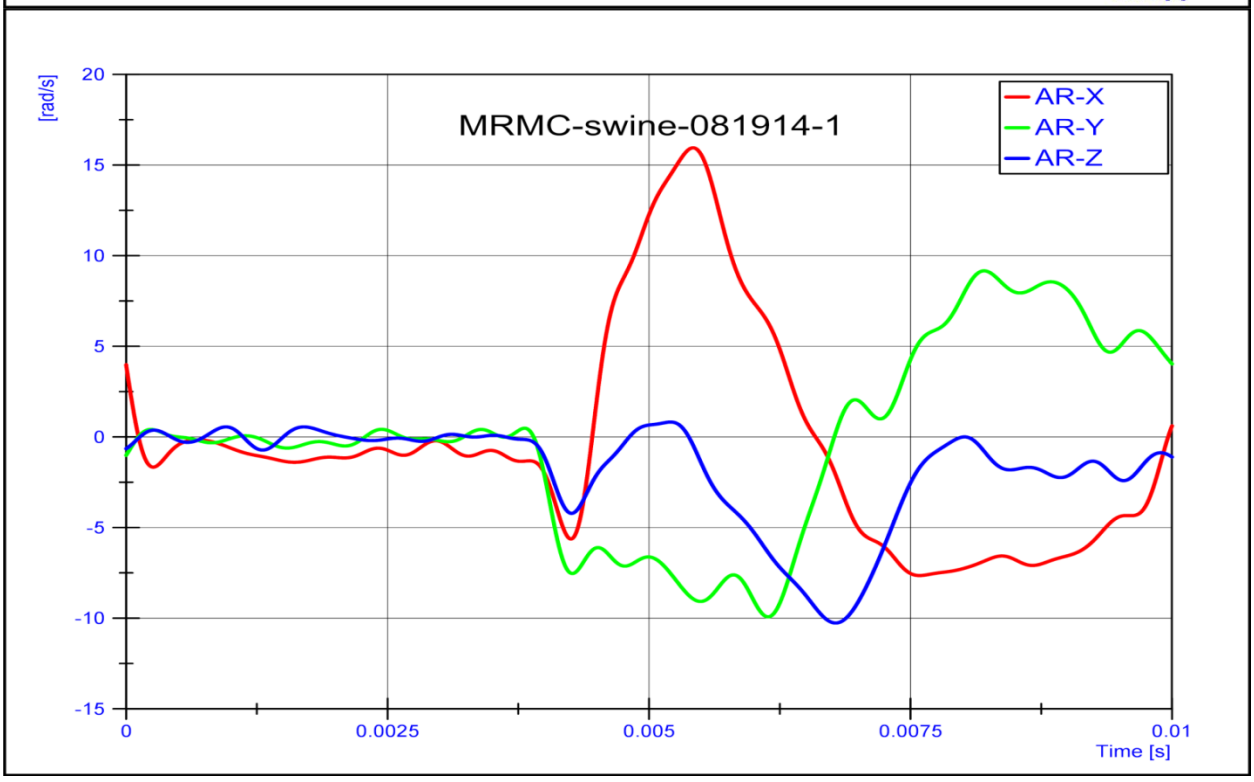
MRMC-swine-081914-1
AR-X
AR-Y
AR-Z
[rad/s]
20
15
10
5
0
-5
-10
-15
0
0.0025
0.005
0.0075
0.01
Time [s]

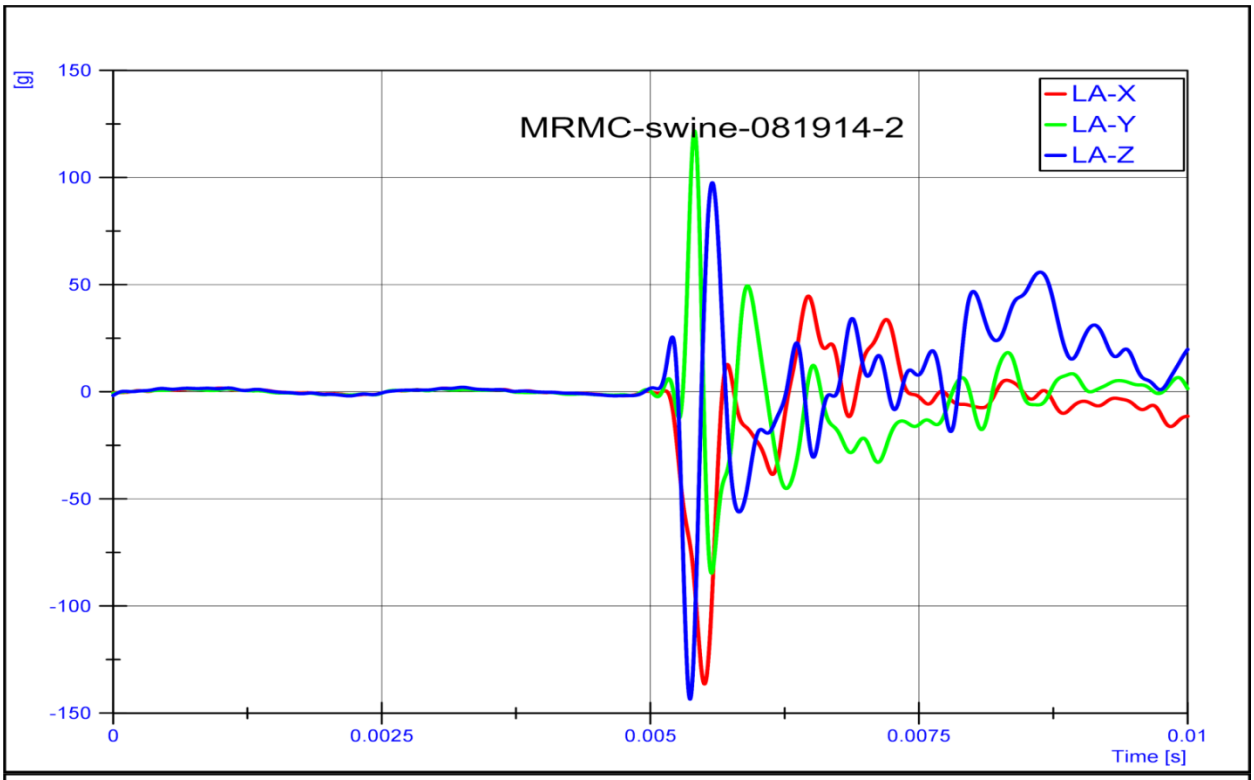
MRMC-swine-081914-2
LA-X
LA-Y
LA-Z
[g]
150
100
50
0
-50
-100
-150
0
0.0025
0.005
0.0075
0.01
Time [s]

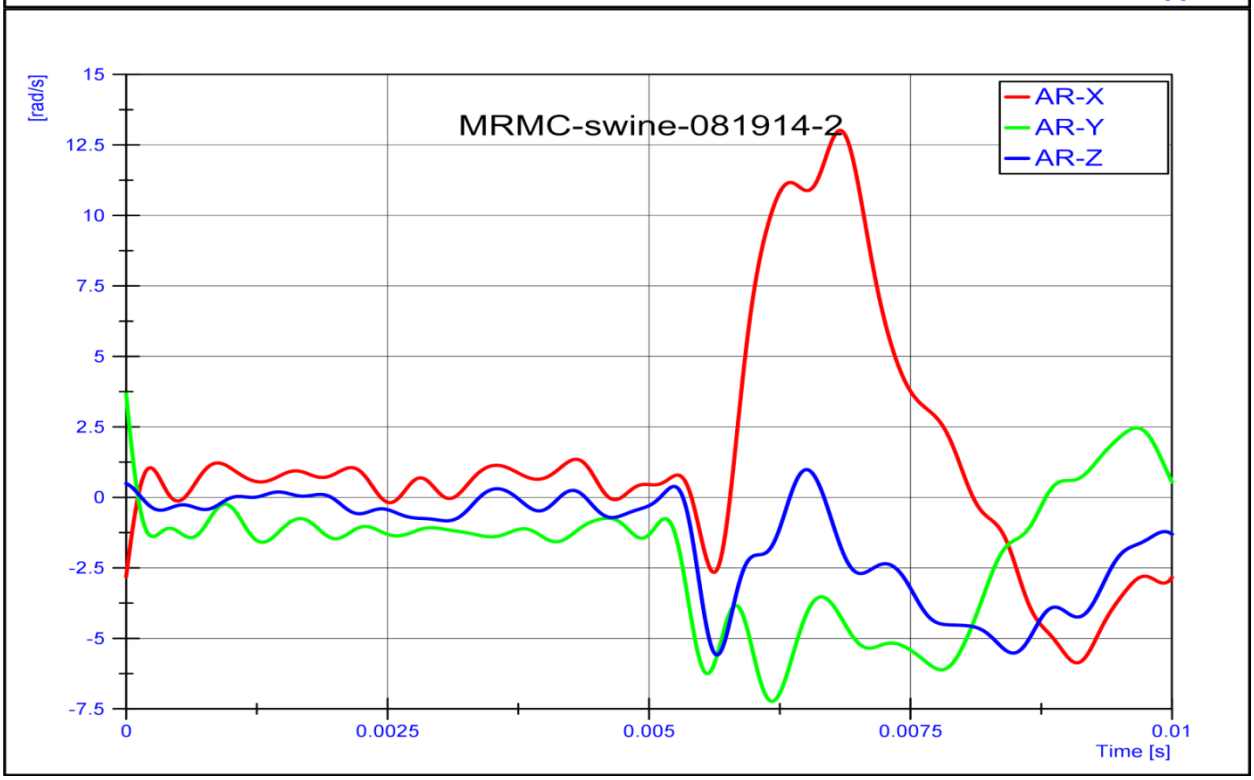
MRMC-swine-081914-2
AR-X
AR-Y
AR-Z
[rad/s]
15
12.5
10
7.5
5
2.5
0
-2.5
-5
-7.5
0
0.0025
0.005
0.0075
0.01
Time [s]

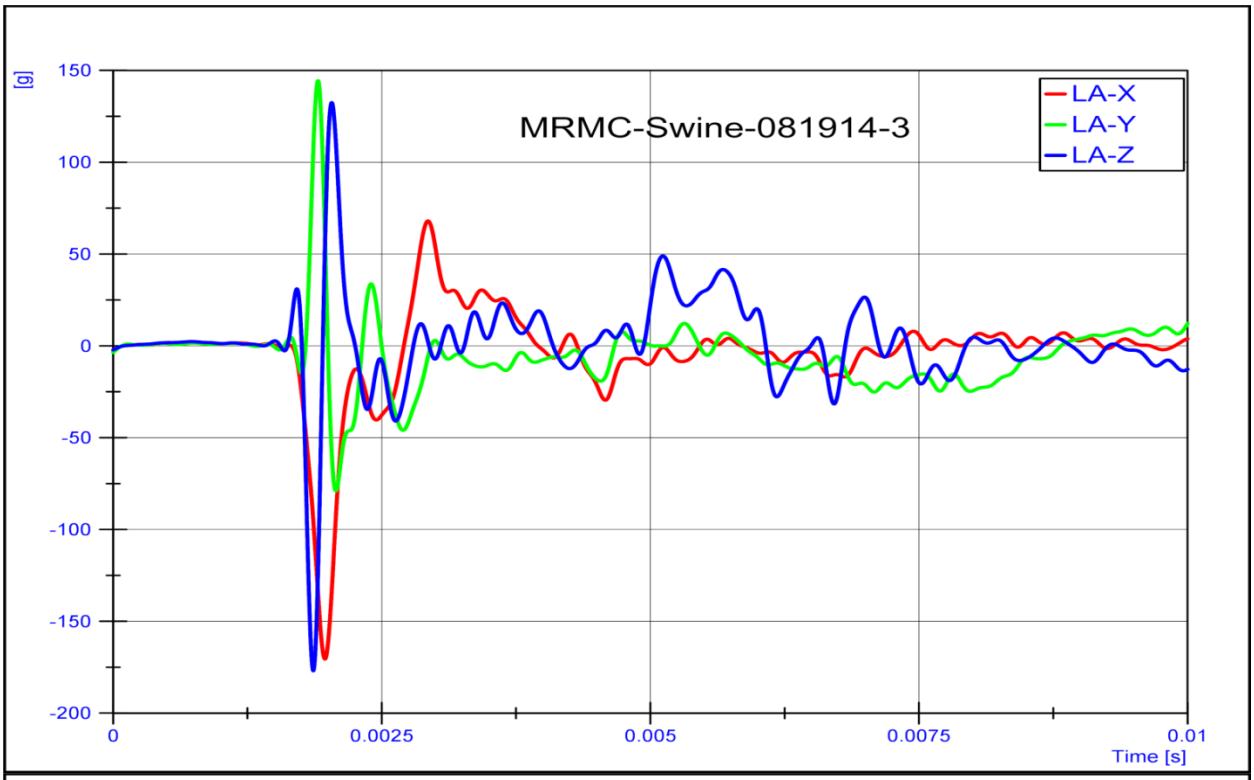
MRMC-Swine-081914-3
LA-X
LA-Y
LA-Z
[g]
150
100
50
0
-50
-100
-150
-200
0
0.0025
0.005
0.0075
0.01
Time [s]

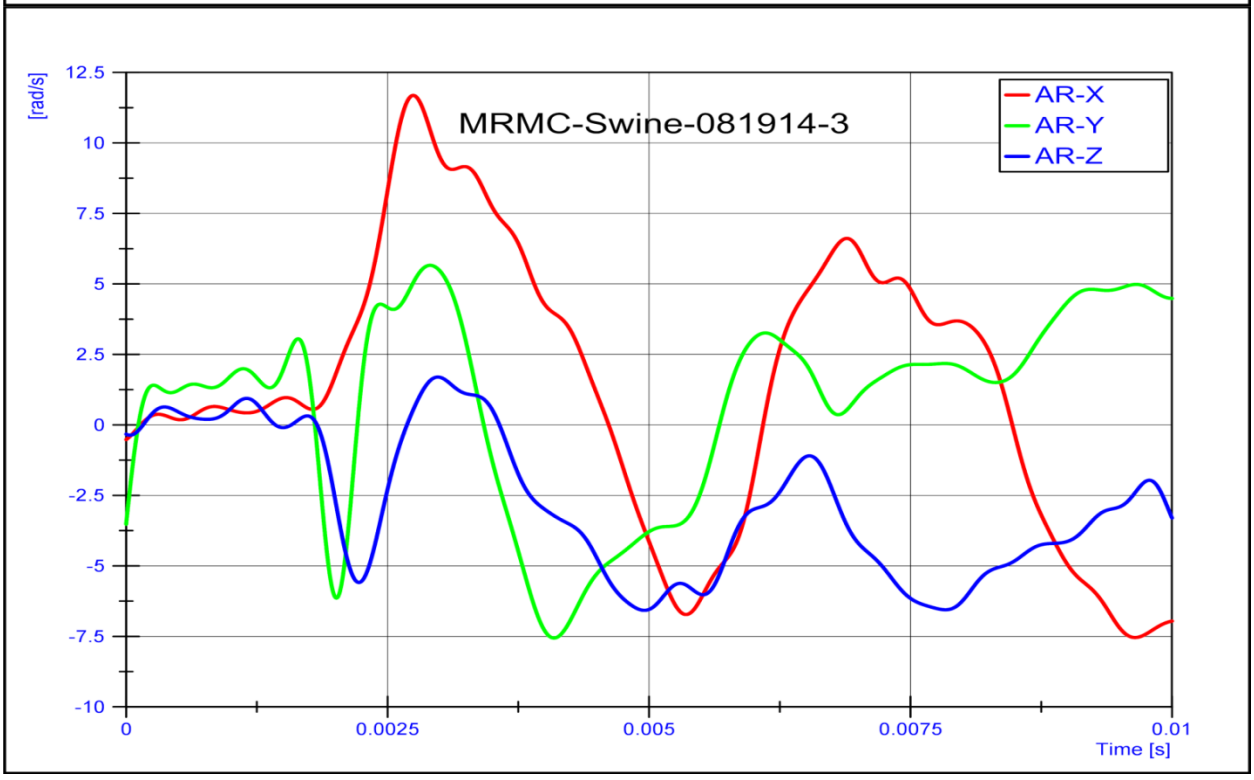
MRMC-Swine-081914-3
AR-X
AR-Y
AR-Z
[rad/s]
12.5
10
7.5
5
2.5
0
-2.5
-5
-7.5
-10
0
0.0025
0.005
0.0075
0.01
Time [s]

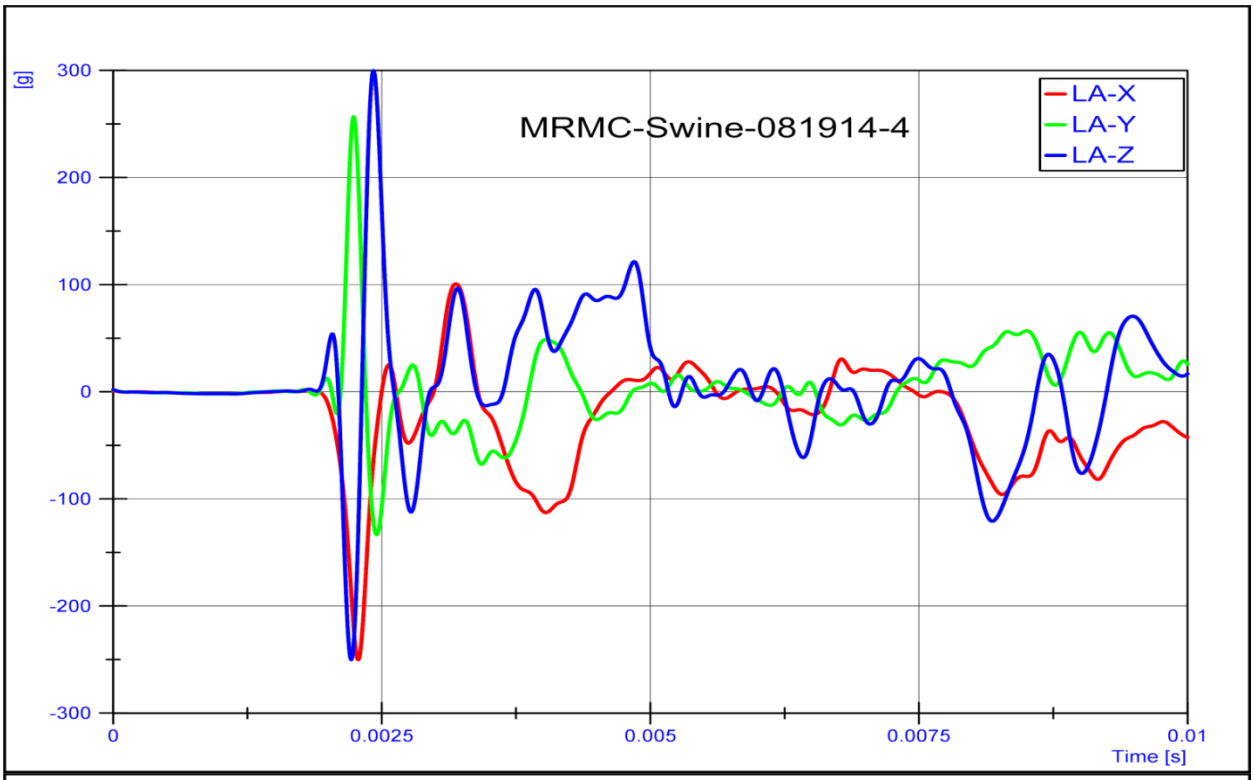
MRMC-Swine-081914-4
LA-X
LA-Y
LA-Z
[g]
300
200
100
0
-100
-200
-300
0
0.0025
0.005
0.0075
0.01
Time [s]

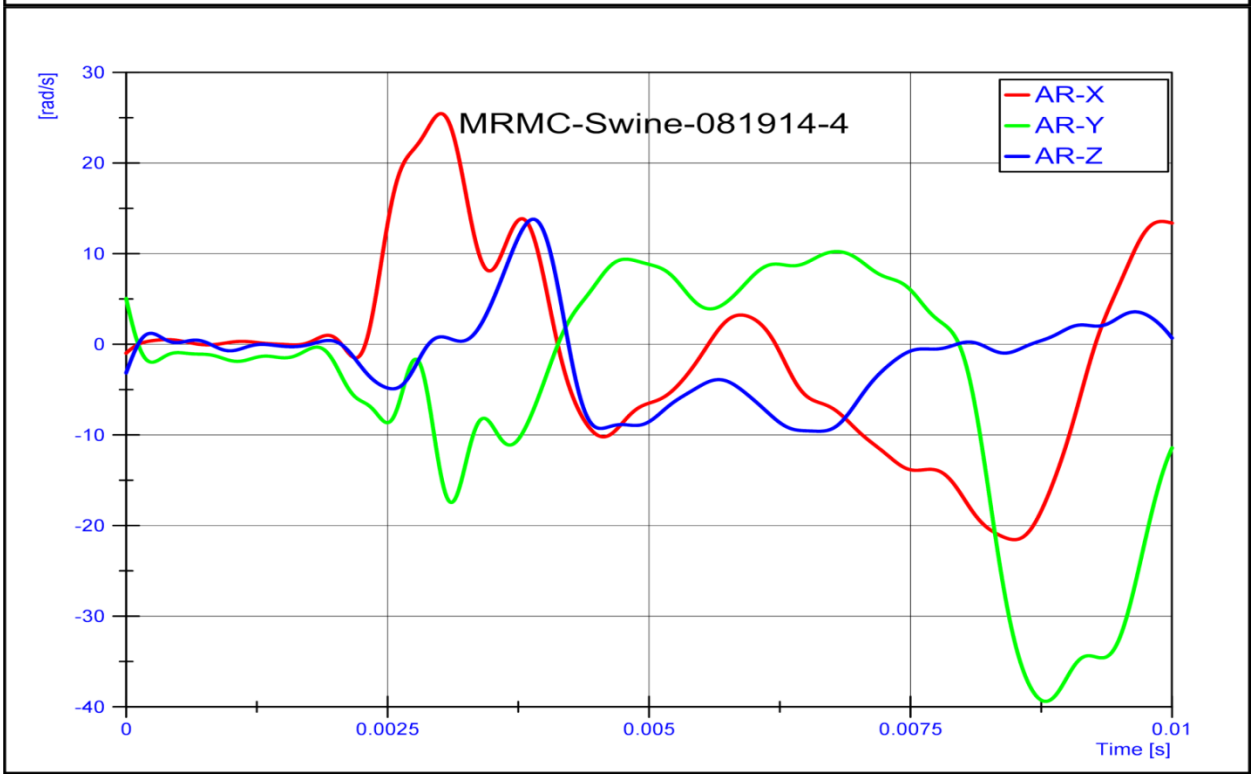
MRMC-Swine-081914-4
AR-X
AR-Y
AR-Z
[rad/s]
30
20
10
0
-10
-20
-30
-40
0
0.0025
0.005
0.0075
0.01
Time [s]

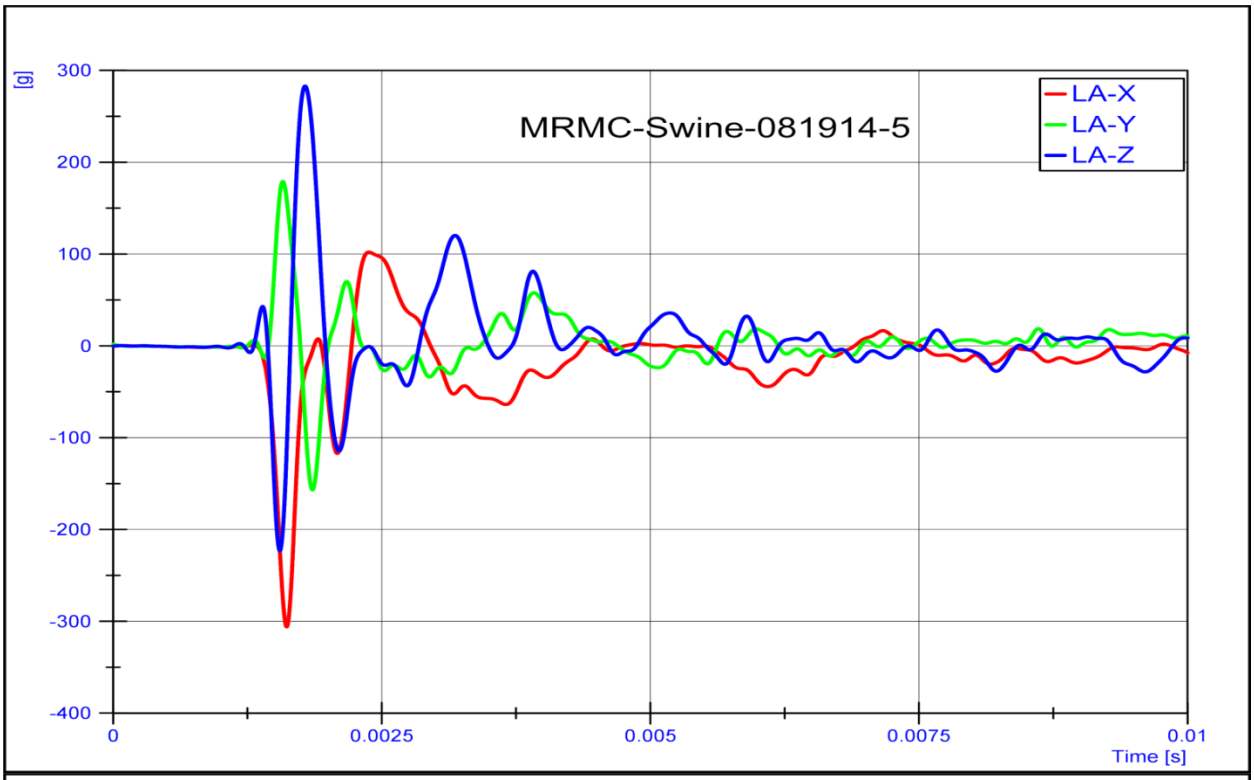
MRMC-Swine-081914-5
LA-X
LA-Y
LA-Z
[g]
300
200
100
0
-100
-200
-300
-400
0
0.0025
0.005
0.0075
0.01
Time [s]

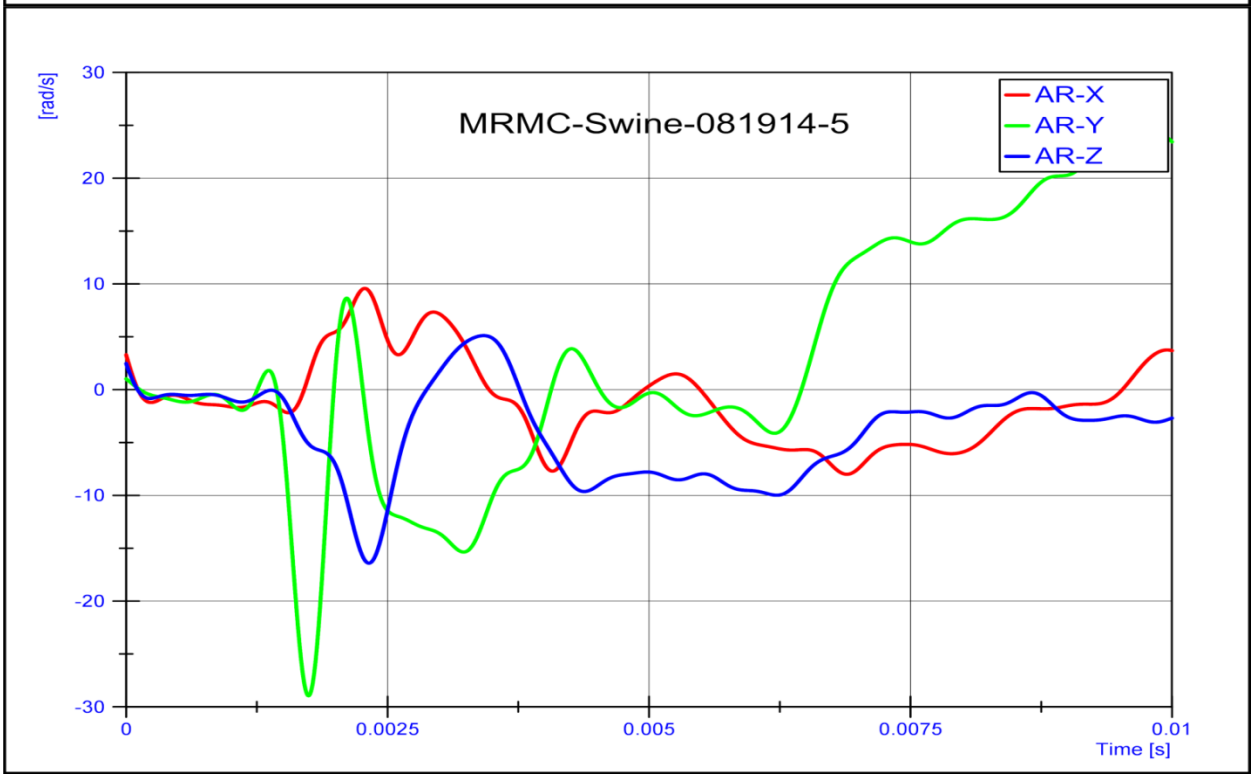
MRMC-Swine-081914-5
AR-X
AR-Y
AR-Z
[rad/s]
30
20
10
0
-10
-20
-30
0
0.0025
0.005
0.0075
0.01
Time [s]

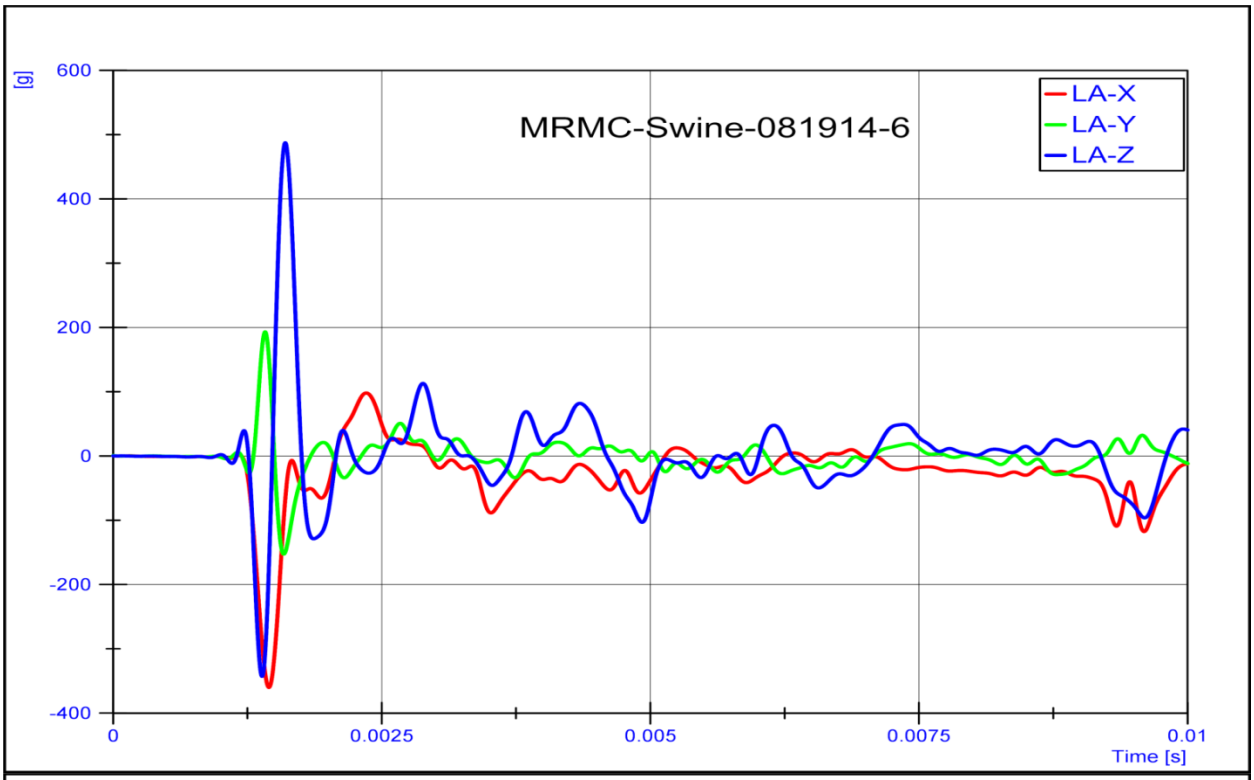
MRMC-Swine-081914-6
LA-X
LA-Y
LA-Z
[g]
600
400
200
0
-200
-400
0
0.0025
0.005
0.0075
0.01
Time [s]

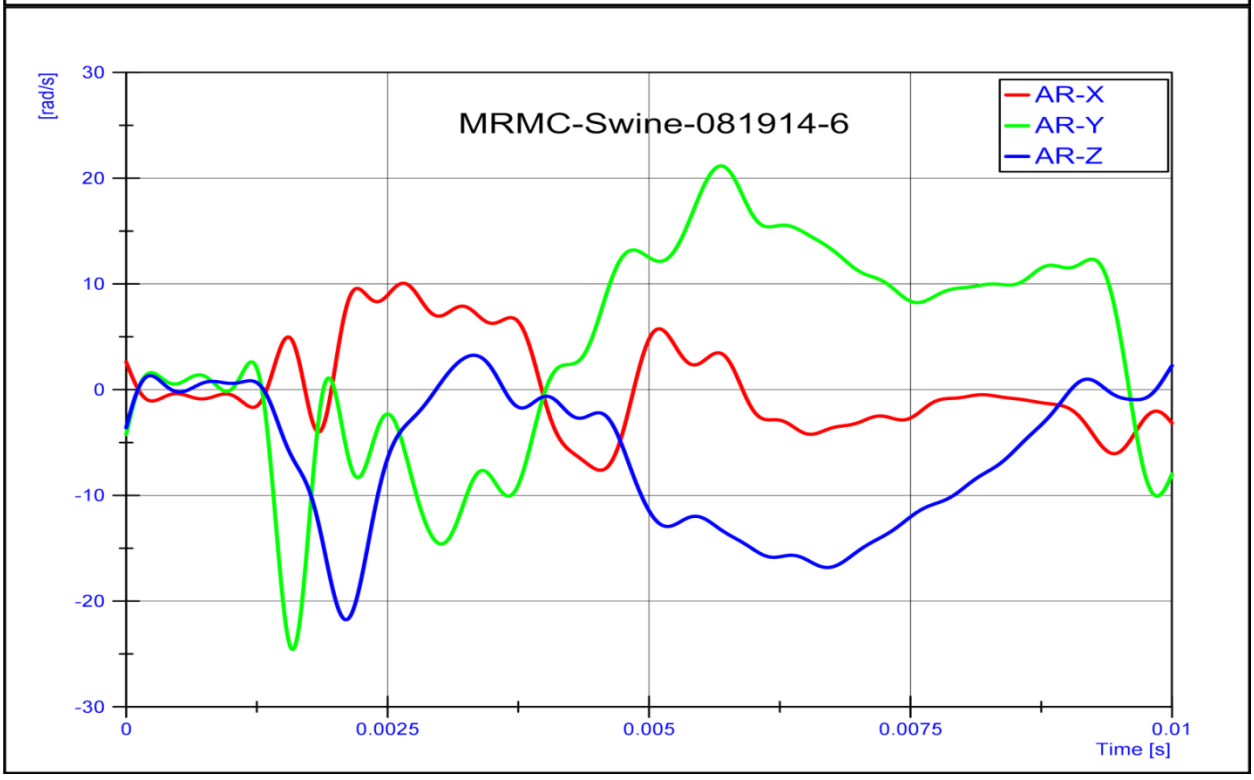
MRMC-Swine-081914-6
AR-X
AR-Y
AR-Z
[rad/s]
30
20
10
0
-10
-20
-30
0
0.0025
0.005
0.0075
0.01
Time [s]

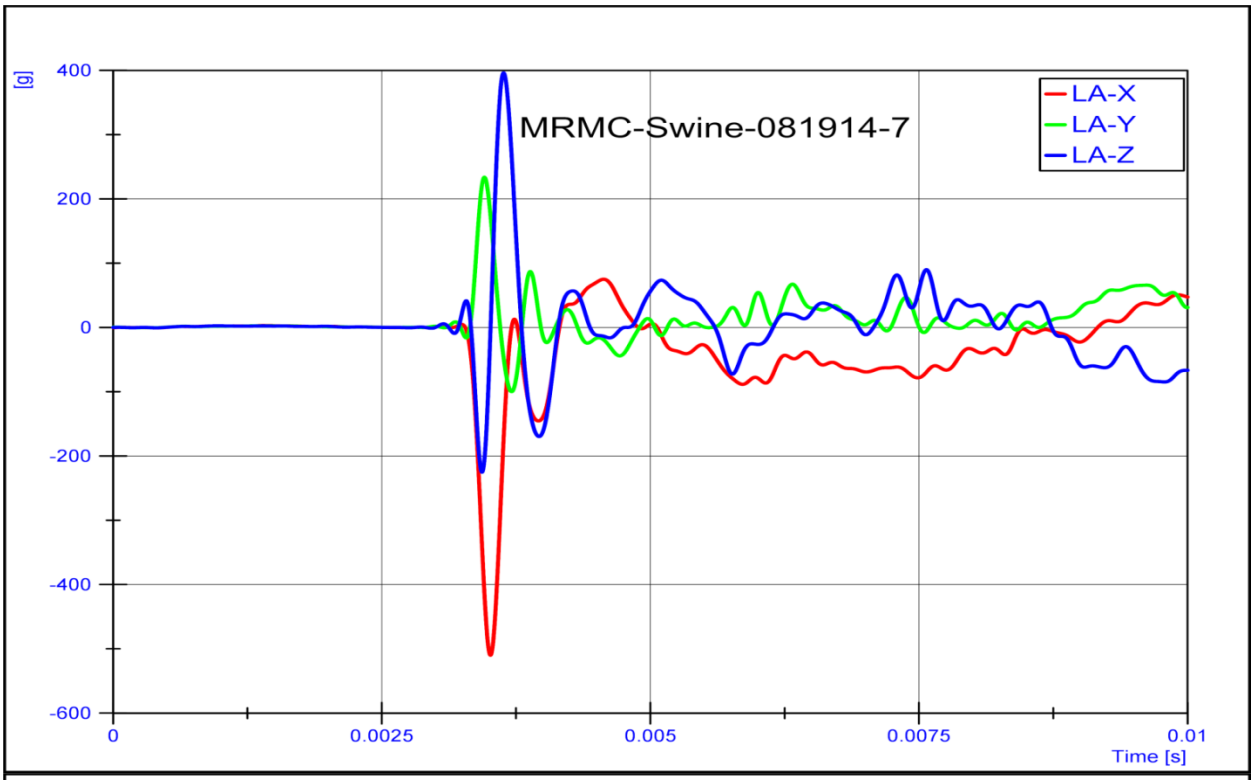
MRMC-Swine-081914-7
LA-X
LA-Y
LA-Z
[g]
400
200
0
-200
-400
-600
0
0.0025
0.005
0.0075
0.01
Time [s]

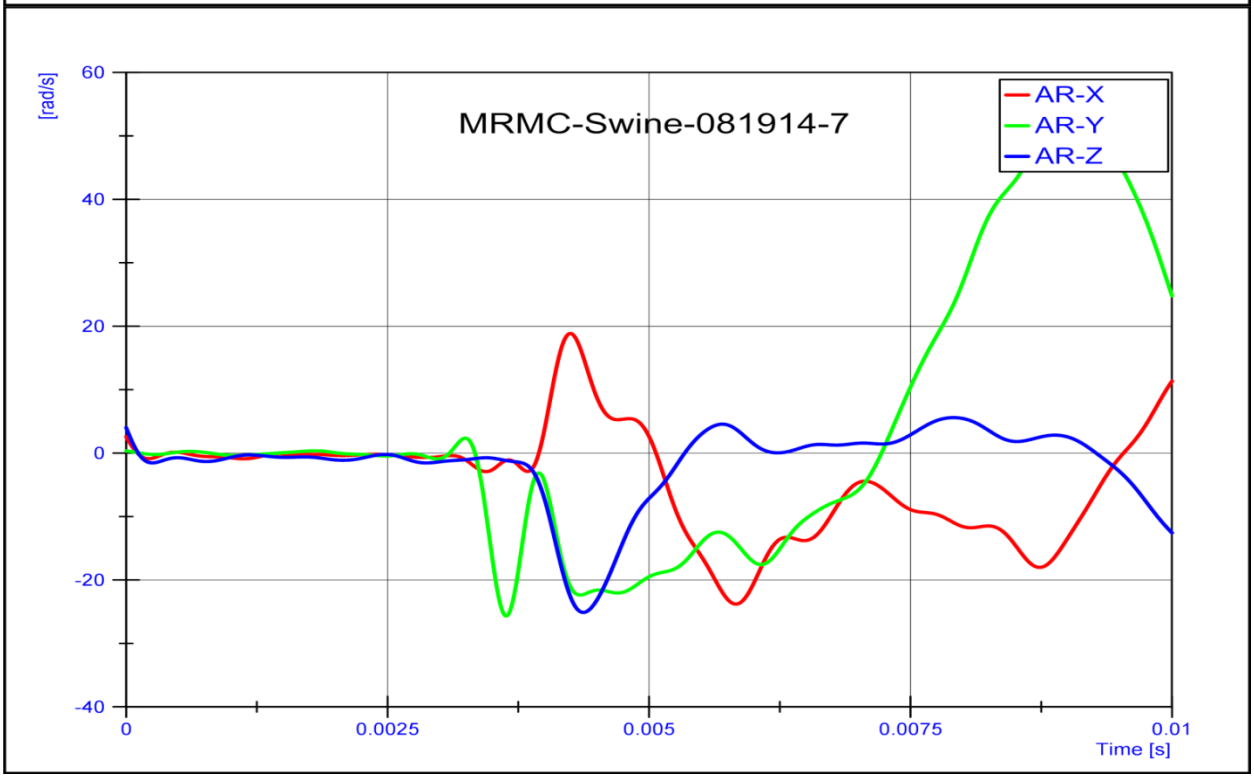
MRMC-Swine-081914-7
AR-X
AR-Y
AR-Z
[rad/s]
60
40
20
0
-20
-40
0
0.0025
0.005
0.0075
0.01
Time [s]

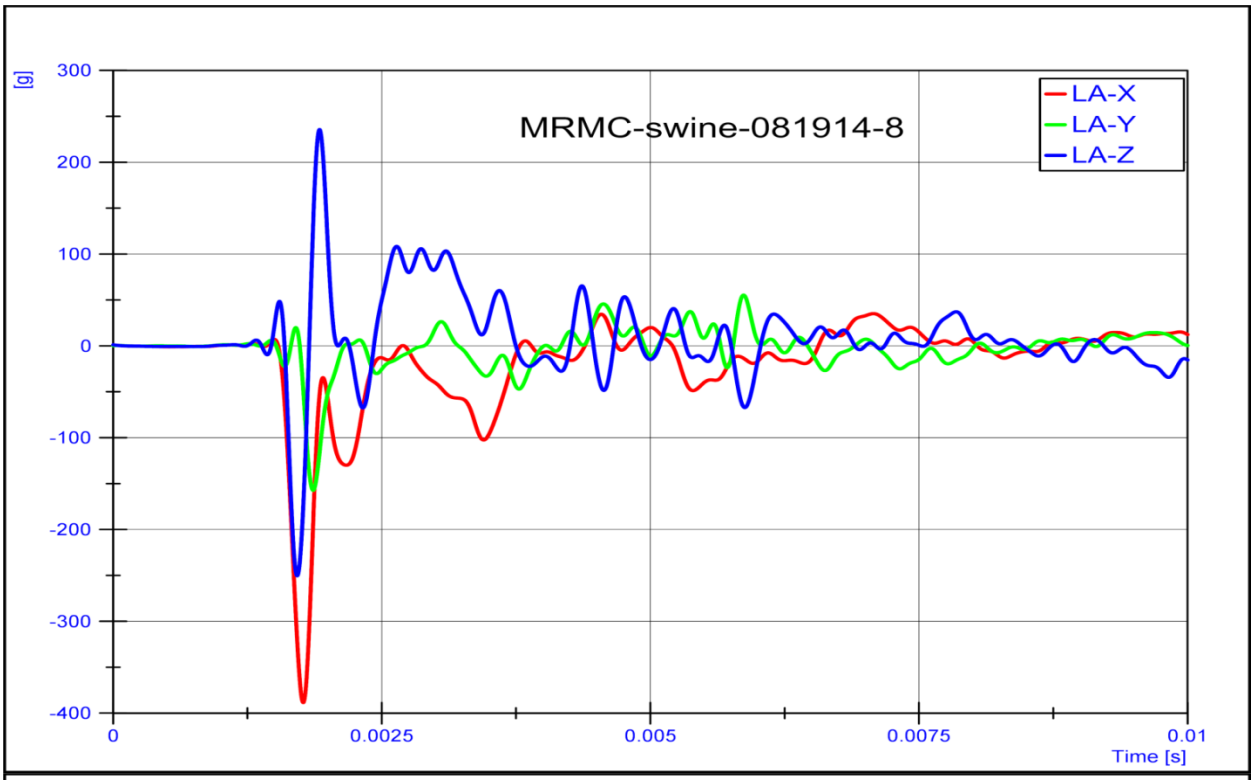
MRMC-swine-081914-8
LA-X
LA-Y
LA-Z
[g]
300
200
100
0
-100
-200
-300
-400
0
0.0025
0.005
0.0075
0.01
Time [s]

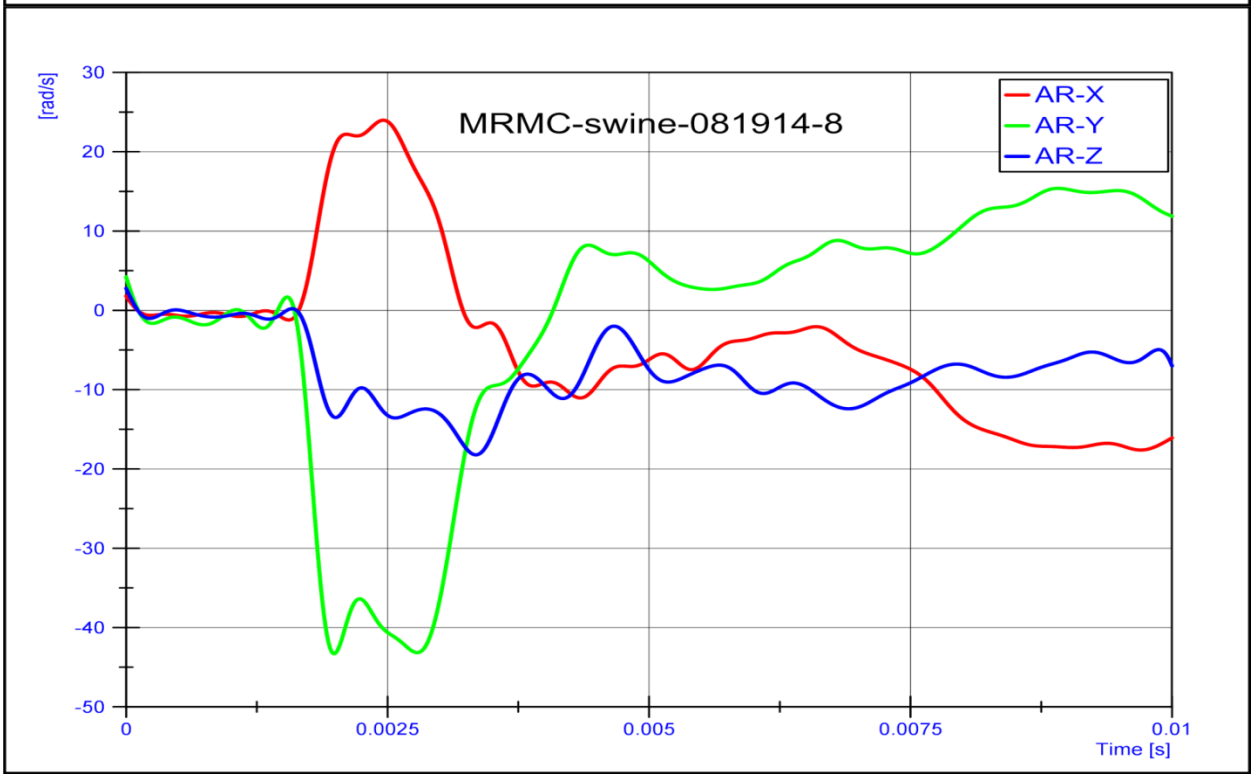
MRMC-swine-081914-8
AR-X
AR-Y
AR-Z
[rad/s]
30
20
10
0
-10
-20
-30
-40
-50
0
0.0025
0.005
0.0075
0.01
Time [s]

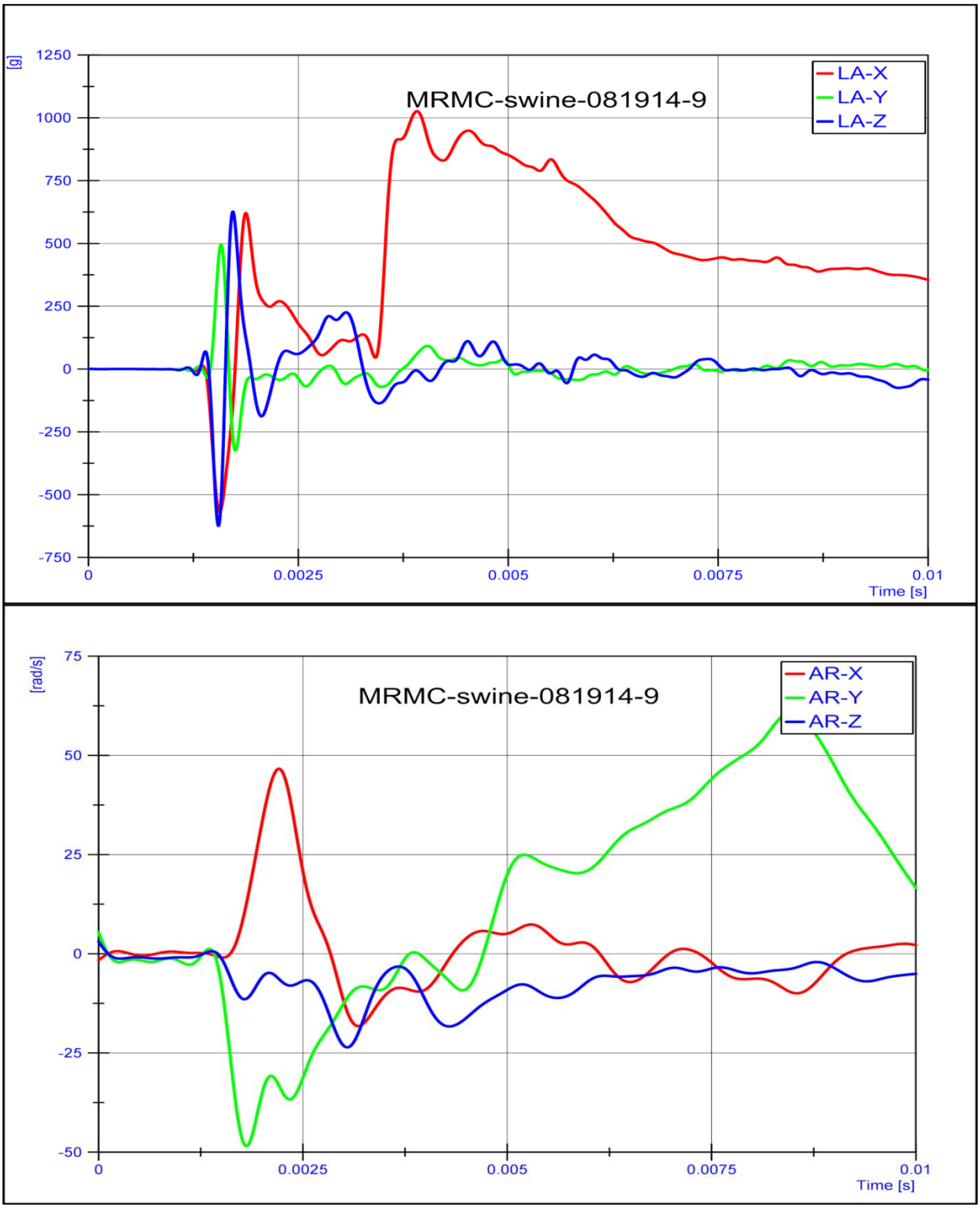
MRMC-swine-081914-9
LA-X
LA-Y
LA-Z
[g]
1250
1000
750
500
250
0
-250
-500
-750
0
0.0025
0.005
0.0075
0.01
Time [s]
MRMC-swine-081914-9
AR-X
AR-Y
AR-Z
[rad/s]
75
50
25
0
-25
-50
0
0.0025
0.005
0.0075
0.01
Time [s]

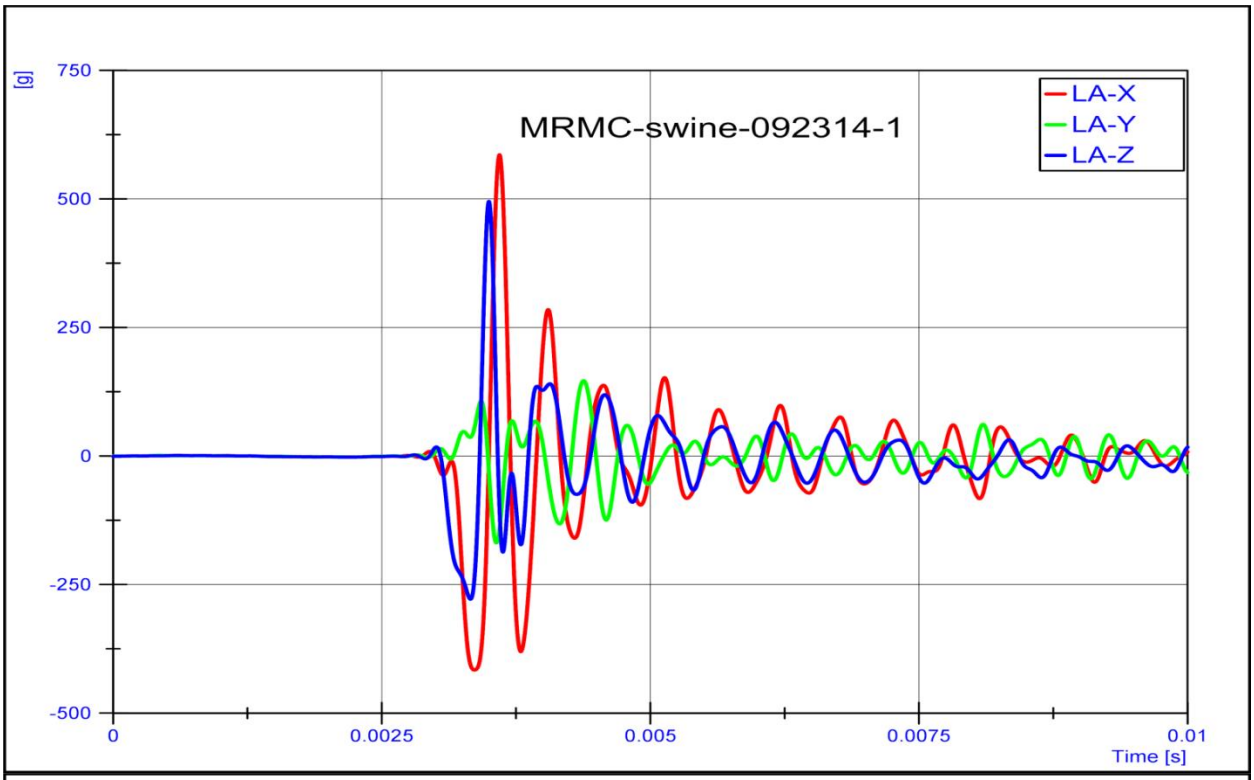
MRMC-swine-092314-1
LA-X
LA-Y
LA-Z
[g]
750
500
250
0
-250
-500
0
0.0025
0.005
0.0075
0.01
Time [s]

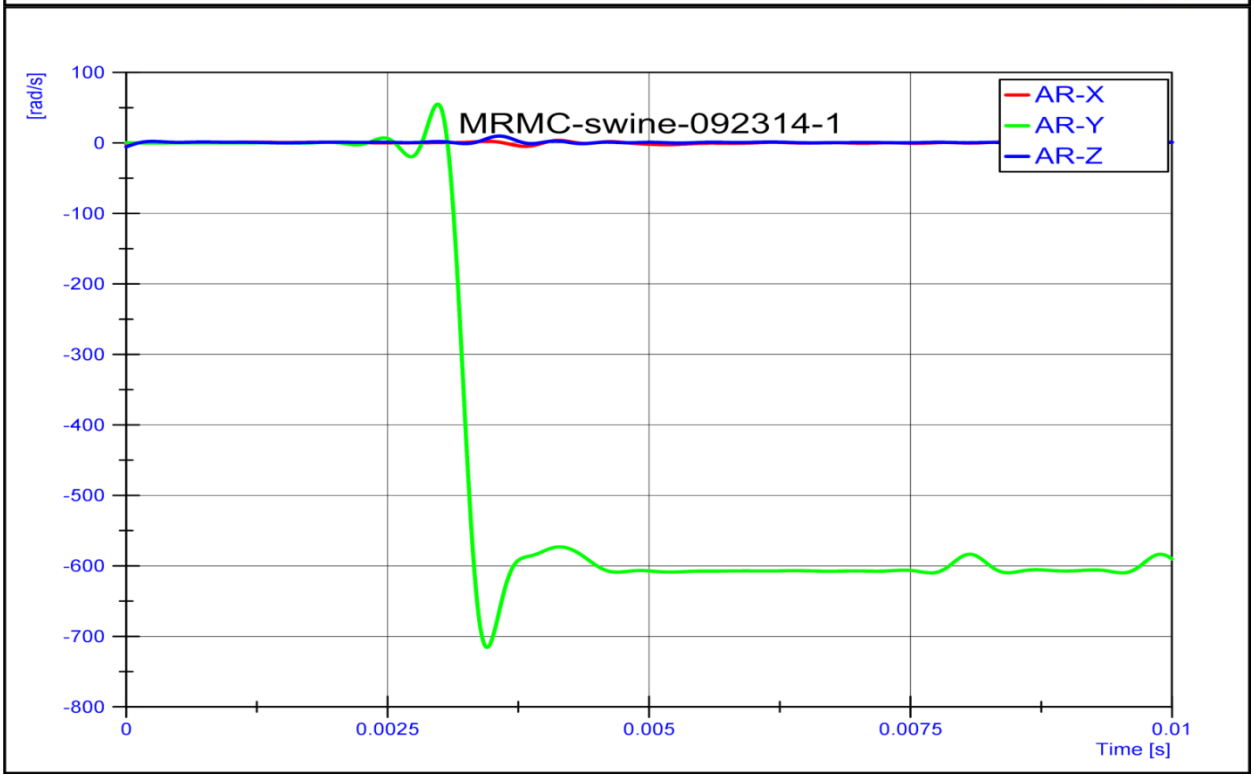
MRMC-swine-092314-1
AR-X
AR-Y
AR-Z
[rad/s]
100
0
-100
-200
-300
-400
-500
-600
-700
-800
0
0.0025
0.005
0.0075
0.01
Time [s]

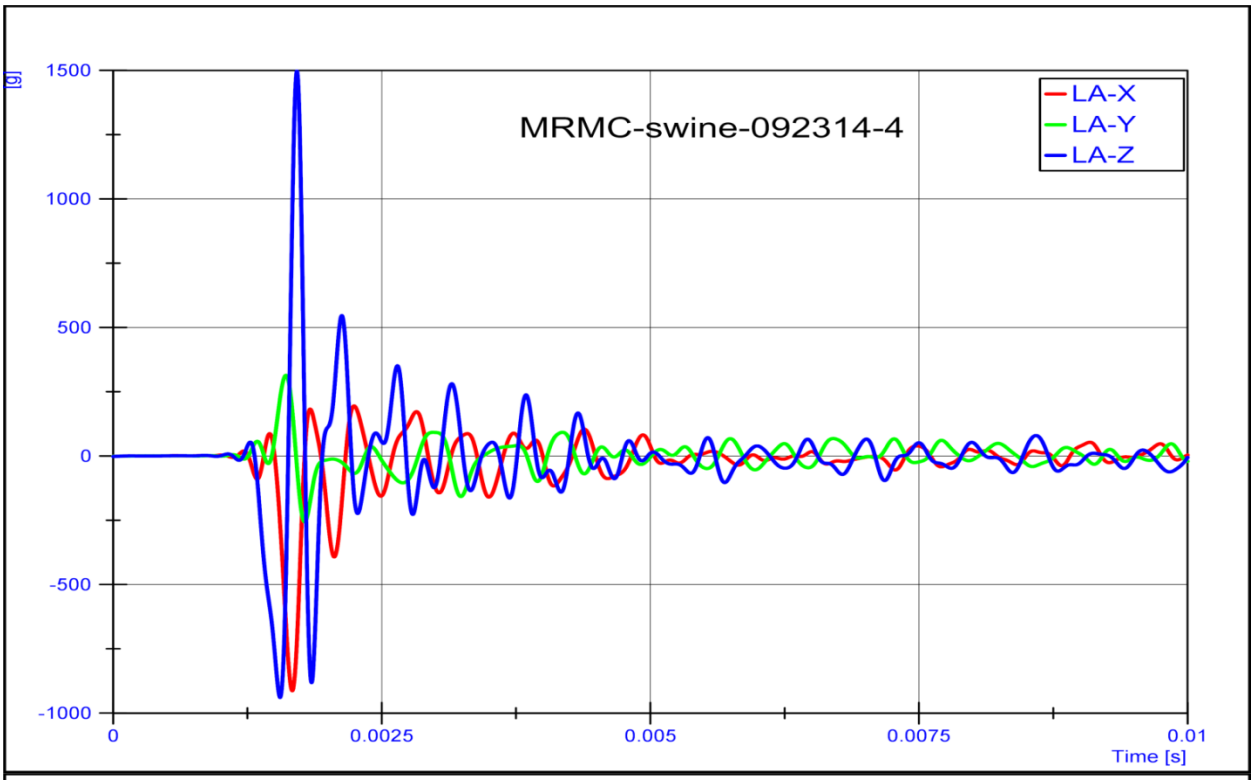
MRMC-swine-092314-4
LA-X
LA-Y
LA-Z
[g]
1500
1000
500
0
-500
-1000
0
0.0025
0.005
0.0075
0.01
Time [s]

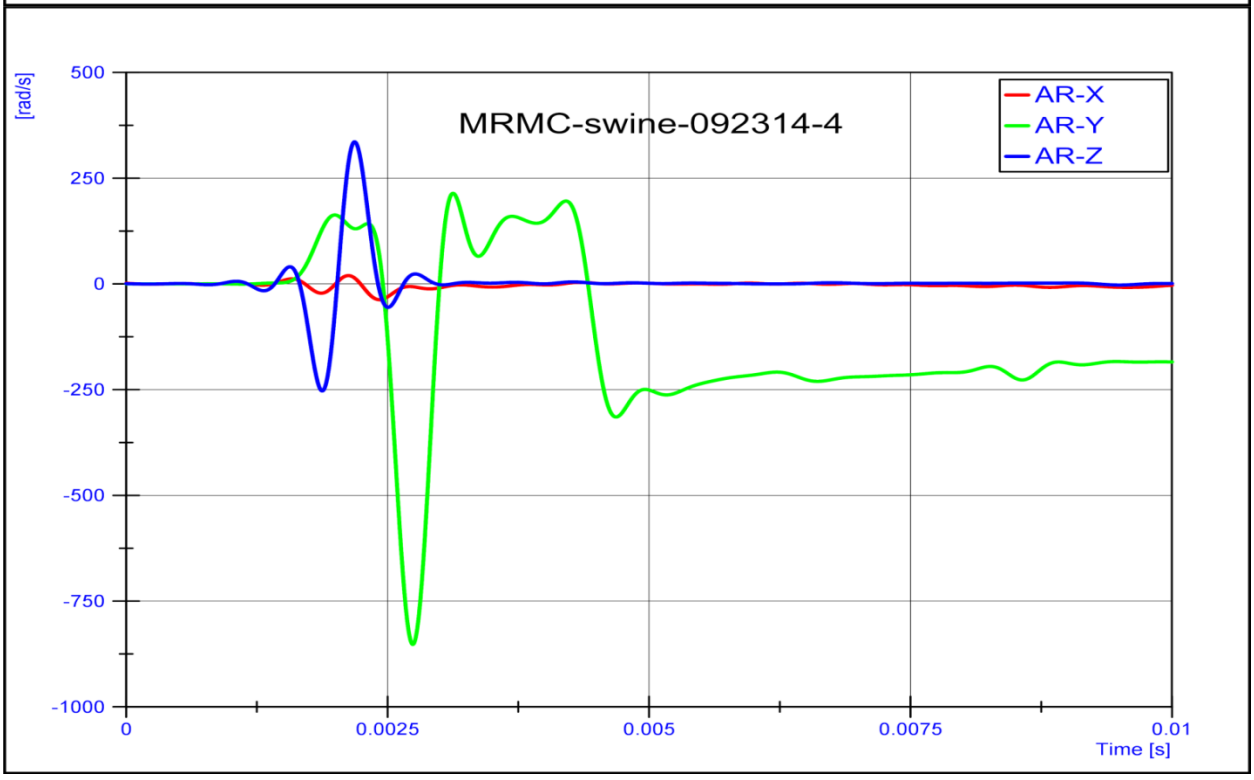
MRMC-swine-092314-4
AR-X
AR-Y
AR-Z
[rad/s]
500
250
0
-250
-500
-750
-1000
0
0.0025
0.005
0.0075
0.01
Time [s]

## 3: REAR BLAST ICP CURVES

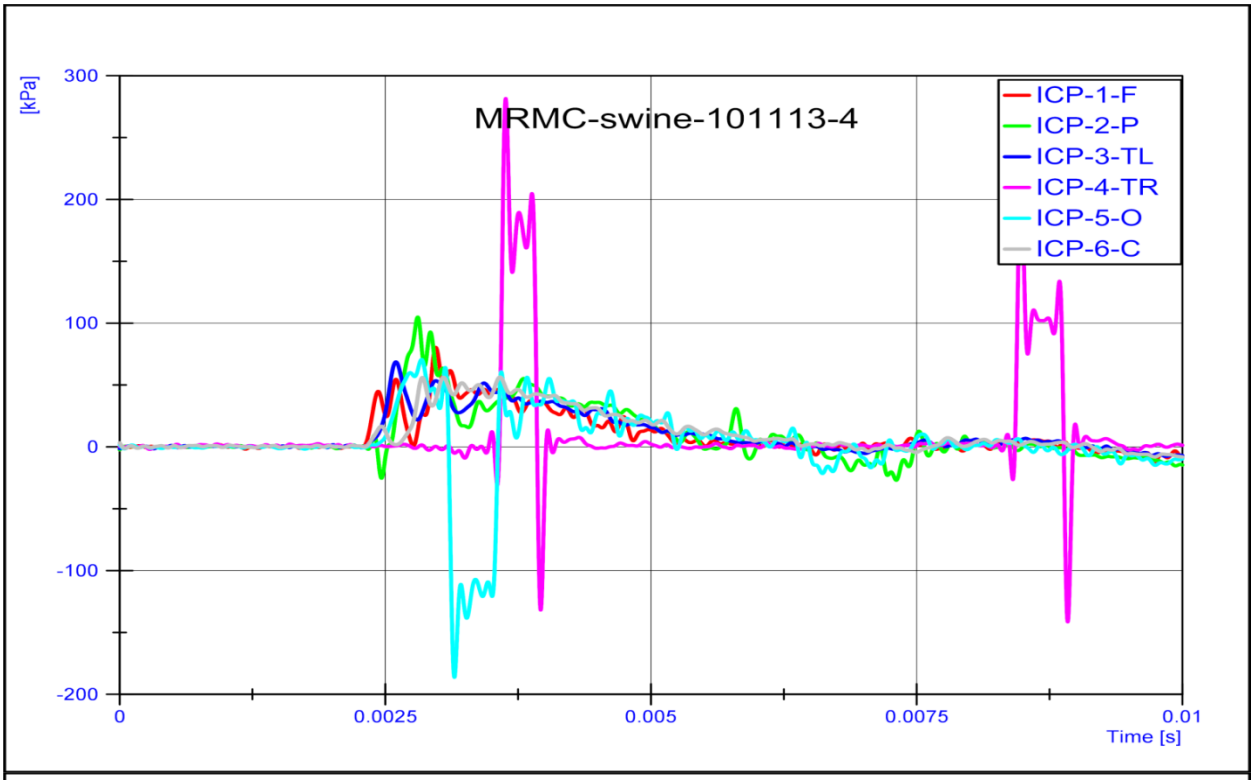


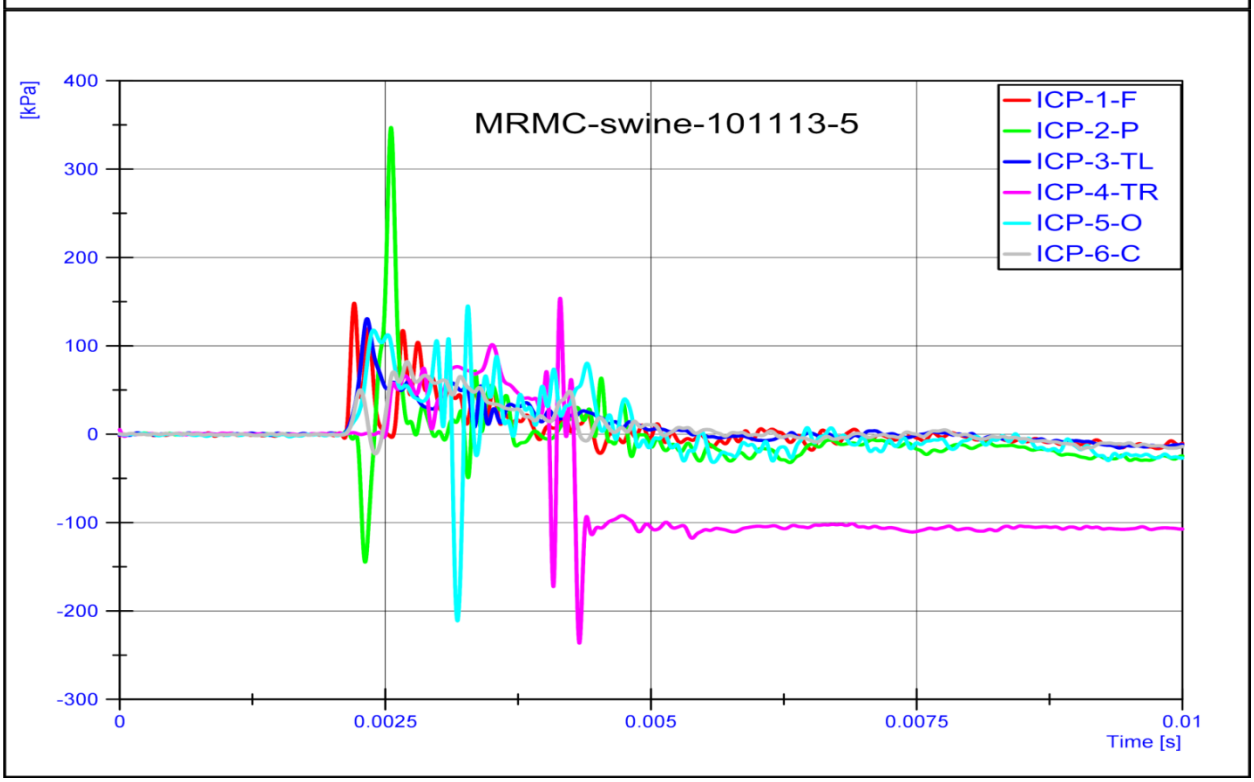

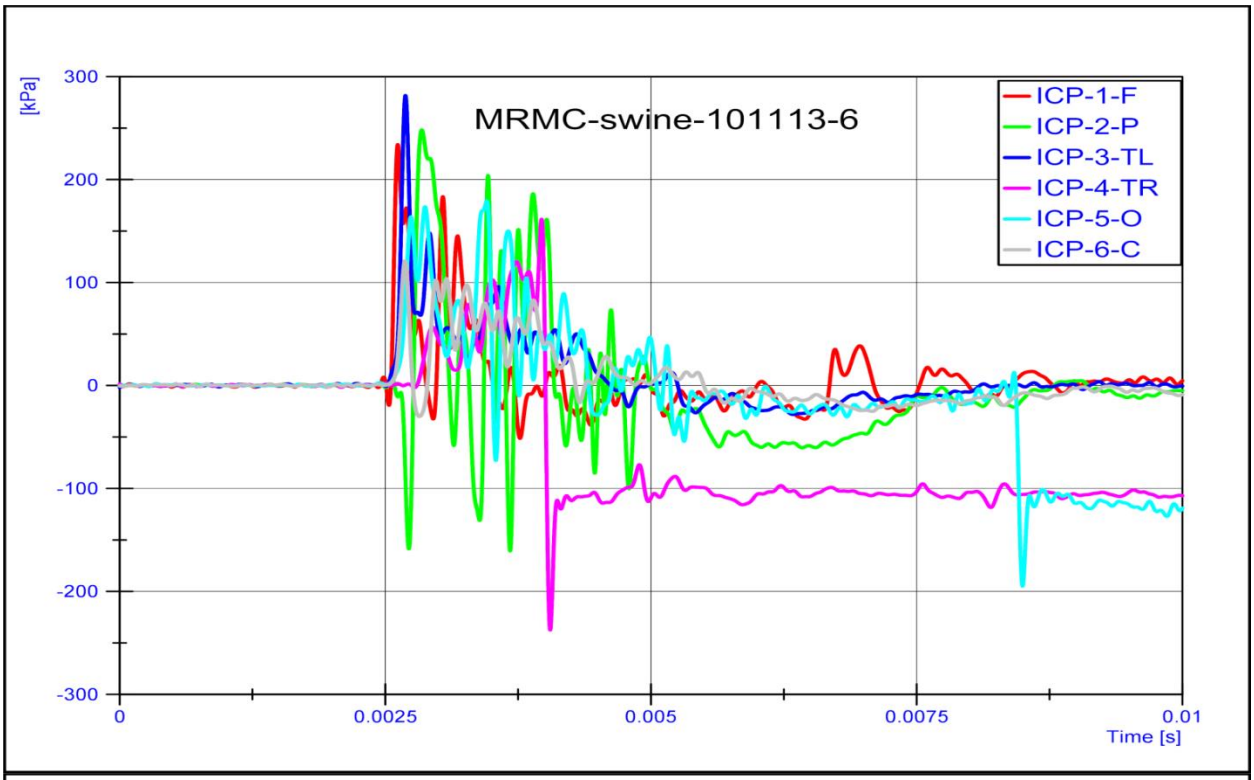
MRMC-swine-101113-6
[kPa]
300
200
100
0
-100
-200
-300
0
0.0025
0.005
0.0075
0.01
Time [s]
ICP-1-F
ICP-2-P
ICP-3-TL
ICP-4-TR
ICP-5-O
ICP-6-C

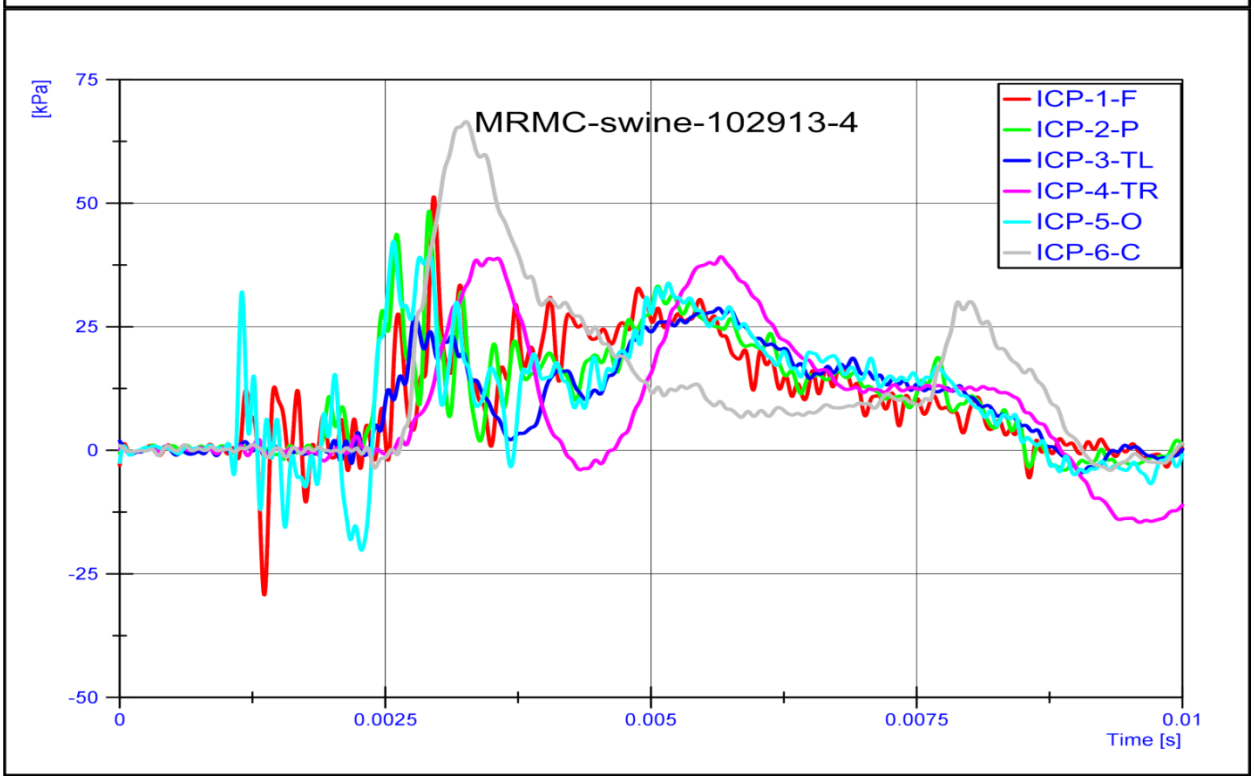
MRMC-swine-102913-4
[kPa]
75
50
25
0
-25
-50
0
0.0025
0.005
0.0075
0.01
Time [s]
ICP-1-F
ICP-2-P
ICP-3-TL
ICP-4-TR
ICP-5-O
ICP-6-C

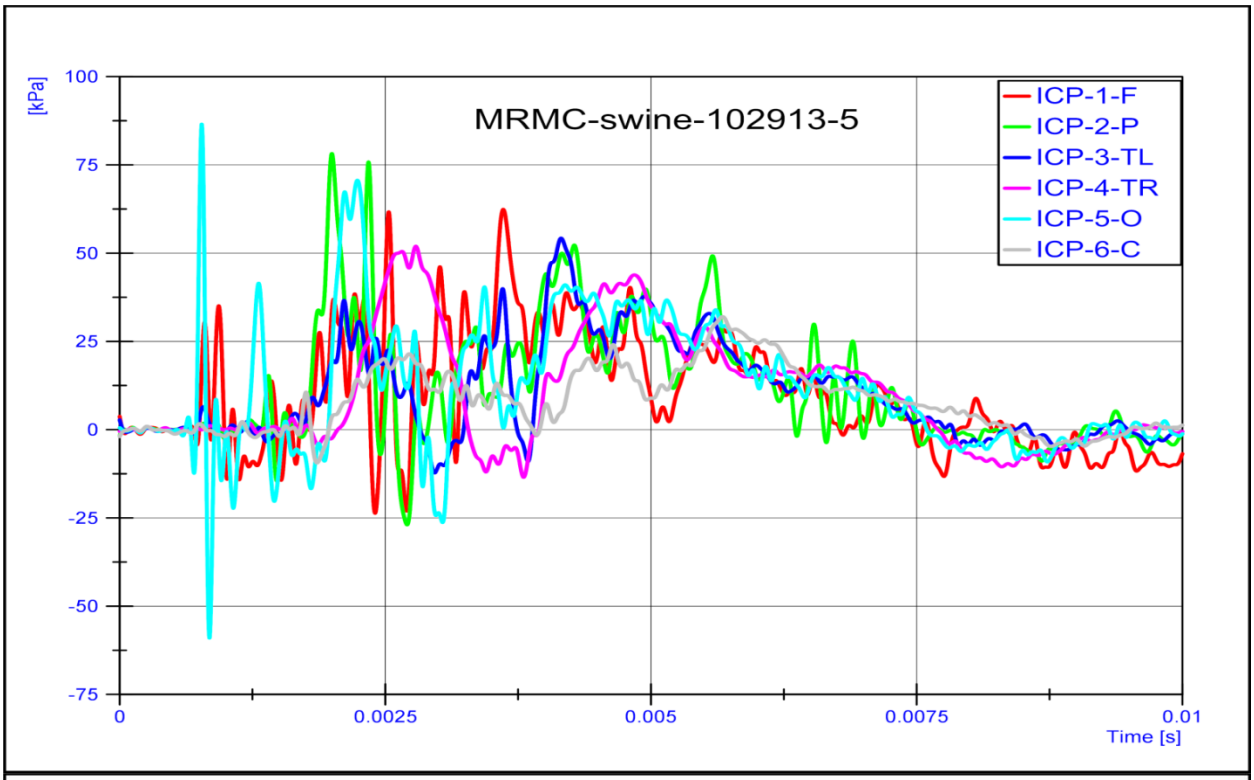
MRMC-swine-102913-5
ICP-1-F
ICP-2-P
ICP-3-TL
ICP-4-TR
ICP-5-O
ICP-6-C
[kPa]
100
75
50
25
0
-25
-50
-75
0
0.0025
0.005
0.0075
0.01
Time [s]

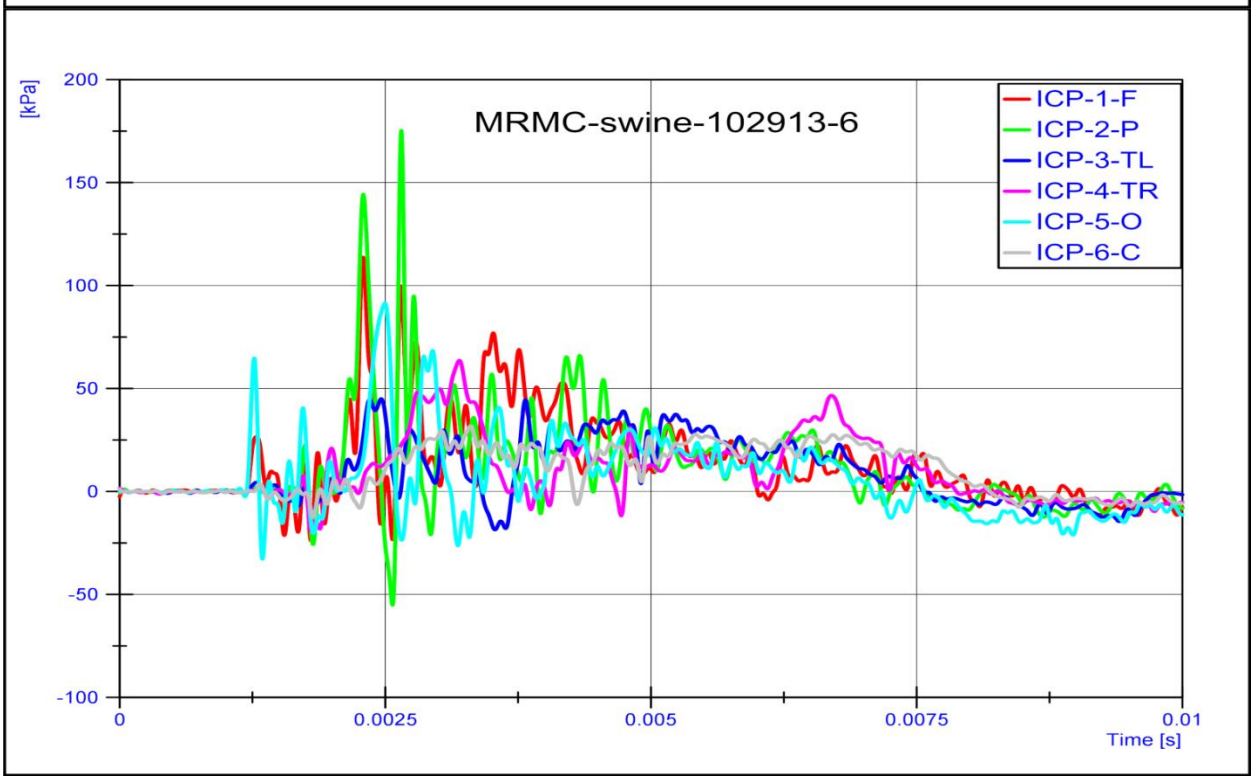
MRMC-swine-102913-6
ICP-1-F
ICP-2-P
ICP-3-TL
ICP-4-TR
ICP-5-O
ICP-6-C
[kPa]
200
150
100
50
0
-50
-100
0
0.0025
0.005
0.0075
0.01
Time [s]

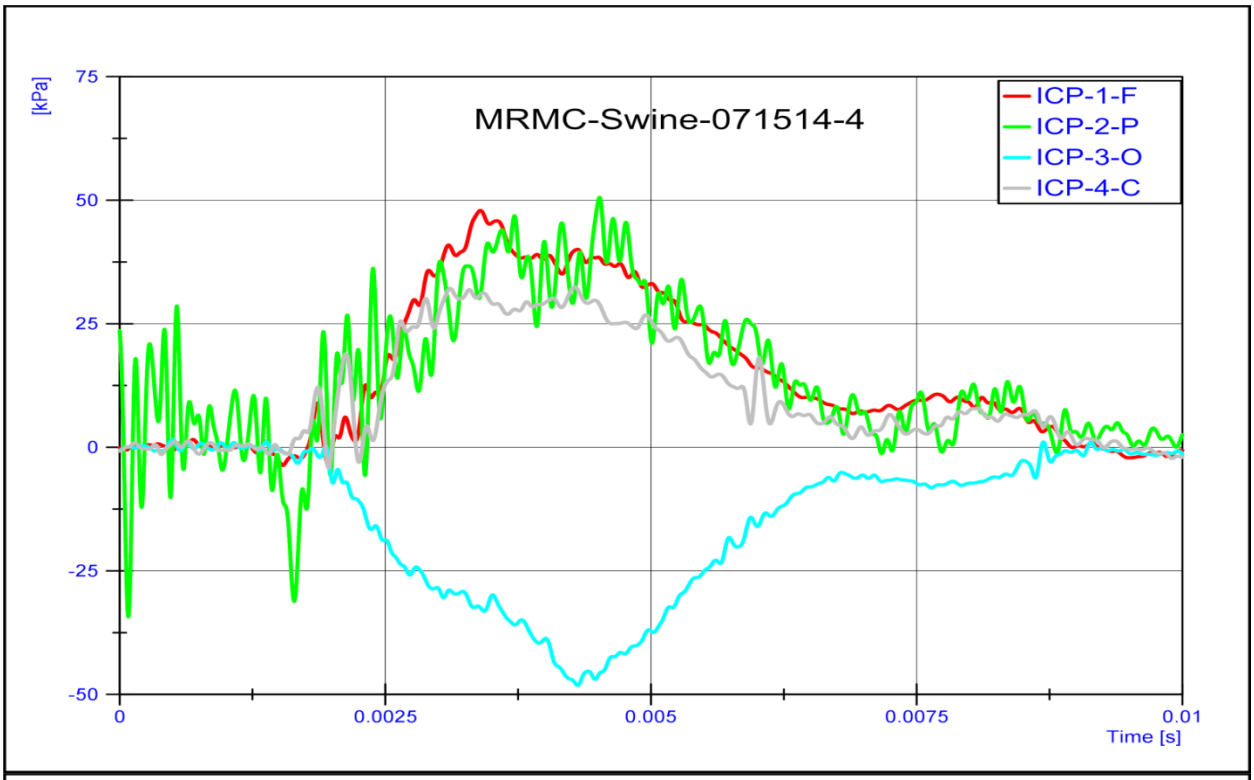
MRMC-Swine-071514-4
ICP-1-F
ICP-2-P
ICP-3-O
ICP-4-C
[kPa]
75
50
25
0
-25
-50
0
0.0025
0.005
0.0075
0.01
Time [s]

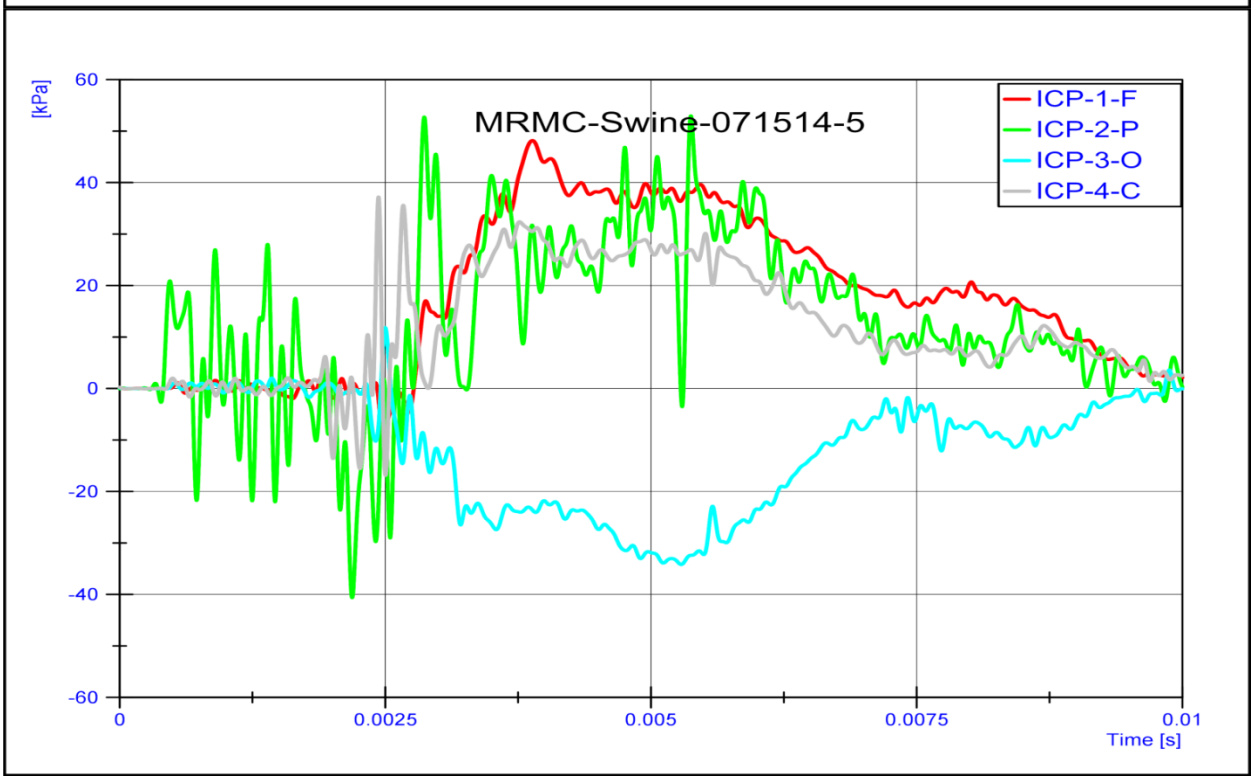
MRMC-Swine-071514-5
ICP-1-F
ICP-2-P
ICP-3-O
ICP-4-C
[kPa]
60
40
20
0
-20
-40
-60
0
0.0025
0.005
0.0075
0.01
Time [s]

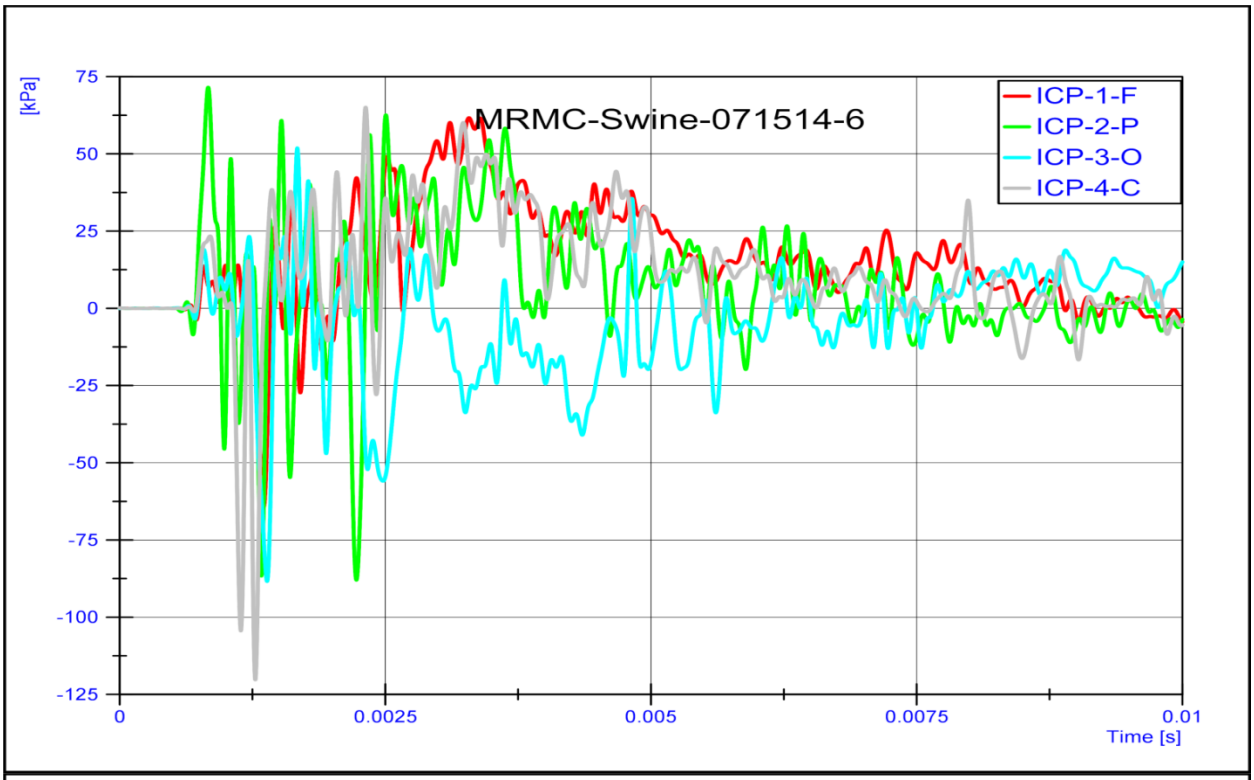
MRMC-Swine-071514-6
ICP-1-F
ICP-2-P
ICP-3-O
ICP-4-C
[kPa]
75
50
25
0
-25
-50
-75
-100
-125
0
0.0025
0.005
0.0075
0.01
Time [s]

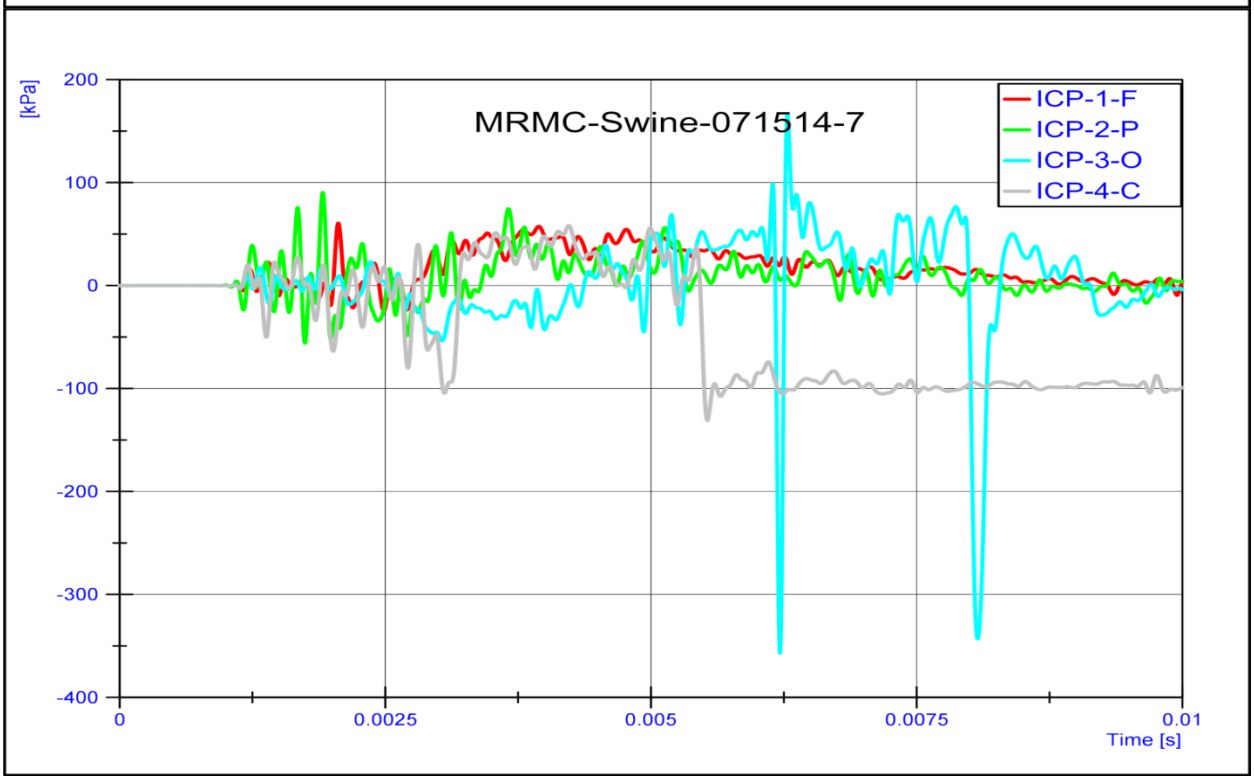
MRMC-Swine-071514-7
ICP-1-F
ICP-2-P
ICP-3-O
ICP-4-C
[kPa]
200
100
0
-100
-200
-300
-400
0
0.0025
0.005
0.0075
0.01
Time [s]

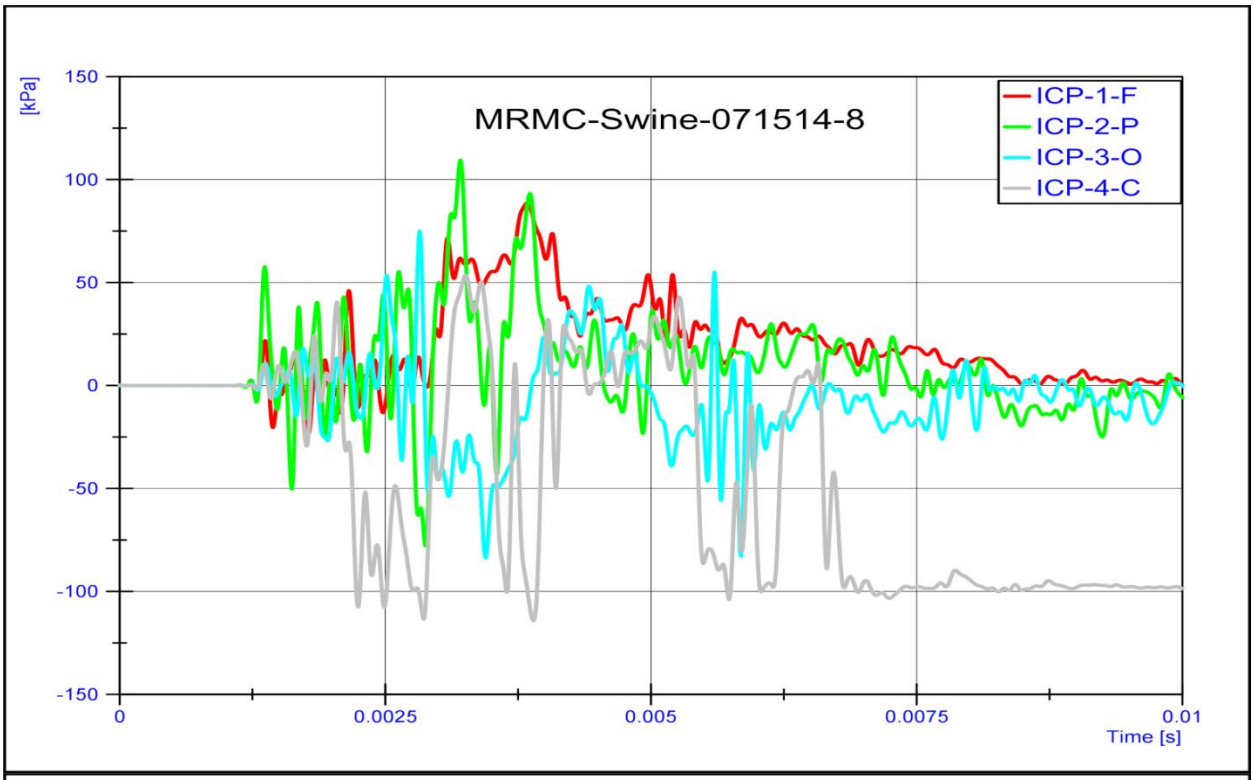
MRMC-Swine-071514-8
ICP-1-F
ICP-2-P
ICP-3-O
ICP-4-C
[kPa]
150
100
50
0
-50
-100
-150
0
0.0025
0.005
0.0075
0.01
Time [s]

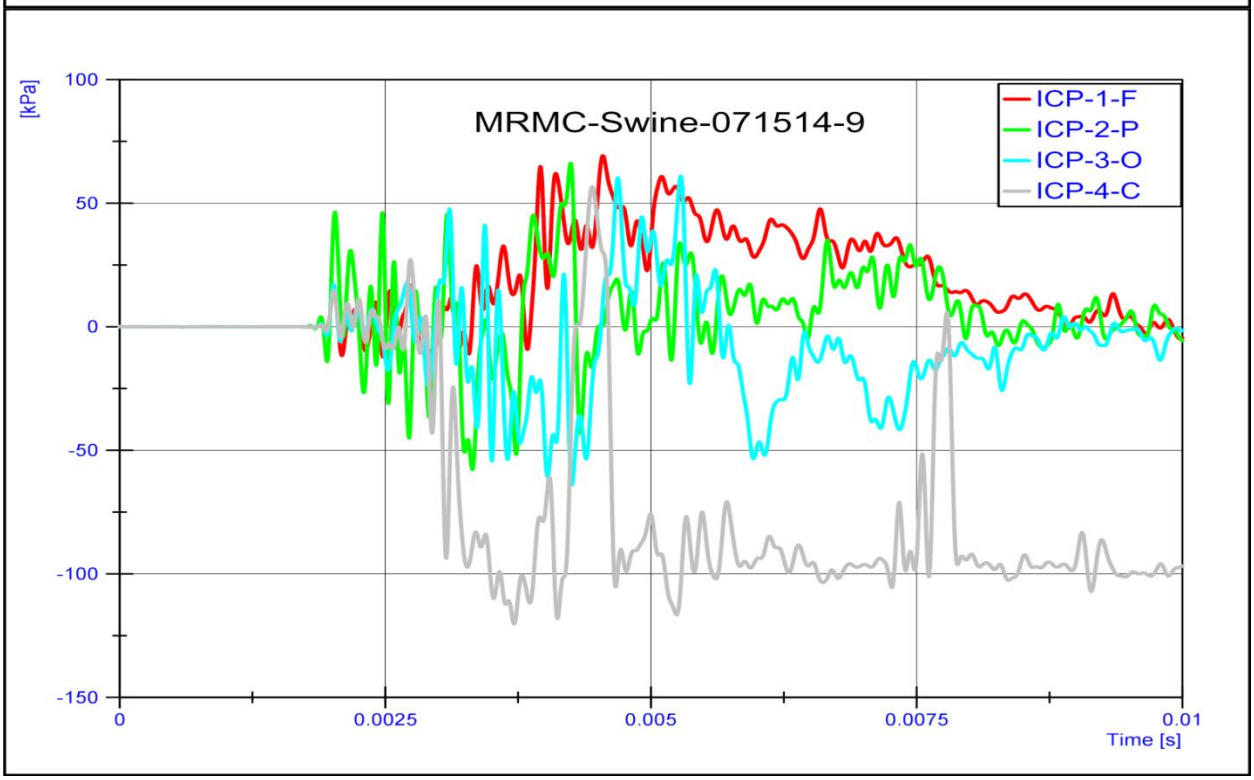
MRMC-Swine-071514-9
ICP-1-F
ICP-2-P
ICP-3-O
ICP-4-C
[kPa]
100
50
0
-50
-100
-150
0
0.0025
0.005
0.0075
0.01
Time [s]

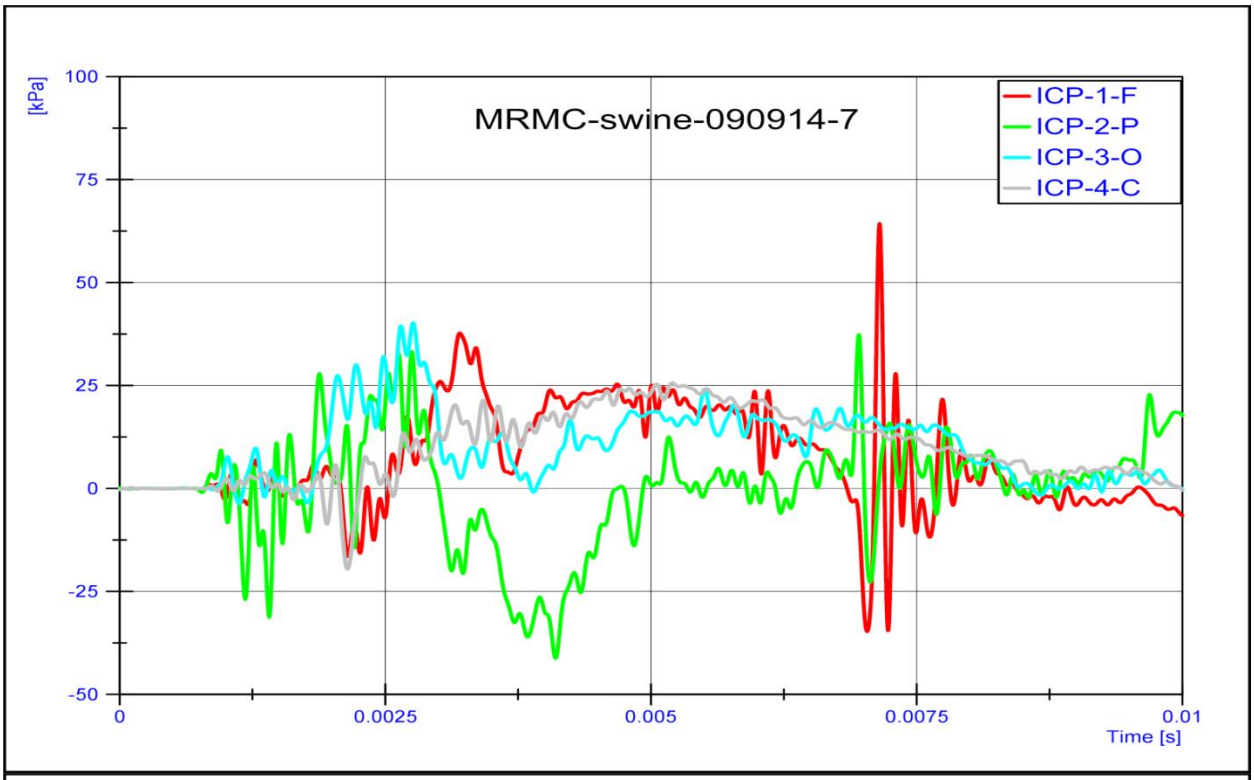
MRMC-swine-090914-7
ICP-1-F
ICP-2-P
ICP-3-O
ICP-4-C
[kPa]
100
75
50
25
0
-25
-50
0
0.0025
0.005
0.0075
0.01
Time [s]

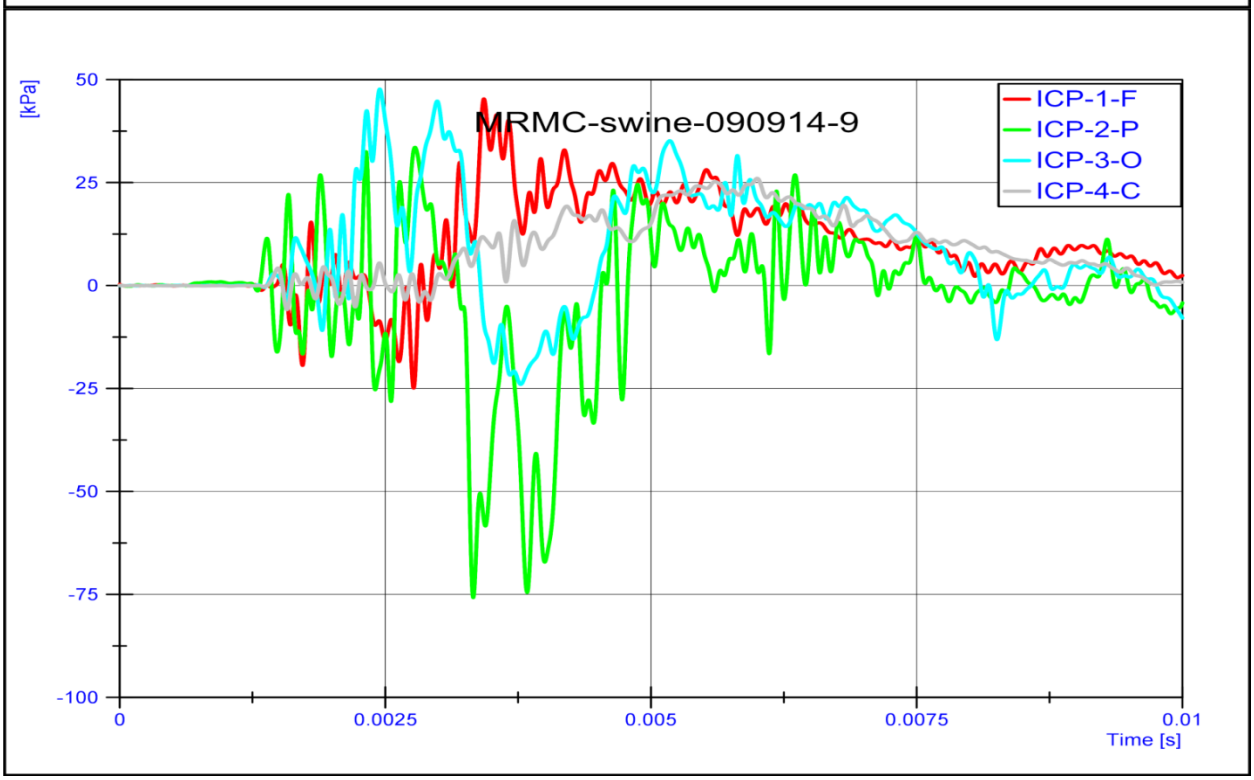
MRMC-swine-090914-9
ICP-1-F
ICP-2-P
ICP-3-O
ICP-4-C
[kPa]
50
25
0
-25
-50
-75
-100
0
0.0025
0.005
0.0075
0.01
Time [s]

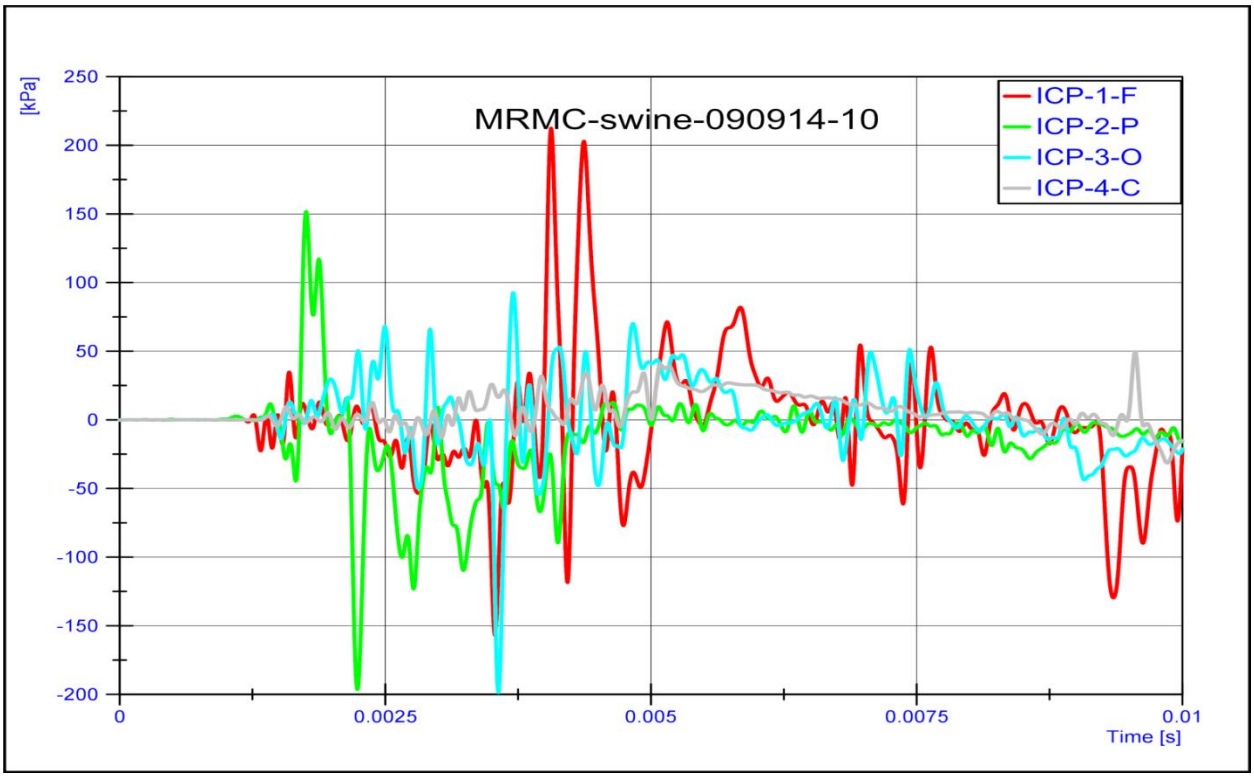
MRMC-swine-090914-10
ICP-1-F
ICP-2-P
ICP-3-O
ICP-4-C
[kPa]
250
200
150
100
50
0
-50
-100
-150
-200
0
0.0025
0.005
0.0075
0.01
Time [s]

## 4.REAR BLAST MOTION OVERVIEW

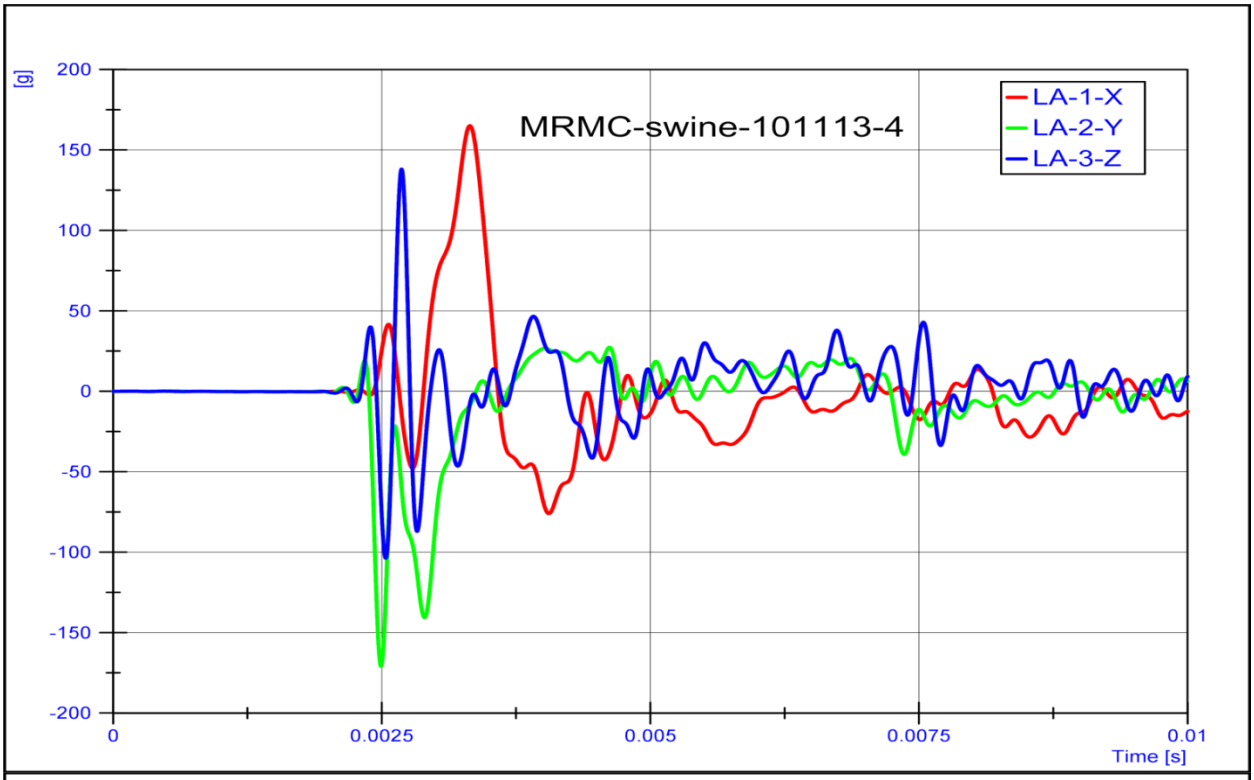


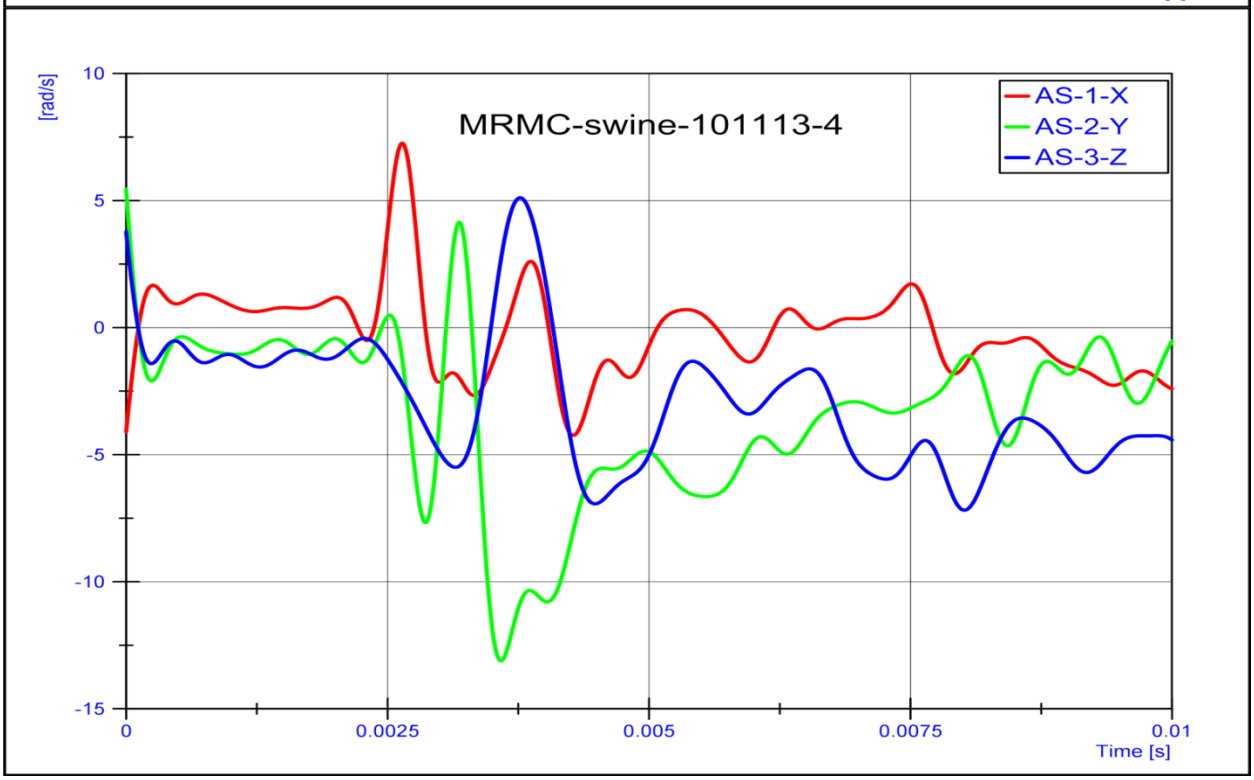

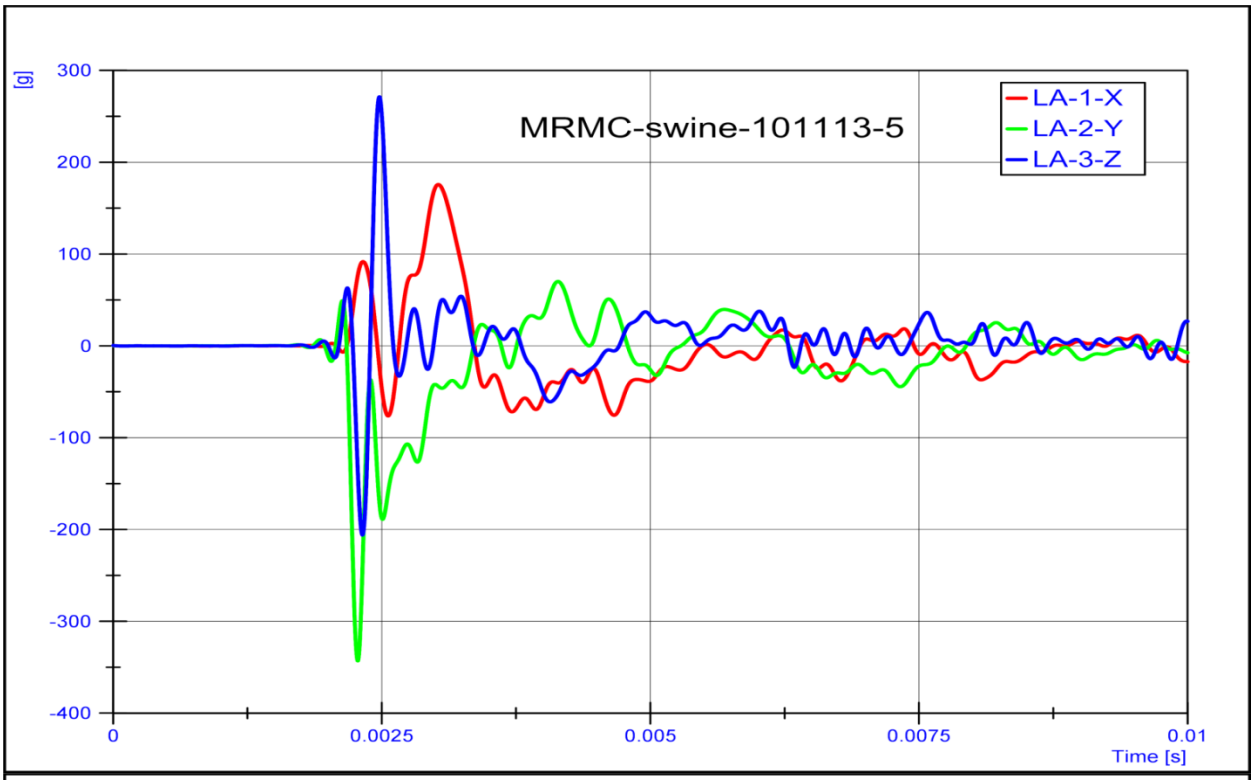
MRMC-swine-101113-5
LA-1-X
LA-2-Y
LA-3-Z
[g]
300
200
100
0
-100
-200
-300
-400
0
0.0025
0.005
0.0075
0.01
Time [s]

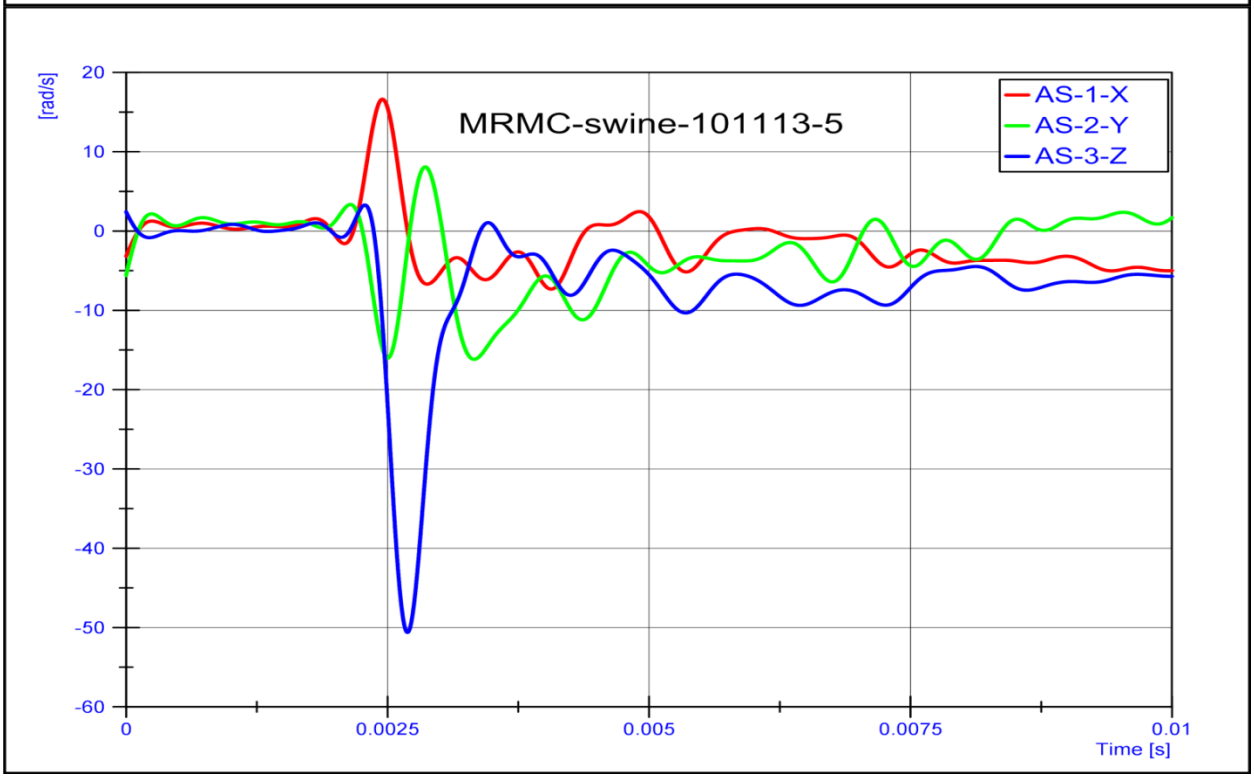
MRMC-swine-101113-5
AS-1-X
AS-2-Y
AS-3-Z
[rad/s]
20
10
0
-10
-20
-30
-40
-50
-60
0
0.0025
0.005
0.0075
0.01
Time [s]

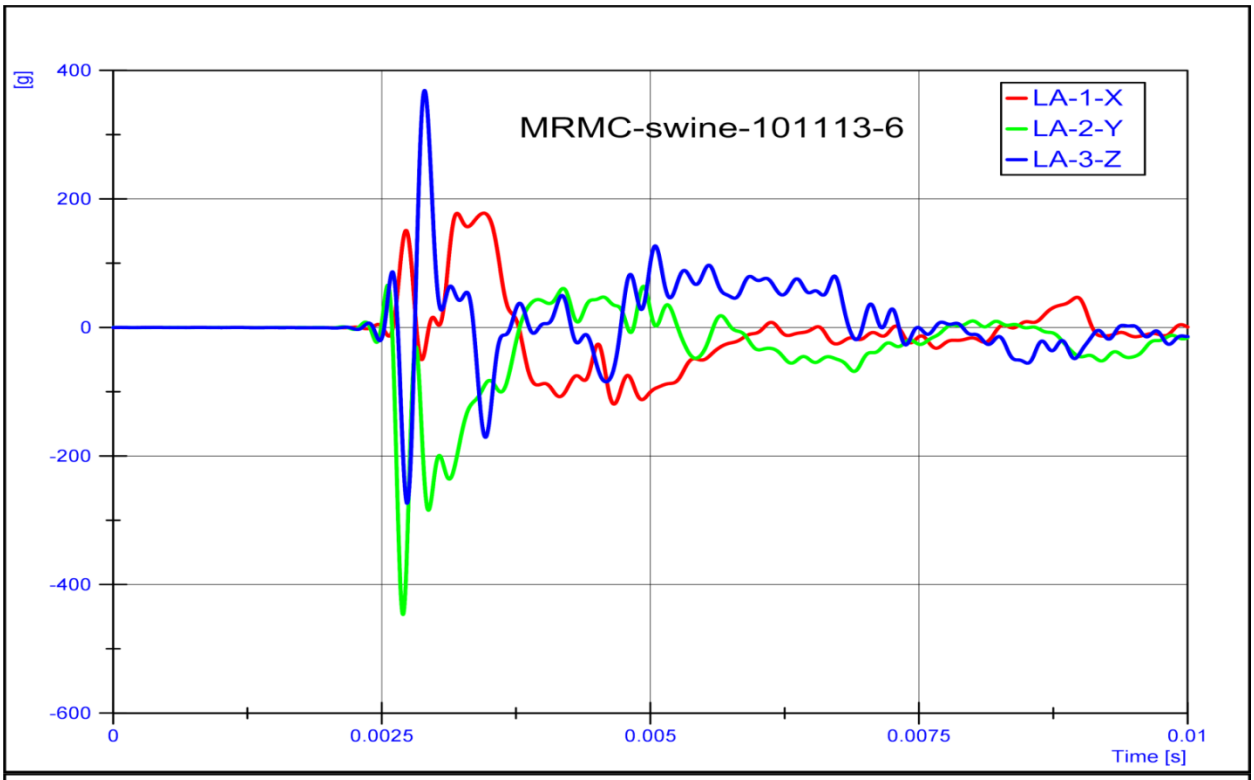
MRMC-swine-101113-6
LA-1-X
LA-2-Y
LA-3-Z
[g]
400
200
0
-200
-400
-600
0
0.0025
0.005
0.0075
0.01
Time [s]

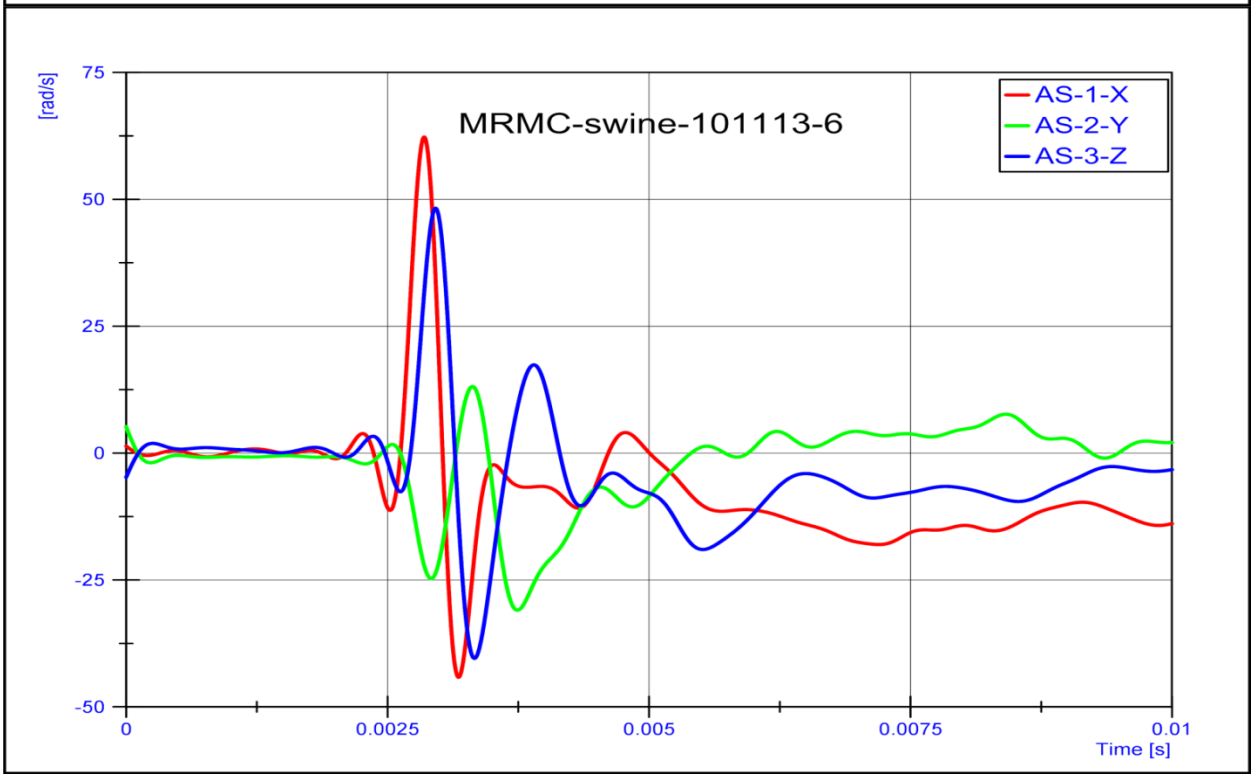
MRMC-swine-101113-6
AS-1-X
AS-2-Y
AS-3-Z
[rad/s]
75
50
25
0
-25
-50
0
0.0025
0.005
0.0075
0.01
Time [s]

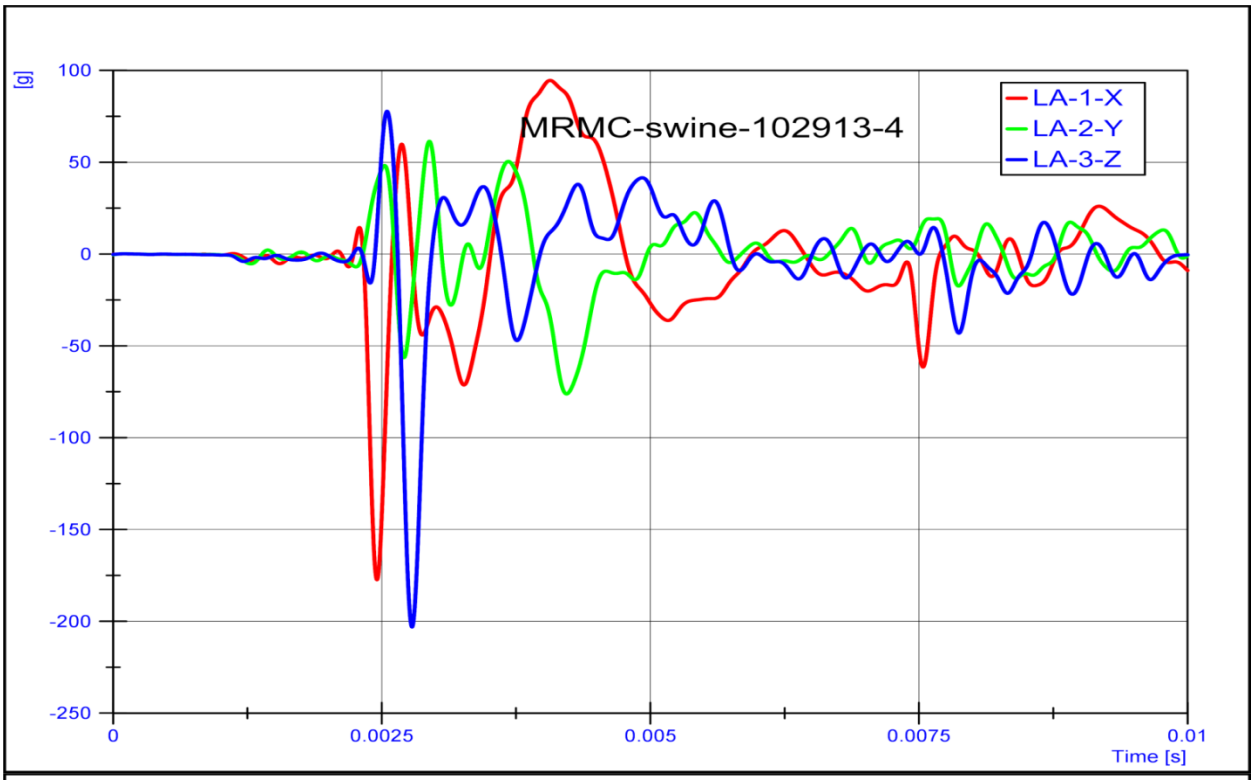
MRMC-swine-102913-4
LA-1-X
LA-2-Y
LA-3-Z
[g]
100
50
0
-50
-100
-150
-200
-250
0
0.0025
0.005
0.0075
0.01
Time [s]

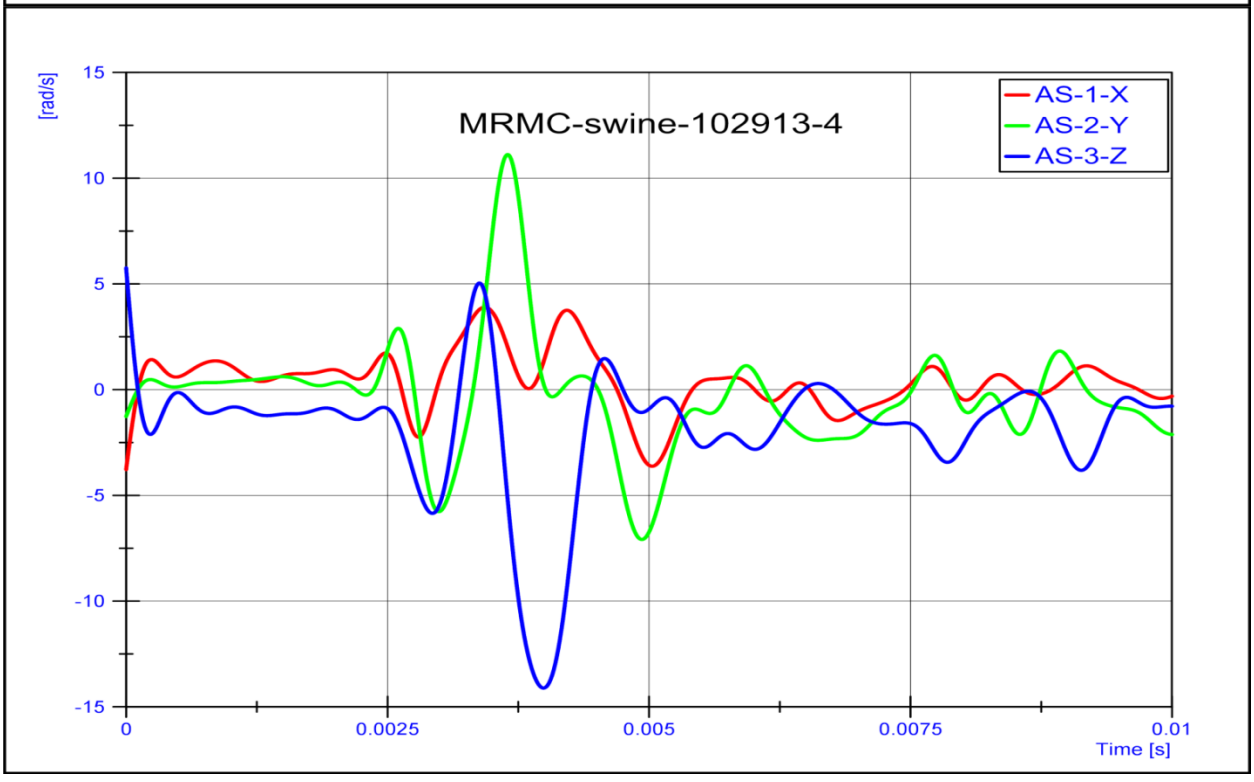
MRMC-swine-102913-4
AS-1-X
AS-2-Y
AS-3-Z
[rad/s]
15
10
5
0
-5
-10
-15
0
0.0025
0.005
0.0075
0.01
Time [s]

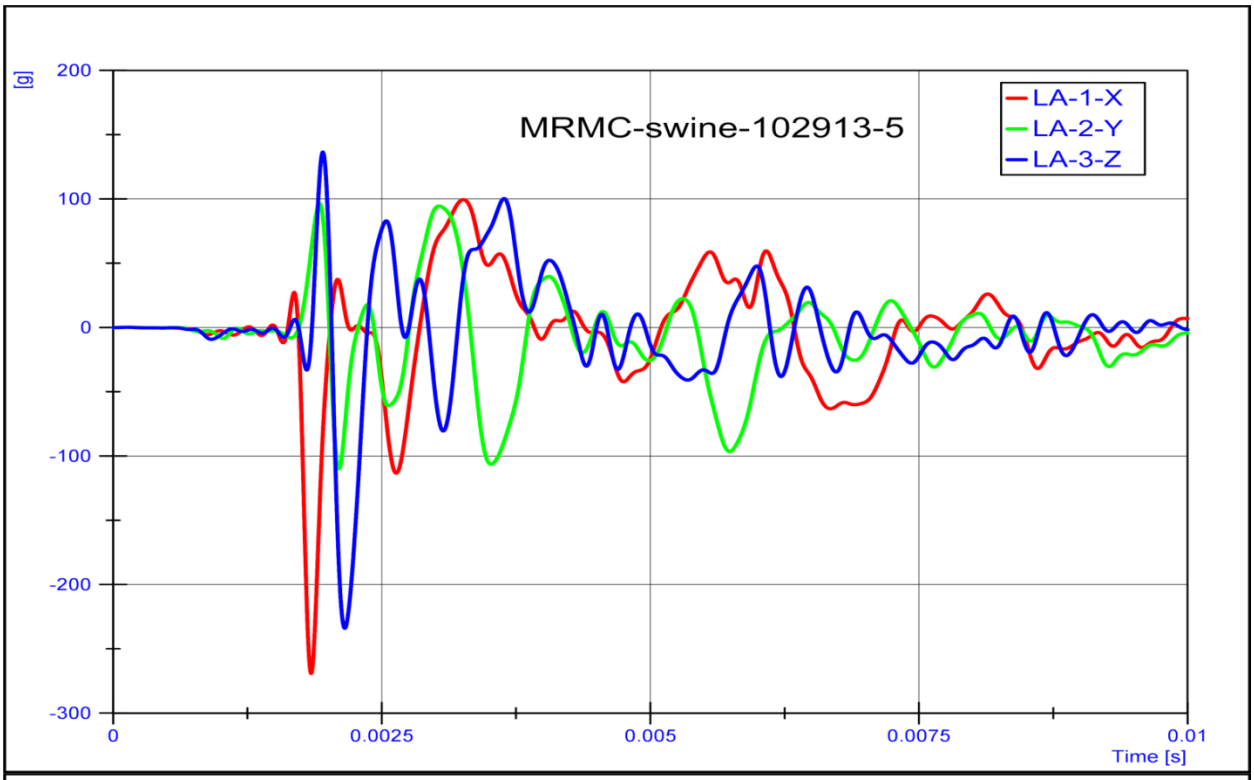
MRMC-swine-102913-5
LA-1-X
LA-2-Y
LA-3-Z
[g]
200
100
0
-100
-200
-300
0
0.0025
0.005
0.0075
0.01
Time [s]

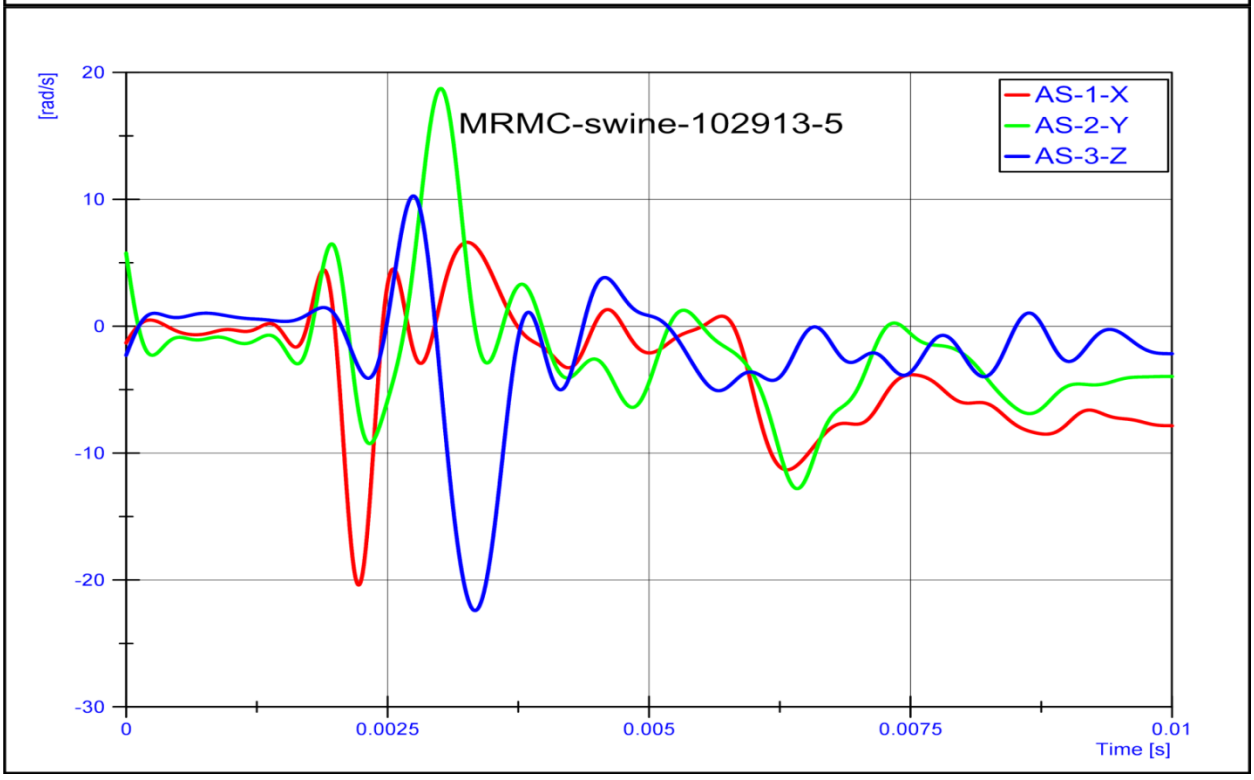
MRMC-swine-102913-5
AS-1-X
AS-2-Y
AS-3-Z
[rad/s]
20
10
0
-10
-20
-30
0
0.0025
0.005
0.0075
0.01
Time [s]

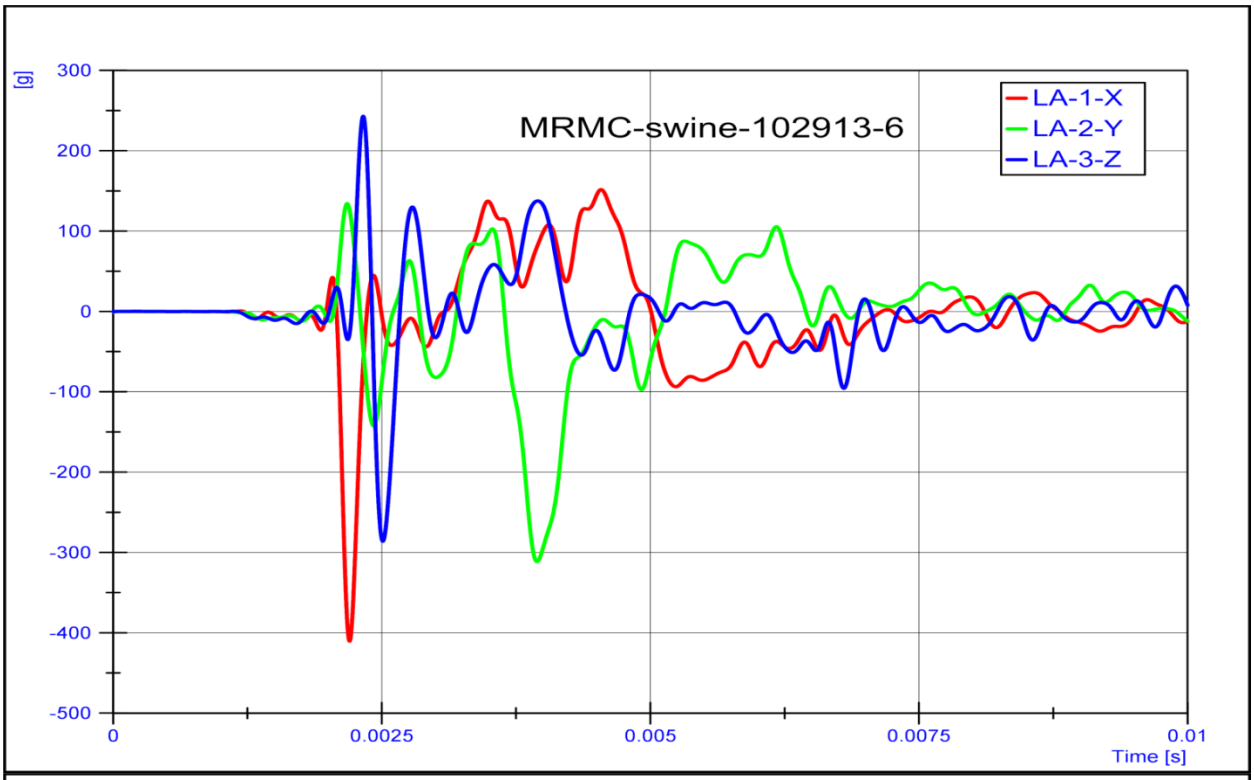
MRMC-swine-102913-6
LA-1-X
LA-2-Y
LA-3-Z
[g]
300
200
100
0
-100
-200
-300
-400
-500
0
0.0025
0.005
0.0075
0.01
Time [s]

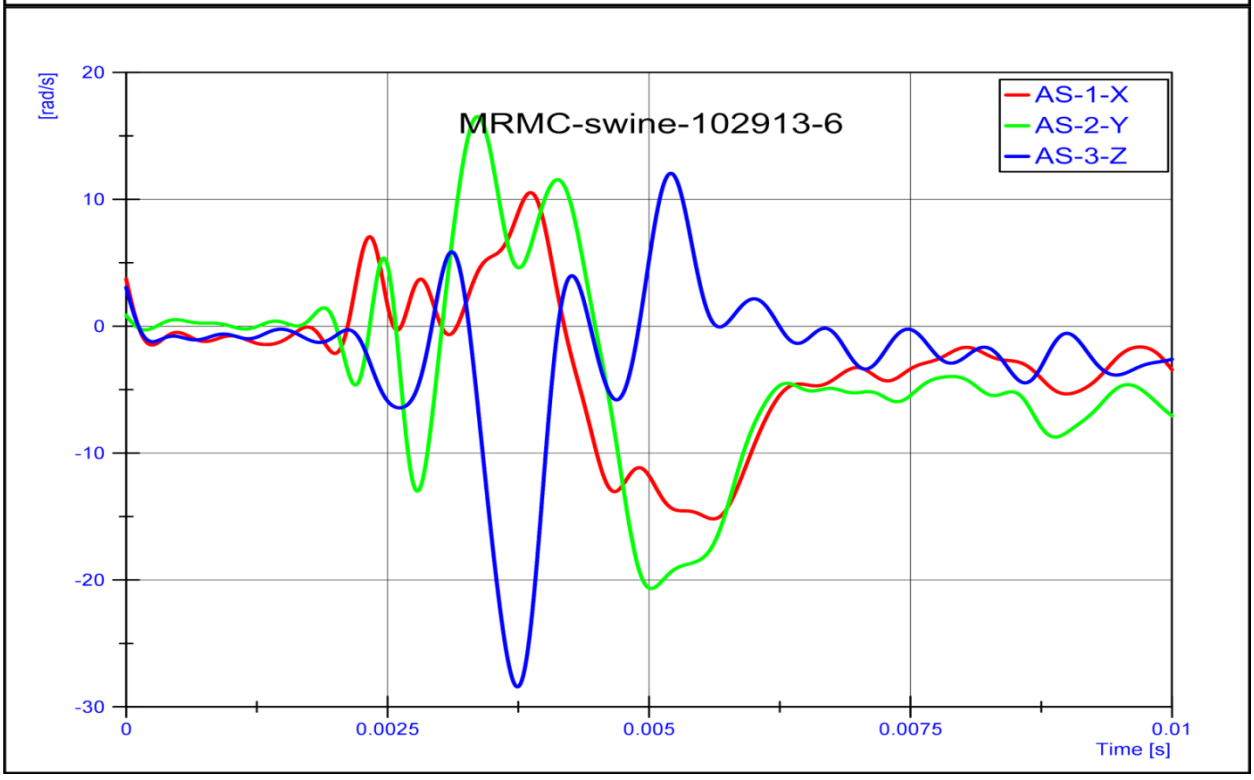
MRMC-swine-102913-6
AS-1-X
AS-2-Y
AS-3-Z
[rad/s]
20
10
0
-10
-20
-30
0
0.0025
0.005
0.0075
0.01
Time [s]

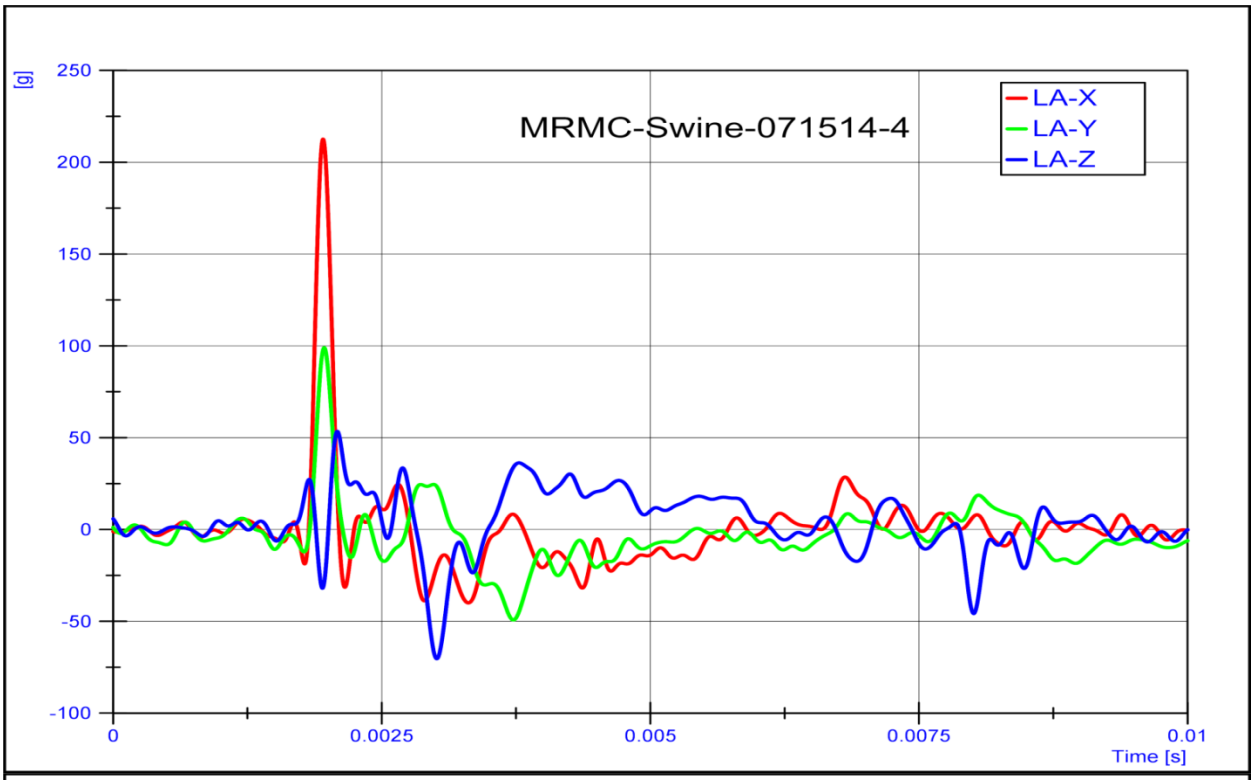
MRMC-Swine-071514-4
LA-X
LA-Y
LA-Z
[g]
250
200
150
100
50
0
-50
-100
0
0.0025
0.005
0.0075
0.01
Time [s]

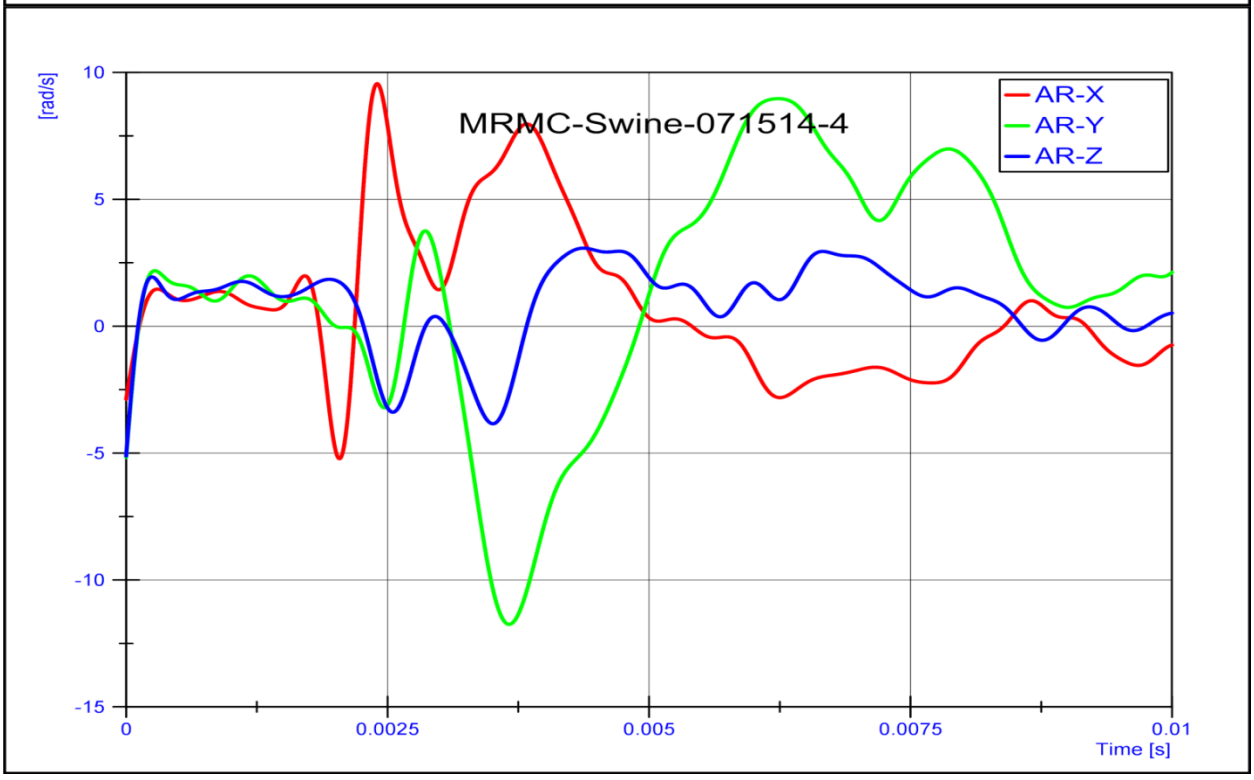
MRMC-Swine-071514-4
AR-X
AR-Y
AR-Z
[rad/s]
10
5
0
-5
-10
-15
0
0.0025
0.005
0.0075
0.01
Time [s]

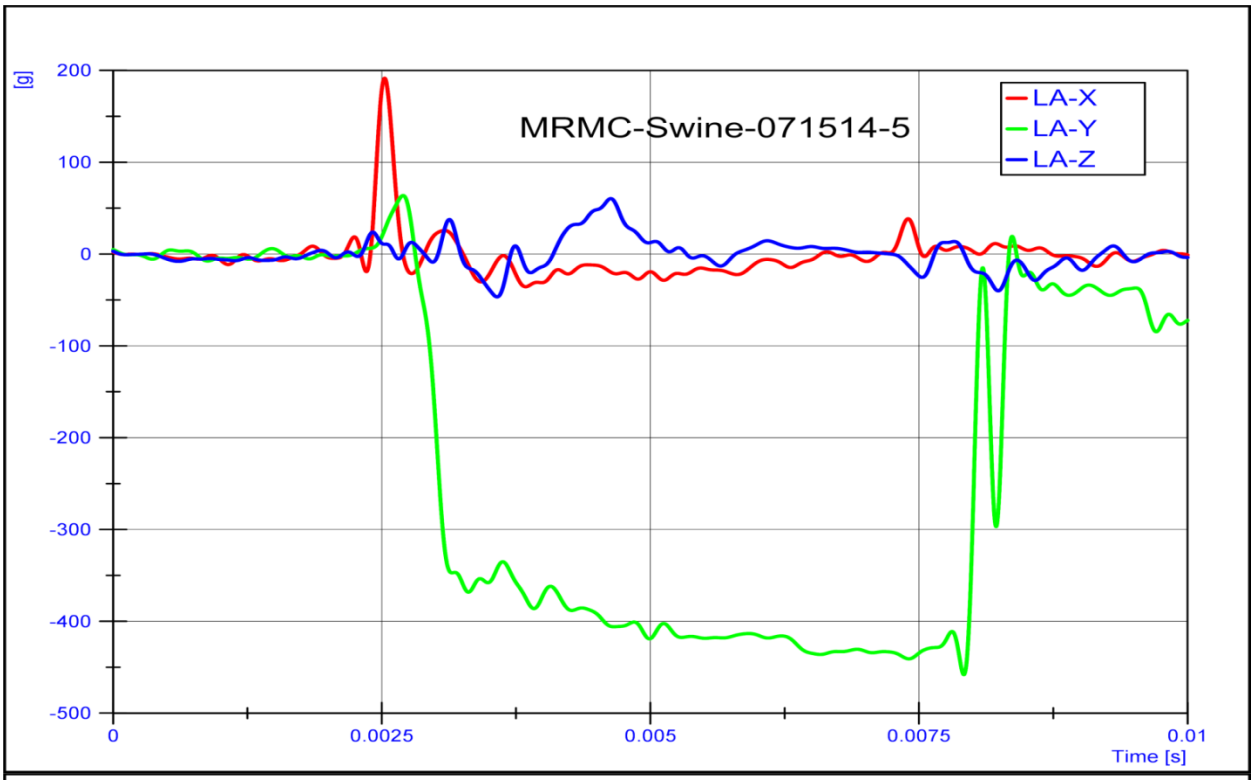
MRMC-Swine-071514-5
LA-X
LA-Y
LA-Z
[g]
200
100
0
-100
-200
-300
-400
-500
0
0.0025
0.005
0.0075
0.01
Time [s]

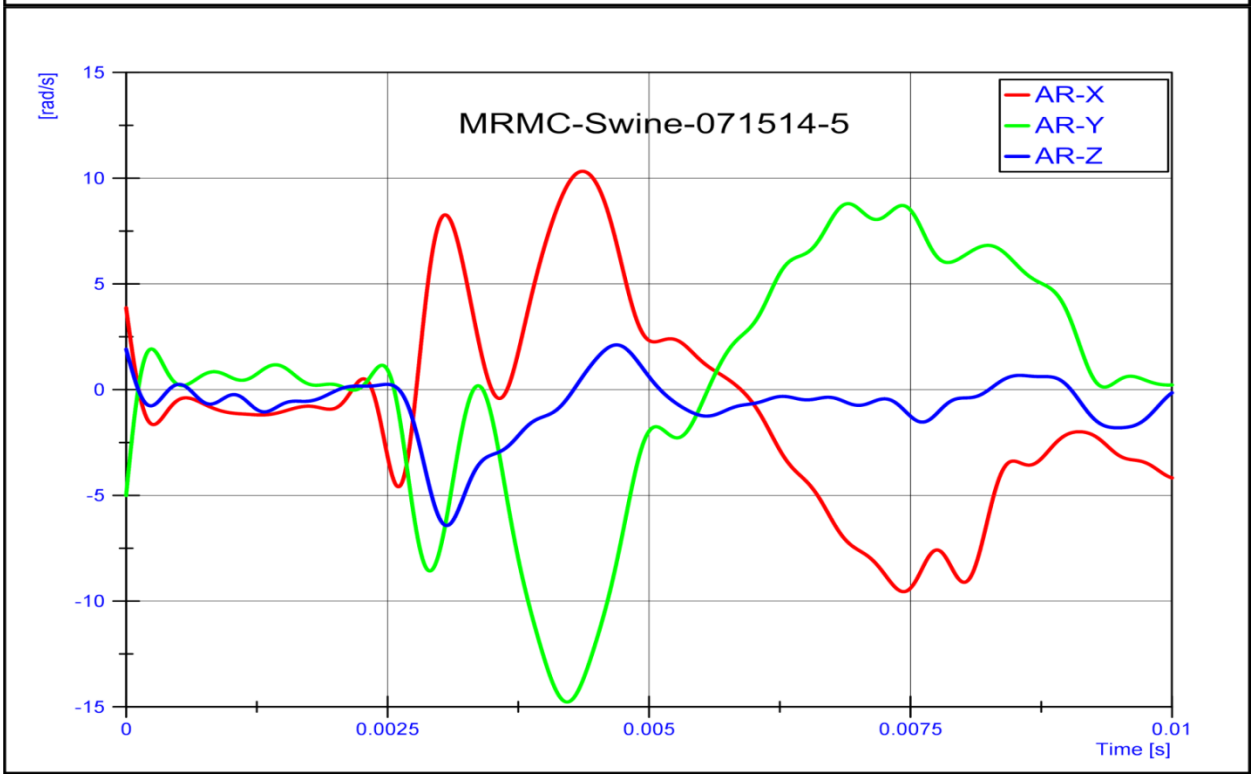
MRMC-Swine-071514-5
AR-X
AR-Y
AR-Z
[rad/s]
15
10
5
0
-5
-10
-15
0
0.0025
0.005
0.0075
0.01
Time [s]

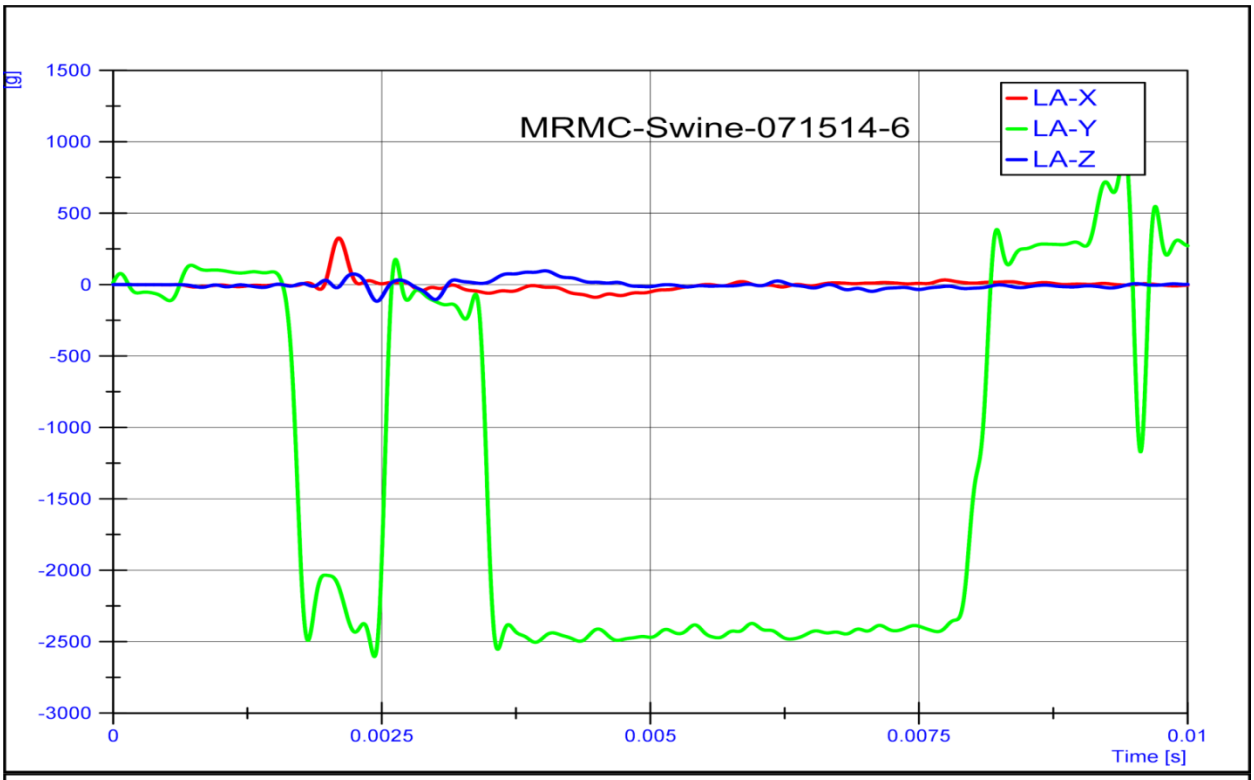
MRMC-Swine-071514-6
LA-X
LA-Y
LA-Z
[g]
1500
1000
500
0
-500
-1000
-1500
-2000
-2500
-3000
0
0.0025
0.005
0.0075
0.01
Time [s]

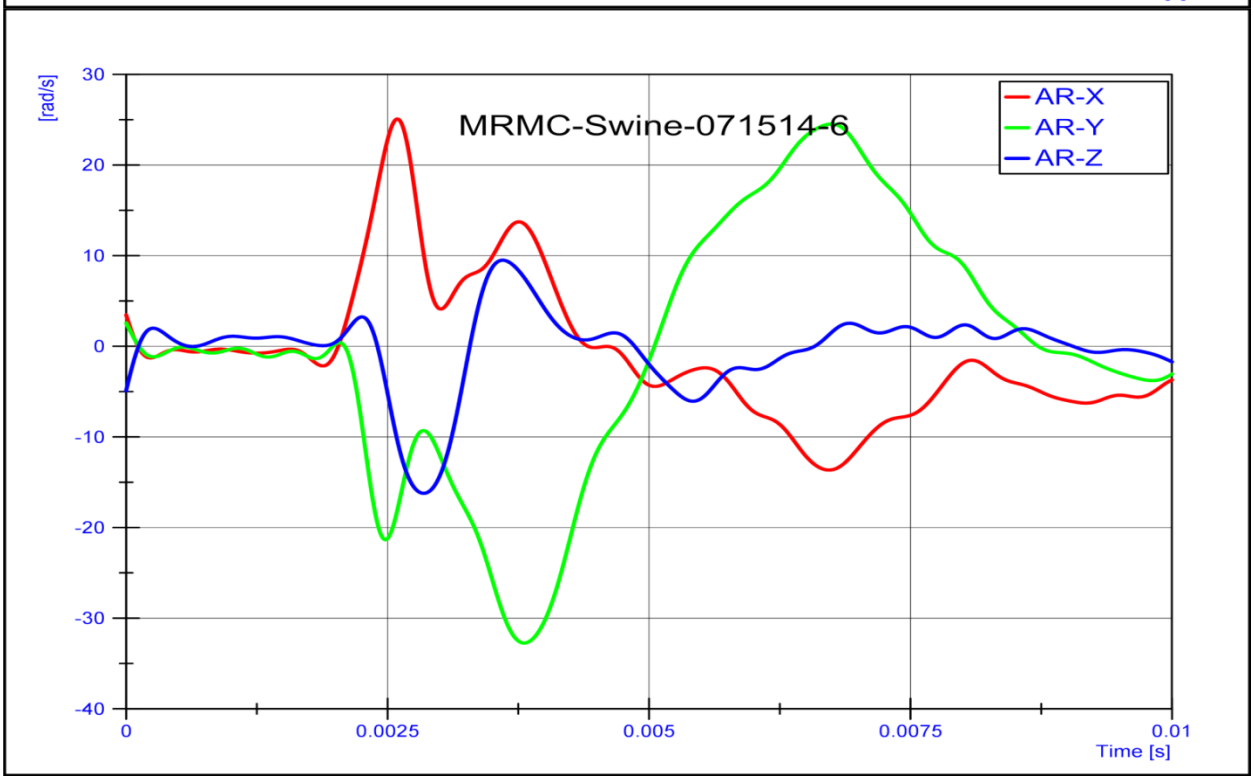
MRMC-Swine-071514-6
AR-X
AR-Y
AR-Z
[rad/s]
30
20
10
0
-10
-20
-30
-40
0
0.0025
0.005
0.0075
0.01
Time [s]

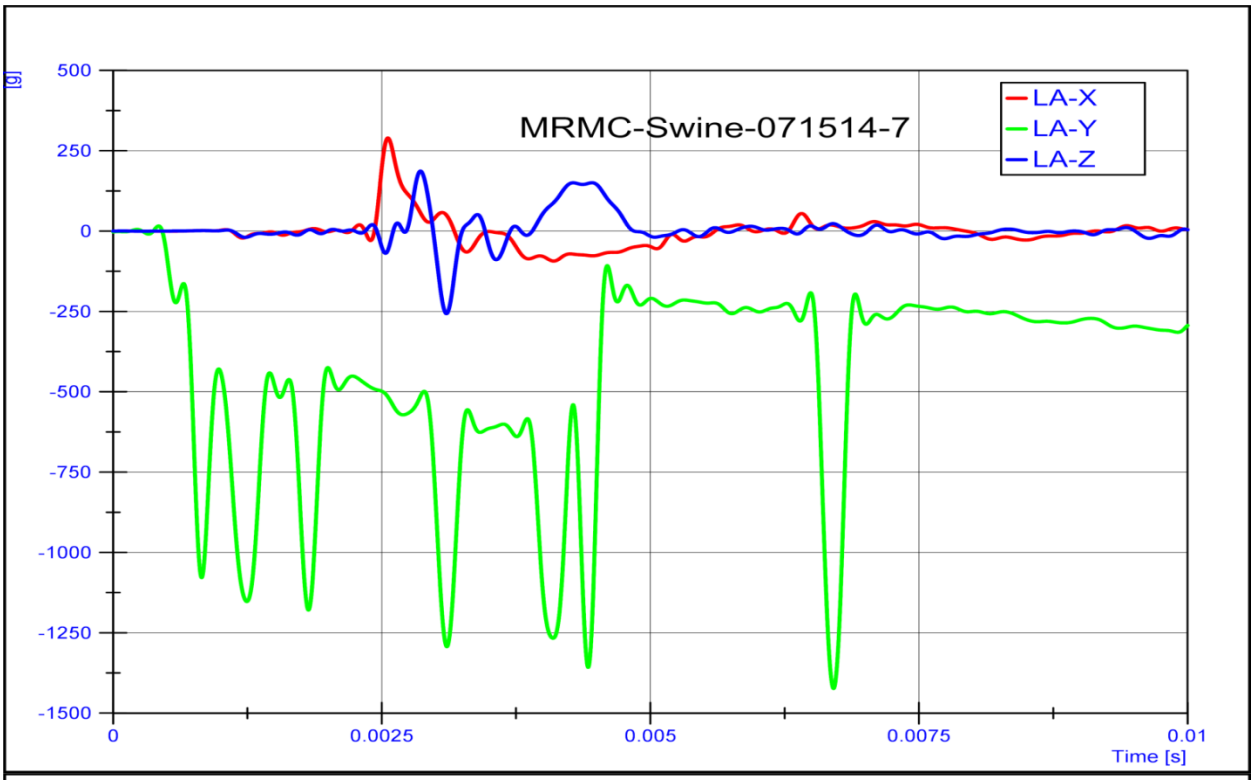
MRMC-Swine-071514-7
LA-X
LA-Y
LA-Z
[g]
500
250
0
-250
-500
-750
-1000
-1250
-1500
0
0.0025
0.005
0.0075
0.01
Time [s]

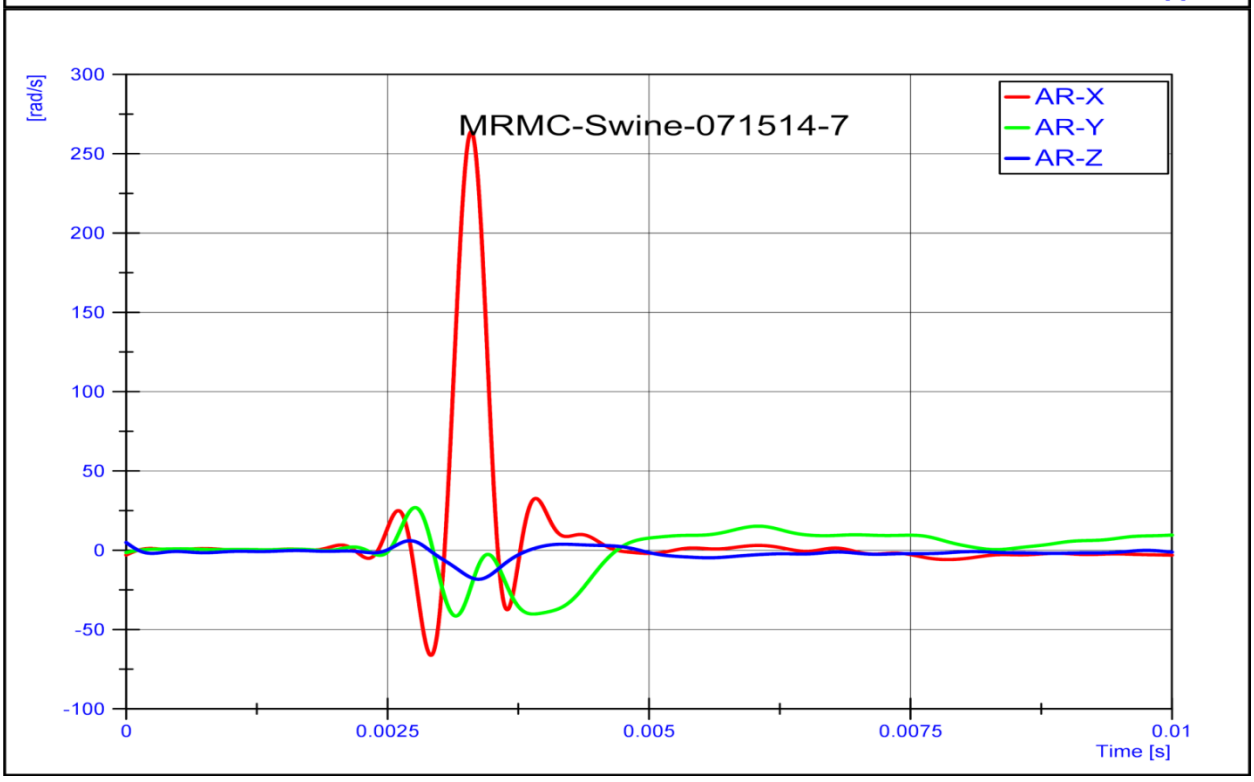
MRMC-Swine-071514-7
AR-X
AR-Y
AR-Z
[rad/s]
300
250
200
150
100
50
0
-50
-100
0
0.0025
0.005
0.0075
0.01
Time [s]

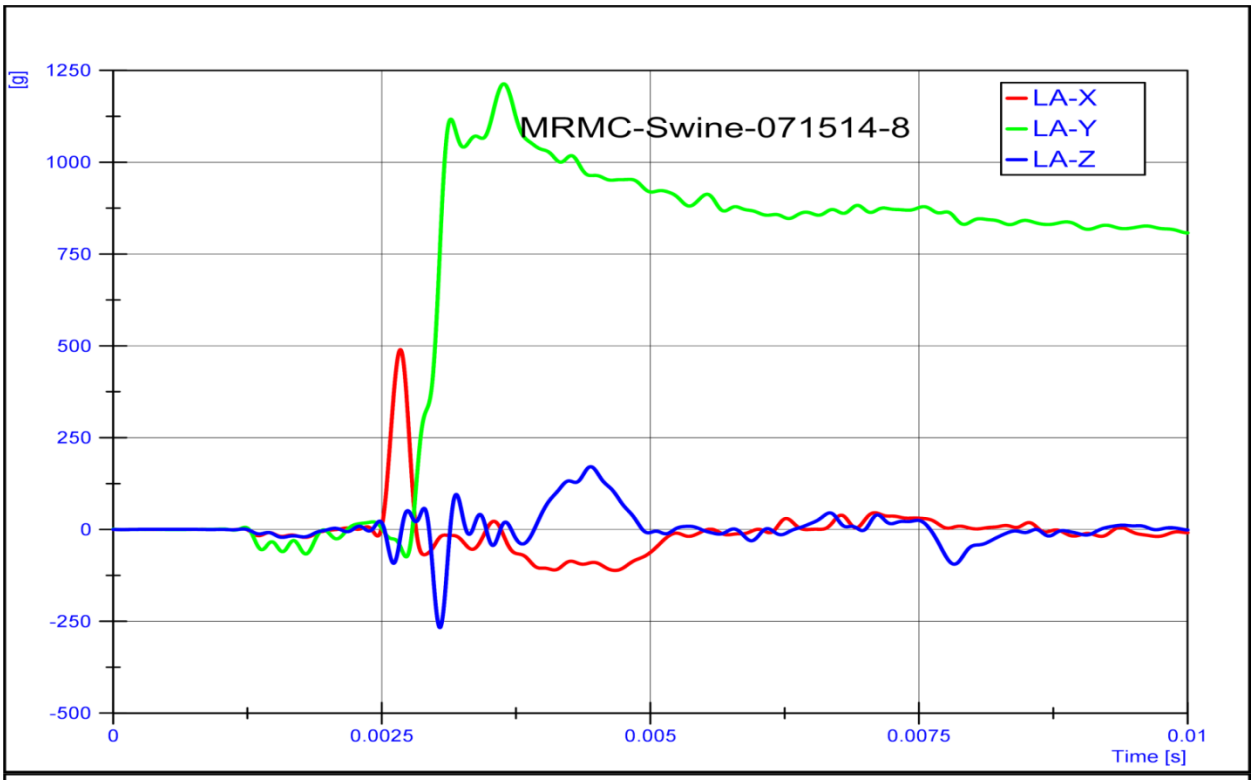
MRMC-Swine-071514-8
LA-X
LA-Y
LA-Z
[g]
1250
1000
750
500
250
0
-250
-500
0
0.0025
0.005
0.0075
0.01
Time [s]

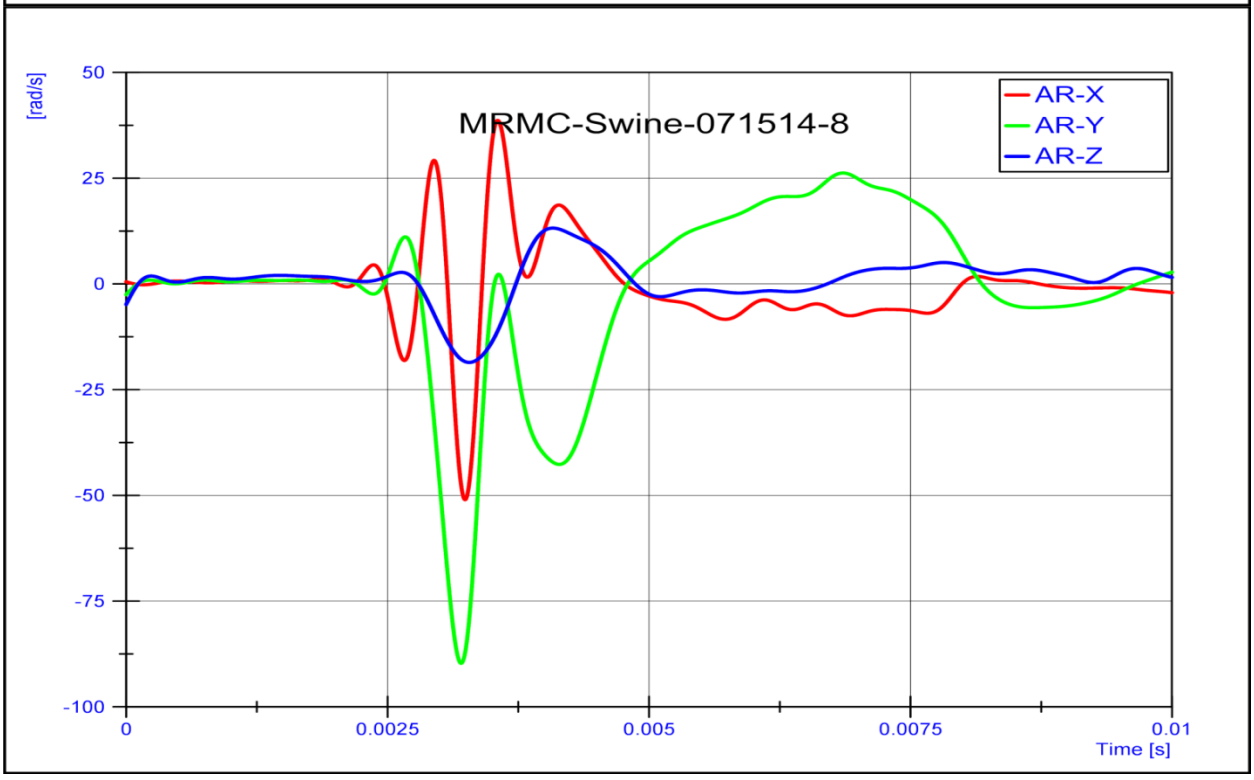
MRMC-Swine-071514-8
AR-X
AR-Y
AR-Z
[rad/s]
50
25
0
-25
-50
-75
-100
0
0.0025
0.005
0.0075
0.01
Time [s]

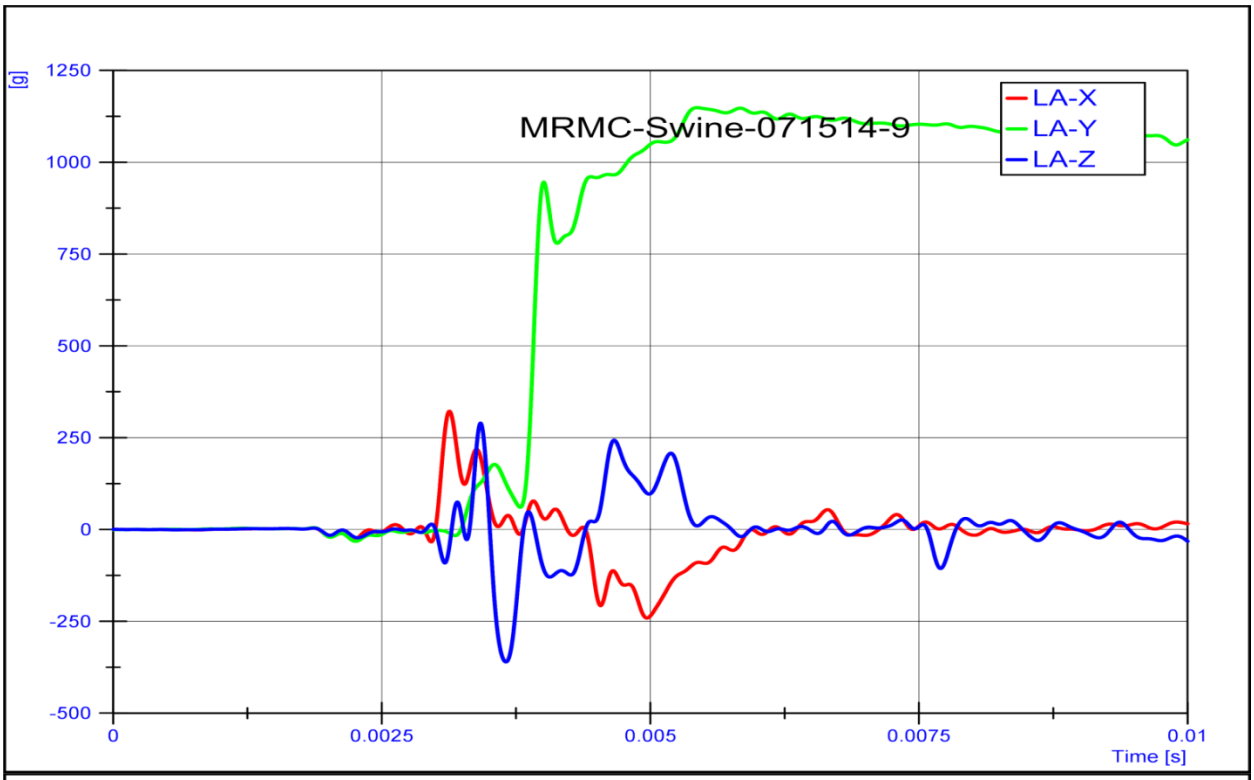
MRMC-Swine-071514-9
LA-X
LA-Y
LA-Z
[g]
1250
1000
750
500
250
0
-250
-500
0
0.0025
0.005
0.0075
0.01
Time [s]

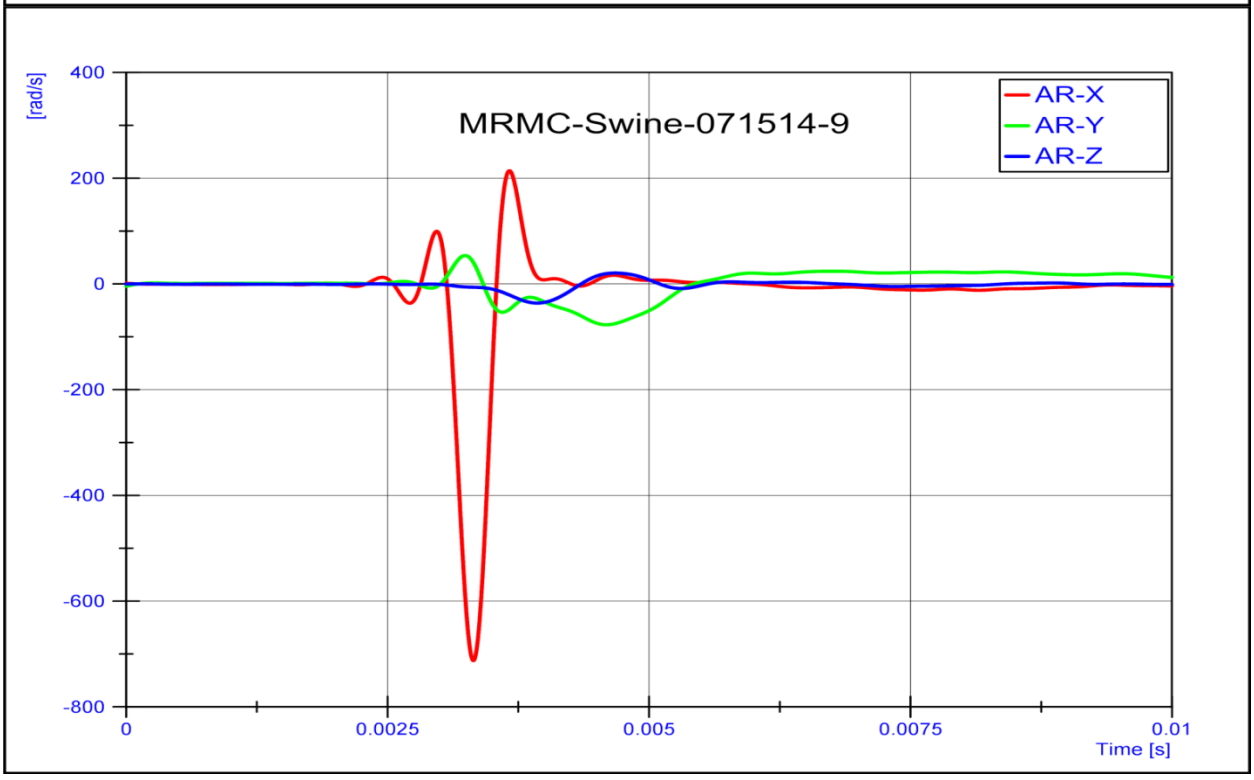
MRMC-Swine-071514-9
AR-X
AR-Y
AR-Z
[rad/s]
400
200
0
-200
-400
-600
-800
0
0.0025
0.005
0.0075
0.01
Time [s]

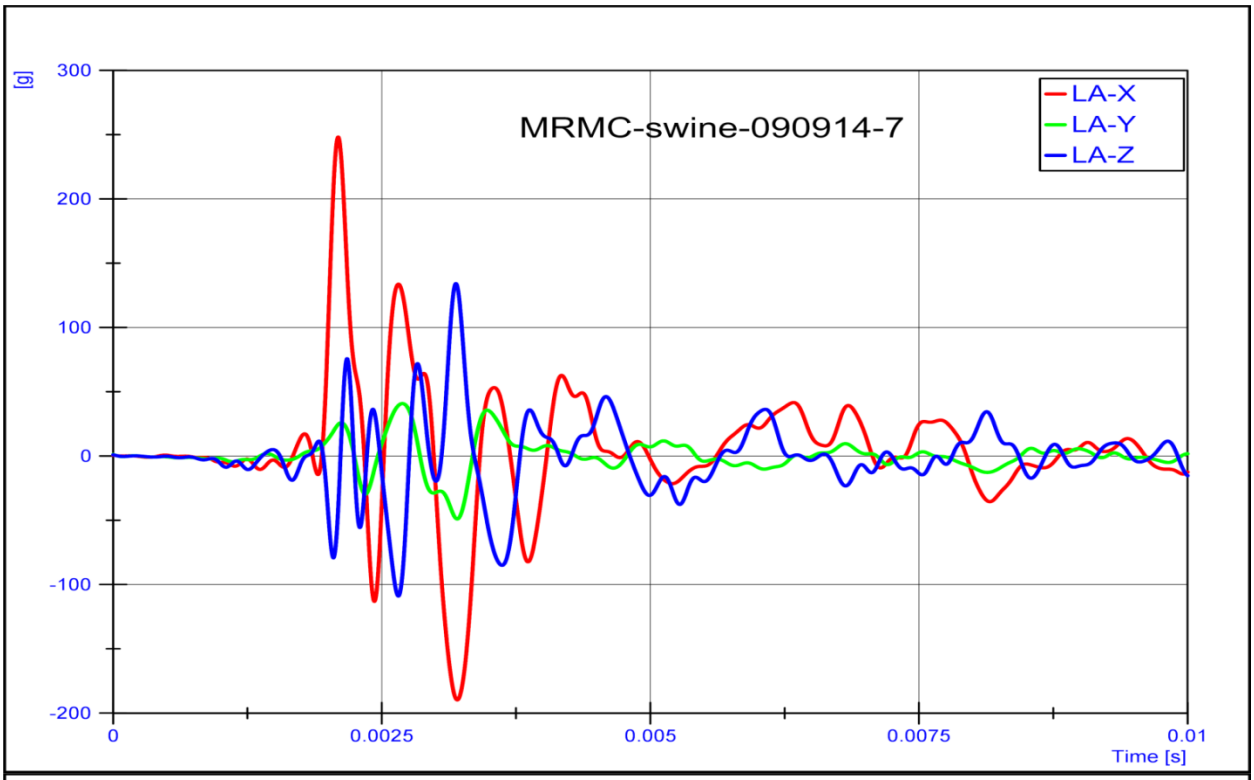
MRMC-swine-090914-7
LA-X
LA-Y
LA-Z
[g]
300
200
100
0
-100
-200
0
0.0025
0.005
0.0075
0.01
Time [s]

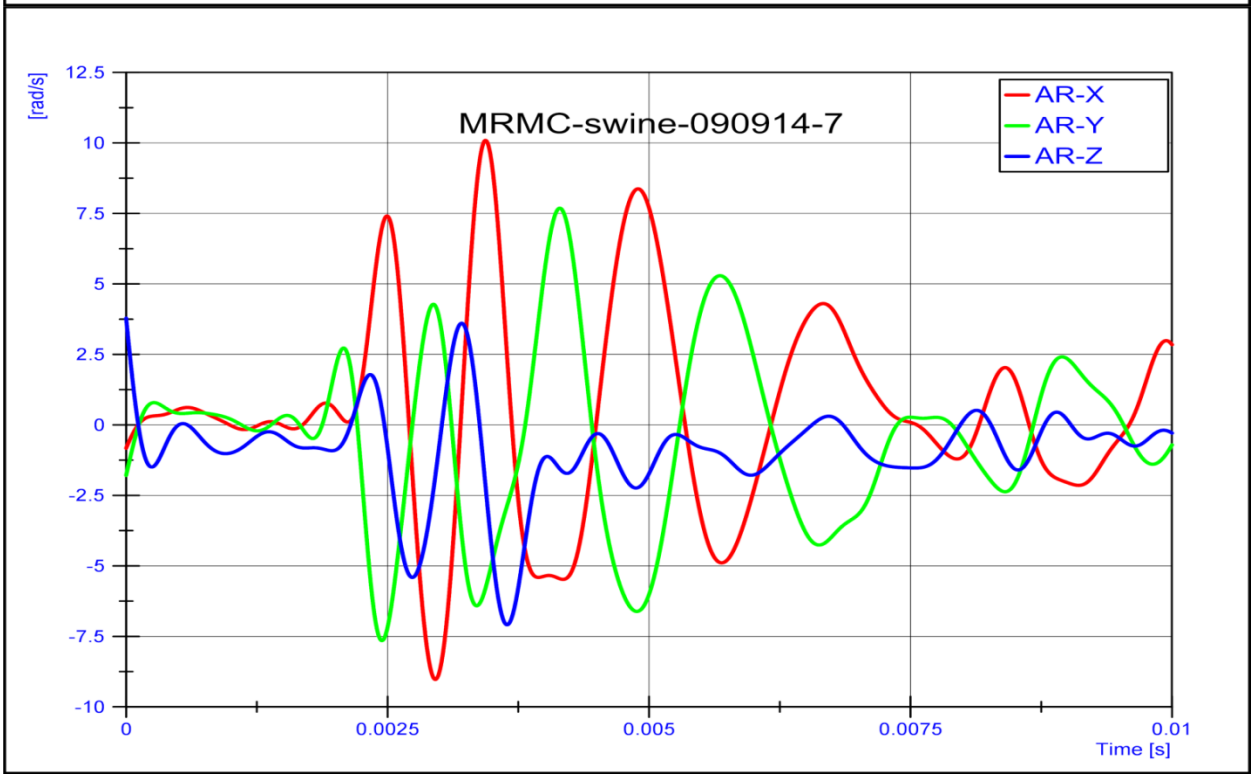
MRMC-swine-090914-7
AR-X
AR-Y
AR-Z
[rad/s]
12.5
10
7.5
5
2.5
0
-2.5
-5
-7.5
-10
0
0.0025
0.005
0.0075
0.01
Time [s]

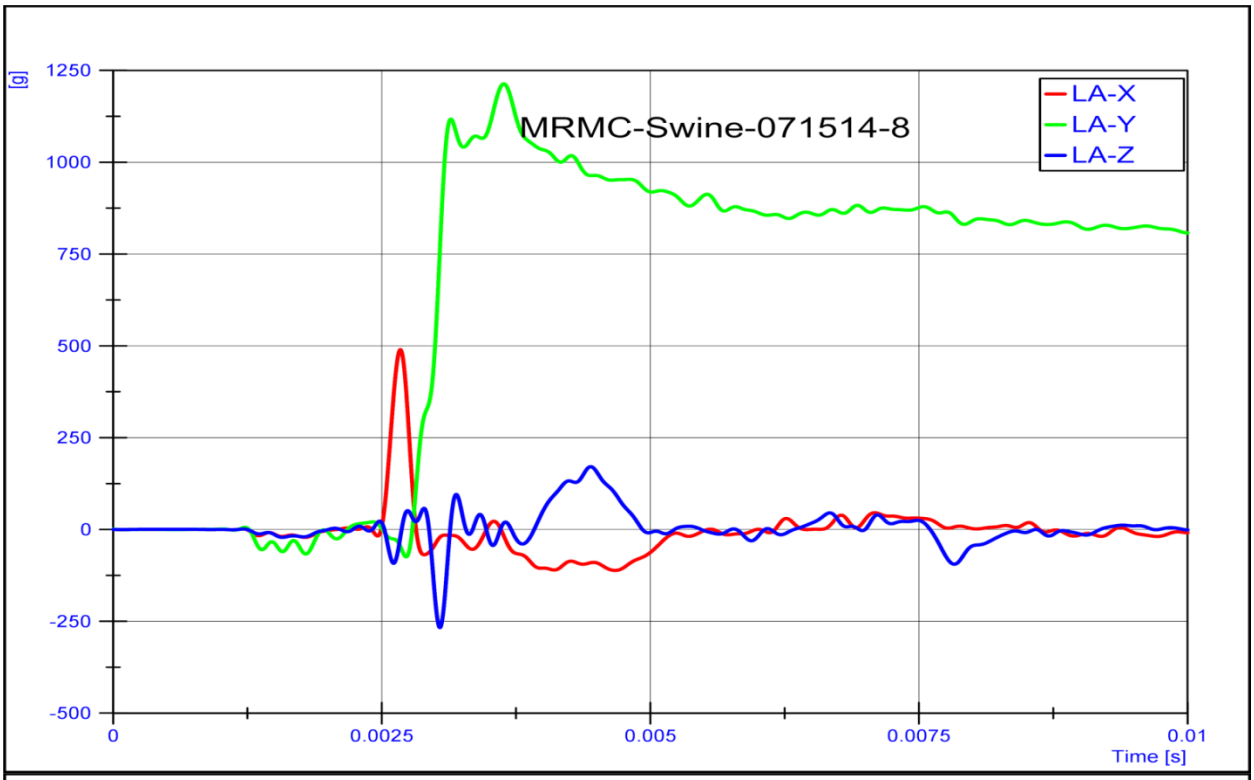
MRMC-Swine-071514-8
LA-X
LA-Y
LA-Z
[g]
1250
1000
750
500
250
0
-250
-500
0
0.0025
0.005
0.0075
0.01
Time [s]

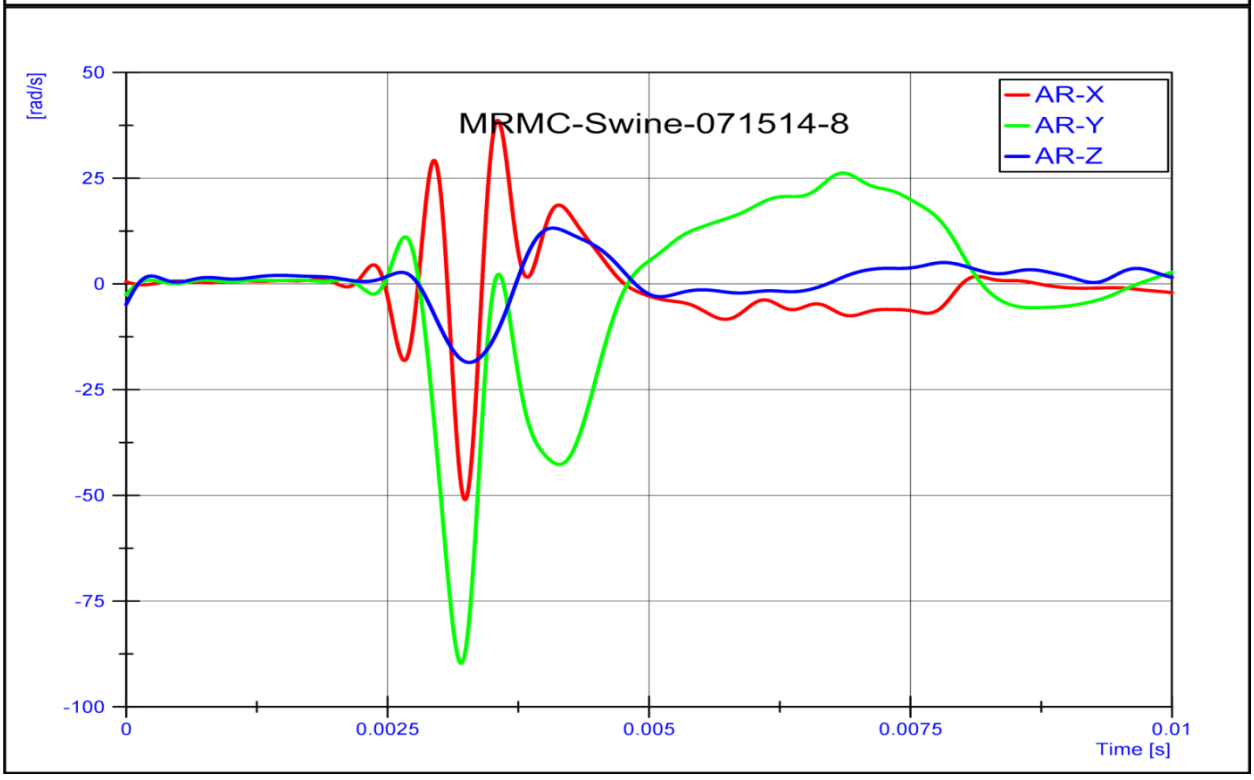
MRMC-Swine-071514-8
AR-X
AR-Y
AR-Z
[rad/s]
50
25
0
-25
-50
-75
-100
0
0.0025
0.005
0.0075
0.01
Time [s]

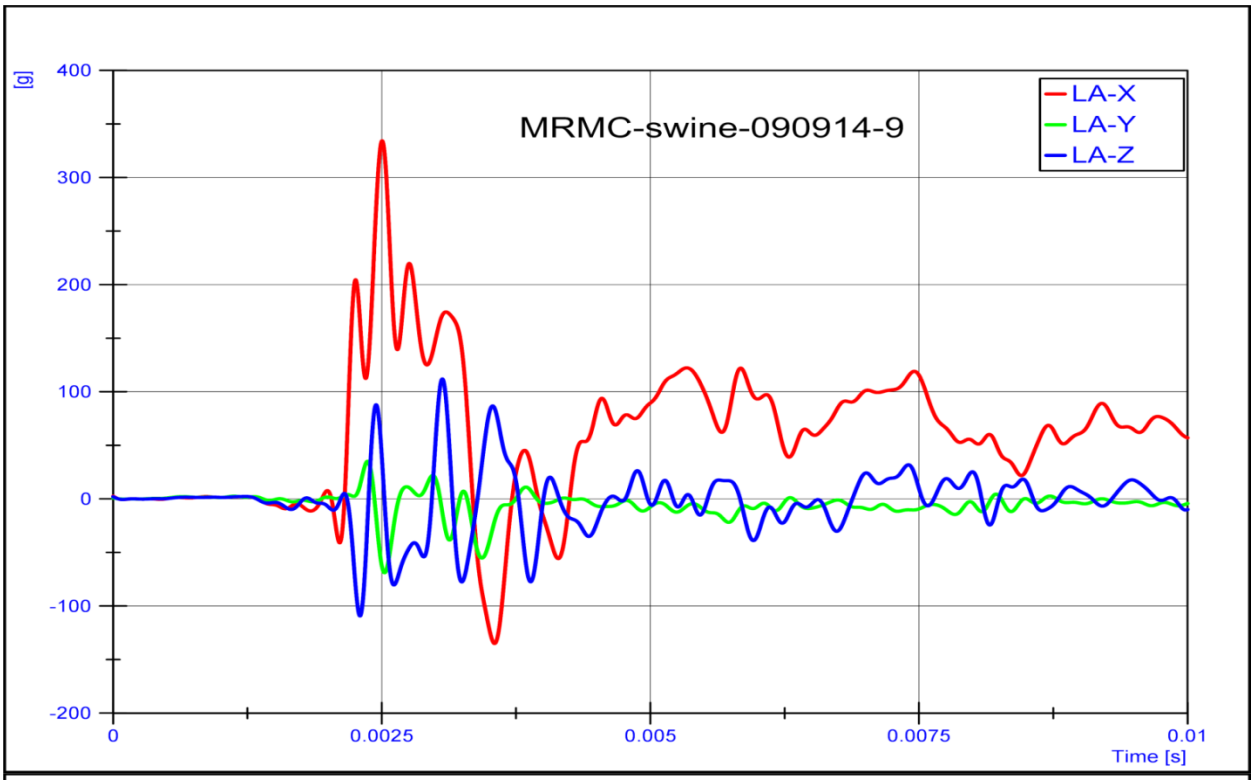
MRMC-swine-090914-9
LA-X
LA-Y
LA-Z
[g]
400
300
200
100
0
-100
-200
0
0.0025
0.005
0.0075
0.01
Time [s]

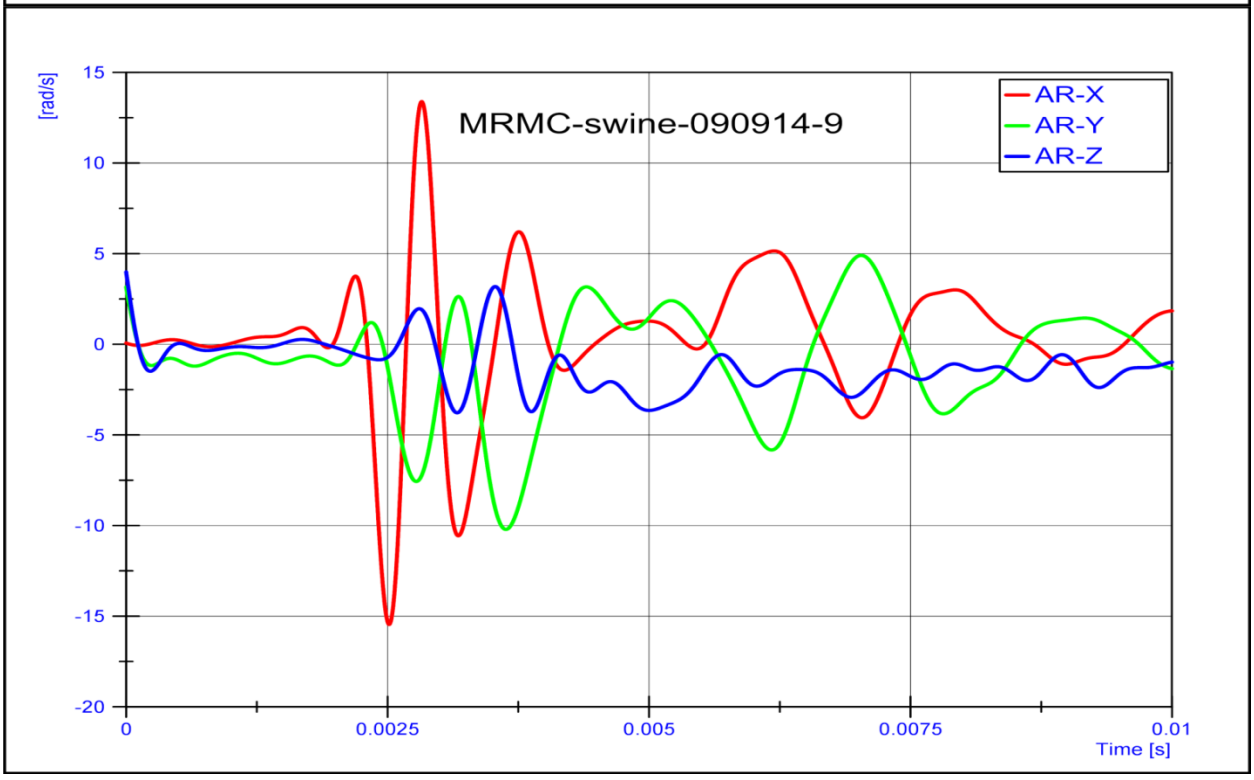
MRMC-swine-090914-9
AR-X
AR-Y
AR-Z
[rad/s]
15
10
5
0
-5
-10
-15
-20
0
0.0025
0.005
0.0075
0.01
Time [s]

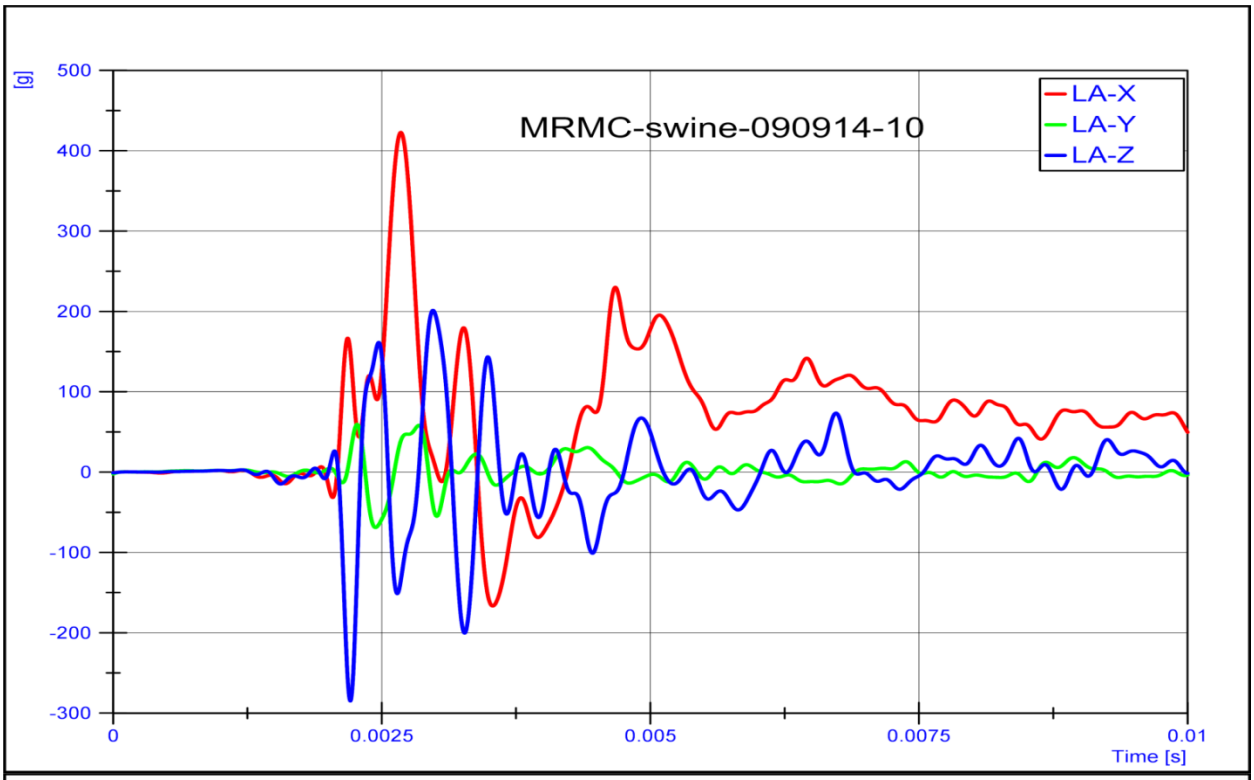
MRMC-swine-090914-10
LA-X
LA-Y
LA-Z
[g]
500
400
300
200
100
0
-100
-200
-300
0
0.0025
0.005
0.0075
0.01
Time [s]

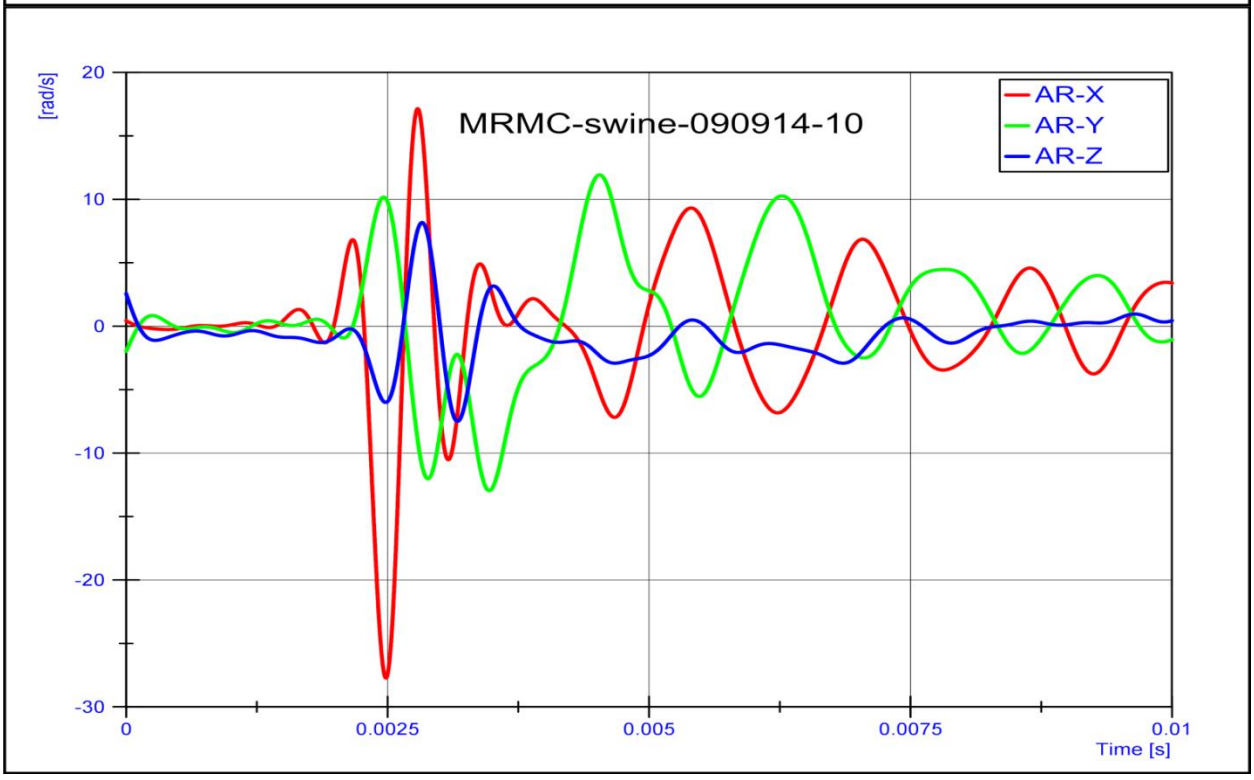
MRMC-swine-090914-10
AR-X
AR-Y
AR-Z
[rad/s]
20
10
0
-10
-20
-30
0
0.0025
0.005
0.0075
0.01
Time [s]

## REFERENCES

1993. Definition of mild traumatic brain Injury the Mild Traumatic Brain Injury Committee of the Head Injury Interdisciplinary Special Interest Group of the American Congress of Rehabilitation Medicine

2017. Defense Medical Surveillance System (DMSS) and Theater Medical Data Store (TMDS) provided by the Armed Forces Health Surveillance Branch (AFHSB).

Abdul-Muneer, P.M., Chandra, N., Haorah, J., 2015. Interactions of oxidative stress and neurovascular inflammation in the pathogenesis of traumatic brain injury. Mol Neurobiol 51, 966-979.

Abdul-Muneer, P.M., Schuetz, H., Wang, F., Skotak, M., Jones, J., Gorantla, S., Zimmerman, M.C., Chandra, N., Haorah, J., 2013. Induction of oxidative and nitrosative damage leads to cerebrovascular inflammation in an animal model of mild traumatic brain injury induced by primary blast. Free radical biology & medicine 60, 282-291.

Ahlers, S.T., Vasserman-Stokes, E., Shaughness, M.C., Hall, A.A., Shear, D.A., Chavko, M., McCarron, R.M., Stone, J.R., 2012. Assessment of the effects of acute and repeated exposure to blast overpressure in rodents: toward a greater understanding of blast and the potential ramifications for injury in humans exposed to blast. Frontiers in neurology 3, 32.

Armonda, R.A., Bell, R.S., Vo, A.H., Ling, G., DeGraba, T.J., Crandall, B., Ecklund, J., Campbell, W.W., 2006. Wartime traumatic cerebral vasospasm: recent review of combat casualties. Neurosurgery 59, 1215-1225; discussion 1225.

Axelsson, H., Hjelmqvist, H., Medin, A., Persson, J.K., Suneson, A., 2000. Physiological changes in pigs exposed to a blast wave from a detonating high-explosive charge. Mil Med 165, 119-126.

Bardet, P.L., Kolahgar, G., Mynett, A., Miguel-Aliaga, I., Briscoe, J., Meier, P., Vincent, J.P., 2008. A fluorescent reporter of caspase activity for live imaging. Proceedings of the National Academy of Sciences of the United States of America 105, 13901-13905.

Bass, C.R., Panzer, M.B., Rafaels, K.A., Wood, G., Shridharani, J., Capehart, B., 2012. Brain injuries from blast. Ann Biomed Eng 40, 185-202.

Bass, C.R., Rafaels, K.A., Salzar, R.S., 2008. Pulmonary injury risk assessment for short-duration blasts. The Journal of trauma 65, 604-615.

Bauman, R.A., Ling, G., Tong, L., Januszkiewicz, A., Agoston, D., Delanerolle, N., Kim, Y., Ritzel, D., Bell, R., Ecklund, J., Armonda, R., Bandak, F., Parks, S., 2009. An introductory characterization of a combat-casualty-care relevant swine model of closed head injury resulting from exposure to explosive blast. J Neurotrauma 26, 841-860.

Ben-Dor, G., 2007. Shock wave reflection phenomena. Springer.

Bian, G.L., Wei, L.C., Shi, M., Wang, Y.Q., Cao, R., Chen, L.W., 2007. Fluoro-Jade C can specifically stain the degenerative neurons in the substantia nigra of the 1-methyl-4-phenyl-1,2,3,6-tetrahydro pyridine-treated C57BL/6 mice. Brain Res 1150, 55-61.

Bir, C., 2011. Measuring blast-related intracranial pressure within the human head. DTIC Document.

Bowen IG, F.E., Richmond DR., 1968. estimate of man's tolerance to the direct effects of air blast.

Bressenot, A., Marchal, S., Bezdetnaya, L., Garrier, J., Guillemin, F., Plenat, F., 2009. Assessment of apoptosis by immunohistochemistry to active caspase-3, active caspase-7, or cleaved PARP in monolayer cells and spheroid and subcutaneous xenografts of human carcinoma. J Histochem Cytochem 57, 289-300.

Cernak, I., 2014. Blast-induced neurotrauma models and their requirements. Frontiers in neurology 5, 128.

Cernak, I., Wang, Z., Jiang, J., Bian, X., Savic, J., 2001a. Cognitive deficits following blast injury-induced neurotrauma: possible involvement of nitric oxide. Brain injury 15, 593-612.

Cernak, I., Wang, Z., Jiang, J., Bian, X., Savic, J., 2001b. Ultrastructural and functional characteristics of blast injury-induced neurotrauma. The Journal of trauma 50, 695-706.

Chafi, M.S., Karami, G., Ziejewski, M., 2010. Biomechanical assessment of brain dynamic responses due to blast pressure waves. Annals of biomedical engineering 38, 490-504.

Chavko, M., Koller, W.A., Prusaczyk, W.K., McCarron, R.M., 2007. Measurement of blast wave by a miniature fiber optic pressure transducer in the rat brain. J Neurosci Methods 159, 277-281.

Cheng, G., Kong, R.H., Zhang, L.M., Zhang, J.N., 2012. Mitochondria in traumatic brain injury and mitochondrial-targeted multipotential therapeutic strategies. Br J Pharmacol 167, 699-719.

Clemedson, C.J., 1956. Blast injury. Physiological reviews 36, 336-354.

Connell, S., Gao, J., Chen, J., Shi, R., 2011. Novel model to investigate blast injury in the central nervous system. Journal of neurotrauma 28, 1229-1236.

Cornelius, C., Crupi, R., Calabrese, V., Graziano, A., Milone, P., Pennisi, G., Radak, Z., Calabrese, E.J., Cuzzocrea, S., 2013. Traumatic brain injury: oxidative stress and neuroprotection. Antioxid Redox Signal 19, 836-853.

Courtney, A., Courtney, M., 2015. The Complexity of Biomechanics Causing Primary Blast-Induced Traumatic Brain Injury: A Review of Potential Mechanisms. Frontiers in neurology 6, 221.

D'Amelio, M., Cavallucci, V., Cecconi, F., 2010. Neuronal caspase-3 signaling: not only cell death. Cell death and differentiation 17, 1104-1114.

de Lanerolle, N.C., Bandak, F., Kang, D., Li, A.Y., Du, F., Swauger, P., Parks, S., Ling, G., Kim, J.H., 2011. Characteristics of an explosive blast-induced brain injury in an experimental model. J Neuropathol Exp Neurol 70, 1046-1057.

De Rosa, M., Fam, F., Palleschi, V.V., Singh, D.P., Vaselli, M., 1992. Derivation of the critical angle for Mach reflection for strong shock waves. Physical review. A 45, 6130-6132.

Effgen, G.B., Hue, C.D., Vogel, E., 3rd, Panzer, M.B., Meaney, D.F., Bass, C.R., Morrison, B., 3rd, 2012. A Multiscale Approach to Blast Neurotrauma Modeling: Part II: Methodology for Inducing Blast Injury to in vitro Models. Frontiers in neurology 3, 23.

Elder, G.A., Dorr, N.P., De Gasperi, R., Gama Sosa, M.A., Shaughness, M.C., Maudlin-Jeronimo, E., Hall, A.A., McCarron, R.M., Ahlers, S.T., 2012. Blast exposure induces post-traumatic stress disorder-related traits in a rat model of mild traumatic brain injury. Journal of neurotrauma 29, 2564-2575.

Elder, G.A., Stone, J.R., Ahlers, S.T., 2014. Effects of low-level blast exposure on the nervous system: is there really a controversy? Frontiers in neurology 5, 269.

Elsayed, N.M., Gorbunov, N.V., Kagan, V.E., 1997. A proposed biochemical mechanism involving hemoglobin for blast overpressure-induced injury. Toxicology 121, 81-90.

Galarneau, M.R., Woodruff, S.I., Dye, J.L., Mohrle, C.R., Wade, A.L., 2008. Traumatic brain injury during Operation Iraqi Freedom: findings from the United States Navy-Marine Corps Combat Trauma Registry. Journal of neurosurgery 108, 950-957.

Gama Sosa, M.A., De Gasperi, R., Janssen, P.L., Yuk, F.J., Anazodo, P.C., Pricop, P.E., Paulino, A.J., Wicinski, B., Shaughness, M.C., Maudlin-Jeronimo, E., Hall, A.A., Dickstein, D.L., McCarron, R.M., Chavko, M., Hof, P.R., Ahlers, S.T., Elder, G.A., 2014. Selective vulnerability

of the cerebral vasculature to blast injury in a rat model of mild traumatic brain injury. Acta neuropathologica communications 2, 67.

Ghavami, S., Hashemi, M., Ande, S.R., Yeganeh, B., Xiao, W., Eshraghi, M., Bus, C.J., Kadkhoda, K., Wiechec, E., Halayko, A.J., Los, M., 2009. Apoptosis and cancer: mutations within caspase genes. J Med Genet 46, 497-510.

Gill, J., Motamedi, V., Osier, N., Dell, K., Arcurio, L., Carr, W., Walker, P., Ahlers, S., LoPresti, M., Yarnell, A., 2017. Moderate blast exposure results in increased IL-6 and TNFalpha in peripheral blood. Brain Behav Immun.

Goldstein, L.E., Fisher, A.M., Tagge, C.A., Zhang, X.L., Velisek, L., Sullivan, J.A., Upreti, C., Kracht, J.M., Ericsson, M., Wojnarowicz, M.W., Goletiani, C.J., Maglakelidze, G.M., Casey, N., Moncaster, J.A., Minaeva, O., Moir, R.D., Nowinski, C.J., Stern, R.A., Cantu, R.C., Geiling, J., Blusztajn, J.K., Wolozin, B.L., Ikezu, T., Stein, T.D., Budson, A.E., Kowall, N.W., Chargin, D., Sharon, A., Saman, S., Hall, G.F., Moss, W.C., Cleveland, R.O., Tanzi, R.E., Stanton, P.K., McKee, A.C., 2012. Chronic traumatic encephalopathy in blast-exposed military veterans and a blast neurotrauma mouse model. Sci Transl Med 4, 134ra160.

Graner, J., Oakes, T.R., French, L.M., Riedy, G., 2013. Functional MRI in the investigation of blast-related traumatic brain injury. Frontiers in neurology 4, 16.

Gullotti, D.M., Beamer, M., Panzer, M.B., Chen, Y.C., Patel, T.P., Yu, A., Jaumard, N., Winkelstein, B., Bass, C.R., Morrison, B., Meaney, D.F., 2014. Significant head accelerations can influence immediate neurological impairments in a murine model of blast-induced traumatic brain injury. Journal of biomechanical engineering 136, 091004.

Gyorgy, A., Ling, G., Wingo, D., Walker, J., Tong, L., Parks, S., Januszkiewicz, A., Baumann, R., Agoston, D.V., 2011. Time-dependent changes in serum biomarker levels after blast traumatic brain injury. J Neurotrauma 28, 1121-1126.

Hofman, M.A., 1985. Size and shape of the cerebral cortex in mammals. I. The cortical surface. Brain Behav Evol 27, 28-40.

Hoge, C.W., McGurk, D., Thomas, J.L., Cox, A.L., Engel, C.C., Castro, C.A., 2008. Mild traumatic brain injury in U.S. Soldiers returning from Iraq. The New England journal of medicine 358, 453-463.

Hu, Z.G., Wang, H.D., Jin, W., Yin, H.X., 2009. Ketogenic diet reduces cytochrome c release and cellular apoptosis following traumatic brain injury in juvenile rats. Ann Clin Lab Sci 39, 76-83.

Hua, F., Reiss, J.I., Tang, H., Wang, J., Fowler, X., Sayeed, I., Stein, D.G., 2012. Progesterone and low-dose vitamin D hormone treatment enhances sparing of memory following traumatic brain injury. Horm Behav 61, 642-651.

Huber, B.R., Meabon, J.S., Martin, T.J., Mourad, P.D., Bennett, R., Kraemer, B.C., Cernak, I., Petrie, E.C., Emery, M.J., Swenson, E.R., Mayer, C., Mehic, E., Peskind, E.R., Cook, D.G., 2013. Blast exposure causes early and persistent aberrant phospho- and cleaved-tau expression in a murine model of mild blast-induced traumatic brain injury. Journal of Alzheimer's disease : JAD 37, 309-323.

Ivanov, M.S., Vandromme, D., Fomin, V.M., Kudryavtsev, A.N., Hadjadj, A., Khotyanovsky, D.V., 2001. Transition between regular and Mach reflection of shock waves: new numerical and experimental results. Shock Waves 11, 199-207.

Kallakuri, S., Desai, A., Feng, K., Tummala, S., Saif, T., Chen, C., Zhang, L., Cavanaugh, J.M., King, A.I., 2017. Neuronal Injury and Glial Changes Are Hallmarks of Open Field Blast Exposure in Swine Frontal Lobe. PLoS One 12, e0169239.

Kato, K., Fujimura, M., Nakagawa, A., Saito, A., Ohki, T., Takayama, K., Tominaga, T., 2007. Pressure-dependent effect of shock waves on rat brain: induction of neuronal apoptosis mediated by a caspase-dependent pathway. Journal of neurosurgery 106, 667-676.

Kuehn, R., Simard, P.F., Driscoll, I., Keledjian, K., Ivanova, S., Tosun, C., Williams, A., Bochicchio, G., Gerzanich, V., Simard, J.M., 2011. Rodent model of direct cranial blast injury. Journal of neurotrauma 28, 2155-2169.

Leonardi, A.D., Bir, C.A., Ritzel, D.V., VandeVord, P.J., 2011. Intracranial pressure increases during exposure to a shock wave. J Neurotrauma 28, 85-94.

Li, H., Sun, J., Wang, F., Ding, G., Chen, W., Fang, R., Yao, Y., Pang, M., Lu, Z.Q., Liu, J., 2016. Sodium butyrate exerts neuroprotective effects by restoring the blood-brain barrier in traumatic brain injury mice. Brain Res.

Li, S., Zaninotto, A.L., Neville, I.S., Paiva, W.S., Nunn, D., Fregni, F., 2015. Clinical utility of brain stimulation modalities following traumatic brain injury: current evidence. Neuropsychiatr Dis Treat 11, 1573-1586.

Ling, G., Bandak, F., Armonda, R., Grant, G., Ecklund, J., 2009. Explosive blast neurotrauma. Journal of neurotrauma 26, 815-825.

Ling, G.S., Ecklund, J.M., 2011. Traumatic brain injury in modern war. Current opinion in anaesthesiology 24, 124-130.

Lockhart, P., Cronin, D., Williams, K., Ouellet, S., 2011. Investigation of head response to blast loading. The Journal of trauma 70, E29-36.

Long, J.B., Bentley, T.L., Wessner, K.A., Cerone, C., Sweeney, S., Bauman, R.A., 2009. Blast overpressure in rats: recreating a battlefield injury in the laboratory. Journal of neurotrauma 26, 827-840.

Lu, J., Ng, K.C., Ling, G., Wu, J., Poon, D.J., Kan, E.M., Tan, M.H., Wu, Y.J., Li, P., Moochhala, S., Yap, E., Lee, L.K., Teo, M., Yeh, I.B., Sergio, D.M., Chua, F., Kumar, S.D., Ling, E.A., 2012. Effect of blast exposure on the brain structure and cognition in Macaca fascicularis. Journal of neurotrauma 29, 1434-1454.

Masel, B.E., DeWitt, D.S., 2010. Traumatic brain injury: a disease process, not an event. J Neurotrauma 27, 1529-1540.

Mattson, M.P., Chan, S.L., 2003. Calcium orchestrates apoptosis. Nature cell biology 5, 1041-1043.

Mayhew, T.M., 1992. A review of recent advances in stereology for quantifying neural structure. J Neurocytol 21, 313-328.

Mayhew, T.M., Mwamengele, G.L., Dantzer, V., Williams, S., 1996. The gyrification of mammalian cerebral cortex: quantitative evidence of anisomorphic surface expansion during phylogenetic and ontogenetic development. Journal of anatomy 188 ( Pt 1), 53-58.

Mayorga, M.A., 1997. The pathology of primary blast overpressure injury. Toxicology 121, 17-28.

McKee, A.C., Stern, R.A., Nowinski, C.J., Stein, T.D., Alvarez, V.E., Daneshvar, D.H., Lee, H.S., Wojtowicz, S.M., Hall, G., Baugh, C.M., Riley, D.O., Kubilus, C.A., Cormier, K.A., Jacobs, M.A., Martin, B.R., Abraham, C.R., Ikezu, T., Reichard, R.R., Wolozin, B.L., Budson, A.E., Goldstein, L.E., Kowall, N.W., Cantu, R.C., 2013. The spectrum of disease in chronic traumatic encephalopathy. Brain : a journal of neurology 136, 43-64.

Meyers, M.A., 1994. Dynamic behavior of materials. Wiley, New York.

Miller, A.P., Shah, A.S., Aperi, B.V., Budde, M.D., Pintar, F.A., Tarima, S., Kurpad, S.N., Stemper, B.D., Glavaski-Joksimovic, A., 2015. Effects of blast overpressure on neurons and glial cells in rat organotypic hippocampal slice cultures. Frontiers in neurology 6, 20.

Miller, A.P., Shah, A.S., Aperi, B.V., Kurpad, S.N., Stemper, B.D., Glavaski-Joksimovic, A., 2017. Acute death of astrocytes in blast-exposed rat organotypic hippocampal slice cultures. PLoS One 12, e0173167.

Moore, D.F., Jerusalem, A., Nyein, M., Noels, L., Jaffee, M.S., Radovitzky, R.A., 2009. Computational biology - modeling of primary blast effects on the central nervous system. NeuroImage 47 Suppl 2, T10-20.

Moss, W.C., King, M.J., Blackman, E.G., 2009. Skull flexure from blast waves: a mechanism for brain injury with implications for helmet design. Physical review letters 103, 108702.

Murray, C.K., Reynolds, J.C., Schroeder, J.M., Harrison, M.B., Evans, O.M., Hospenthal, D.R., 2005. Spectrum of care provided at an echelon II Medical Unit during Operation Iraqi Freedom. Military medicine 170, 516-520.

Needham, C.E., Ritzel, D., Rule, G.T., Wiri, S., Young, L., 2015. Blast Testing Issues and TBI: Experimental Models That Lead to Wrong Conclusions. Frontiers in neurology 6, 72.

Ngo, T., Mendis, P., Gupta, A., Ramsay, J., 2007. Blast loading and blast effects on structures–an overview. Electronic Journal of Structural Engineering 7, 76-91.

Nyein, M.K., Jason, A.M., Yu, L., Pita, C.M., Joannopoulos, J.D., Moore, D.F., Radovitzky, R.A., 2010. In silico investigation of intracranial blast mitigation with relevance to military traumatic brain injury. Proceedings of the National Academy of Sciences of the United States of America 107, 20703-20708.

Okie, S., 2005. Traumatic brain injury in the war zone. N Engl J Med 352, 2043-2047.

Omalu, B.I., DeKosky, S.T., Minster, R.L., Kamboh, M.I., Hamilton, R.L., Wecht, C.H., 2005. Chronic traumatic encephalopathy in a National Football League player. Neurosurgery 57, 128-134; discussion 128-134.

Panzer, M.B., Myers, B.S., Capehart, B.P., Bass, C.R., 2012. Development of a finite element model for blast brain injury and the effects of CSF cavitation. Annals of biomedical engineering 40, 1530-1544.

Rafaels, K., Bass, C.R., Salzar, R.S., Panzer, M.B., Woods, W., Feldman, S., Cummings, T., Capehart, B., 2011. Survival risk assessment for primary blast exposures to the head. Journal of neurotrauma 28, 2319-2328.

Rafaels, K.A., Bass, C.R., Panzer, M.B., Salzar, R.S., Woods, W.A., Feldman, S.H., Walilko, T., Kent, R.W., Capehart, B.P., Foster, J.B., Derkunt, B., Toman, A., 2012. Brain injury risk from primary blast. J Trauma Acute Care Surg 73, 895-901.

Ramasamy, A., Newell, N., Masouros, S., 2014. From the battlefield to the laboratory: the use of clinical data analysis in developing models of lower limb blast injury. Journal of the Royal Army Medical Corps 160, 117-120.

Ravin, R., Blank, P.S., Steinkamp, A., Rappaport, S.M., Ravin, N., Bezrukov, L., Guerrero-Cazares, H., Quinones-Hinojosa, A., Bezrukov, S.M., Zimmerberg, J., 2012. Shear forces during blast, not abrupt changes in pressure alone, generate calcium activity in human brain cells. PloS one 7, e39421.

Reneer, D.V., Hisel, R.D., Hoffman, J.M., Kryscio, R.J., Lusk, B.T., Geddes, J.W., 2011. A multi-mode shock tube for investigation of blast-induced traumatic brain injury. Journal of neurotrauma 28, 95-104.

Richmond, D.R., Damon, E.G., Fletcher, E.R., Bowen, I.G., White, C.S., 1968. The relationship between selected blast-wave parameters and the response of mammals exposed to air blast. Annals of the New York Academy of Sciences 152, 103-121.

Richmond, D.R., Goldizen, V.C., Clare, V.R., Pratt, D.E., Sherping, F., Sanchez, R.T., Fischer, C.C., White, C.S., 1962. The biologic response to overpressure. III. Mortality in small animals exposed in a shock tube to sharprising overpressures of 3 to 4 msec duration. Aerospace medicine 33, 1-27.

Risling, M., Davidsson, J., 2012. Experimental animal models for studies on the mechanisms of blast-induced neurotrauma. Front Neurol 3, 30.

Rosenfeld, J.V., Bell, R.S., Armonda, R., 2015. Current concepts in penetrating and blast injury to the central nervous system. World J Surg 39, 1352-1362.

Rosenfeld, J.V., McFarlane, A.C., Bragge, P., Armonda, R.A., Grimes, J.B., Ling, G.S., 2013. Blast-related traumatic brain injury. The Lancet. Neurology 12, 882-893.

Roura, E., Koopmans, S.J., Lalles, J.P., Le Huerou-Luron, I., de Jager, N., Schuurman, T., Val-Laillet, D., 2016. Critical review evaluating the pig as a model for human nutritional physiology. Nutr Res Rev 29, 60-90.

Rubovitch, V., Ten-Bosch, M., Zohar, O., Harrison, C.R., Tempel-Brami, C., Stein, E., Hoffer, B.J., Balaban, C.D., Schreiber, S., Chiu, W.T., Pick, C.G., 2011. A mouse model of blast-induced mild traumatic brain injury. Experimental neurology 232, 280-289.

Saljo, A., Arrhen, F., Bolouri, H., Mayorga, M., Hamberger, A., 2008. Neuropathology and pressure in the pig brain resulting from low-impulse noise exposure. J Neurotrauma 25, 1397-1406.

Saljo, A., Mayorga, M., Bolouri, H., Svensson, B., Hamberger, A., 2011. Mechanisms and pathophysiology of the low-level blast brain injury in animal models. Neuroimage 54 Suppl 1, S83-88.

Salvesen, G.S., 2002. Caspases: opening the boxes and interpreting the arrows. Cell death and differentiation 9, 3-5.

Sarntinoranont, M., Lee, S.J., Hong, Y., King, M.A., Subhash, G., Kwon, J., Moore, D.F., 2012. High-strain-rate brain injury model using submerged acute rat brain tissue slices. Journal of neurotrauma 29, 418-429.

Sawyer, T.W., Lee, J.J., Villanueva, M., Wang, Y., Nelson, P., Song, Y., Fan, C., Barnes, J., McLaws, L., 2017. The Effect of Underwater Blast on Aggregating Brain Cell Cultures. Journal of neurotrauma 34, 517-528.

Schmued, L.C., Albertson, C., Slikker, W., Jr., 1997. Fluoro-Jade: a novel fluorochrome for the sensitive and reliable histochemical localization of neuronal degeneration. Brain Res 751, 37-46.

Schmued, L.C., Stowers, C.C., Scallet, A.C., Xu, L., 2005. Fluoro-Jade C results in ultra high resolution and contrast labeling of degenerating neurons. Brain Res 1035, 24-31.

Shellington, D.K., Du, L., Wu, X., Exo, J., Vagni, V., Ma, L., Janesko-Feldman, K., Clark, R.S., Bayir, H., Dixon, C.E., Jenkins, L.W., Hsia, C.J., Kochanek, P.M., 2011. Polynitroxylated pegylated hemoglobin: a novel neuroprotective hemoglobin for acute volume-limited fluid resuscitation after combined traumatic brain injury and hemorrhagic hypotension in mice. Crit Care Med 39, 494-505.

Shetty, A.K., Mishra, V., Kodali, M., Hattiangady, B., 2014. Blood brain barrier dysfunction and delayed neurological deficits in mild traumatic brain injury induced by blast shock waves. Frontiers in cellular neuroscience 8, 232.

Shridharani, J.K., Wood, G.W., Panzer, M.B., Capehart, B.P., Nyein, M.K., Radovitzky, R.A., Bass, C.R., 2012. Porcine head response to blast. Front Neurol 3, 70.

Singer, P., Cohen, J.D., Stein, M., 2005. Conventional terrorism and critical care. Critical care medicine 33, S61-65.

Skotak, M., Wang, F., Alai, A., Holmberg, A., Harris, S., Switzer, R.C., Chandra, N., 2013. Rat injury model under controlled field-relevant primary blast conditions: acute response to a wide range of peak overpressures. Journal of neurotrauma 30, 1147-1160.

Smith, M., Piehler, T., Benjamin, R., Farizatto, K.L., Pait, M.C., Almeida, M.F., Ghukasyan, V.V., Bahr, B.A., 2016. Blast waves from detonated military explosive reduce GluR1 and synaptophysin levels in hippocampal slice cultures. Experimental neurology 286, 107-115.

Sosa, M.A., De Gasperi, R., Paulino, A.J., Pricop, P.E., Shaughness, M.C., Maudlin-Jeronimo, E., Hall, A.A., Janssen, W.G., Yuk, F.J., Dorr, N.P., Dickstein, D.L., McCarron, R.M., Chavko, M., Hof, P.R., Ahlers, S.T., Elder, G.A., 2013. Blast overpressure induces shear-related injuries in the brain of rats exposed to a mild traumatic brain injury. Acta neuropathologica communications 1, 51.

Springer, J.E., 2002. Apoptotic cell death following traumatic injury to the central nervous system. J Biochem Mol Biol 35, 94-105.

Stein, M.B., McAllister, T.W., 2009. Exploring the convergence of posttraumatic stress disorder and mild traumatic brain injury. The American journal of psychiatry 166, 768-776.

Sundaramurthy, A., Chandra, N., 2014. A parametric approach to shape field-relevant blast wave profiles in compressed-gas-driven shock tube. Frontiers in neurology 5, 253.

Swindle, M.M., 1984. Swine as replacements for dogs in the surgical teaching and research laboratory. Lab Anim Sci 34, 383-385.

Taylor, P.A., Ford, C.C., 2009. Simulation of blast-induced early-time intracranial wave physics leading to traumatic brain injury. Journal of biomechanical engineering 131, 061007.

Teasdale, G., Jennett, B., 1974. Assessment of coma and impaired consciousness. A practical scale. Lancet 2, 81-84.

Uguz, A.C., Naziroglu, M., Espino, J., Bejarano, I., Gonzalez, D., Rodriguez, A.B., Pariente, J.A., 2009. Selenium modulates oxidative stress-induced cell apoptosis in human myeloid HL-60 cells through regulation of calcium release and caspase-3 and -9 activities. J Membr Biol 232, 15-23.

Walters, J., Pop, C., Scott, F.L., Drag, M., Swartz, P., Mattos, C., Salvesen, G.S., Clark, A.C., 2009. A constitutively active and uninhibitable caspase-3 zymogen efficiently induces apoptosis. The Biochemical journal 424, 335-345.

Wang, C., Pahk, J.B., Balaban, C.D., Miller, M.C., Wood, A.R., Vipperman, J.S., 2014. Computational study of human head response to primary blast waves of five levels from three directions. PloS one 9, e113264.

Wang, E.W., Huang, J.H., 2013. Understanding and treating blast traumatic brain injury in the combat theater. Neurol Res 35, 285-289.

Wang, J.W., Wang, H.D., Zhong, W.Z., Li, N., Cong, Z.X., 2012. Expression and cell distribution of metabotropic glutamate receptor 5 in the rat cortex following traumatic brain injury. Brain Res 1464, 73-81.

Wang, Y., Wei, Y., Oguntayo, S., Wilkins, W., Arun, P., Valiyaveettil, M., Song, J., Long, J.B., Nambiar, M.P., 2011. Tightly coupled repetitive blast-induced traumatic brain injury: development and characterization in mice. Journal of neurotrauma 28, 2171-2183.

Warden, D.L., French, L., 2005. Traumatic brain injury in the war zone. N Engl J Med 353, 633-634.

White, C.S., Bowen, I.G., Richmond, D.R., 1965. Biological tolerance to air blast and related biomedical criteria. CEX-65.4. CEX [reports]; civil effects exercise. U.S. Atomic Energy Commission, 1-239.

Wojcik, B.E., Stein, C.R., Bagg, K., Humphrey, R.J., Orosco, J., 2010. Traumatic brain injury hospitalizations of U.S. army soldiers deployed to Afghanistan and Iraq. Am J Prev Med 38, S108-116.

Wood, A., 1966. Acoustics. Dover Publications, New York,.

Xu, J., Wang, H., Ding, K., Lu, X., Li, T., Wang, J., Wang, C., Wang, J., 2013. Inhibition of cathepsin S produces neuroprotective effects after traumatic brain injury in mice. Mediators Inflamm 2013, 187873.

Xu, S., Liu, J., Zhang, Y., Wang, C., Wang, J., Yang, Y., Huo, J., Sun, W., 2012. Apoptosis-related protein expression in rabbits with blast brain injury following early hyperbaric oxygen therapy. Neural regeneration research 7, 1318-1324.

Yatsiv, I., Grigoriadis, N., Simeonidou, C., Stahel, P.F., Schmidt, O.I., Alexandrovitch, A.G., Tsenter, J., Shohami, E., 2005. Erythropoietin is neuroprotective, improves functional recovery, and reduces neuronal apoptosis and inflammation in a rodent model of experimental closed head injury. FASEB J 19, 1701-1703.

Zhang, L., Makwana, R., Sharma, S., 2013. Brain response to primary blast wave using validated finite element models of human head and advanced combat helmet. Front Neurol 4, 88.

Zhang, X., Chen, Y., Jenkins, L.W., Kochanek, P.M., Clark, R.S., 2005. Bench-to-bedside review: Apoptosis/programmed cell death triggered by traumatic brain injury. Crit Care 9, 66-75.

Zhu, F., Mao, H., Dal Cengio Leonardi, A., Wagner, C., Chou, C., Jin, X., Bir, C., Vandevord, P., Yang, K.H., King, A.I., 2010. Development of an FE model of the rat head subjected to air shock loading. Stapp car crash journal 54, 211-225.

Zhu, F., Skelton, P., Chou, C.C., Mao, H., Yang, K.H., King, A.I., 2013. Biomechanical responses of a pig head under blast loading: a computational simulation. International journal for numerical methods in biomedical engineering 29, 392-407.

Zhu, F., Wagner, C., Dal Cengio Leonardi, A., Jin, X., Vandevord, P., Chou, C., Yang, K.H., King, A.I., 2012. Using a gel/plastic surrogate to study the biomechanical response of the head under air shock loading: a combined experimental and numerical investigation. Biomech Model Mechanobiol 11, 341-353.

## ABSTRACT

# AN INVESTIGATION OF THE MECHANISM OF TRAUMATIC BRAIN INJURY FROM BLAST IN THE OPEN FIELD

by

**KE FENG**

**May 2017**

**Advisor:** Dr. John Cavanaugh

**Major:** Biomedical Engineering

**Degree:** Doctor of Philosophy

Blast-induced traumatic brain injury (bTBI) is a signature wound of modern warfare. The current incomplete understanding of its injury mechanism impedes the development of strategies for effective protection of bTBI. Despite a considerable amount of experimental animal studies focused on the evaluation of brain neurotrauma caused by blast exposure, there is very limited knowledge on the biomechanical responses of the gyrenecephalic brain subjected to primary free-field blast waves imposed in vivo, and the correlation analysis between the biomechanical responses and its injury outcomes. Such information is crucial to the development of injury criteria of bTBI.

This study aims to evaluate the external and internal mechanical responses of the brain against different levels of blast loading with Yucatan swine in free field, and to conduct correlational studies with brain tissue damage. To better understand primary bTBI, we have implemented an open field experimental model to apply controlled shock waves on swine head. The applied pressure levels of shock waves were predicted by finite element modeling and verified

with calibrated testing. Biomechanical responses of primary blasts such as intracranial pressure (ICP), head kinetics, strain rate of skull, were measured *in vivo* during the blasts. A positive correlation between incident overpressure (IOP) and its corresponding biomechanical responses of the brain was observed. A parallel group of non-instrumented animals were used to collect injury data 72 hours post experiment. Cellular responses governed by primary blasts, such as neuronal degeneration and apoptosis were studied via immunohistochemistry. Representative fluorescent-stained images were examined under microscope. A positive correlation was found between the amount of degenerative neurons and the blast level. Significant elevation of apoptosis was found in the high-level blast. Comparisons between brains with varies ICP readings demonstrate differences of the numbers of neuronal degeneration and apoptosis within the imaged volume. Additionally, comparisons between sections at different locations of the head did not show spatial changes for cellular responses. These metrics provide a pathway for direct connection between the cellular damage and the measured biomechanical responses of the brain within the same experimental model, and could be critical in understanding the mechanisms of bTBI. This experimental data can be used to validate computer models of bTBI.

# AUTOBIOGRAPHICAL STATEMENT
# KE FENG

**EDUCATION:**

- Ph.D. Biomedical Engineering, Wayne State University, Detroit, Michigan, 2017.
- M.S., Biomedical Engineering, Wayne State University, Detroit, Michigan, 2010
- B.E. Biomedical Engineering, South-Central University for Nationalities, Wuhan, China, 2008.

**EXPERIENCE:**

- Graduate Research Assistant, Biomedical Engineering Department 08/12 - 08/16
  College of Engineering, Wayne State University, Detroit, MI
- Graduate Teaching Assistant, Biomedical Engineering Department 08/10 - 05/12
  College of Engineering, Wayne State University, Detroit, MI